

**END MILLING MACHINABILITY STUDIES FOR
STEEL, A NICKEL-BASE ALLOY (INCONEL 718) AND
A METAL MATRIX COMPOSITE**

A thesis submitted to
Dublin City University
in fulfilment of the requirements
for the award of the degree of
Doctor of Philosophy

by

Mohammed Alauddin B. Sc., M. Sc.(Eng.)
School of Mechanical and Manufacturing Engineering
Dublin City University, Dublin 9
Ireland

July 1993

LIBRARY
DUBLIN CITY
UNIVERSITY

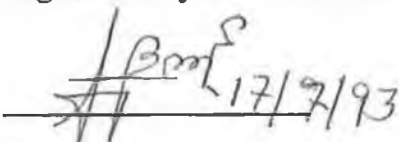
Dedicated To My Family

DECLARATION

I hereby declare that all the work reported in this thesis was carried out by me at Dublin City University during the period of July 1990 to July 1993.

To the best of my knowledge, the results presented in this thesis originated from the present study, except where references have been made. No part of this thesis has been submitted for a degree at any other institution.

Signature of Candidate: _____

 17/7/93

Mohammed Alauddin

ACKNOWLEDGEMENTS

The author is indebted to his supervisors, Dr. M.A. El Baradie and Professor M.S.J. Hashmi for their valuable advice, wholehearted aid and encouragement at all stages of the work.

Sincerest thanks are due to Mr. Liam Domican, Mr. Martin Johnson, Mr. Stuart Doherty, Mr. Ian Hooper, Mr. Tom Walsh , the staff of the School of Mechanical and Manufacturing Engineering for providing great help during the course of this research, and to Mr. George Anderson, the ex staff member of the school of Mechanical and Manufacturing Engineering for his valuable assistance. Thanks are also due to Ms. Lesley Lawlor, the secretary of the school of Mechanical and Manufacturing Engineering for her co-operation in connection with the work.

The author is grateful to Materials Ireland (EOLAS) for providing funds in support of this research, and to Devtec Ltd., a subsidiary of Aer lingus for providing workpiece materials used in this work.

The author owes thanks to Mr. Hemayet uddin Talukder, a deputy secretary of the Ministry of Establishment, The Government of Bangladesh who has always been supportive and provided encouragement for the author's higher studies.

Finally, the author would like to express his special thanks to his wife, Nazmun Nahar who helped greatly in the preparation of this thesis.

About The Author

The author received his B.Sc.in Engineering (Mechanical) from the Bangladesh University of Engineering and Technology (BUET), Dhaka in the year 1976. After graduation the author worked in industry for about five years and then joined as an Assistant Professor, Dhaka Engineering College (DEC) in 1982. In 1985, the author came to the U.K to pursue his M.Sc. in Advanced Manufacturing Technology (AMT) in the department of Mechanical Engineering at the University of Manchester Institute of Science and Technology (UMIST) under the BTA (British Technical Assistance) programme. After receiving M.Sc. in 1987, the author returned to his post in the Bangladesh Institute of Technology (BIT¹) Dhaka. In 1990, the author received a studentship from the School of Mechanical and Manufacturing Engineering of Dublin City University to pursue this Ph.D study.

¹ In 1986 DEC was converted into BIT Dhaka

CONTENTS

	Page
DECLARATION	
ACKNOWLEDGEMENTS	
ABSTRACT	
ABOUT THE AUTHOR	
NOTATION	
CHAPTER 1: INTRODUCTION	1
CHAPTER 2: LITERATURE SURVEY	
2.1 Introduction	7
2.2 Cutting forces in milling	7
2.3 Tool life in milling	19
2.4 Surface finish in milling	35
2.5 Machinability of advanced materials	39
CHAPTER 3: GENERAL DISCUSSION ON MACHINABILITY	
3.1 Introduction	46
3.2 Machinability assessment	47
3.3 Factors influencing machinability	47
3.3.1 End Milling process	47
3.3.1.1 Cutting force aspects in end Milling	62
3.3.1.2 Tool life aspects in end Milling	80
3.3.1.3 Surface integrity aspects in end milling	106
CHAPTER 4: RESPONSE SURFACE METHODOLOGY AND DEVELOPMENT OF MACHINABILITY MODELS	
4.1 Response Surface Methodology(RSM)	121
4.1.1 The response function and the response surface	122
4.1.2 Representation of the response surface by contour	122
4.1.3 General steps involved in the application of Response Surface Methodology	125
4.2 Development of machinability models by RSM	141

CHAPTER 5: EXPERIMENTAL SET-UP AND PROCEDURE

5.1	Introduction	143
5.2	Experimental apparatus, equipment and machine	143
5.3	Experimental workpiece materials	144
5.4	Experimental cutting tools	148
5.5	Measurement of average cutting forces	148
5.6	Measurement of flank wear of end mill cutter	155
5.7	Measurement of surface roughness	155

CHAPTER 6: INVESTIGATION OF CUTTING FORCES IN END MILLING STEEL (190 BHN) AND INCONEL 718

6.1	Introduction	157
6.2	Development of cutting force model in end milling steel (190 BHN)	157
6.3	Influence of machining conditions on cutting forces in end milling Inconel 718	166
6.4	Development of cutting force model in end milling Inconel 718	194

CHAPTER 7: INVESTIGATION OF TOOL LIFE IN END MILLING STEEL (190 BHN) AND INCONEL 718.

7.1	Introduction	200
7.2	Development of tool life models in end milling steel (190 BHN)	200
7.3	Tool deterioration with cutting time in end milling Inconel 718	210

CHAPTER 8: INVESTIGATION OF SURFACE FINISH IN END MILLING STEEL (190 BHN), INCONEL 718 AND 2618 MMC

8.1	Introduction	220
8.2	Development of surface roughness models in end milling <u>steel</u> (190 BHN)	220
8.3	Influence of machining conditions on surface roughness in end milling <u>Inconel</u> 718	232
8.4	Development of surface roughness models in end milling <u>Inconel</u> 718	235
8.5	Development of surface roughness models in end milling 2618 <u>MMC</u>	243

CHAPTER 9: GENERAL CONCLUSIONS AND SUGGESTIONS FOR FURTHER DEVELOPMENT		
9.1	General conclusions	253
9.2	Recommendations further development	255
REFERENCES		258
APPENDICES		
APPENDIX 1: The experimental machine tool, workpiece & measurement of cutting forces, tool life and surface roughness		269
APPENDIX 2: The calculation of model parameters, results of analysis of variance, significance testing of the individual variables and confidence intervals for cutting force models for steel (190 BHN) and Inconel 718		283
APPENDIX 3: The Calculation of model parameters, results of analysis of variance, significance testing of the individual variables and confidence intervals for tool life models for steel (190 BHN) and SEM image of the flank wear of the carbide inserts in end milling Inconel 718		292
APPENDIX 4: The results of analysis of variance, significance testing for individual variables and confidence intervals for the predictive surface roughness models for steel (190 BHN), Inconel 718 and 2618 MMC		301
APPENDIX 5: Publications		312

List of Figures

<u>Fig. No.</u>		Page
2.1	Taylor's tool life equation	26
2.2	General trend of tool life with speed, feed and depth of cut	26
2.3	Kronenberg method of modifying a curved Taylor's plot	26
2.4	Influence of chip equivalent on cutting temperature	29
3.1	Factors influencing machinability of a material	48
3.2	End milling process	56
3.3	Milling mode	56
3.4	Slot milling	57
3.5	End milling ($a_a > a_r$)	57
3.6	End milling ($a_a < a_r$)	58
3.7	End milling processes	58
3.8	The chip geometry of an end mill cutter	59
3.9	The simplified model of end milling process	59
3.10	Cutting processes in the effective cutting plane (simplified end milling process)	60
3.11	Relationship between feed/tooth and feed/min in end milling process	61
3.12	Relationship between feed/tooth and feed ratio in end milling process	61
3.13	Cutting force components acting on one tooth of an end mill	64
3.14	Variation of the feed force in slot milling operation	67
3.15	Factors influencing cutting forces in end milling processes	74
3.16	Flank wear on a solid end mill cutter	82
3.17	Flank wear of a carbide insert of an end mill	83
3.18	Schematic illustration of adhesion of a material	89
3.19	Schematic illustration of two body and three body abrasive wear	89
3.20	Wear by diffusion	89
3.21	Stress distribution around the interlocking asperities	89
3.22	Tool deterioration values for a number of tests runs plotted against cutting time	92

3.23	Arithmetic mean values of tool deterioration for a number of test runs against cutting time	92
3.24	Factors influencing tool life in end milling processes	94
3.25	Face milling process	103
3.26	A typical plot of tool life (T) against off set	103
3.27	A plot of tool life against distance off set in machining hard or extremely workhardening materials	104
3.28	Schematic illustration of a tooth contact with workpiece in end (Face) milling process	104
3.29	Kinds of surface profiles	110
3.30	Lay direction in slot milling by an end mill insert	110
3.31	Common surface roughness parameters	110
3.32	Definition of R_a	111
3.33	Factors influencing surface finish in end milling processes	112
4.1	A response surface	124
4.2	Response contours for the surface of Fig.4.1	124
4.3	First-order orthogonal design for 2 factors	133
4.4	First-order orthogonal design for 3 factors	133
4.5	Central Composite rotatable design for 2 factors	134
4.6	Central composite design for 3 factors	134
5.1	Schematic diagram of force measuring system	150
5.2	Measurement of average cutting force of a section of cutting force signal from the light beam recorder	154
6.1	Contour surfaces for resultant cutting forces in end milling steel in 3 dimensional factor space	163
6.2	Resultant cutting force contours (first-order model) for steel in speed -axial depth of cut plane at selected levels of feed	164
6.3	Effect of cutting speed on average feed force in slot milling Inconel 718 at 3 selected levels of feed/min	168
6.4	Effect of cutting speed on average normal force in slot milling Inconel 718 at 3 selected levels of feed/min	169
6.5	Effect of cutting speed on average vertical force in slot milling Inconel 718 at 3 selected levels of feed/min	169

6.6	Effect of cutting speed on average tangential force in slot milling Inconel 718 at 3 selected levels of feed/min	170
6.7	Effect of cutting speed on average resultant force in slot milling Inconel 718 3 selected levels of feed/min	170
6.8	Effect of cutting speed on average table system of cutting forces in slot milling Inconel 718 at feed rate of 45 mm/min and axial depth of cut of 1.2 mm	171
6.9	Effect of cutting speed on average table system of cutting forces in slot milling Inconel 718 at f_z of 0.10 mm/tooth and a_a of 0.50 mm	171
6.10	Effect of feed (f_m) on average feed force in slot milling Inconel 718 3 selected levels of speed	173
6.11	Effect of feed (f_m) on average normal force in slot milling Inconel 718 at 3 selected levels of speed	173
6.12	Effect of feed on average vertical force in slot milling Inconel 718 3 selected levels of speed	174
6.13	Effect of feed on average tangential force in slot milling Inconel 718 at 3 selected levels of speed	174
6.14	Effect of feed on average resultant force in slot milling Inconel 718 at 3 selected levels of speed	175
6.15	Effect of feed on average table system of cutting forces in slot milling Inconel 718 at speed of 16.17 m/min and axial depth of cut of 1.2 mm	175
6.16	Effect of axial depth of cut on average feed force in slot milling Inconel 718 at 3 selected levels of speed	177
6.17	Effect of axial depth of cut on average normal force in slot milling Inconel 718 at 3 selected levels of speed	177
6.18	Effect of axial depth of cut on average vertical force in slot milling Inconel 718 at 3 selected levels of speed	178
6.19	Effect of axial depth of cut on average tangential force in slot milling Inconel 718 at 3 selected levels of speed	178
6.20	Effect of axial depth of cut on average resultant force in slot milling Inconel 718 at 3 selected levels of speed	179
6.21	Effect of axial depth of cut on average table system of cutting forces in slot milling Inconel 718 at 3 selected levels of speed	179

6.22	Effect of speed on average table system of cutting forces in half immersion up end milling Inconel 718 at feed rate of 32 mm/min	181
6.23	Effect of speed on average tangential force in half immersion up end milling Inconel 718 at feed rate of 32 mm/min	181
6.24	Effect of speed on average resultant force in half immersion up end milling Inconel 718 at feed rate of 32 mm/min	182
6.25	Effect of feed on average table system of cutting forces in half immersion up end milling Inconel 718 at cutting speed of 16.17 m/min	183
6.26	Effect of feed on average tangential force in half immersion up end milling Inconel 718 at cutting speed of 16.17 m/min	183
6.27	Effect of feed on average resultant force in half immersion up Inconel 718 at cutting speed of 16.17 m/min	184
6.28	Effect of axial depth of cut on average table system of cutting forces in half immersion up end milling Inconel 718 at speed of 16.17 m/min	185
6.29	Effect of axial depth of cut on average tangential force in half immersion up end milling Inconel 718 at speed of 16.17 m/min	185
6.30	Effect of axial depth of cut on average resultant cutting force in half immersion up end milling Inconel 718 at speed of 16.17 m/min	186
6.31	Effect of speed on average table system of cutting forces in half immersion down milling Inconel 718 at feed rate of 32 mm/min	187
6.32	Effect of speed on average tangential force in half immersion down end milling Inconel 718 at feed rate of 32 mm/min	188
6.33	Effect of speed on average resultant cutting force in half immersion down end milling Inconel 718 at feed rate of 32 mm/min	188
6.34	Effect of feed on average table system of cutting forces in half immersion down end milling Inconel 718 at speed of 16.17 m/min	189
6.35	Effect of feed on average tangential force in half immersion down end milling Inconel 718 at speed of 16.17 m/min	190
6.36	Effect of feed on average resultant force in half immersion down end milling Inconel 718 at cutting speed of 16.17 m/min	190
6.37	Effect of axial depth of cut on average table system of cutting forces in half immersion down end milling Inconel 718 at speed of 16.17m/min	191

6.38	Effect of axial depth of cut on average tangential force in half immersion down end milling Inconel 718 at speed of 16.17 m/in	192
6.39	Effect of axial depth of cut on average resultant force in half immersion down end milling Inconel 718 at speed of 16.17 m/min	192
6.40	Tangential force contours in axial depth of cut-feed plane at a selected level of cutting speed of 16.17 m/min	198
7.1	Contour surface for tool life in end milling steel in 3 dimensional space	206
7.2	Tool life contours (first-order model) for steel in speed-feed plane at selected level of axial depth of cut	206
7.3	Tool life contours (second-order model) for steel in speed-feed planes at selected level of axial depth of cut	207
7.4	Contours of tool life (second-order model) and material removal rates for steel in speed-feed planes at an axial depth of cut of 0.60 mm	207
7.5	Tool deterioration values for a number of test runs plotted against cutting time in full immersion end milling Inconel 718 at $v = 19.32$ m/min, $f_z = 0.091$ mm/tooth and $a_a = 1.00$ mm	212
7.6	Arithmetic mean values of tool deterioration which is obtained from Fig.7.5 plotted against cutting time	212
7.7	Tool deterioration values for a number of test runs plotted against cutting time in full immersion end milling Inconel 718 at $v = 29.05$ m/min, $f_z = 0.086$ mm/tooth and $a_a = 1.00$ mm	213
7.8	Arithmetic mean values of tool deterioration which is obtained from Fig.7.7 is plotted against cutting time	213
7.9	Tool deterioration values for a number of test runs plotted against cutting time in half immersion up cut end milling Inconel 718 at $v = 19.32$ m/min, $f_z = 0.091$ mm/tooth and $a_a = 1.00$ mm	215
7.10	Arithmetic mean values of tool deterioration which is obtained from Fig.7.9 plotted against cutting time	215
7.11	Tool deterioration values of test runs plotted against cutting time in half immersion down cut end milling Inconel 718 at $v = 19.32$ m/min, $f_z = 0.091$ mm/tooth and $a_a = 1.00$ mm	217

7.12	Arithmetic mean values of tool deterioration which is obtained from Fig.7.11 plotted against cutting time	217
7.13	Comparison of tool life between half immersion and full immersion end milling Inconel 718	219
8.1	Contour surfaces for surface roughness in end milling steel in a 3 dimensional factor space	226
8.2	Surface roughness contours (first-order model) for steel in speed-feed planes at selected levels of axial depth of cut	227
8.3	Surface roughness contours (second-order model) for steel in speed feed planes at selected levels of axial depth of cut	229
8.4	Contours of surface roughness (second-order model) and material removal rates for steel in speed-feed planes	230
8.5	Surface roughness versus speed for slot milling Inconel 718 using sharp uncoated carbide under dry condition	234
8.6	Surface roughness versus feed for slot milling Inconel 718 using sharp uncoated carbide insert under dry condition	234
8.7	Surface roughness contours (first-order model) for Inconel 718 in speed-feed planes at 0.50 mm axial depth of cut	240
8.8	Surface roughness contours (second-order model) for Inconel 718 in speed-feed planes at a selected level of axial depth of cut	240
8.9	Contours of surface roughness (second-order model) and material removal rates for Inconel 718 in speed-feed planes at $a_p = 0.50$ mm	241
8.10	Contour surfaces for surface roughness in end milling MMC (Al/SiC) in 3 dimensional factor space	248
8.11	Surface roughness contours (First-order model) for MMC (Al/SiC) in speed-feed planes at a selected level of axial depth of cut	248
8.12	Surface roughness contours (second-order model) for MMC (Al/SiC) in speed-feed planes at 1.00 mm axial depth of cut	250
8.13	Contours of surface roughness (second-order model) and material removal rates in a speed-feed planes at 1.00 mm axial depth of cut	250
1	Angular geometries of a slot drill	275
2	Dimension of the carbide insert of the end mill cutter	276

3	SEM image of the flank wear of the carbide insert in full immersion end milling Inconel 718 at $v = 19.32$ m/min, $f_z = 0.091$ mm/tooth and $a_a = 1.00$ mm	299
4	SEM image of the flank wear of the carbide insert in full immersion end milling Inconel 718 at $v = 29.05$ m/min, $f_z = 0.086$ mm/tooth and $a_a = 1.00$ mm	299
5.	SEM image of the flank wear of the carbide insert in half immersion end milling Inconel 718 at up cut mode at $v = 19.32$ m/min, $f_z = 0.091$ mm/tooth and $a_a = 1.00$ mm	300
6	SEM image of the " V " shaped localized flank wear of the carbide insert in half immersion end milling Inconel 718 at down cut mode at $v = 19.32$ m/min, $f_z = 0.091$ mm/tooth and $a_a = 1.00$ mm	300

List of Tables

<u>Table No.</u>		
2.1	Summary of static cutting force equations	18
2.2	Summary of dynamic cutting force equations	18
2.3	Summary of tool life equations	34
2.4	Summary of surface roughness equations	38
4.1	Orthogonal Composite Designs	130
4.2	Orthogonal and Uniform-Precision rotatable Central Composite Designs	132
4.3	Formulae for ANOVA for First-order Model	137
4.4	Formulae for ANOVA for Second-order Model	138
5.1	Chemical composition of steel (190 BHN)	144
5.2	Chemical composition of Inconel 718	145
5.3	Chemical Composition of matrix metal of 2618 MMC	147
5.4	Reference Cut-off values	156
6.1	Levels of the independent variables and coding identification for cutting force (steel)	160
6.2	Experimental Conditions and Results for cutting force (Steel)	161
6.3	Levels of the independent variables and coding identification for cutting force (Inconel 718)	196
6.4	Results and cutting conditions for cutting force (Inconel 718)	197
7.1	Levels of the independent variables and coding identification for tool life (steel)	203
7.2	Cutting conditions and Results for tool life (steel)	205
8.1	Levels of the independent variables and coding identification for surface roughness (steel)	223
8.2	Experimental Conditions and Results for surface roughness(steel)	224
8.3	Levels of the independent variables and coding identification for surface roughness (Inconel 718)	237
8.4	Experimental results and conditions for surface roughness (Inconel 718)	238

8.5	Levels of the independent variables and coding identifications for surface roughness (MMC)	245
8.6	Experimental results and cutting conditions for surface roughness (MMC)	246
8.7	Summary of surface roughness equations of the investigated workpiece materials (steel, Inconel 718 and MMC)	252
1	Mechanical properties of steel (190 BHN)	272
2	Thermal properties of steel (190 BHN)	272
3	Physical constants of Inconel 718	273
4	Thermal properties of Inconel 718	273
5	Mechanical properties of Inconel	718
6	Physical properties of 2618 MMC	273
7	Mechanical properties of 2618 MMC	274
8	Chemical composition of HSS slot drill	274
9	Tool geometry and tolerances for HSS slot drills	275
10	ANOVA for the predictive cutting force model, steel (12 tests)	287
11	Significance testing for individual variables (cutting force model, steel)	287
12	Confidence intervals (cutting force models, steel)	289
13	ANOVA for the cutting force model for Inconel 718	290
14	Significance testing for individual variables (tangential cutting force model, Inconel 718)	290
15	Confidence intervals for cutting force model for Inconel 718	291
16	ANOVA for the first-order tool life model (steel)	294
17	ANOVA for the second-order tool life model (steel)	294
18	Significance testing for individual variables (First-order tool life Model, steel)	295
19	Significance testing for individual variables (second-order tool life Model, steel)	295
20	Confidence intervals for tool life (First-order Model, steel)	297
21	Confidence intervals for tool life (second-order Model, steel)	298
22	ANOVA for the First-order surface roughness model (steel)	301
23	ANOVA for the Second-order surface roughness model (steel)	301

24	Test for Significance of independent variables (First-order surface roughness model, steel)	302
25	Test for Significance of individual variables (second-order surface roughness model, steel)	302
26	Confidence intervals for surface roughness (First-order Model, steel)	303
27	Confidence intervals of surface roughness (Second-order Model, steel)	304
28	ANOVA for the First-order surface roughness model (Inconel)	305
29	ANOVA for the Second-order surface roughness model (Inconel)	305
30	Test of significance for the individual variables (First-order surface roughness model, Inconel 718)	306
31	Test of significance for the individual variables (second-order surface roughness model, Inconel 718)	306
32	Confidence intervals for the First-order surface roughness model, Inconel 718)	307
33	Confidence intervals for the Second-order surface roughness model, Inconel 718)	307
34	ANOVA for the First-order surface roughness model (MMC)	308
35	ANOVA for the Second-order surface roughness model (MMC)	308
36	Test of significance for the individual variables for the First-order surface roughness model, MMC	309
37	Test of significance for individual variables (Second-order surface roughness model, MMC)	309
38	Confidence intervals(First-order surface roughness model, MMC)	310
39	Confidence intervals(Second-order surface roughness model, MMC)	311

ABSTRACT

Nickel based superalloys and MMCs are advanced materials which are used in aerospace, automotive, defence industries etc.. In general, these materials are difficult to machine. This thesis describes a study of machinability assessment of Inconel 718ⁱⁱ, a nickel base superalloy and 2618ⁱⁱⁱ MMC, a MMC based on aluminium alloy (matrix metal) and 12% vf. SiC_p (reinforcement), using uncoated carbide inserts. In addition to the machining of these two materials preliminary cutting tests were carried out on steel (190 BHN) using HSS solid end mills. Through out the experiment the cutting tests were conducted under dry conditions. The experiments may be summarised as follows:

- An investigation of cutting forces, tool life and surface finish in end milling Inconel 718

- Development of the mathematical models for machining responses by Response Surface Methodology: The mathematical models for machining responses (cutting forces, tool life and surface finish) are developed in terms of primary machining variables like cutting speed, feed and axial depth of cut. The mathematical models for machining responses cover the following areas:
 - (a) Cutting force models for slot milling steel (190 BHN) and Inconel 718

 - (b) Tool life models for slot milling steel (190 BHN)

 - (c) Surface roughness models for slot milling steel (190 BHN), Inconel 718 and 2618 MMC.

ⁱⁱ - Trade mark of INCO (The International Nickel Company Inc.)

ⁱⁱⁱ - Trade mark of ALCAN (Aluminium Canada)

NOMENCLATURE

a_a	axial depth of cut
a_r	radial depth of cut
a_r/D	immersion ratio
$b_1..b_{33}$	model parameters
$b_{11}..b_{33}$	model parameters
b_c	chip width
b_m	the matrix of parameters estimates
d_{zi}	current deflection of the cutter normal to the surface of the cut
d_{z0}	deflection of tooth which previously generated
E_c	energy per chip
e_r	cutter runout
f_z	feed per tooth (multi point tool)
f_r	feed per revolution
f_m	feed per minute
F_a	axial force
F_r	radial force
F_R	resultant cutting force (table system)
\acute{F}_R	resultant cutting force (cutter system)
F_{ratio}	a test static
F_s	shear force in shear plane
F_t	tangential force acting on one tooth
F_x	feed force acting on one tooth
F_X	feed force per cut in multi-tooth cutting
F_{Xm}	mean value feed force per cut in X direction for multi-tooth cutting
F_y	normal force
F_Y	normal force per cut in multi-tooth cutting
F_{Ym}	mean value of normal force per cut in Y direction
F_z	vertical force
F_Z	vertical force per cut in multi-tooth cutting
F_{Zm}	mean value of vertical force per cut in Z direction
F_{zeq}	equivalent feed

h_e	equivalent chip thickness
h^*	critical chip thickness
K	number of factors
K'	stiffness of the cutter
k_s	specific cutting pressure
k_m	mean cutting pressure
N_s	spindle speed
P_u	specific power unit
P_s	power required at the spindle
q	chip equivalent
Q	metal removal rate
R	radius of cutter
r_a	tool nose radius
R_a	surface roughness parameter (centre line average)
\hat{R}_s	predicted response (natural scale)
s	standard deviation
T	tool life
T_1	tool life for cutting speed v_1
T_2	tool life for cutting speed v_2
$t_{c(max)}$	maximum chip thickness
t_{ca}	average chip thickness
t_{ci}	instantaneous chip thickness
T^*	a certain tool life
t_m	middle chip thickness
v	cutting speed (peripheral) of cutter
v_T	cutting speed for tool life T min
VB	average flank wear
$VB1$	uniform flank wear
$VB2$	non uniform flank wear
$VB3$	localized flank wear
W_c	width of crater wear
x	coded value of any factor corresponding to its natural value X_n
x_1	coded value (logarithmic transformation) of cutting speed

x_2	coded value of feed per tooth
x_3	coded value of axial depth of cut
X_m	the matrix of independent variables
X_T	thermal fatigue factor
y	level of experimental response on natural logarithmic scale
\hat{y}	the predicted response on natural logarithmic scale
Y_m	matrix of experimental response on natural logarithmic scale
z	number of teeth
α	augment distance
α_n	normal rake angle in normal plane
α_e	effective rake angle in oblique cutting
$d\alpha$	change of rake angle
$d\alpha$	time derivative of rake angle
$d\alpha$	time derivative of rake angle
α_1	a constant
α_{o1}	tool orthogonal clearance angle(first flank)
α_1	level of confidence interval
β	mean friction angle
η_s	angle shear velocity and a normal of the cutting edge in the shear plane
Θ	absolute temperature
λ_s	helix angle
τ	shear strength of the workpiece material
τ_s	shear stress in shear plane
τ_c	cutting stress
ϕ_n	normal shear angle
ϕ_t	angle between the consecutive teeth
ψ	current angle of rotation of a cutter
ψ_s	swept angle

CHAPTER 1

INTRODUCTION

The development of better and more advanced materials is crucially important for the advancement in technology. This is especially true in high technology industries like aerospace, defence, nuclear power engineering etc. The trend in the aerospace industry in the recent past has been towards the development of materials for constructions that are:

- (1) of greater strength
- (2) resistant to oxidation, particularly at high temperature
- (3) exhibit small deformations at high temperatures
- (4) of lighter weight
- (5) not brittle at low temperature

Advanced materials such as superalloys and metal matrix composites (MMCs) have been introduced to meet these requirement. Besides, the use of metal matrix composites continues to increase in the automotive and leisure industries. Hence, nowadays the ability to machine these advanced materials like nickel based superalloys and metal matrix composites is increasingly demanded. Metal machining has a long history and there are now good cutting methods to machine traditional materials under orthodox conditions. Even though new cutting tools like coated carbide, oxide, sialon etc. have been developed, still advanced materials like nickel base superalloys and metal matrix composites are difficult to machine. There are various types of nickel based alloys [1,2], for example Inconel, Monel, Incoloy, Permanickel, Duranickel, Nimonics etc. of which Inconel 718 is being used increasingly in industries. Metal matrix composites are a relatively new range of advanced materials. They are being manufactured in a variety of grades since different forms of reinforcement are included in a varying percentage of matrix metals. They are also being manufactured by different routes, of which codeposition technique is an economical method and has got industrial status.

MMCs based on the aluminium alloy 2618 manufactured by codeposition technique are high temperature metal matrix composites [3]. This MMC is lower cost than the 7000 series based MMCs. It is thus more attractive for applications that are more cost sensitive, for example high performance automotive. The machinability of MMCs is yet to be established.

The basic aim of machinability assessment is the provision of sufficient technological data to ensure the efficient use of machine tools and personnel. The accelerated application of computer aided manufacturing (CAM) in the machining operation by the use of CNC and DNC machine tool has focused on the desirability of developing reliable machining data systems to ensure optimum production from the expensive equipment involved. The machinability data system is essential for the selection of optimum cutting conditions during process planning and it has become an important component in the implementation of Computer Integrated Manufacturing system (CIMS).

Computerized machinability data systems have been classified into two general types:

- (1) Simple data retrieval system
- (2) Mathematical model system.

The simple data retrieval systems are based on the systematic collection and storage of large quantities of data from laboratory and industry resulting in so called "Machinability data banks" and then simply retrieving recommended cutting speeds, feed rates and cost information for any specific cutting operation. Whilst data from industry may be reliable in the sense that it has been used successfully in practice, it is usually incomplete in that no information will be available to indicate the influence of moving away from the given machining conditions. Hence if data banks are to be truly useful then methods of assessing machinability under laboratory or controlled industrial conditions are required to produce the original unconstrained relationship between the machining parameters and the dependent variables of cutting force, power requirement, tool life and surface finish. It is also necessary that the recipients of data in this form should be capable of modifying it to fit their particular needs.

The conventional method of obtaining machinability data under laboratory conditions is to conduct actual machining tests over a range of cutting conditions in order to express machining responses (cutting force, tool life and surface finish) as an empirical function of these conditions. Whilst this method gives reasonable results in most cases, the evaluation of the constants in these empirical equations (mathematical models) are usually done in a conventional way (one variable at a time) which is expensive and time consuming process. Hence, the need for a method of assessing machinability tests both quickly and cheaply has encouraged considerable interest in the past. A recent approach to the problem of designing a suitable machining data selection system for Computer Integrated Manufacturing (CIM) applications is to use mathematical model type data base systems. In the mathematical model type systems, the machining response data such as cutting force , tool life , surface finish etc. is used as the primary data. Mathematical model of these machining responses as functions of the machining variables are developed using a model building module. The mathematical model system attempts to predict the optimum cutting conditions for a specific operation. The model parameters and other economic factors are used to derive the optimum set of cutting conditions. Data gathered from the machinability experiments performed under laboratory conditions is used as the start-up data for the system. Because of the diversity of machining situations encountered in manufacturing, start up laboratory based data sets for some of the machining operations may not be available for use in the machinability data base. However, based on similarities between the various operations and the use of engineering judgement, start-up model parameters can be obtained for such cases. The subjective information regarding the functional relationship is then adapted to the required machining environment. The model building module in this case must be able to utilize the subjective prior information regarding the model parameters. So , the objectives of this work are:

- (1) to develop machining data for advanced materials for industry or machining data bank
- (2) to determine how relevant the mathematical models (empirical equations) are to machinability parameters of advanced materials
- (3) to ascertain optimum machining conditions for machinability assessment of a material particularly for advanced materials

It may be noted that preliminary cutting tests were conducted using steel (190 BHN) with an intention to observe the suitability of developing mathematical machinability models in terms of primary machining variables like speed, feed and axial depth of cut by response surface methodology (RSM). RSM is a combination of mathematical and statistical techniques used in an empirical study of relationships and optimization, where several independent variables influence a dependent variable or response. In RSM, the relationship between the responses and investigated independent variables is commonly approximated by polynomial functions, while model parameters are obtained by a small number of experiments utilizing a design of experiment and multiple regression techniques. In RSM, response surface contours can be constructed by computer and can be used for determining the optimum cutting conditions for a required machining response.

Various types of machining processes (conventional i.e. turning, milling drilling etc. and unconventional i.e. electro-discharge, electro-chemical, waterjet etc.) are used in industry. But this work is confined to end milling process. End milling is one of the most widely used material cutting operations in industry. The aerospace industry places heavy demands on the end milling process due to both the shape and complexity of the parts machined and the accuracy required in the finished part dimensions.

The reference work material steel (190 BHN) was machined using solid uncoated HSS (high speed steel) slot drills while the advanced materials like Inconel 718 and 2618 MMC were machined using an end mill with uncoated carbide inserts under dry conditions.

This thesis contains nine chapters:

Chapter 2 gives a review of the literature of the predictive models (equations) pertaining to cutting forces, tool life and surface finish in the end milling process and machinability of advanced materials like nickel based superalloys and metal matrix composites.

Chapter 3 is a general discussion on machinability assessment of a material covering the areas of the basic geometry and process mechanics of end milling processes and factors influencing cutting force, tool life and surface finish in end milling and provision to supply machinability data.

Chapter 4 describes response surface methodology and development of machinability models by this methodology.

Chapter 5 describes reference work materials, machine tools used in the experimental set up and the procedure to measure cutting force, tool life and surface finish end milling.

In chapter 6, the investigation of cutting force in end milling steel (190 BHN) and Inconel 718 is presented. Here, firstly, the mathematical model for cutting force in end milling steel (190 BHN) is developed by RSM and the adequacy of the model is checked by analysis of variance. Secondly, the influence of cutting conditions (i.e. cutting speed, feed and axial depth of cut) on the cutting forces in end milling Inconel 718 has been investigated and subsequently a mathematical model for cutting force in end milling Inconel 718 is developed. The model accuracy is also verified by analysis of variance. It may be noted that the cutting force in end milling MMC could not be investigated due to unavailability of MMC workpiece material of proper size to fit the table type dynamometer used in this experiment.

In chapter 7, the investigation of tool life in end milling steel (190 BHN) and Inconel 718 is shown. The mathematical models (First and second order) for tool life in end milling steel (190 BHN) are developed. Due to limiting cutting conditions in the milling machine, the mathematical model for tool life in end milling Inconel 718 could not be developed. So, in this case, only tool wear curves in end milling Inconel have been shown. Tool life tests in end milling 2618 MMC could not be investigated due to unavailability of sufficient quantity of MMC work piece material.

In chapter 8, the mathematical prediction models (First and second-order) for surface roughness in end milling steel (190 BHN), Inconel 718 and 2618 MMC are developed.

It may be noted that in the case of Inconel 718, the influence of cutting speed and feed on surface roughness has also been shown.

Chapter 9 contains the general conclusions on machinability assessment of the investigated materials and provides suggestions for the further development of the work.

CHAPTER 2

LITERATURE SURVEY

2.1 Introduction

A review of literature pertaining to machinability assessment of advanced materials by end milling processes can be divided into four sections as follows:

- (1) Cutting forces in milling processes
- (2) Tool life in milling processes
- (3) Surface finish in milling processes
- (4) Machinability of nickel base superalloys and MMCs.

2.2 Cutting forces in milling processes

A standard method of assessing the machinability of a material is to measure the cutting forces produced during a material cutting operation. Generally these forces are measured using a dynamometer. Many researchers [4] have shown that how cutting forces affect machining parameters, such as the power required, temperature, vibration and surface finish. A literature survey on cutting forces in milling can be divided into two parts as :

- (1) The static (average or D.C) cutting forces in milling processes
- (2) The dynamic (varying instantaneous or A.C) cutting forces in milling processes

2.2.1 The static (average or D.C) cutting forces in milling processes

In the past, a considerable amount of work, both analytical and experimental, has been published on the determination of the power required during the milling processes.

Whilst some analytical work on the cutting force wave form has been carried out, comparatively little experimental work appears to have been done to confirm the results of such analyses. The reason for this seems to be difficulties encountered when trying to measure directly and continuously the magnitude of the fluctuating forces in the milling processes under actual working conditions. Some measurements of the milling forces have been carried out, no doubt, but the dynamometers employed were either unsuitable for work at high speeds or indicated only one component of cutting force [5].

Several investigators carried out investigations to determine the work done during the milling process [6-8]. For determining the work done per tooth and the power requirements, the concept of mean cutting pressure k_m was investigated. Schlesinger developed a simple formula in which he combined the theoretical and practical results in such a manner as to obtain general, very comprehensive and yet simple equations as:

- (a) If cutting is intermittent, i.e. if one tooth exits the workpiece before the following tooth has entered, then the mean cutting pressure:

$$k_m = \frac{F_t * v * \psi_s * z}{a_r * a_a * f_z * 2\pi} \quad (2.1)$$

Where

k_m = mean cutting pressure (determined from middle chip thickness)

F_t = average or mean tangential force/tooth

v = tangential (peripheral) velocity of the cutter

ψ_s = total angle of engagement of the cutter tooth with the workpiece.

z = number of teeth in the cutter

a_a = axial depth of cut

a_r = radial depth of cut

f_z = feed per tooth

- (b) If cutting is continuous, i.e. if one tooth leaves the cut when the following one takes over, or more teeth than one are cutting at the same time then the mean pressure:

$$k_m = \frac{F_t * v}{a_r * a_a * f_z} \quad (2.2)$$

Where

F_t - average tangential force per tooth, the period of which ψ_t
 (ψ_t - angle between two consecutive teeth of the cutter).

Boston and Kraus developed the following formula for the energy per chip and commented that middle chip thickness was not a suitable criterion for the power determination:

$$E_c = C_1 a_r f_z^{a_1} a_a^{b_1} \quad (2.3)$$

Where

E_c = energy per chip (the unit of which depends on exponents a_1, b_1)

C_1 = constant depending upon the shape of the cutter, material cut and cutting fluid used.

a_r = width of cut

f_z = feed per tooth

a_a = axial depth of cut

a_1 and b_1 are exponents determined experimentally

Boston and Gilbert studied the influence of rake angles on the power requirement in milling, by means of a wattmeter which recorded the gross power input to the machine. The net power at the cutter could be calculated after the efficiency of the machine had been measured by means of a prony brake.

Schmidt developed a thermo-analytical technique to determine the power required and investigated the effect of rake angle in case of face milling operations.

Onger and Fleck, Leyk and Weilemann assumed certain material constants and used these to determine the power requirements from purely geometrical considerations.

Some expressions for amplitude of the cutting forces in milling have been developed, again from purely geometrical considerations. One of the parameters affecting the

cutting force is the specific cutting pressure, k_s , which is not function of only the workpiece and cutter materials, but also of the cutting conditions. An equation was established for the cutting force wave form for the purpose of determining the work done by a straight tooth milling cutter. The equation was based on the assumption that the specific cutting pressure, k_s , is a function of the chip thickness according to the relationship:

$$k_s = C_2 t_{ci}^{a_2} \quad (2.4)$$

Where

t_{ci} = chip thickness at any instant

' C_2 ' and ' a_2 ' are constant depending on the workpiece material and the milling cutter

The cutting force equations for straight and helical tooth cutters were developed by several researchers, whilst one researcher considered " k_s " to be constant for a given material and cutter, other researcher assumed that:

$$k_s = F_u * \frac{1.8}{\sqrt[4]{t_{c(max)}}} \quad (2.5)$$

Where F_u = ultimate tensile strength of the material

$t_{c(max)}$ = maximum chip thickness

Some other expressions developed for k_s are found in the reference [7] which are listed below :

$$k_s = C_3 d^{-a_3} f_z^{-b_3} \quad \text{Taylor} \quad (2.6)$$

$$k_s = C_4 A^{-0.25} \quad \text{Hipler} \quad (2.7)$$

$$k_s = k_{\alpha 1} + k_{\beta 1} t_c^{-1} \quad \text{Pohl} \quad (2.8)$$

$$k_s = k_{\delta 1} t_c^{a_4} \quad \text{Kienzle} \quad (2.9)$$

$$k_s = C_5 (1 + C_6 t_c^{-1}) \quad \text{Richter} \quad (2.10)$$

Where C_3 , C_4 , $k_{\alpha 1}$, $k_{\beta 1}$, $k_{\delta 1}$, C_5 and C_6 are constants depending upon the shape of the

cutter, the work piece material used, the coolant used etc. and

d = depth of cut

f_z = feed per tooth

t_c = chip thickness at any instant

A = area at any instant

a_3, b_3, a_4 are exponents to be determined experimentally.

The above analyses of the peripheral (slab) milling processes were mostly based on the assumption that the tooth path is circular.

Martellotti [9,10] considered the path of the cutter as tracheidal and then proceeded to derive expressions for the chip thickness, length of the tooth path and radius of the curvature etc.. The assumption of a circular tooth path is a close approximation to the tracheidal form and the simpler expressions obtained are of greater value. Koneigsberger and Sabberwal [11] considered that cutting forces depend on the area of cut taken by each tooth. In milling the size of cut taken by each tooth will depend on the undeformed chip thickness and depth of cut. Assuming cutter path circular, they developed the following expression for face milling as :

$$F_t = k_s a_a f_z \sin \psi \quad (2.11)$$

Where k_s - specific cutting pressure which is a function of chip thickness, a_a - axial depth of cut, f_z - feed per tooth and ψ - the angle of rotation of the cutter in the workpiece.

They [11] developed nomograms for average and maximum forces and power consumption in face milling and slab milling.

Kline et.al [12] developed a mechanistic model of the cutting force system in end milling in which cutting force is assumed to be directly proportional to chip area. This model is called a mechanistic model because the chip load and the cutting forces are computed based on the cutter geometry and the cutting condition. The end milling process is examined by dividing the end mill into axial segments. In this model the equations which relate the elemental chip loading to cutting forces:

$$DF_t = k_T D_z t_c \quad (2.12)$$

$$DF_r = k_r DF_t \quad (2.13)$$

Where DF_t - elemental tangential force, DF_r - elemental radial force on a flute, D_z - thickness of the axial disk, t_c - chip thickness and k_T, k_R - constants

Kline and DeVor [13] extended the above mechanistic model of cutting force taking account of cutter runout if present.

Yellowley [14] developed a cutting force model which is made up of two components one of which is directly proportional to an undeformed area of cut, and the other directly proportional to length of cutting edge engaged as:

$$F_t = k_s a_a f_z \sin \psi + x_c^* a_a \quad (2.14)$$

$$F_r = k_s a_a f_z (r_1 \sin \psi + r_2 \frac{h^*}{f_z}) \quad (2.15)$$

Where k_s - specific cutting pressure, a_a - axial depth of cut, f_z - feed per tooth, ψ - instantaneous angle of rotation and x_c^* - edge force constant ($x_c^* = k_x h^*$), h^* - critical chip thickness, r_1, r_2 - force ratio constants.

Papazafiriou [15] extended above the force model [14] into another form by taking consideration of flank wear land width. For steady state cutting, the tangential and radial cutting forces of a single cutting edge are given by:

$$F_t = k_s a_a f_z \sin \psi + a_a C_w VB \quad (2.16)$$

$$F_r = r_1 k_s a_a f_z \sin \psi + r_2 a_a C_w VB \quad (2.17)$$

Where k_s - specific cutting pressure, a_a - axial depth of cut, f_z - feed per tooth, ψ - instantaneous angle of rotation, r_1 & r_2 - force ratio constant, VB - average width of flank wear and C_w - edge force constant.

The first term is due to the formation of the chip; the second term is due to friction caused by flank wear.

One of the most basic, yet a very popular way of determining average tangential cutting force, which relies on the metal removal rate(Q) as found in literature [16,17] as:

$$F_{tm} = \frac{P_u * a_r * a_a * f_z * z * N_s}{v} \quad (2.18)$$

Where F_{tm} - average tangential force per cut, N_s - spindle speed and P_u - specific power. For common materials, the values for P_u are available in the literature [e.g.,18].

Armarego et al.[19] developed a predictive model of cutting force based on mechanics of cutting for simulated oblique rotary cutting tool. Rotary tools for cutting processes are ingenious innovations of traditional practical machining processes such as turning and milling. They developed expressions for predicting the cutting force for a simulated rotary oblique cutting tool assuming the cutting process an equivalent classical orthogonal model (thin shear zone). They developed the cutting force expression as:

$$F_c = \frac{\tau_s b t_c \cos i [\cos(\beta_n - \alpha_n) + \tan \eta_c \sin \beta_n \tan i]}{M \sin \phi_n \cos i_s} \quad (2.19)$$

Where F_c - cutting force component in cutting direction, τ_s - shear stress in shear plane, b - width of work, t_c - chip thickness, i - inclination angle, β_n - friction angle in normal plane, α_n - normal rake angle in normal plane, η_c - chip flow angle, ϕ_n - normal shear angle, i_s - static inclination angle and $M = \sqrt{[\cos^2(\phi_n + \beta_n - \alpha_n) + \tan^2 \eta_c \sin^2 \beta_n]}$.

Man liu and Steven [20] have attempted to develop an expression for the frictional force on the rake face of an end mill cutter based on mechanics of cutting assuming cutting process an equivalent oblique cutting model(thin shear zone). But they [20] have taken data for equivalent oblique cutting from classical orthogonal cutting. They developed the following expression for frictional force as:

$$F_f = \tau f_z a_a \frac{\sin \beta \cos \alpha_e \cos \eta_s}{\cos(\phi_e + \beta - \alpha_e) \cos \alpha_n \sin \phi_e \cos^2 \lambda_s} \quad (2.20)$$

Where τ - shear strength of the work piece material, f_z - feed per tooth, a_a - axial depth of cut, β - mean friction angle in the secondary zone, α_e - effective rake angle in oblique cutting, η_s - angle between shear velocity and a normal of the cutting edge in the shear

plane, α_n - normal rake angle of the cutter and λ_s - helix angle of the cutter

Up to this point no analytical expression for predicting important cutting forces in milling based solely on mechanics of chip formation (Merchant like equation [21]) is found in literature. This is due to the general lack of information on dynamic shear stress (τ), dynamic shear angle (ϕ), dynamic friction angle (β) etc.

2.2.2 Dynamic cutting force

Past researches on cutting forces in milling have been concentrated mostly in static (average) forces. But milling is a dynamic cutting process which has complex geometry with varying cutting force direction and stiffness .Probably the first analytical expression for dynamic cutting force was proposed by Tobias and Fishwick [22]. Tobias and Fishwick considered that under dynamic cutting conditions, the incremental cutting force dF_c depends upon:

- (a) the chip thickness variation " dt_c "
- (b) the speed variation " dv " or " $d\omega$ ", where $d\omega$ is the change in angular velocity
- (c) the variation of tool penetration rate or feed rate " df_t "

They [22] expressed the incremental cutting force dF_c as:

$$dF_c = k_1 dt_c + k_2 d\omega + k_3 df_t \quad (2.21)$$

Where k_1 , k_2 and k_3 are cutting co-efficients.

The experimental determination of the dynamic cutting co-efficients requires considerable effort because of their dependence on the machined conditions. An experimental approach to determine the dynamic co-efficient contained in the incremental force equation was proposed by Tobias [23] and actual measurements were carried out by Smith and Tobias [24].

Sabri [25] assumed that the dynamic cutting force is a function of the instantaneous rake angle, α and its time derivatives $d\alpha/dt$ and $d^2\alpha/dt^2$. Sabri expressed the incremental cutting force dF_c as:

$$dF_c = k_\alpha d\alpha + k_{\alpha 1} d\dot{\alpha} + k_{\alpha 2} d\ddot{\alpha} \quad (2.22)$$

Where k_α , $k_{\alpha 1}$, $k_{\alpha 2}$ are assumed to be constants representing the changes of the cutting force for unit changes of rake angle, angular velocity, and angular acceleration respectively.

Sabri [25] justified his assumptions from dynamic cutting tests carried out on a rig which oscillated the cutting tool about its tip. Sabri found that the cutting force components lead the angular oscillation of the tool.

Shumsheruddin [26] carried out extensive cutting tests in which he investigated the effect of cutting speed and feed on the dynamic cutting co-efficient. He suggested that the dynamic cutting forces depend upon the variation in rate of change of chip thickness, in addition to the variations of the chip thickness, cutting speed and penetration rate assumed by Tobias and Fishwick [22].

The experimental determination of the dynamic cutting co-efficient requires a very substantial effort in view of their dependence on the machining conditions. Das and Tobias [27,28] proposed a model by which the co-efficient can be derived from steady state cutting data. The basis of the model was the assumption that the main cutting force (F_c) and shear force F_s are linear functions of shear plane area (A_s) and that the ratio of the slopes of these lines, τ_c/τ_s is a material constant, called "Universal Machinability Index" ; Where τ_c - cutting stress and τ_s - machining shear stress along the shear plane area.

MacManus [29] found, from metallographic examination of wavy chips which were produced by dynamic hot machining, that a dynamic variation of effective shear angle occurs. Consequently, MacManus [29] repudiated the assumption of a stationary shear plane made by Das [27].

Kainth [30] modified the model due to Das and Tobias [27,28] by including the shear plane oscillations in response to the dynamic variations of both the chip thickness and the rake angle.

Other analytical models [31-33] of the dynamic cutting forces have been proposed by considering the characteristics of the friction on the tool rake face and shear angle oscillations in dynamic cutting. In these models, the amplitude and direction of the resultant cutting force were considered as constant in dynamic cutting.

The above analyses of dynamic cutting force were concerned mainly with single point cutting tools. In milling similar analyses are needed to be investigated. But few research works on dynamic cutting forces in milling are found in literatures.

The investigators [34] have shown quantitatively the dynamic behaviour of cutting force in milling by a factor which is a ratio of maximum cutting force to mean cutting force. They [34] measured the cutting forces in plain milling by an optical method.

Thusty et.al [17,35-37] have contributed a significant amount of knowledge in modelling the physics of dynamic cutting in milling. A time domain simulation of dynamic regenerative cutting force in vibrating end mill was developed to illustrate chatter growth and loss of contact between the tooth and workpiece. They considered the basic non-linearity of the process which is due to the fact that the vibration is large enough so that the tool jumps out of the cut for a part of its vibratory period. During this time the force is no longer proportional to chip thickness but simply zero. Thusty et.al have shown in their dynamic chip thickness regeneration model that the force on any tooth is:

$$F_{I+1} = k_s a_a (f_z + dz_i - dz_0) \quad (2.23)$$

Where I - counter denoting the time step, dz_i - current deflection of the cutter normal to the surface of the cut, dz_0 - deflection of the tooth which previously generated the surface (can be any time step), a_a - axial depth of cut, and f_z - feed per tooth.

Sutherland [38,39] recently extended Kline's static flexible end mill model [12] and Thusty's dynamic chip thickness regeneration model [37] to obtain improved chip

thickness and force prediction using a continuous structural model for the end mill.

A comprehensive dynamic milling model to predict cutting forces in vibrating mill is discussed in the reference [40]. The model identifies the chip thickness using tracheidal tool motion. This model incorporates discrete structural dynamics of the flexible tool and flexible workpiece in two direction. The cutting forces are predicted by identifying the relative positions and velocities of the vibrating tool and workpiece.

A mechanistic dynamic model for predicting the force in end milling when process inputs of feed rate, spindle speed and / or cut geometry can change is discussed in the reference [41]. This model accounts for milling process chip formation mechanics by incorporating and extending a steady state mechanistic model [36] to include feed and speed drive dynamics.

Any change in the condition of tool such as caused by increased amount of flank wear would also appear as changes in the signature profile of cutting force spectrum. The authors [15] have shown the variation of cutting force harmonics in frequency domain with different amounts of flank wear.

Table 2.1: Summary of static (average) cutting force equations

Source	Equation	Advantage	Disadvantage
Konigberger & Sabberwal [7],1961	$F_i = k_s a_s f_z \sin \psi$	Average forces can be predicted regardless of the geometry of cutter.	Tooth path is assumed to be circular and work-tool system is assumed to be rigid.
Reference [16], 1980	$F_{im} = \frac{p_u * a_a * f_z * z * N_s}{v}$	popular way to predict average force force as a first appoximation.	specific power unit other than common material not available in the literature
Kline et. al [12], 1982	$DF_i = K_T D_z t_c$	Cutting force data with small number of experiments.	Cutting forces computed based on the cutter geometry & cutting conditions; work-tool system assumed rigid.
Yellowley [14], 1985	$F_i = k_s a_s f_z \sin \psi + x_c a_a$	Forces measured may be applied to adaptive strategies.	Cutting edge assumed to be straight with no nose radius.
Papazafiriou[15], 1989	$F_i = k_s a_s f_z \sin \psi + a_a C_w VB$	Force measured can be applied to adaptive control strategies.	Monitoring of flank wear is not easy.
Armarego et.al[19], 1991	$F_c = \frac{\tau b t_c \cos i [\cos(\beta_n - \alpha_n) + \tan \eta_c \sin \beta_n \tan i]}{M \sin \phi_n \cos i_s}$	Attempt to predict cutting forces in simulated rotary cutting tools based solely on mechanics of cutting.	Data taken from classical orthogonal cutting.
Man Liu & Steven[17],1991	$F_f = \tau f_s a_a \frac{\sin \beta \cos \alpha_c \cos \eta_c}{\cos(\phi_c + \beta - \alpha_c) \cos \alpha_n \sin \phi_c \cos^2 \lambda_c}$	Attempt to predict cutting forces in end milling based on mechanics of cutting.	Data taken from classical orthogonal cutting.

Table 2.2: Summary of dynamic cutting force equations.

Source	Equation	Advantage	Disadvantage
Tobias and Fishwick[22], 1958	$dF_c = k_1 + k_2 d\omega + k_3 df$	Simple analytical formula to predict dynamic cutting forces.	Co-efficients determined from steady state cutting.
Sabri[25], 1964	$dF_c = k_{\alpha} d\alpha + k_{\alpha 1} d\dot{\alpha} + k_{\alpha 2} d\ddot{\alpha}$	Simple formula to predict dynamic cutting forces.	Dynamic cutting force is a function of rake angle and its time derivatives.
Tlusty[36], 1981	$F_{i,t+1} = k_s a_s (f_z + dz_i - dz_0)$	Realistic way to predict dynamic cutting forces in milling and capable of accomodating nonlinearities that occur in the ophysical machining process.	Complicated; tooth path is assumed to be circular.

2.3 Tool life in milling

Tool life assessment is extremely important in machinability assessment. A literature survey on tool life in milling can be divided into two parts as:

- (1) Tool life criteria
- (2) Tool life equations

2.3.1 Tool life criteria

In the past many methods have been used to evaluate the life of a cutting tool. Tool life between replacement or resharpening can be specified in many ways as:

- (a) Actual cutting time to failure (if cutting is continuous)
- (b) Total cutting time to failure (if cutting is intermittent)
- (c) Volume of material removed to failure
- (d) Number of components produced to failure
- (e) Length of components produced to failure

Generally these methods depend on the particular application i.e in a production environment the number of pieces produced by a cutting edge is often monitored. Discrete tool life values find wide usage in industrial applications.

Sabberwal and Fleischer [42] used volume of material removed for certain flank wear land width as criteria for tool life.

To increase reliability and comparability of test results it is essential that tool life be defined as the total cutting time of the tool to reach a specified value of tool life criterion [43,44].

In general, a tool reaches the end of its useful life through many modes of degradation, some of which progress gradually with time and others which are catastrophic in nature.

It is evident that catastrophic failure of the tool is an unacceptable criterion for most applications. Moreover catastrophic failure through either brittle fracture or plastic deformation of the tool material will normally occur only when the amount of degradation of the tool through the normal wearing processes has already reached unreasonable proportions. To assess tool life criteria under the conditions of edge fracture or plastic deformation is currently under study of ISO [43,44]. So, tool life criteria under the conditions as a result of which tool deterioration is due predominantly to wear are usually accepted.

Wear usually takes place on the flank and rake faces of cutting tool. Both affect the cutting edges. Flank wear is usually accepted as a criterion of tool life. In the case of flank wear, a particular width of flank wear land is almost always taken as the criterion of tool failure.

In 1957 , Niklasson [45] used maximum flank wear land width of 0.7 mm for a H.S.S milling cutter to consider the tool to reach its end of tool life.

Sabberwal and Fiescher [42] considered average flank wear of 0.76 mm (0.03") as the criterion for their tool-workpiece combination. The development of flank wear with time was observed by some researchers to occur in three stages for carbide tips tools.

But Colding [46] emphasizes that crater wear is important in determining tool life when work material yields long, continuous chips. The "tougher" the material the more important is the rake wear in determining the failure of the tool. The rake wear is also considered important when cutting speed and feed rate are high for the tough material. Various research works have investigated the dependence of tool failure on the ratio of crater depth to crater width. It is found in the literature that in turning, the crater angle is 18° at failure. But Sabberwal and Flesischer [42] reported that tool failure in face milling does not occur at a specific crater angle. One of the causes of this deviation probably lies in tools of low rake angle failing because of the rapidly increasing flank wear. The tools with small rake angles fail before the necessary crater depth develops sufficiently for a crater angle of 18° to be produced.

Comprehensive studies of crater wear have been conducted by several investigators which are shown in the reference [47]. The tool life criterion based on crater wear for continuous cut and in the absence of chatter:

$$\frac{D_c}{K_c} = \frac{KTl}{KM} = 0.40 \quad (2.24)$$

Where

W_c = width of crater

D_c = depth of crater(KTl)

K_c = distance from centre to cutting edge(KM)

It may be noted that Opitz, Amarellar and Koelzer observed that the physical properties of the work materials influencing the rate of crater wear could be summarised for similar work materials by its shear strength. Moreover the cutting speed for a given tool life with respect to cratering, varies exponentially with the shear strength of the work material. Its composition determines the position and slope of the exponential curve.

Kuljanic [48] had taken tool wear measurement on a single tooth for a face milling cutter. He considered that the measurement of the tool wear in milling is, due to the nature of multi-tooth cutters, a complicated and time consuming process. Hence, Kuljanic used maximum flank wear of 0.76 mm (0.03") on a single tooth as the criterion for the carbide inserts for face mill cutter. This VB_{max} corresponded to the arithmetical mean of tool wear values measured on each tooth in the cutter. He considered this criterion because there was a irregular shape of flank wear for face milling stainless steel with carbide tools, i,e chipping was present under heavier feed and higher speed.

Yellowley [49] was of the opinion that in general , a cutting tool wears steadily on the flank and rake face surfaces. Whilst the stipulation of the crater wear ratio, was often used as a criterion of tool life, it has since been realized in both industry and research establishments that both the stipulation of reliable limits for crater wear and measurement of actual crater wear are difficult. Moreover, the advent of the more highly alloyed carbide tool material has meant that , even at high cutting speeds tool failure is generally attributable to flank wear and not to crater wear.

It has been found that, providing the machining conditions (and in particular the tool material), are correctly chosen the life of carbide tools is determined by flank wear. Hence, he [49] considered uniform flank wear land width, $VB_1 = 0.38 \text{ mm} (0.015")$ and localized flank wear land width, VB_3 (notch wear, VN or groove wear, VG) of $0.76 \text{ mm} (0.030")$ as the criterion for end milling high strength material with carbide inserts.

McGoldrick and Hijazi [50] assessed the tool life in end milling by considering certain amount of weight lost from the tool as result of the total tool wear during machining. This method does not distinguish between flank wear and crater wear.

The authors [51] have given their opinions that many wear mechanisms play a role in determining the life of a cutting tool. Under normal conditions of machining the flank wear is likely to be more prevalent and is usually chosen as the basis of tool wear for cutting tool. This flank wear was determined by averaging the flank wear on the major cutting edge.

Many investigators have shown that notching (localized flank wear) is the major problem when machining nickel base alloys with uncoated carbide tips [52].

Focke et al.[53] showed that when machining Inconel 718 with a variety of single point tool materials that the crater started immediately behind the cutting edge, that is, there is no plateau of unworn material on the rake face. They noticed that as the cutting speed was increased, the crater profile changed; the deepest point moving closer to the cutting edge, where the highest temperatures are developed. With the temperature distributions as described, wear lands developed very quickly on the flank and rake faces of the tool.

The investigators [54] at Warwick University considered tool life for carbide inserts for face mill cutters when $VB_2 = 0.76 \text{ mm}$ on any of the inserts when face milling nickel base alloys (Nimonic 75). But the authors [55] have also carried out cutting tests on Inconel 718 using single point ceramic tools. They rejected these inserts under the following conditions:

- (a) uniform flank wear ≥ 0.40 mm
- (b) maximum flank wear ≥ 0.70 mm
- (c) crater wear, ≥ 0.14 mm
- (d) notching (localized flank wear,) ≥ 1.0 mm

But Shaw [56] has shown that high temperature alloys should not be machined with tools having flank wear values that are as high as those normally employed in cutting steel. Tools should be taken out of service when flank wear reaches 0.25 - 0.38 mm instead of the usual 0.75 mm.

ISO recommends that a certain width of flank wear land (VB) is the most commonly used criterion for H.S.S end mill cutters and carbide inserts. ISO also recommends that a certain depth of face wear is sometimes used as a criterion. Catastrophic criterion can occur inadvertently and should not be used as a primary criterion for tool life criteria. A detailed discussion on tool life criteria for end mill and face mill cutters is found in reference [43,44].

2.3.2 Tool life equations

Many investigations in the field of material cutting have been carried out and expressed the tool life of cutting tools in a mathematical form. Although it is not essential that tool life data be expressed in a mathematical form, it is certainly convenient and important part of machinability assessment. Most researchers use some form of tool life equations which are expressed, usually as a function of various machining variables involved in different material cutting operations.

Before F.W Taylor [57], the relation between cutting speed and tool life is found in the reference [58] as:

$$v T^{\frac{1}{8}} = C_7 \tag{2.25}$$

Where v - cutting speed (m / min), T - tool life (minute) and C_7 - constant.

But F.W Taylor [57], later on reached the conclusion that equation (2.25) does not hold good under all conditions and hence he modified the equation (2.25) as:

$$v T^n = C_8 \quad (2.26)$$

Where n is the slope of the Log T - Log v plot.

This equation is known as Taylor's equation and was developed for turning. In milling similar types of tool life equation hold, but many variables in this process make the equations more limited than in turning [59]. One of the inherent faults of this formula is that it assumes the relationship between Log v and Log T is linear (i.e n is constant). However, many cases of non-linear Taylor curves have been reported [60] as shown in Fig. (2.1).

It has been shown [61,62] that non-linear Taylor plots are most likely to occur when machining high strength alloys, machining at high rates of material removal, and machining under conditions giving long tool life. Pilafides [63] conducted a literature survey on tool life. He has selected 140 tool life curves from published literature for different machining operations which include turning, end milling, face milling etc. He found that the values " n " varied with work piece material, tool material and type of machining. So, Pilafidis concludes that the values of " n " should not be made in terms of discrete values but rather in terms of ranges when " n " fluctuates for specific types of process and workpiece-tool material combination. Several investigators found that the Taylor equation was not capable of covering the full range of cutting speeds. They explained that the exponent " n " of the Taylor's equation is a special case which occurs in certain conditions.

Woxen was one of the first researchers to find that a non-linear relationship, a slightly bent curve on log-log graph paper is obtained in tool life tests, Fig.(2.2). Later on other researchers [64,65] had noticed this phenomenon.

Kronenberg [61] has suggested that a method of straightening a curved Log v - Log T plot, Fig.(2.3). This is achieved by adding or subtracting a constant straightening factor, \dot{K} , to or from all values of speed and tool life, and replotting the results in the form:

$$(v \pm \dot{K}) T^{n_1} = C_8 \pm \dot{K} \quad (2.27)$$

The curvature of the original data determines whether the straightening factor is added or subtracted, as indicated in Fig. 2.3. Kronenberg [66] used trial and error to determine \dot{K} , and checked his guess by the equation :

$$n_1 = \frac{\log [v_2 + (\dot{K}/v_1) + \dot{K}]}{\log (T_1/T_2)} \quad (2.28)$$

Barrow [62] has shown that equation (2.28) implies that

$$n = n_1 \pm \frac{\dot{K} n_1}{v} \quad (2.29)$$

Therefore, if the amount of non-linearity is small, \dot{K} and n_1 can be obtained by plotting " $1/v$ " against " n " .

Equation (2.26) only relates cutting speed to tool life for particular tool-workpiece combination, and does not consider other cutting variables and tool geometry. To connect tool life with several variables, Taylor derived the equation which is found in the reference [62]:

$$v_T = \frac{C_9 [1 - \frac{8}{7} (32r_a)^2]}{\{ f^{\frac{2}{5}} + 5 + (\frac{2.12}{32r_a}) (\frac{48a}{32r_a})^{\frac{2}{15}} + 0.16(32r_a)^{\frac{1}{2}} + \frac{0.8(32r_a)}{[6(32r_a) + 48a]} \}} \quad (2.30)$$

Where v_T - cutting speed for tool life T, f - feed, a - depth of cut, r_a - tool nose radius and C_9 - a constant.

Although this equation includes the important variables, feed and depth of cut, it is too complex and limited to be of any practical use. Taylor considered that feed and depth of cut could not be combined into a single variable.

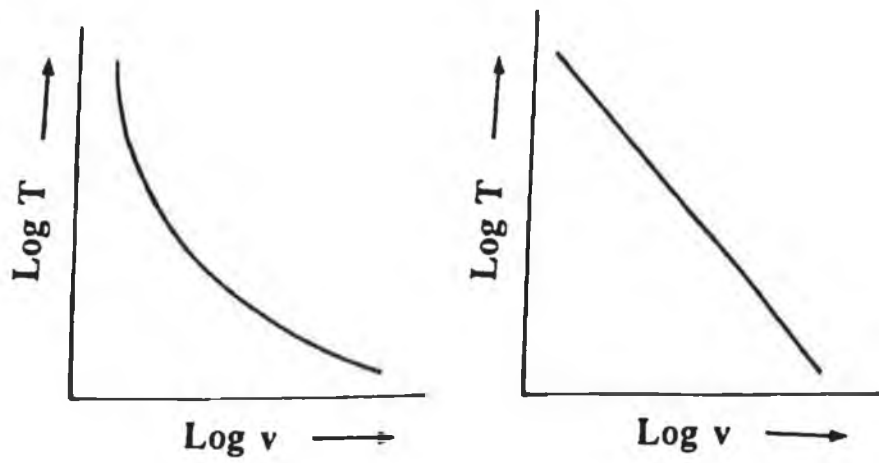


Fig.2.1: Taylor's tool life equation

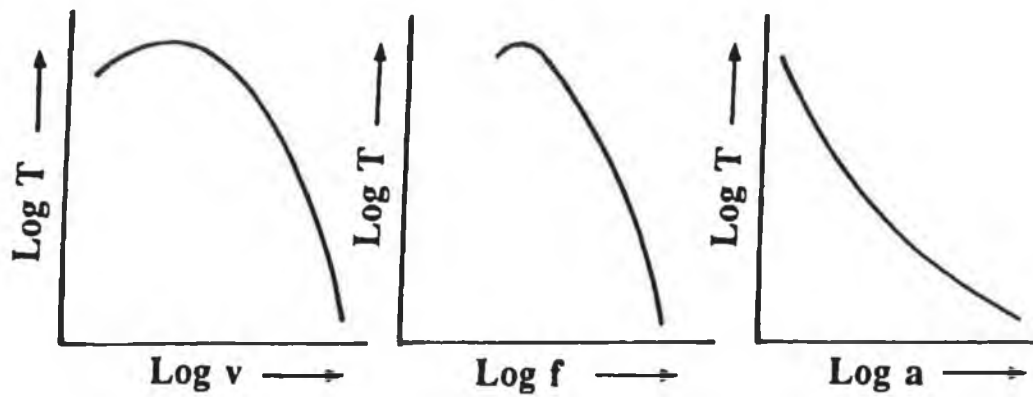


Fig.2.2: General trend of tool life(T) with speed(v), feed(f) and depth of cut(a)

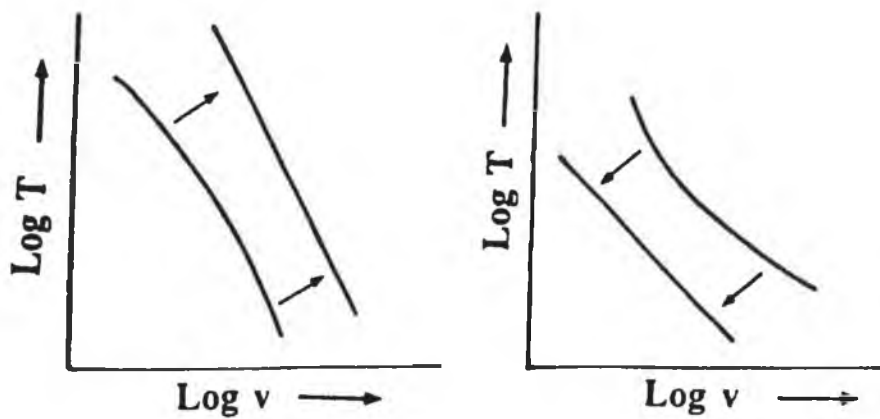


Fig.2.3: Kronenberg method of modifying a curved Taylor's plot

But, Kronenberg [66] used the data obtained by Taylor and found that in most cases the area of cut ($A = f * a$) could be used as a single variable. By plotting data in the form of $\log v_T - \log A$, he developed the relationship

$$vT^n = \frac{C_{10} \left(\frac{G}{5}\right)^u 60^n}{(1000A)^{z_1}} \quad (2.31)$$

Where u - a constant and the term $G/5$ relates G (slenderness ratio = depth of cut / feed) to an average value of G which Kronenberg considered to be 5 and z_1 - the slope of the $\log v_T - \log A$ plot.

Other researchers [69-70] have extended the Taylor equation to include other variables to the form, as for example:

$$T = \frac{C_{11}}{v^{\frac{1}{n}} f_z^{\frac{1}{p}} a_a^{\frac{1}{p_1}}} \quad (2.32)$$

$$T = \frac{C_{12}}{v^{\frac{1}{n}} f_z^{\frac{1}{p_1}} a_a^{\frac{1}{p_2}} a_r^{\frac{1}{p_3}} z^{\frac{1}{p_4}}} \quad (2.33)$$

and these equations are known as extended Taylor equations. Where $n, p, p_1, p_2, p_3, p_4, C_{11}$ & C_{12} are constant.

Tool life equation based on temperature

The effect of temperature in material cutting, together with the dependence of the tool wear on temperature, has been examined by many investigators which is shown in the reference [42]. They have shown that the relationship between tool life T and absolute temperature, Θ :

$$T\Theta^{n_2} = C_{13} \quad (2.34)$$

Where C_{13}, n_2 are constants depending on material and cutting condition. The magnitude of the index " n_2 " have been reported to be as high as 20.

Equation based on the chip equivalent

In 1930's Woxen suggested that tool life could be related to cutting temperature by evaluating a heat balance in steady-state cutting conditions which is found in references [60,62]. He showed that cutting temperature was a direct function of the chip equivalent, q for a given cutting tool workpiece combination. "q" is defined as the ratio between the length of the tool cutting edge contacting the work (L) and the area of cut (A) as:

$$q = \frac{L}{A} \quad (2.35)$$

In some cases the inverse of the chip equivalent is used and is called the equivalent chip thickness, h_c ($= 1/q$). The proposal by Woxen that temperature is a function of chip equivalent has been substantiated by several workers using tool-work thermocouple techniques. Woxen assumed that the condition resulting in constant temperature also resulted in a constant tool life. Using this assumption he was able to predict the shape of $v_T - \Theta$ plot, as shown in Fig. 2.4 (a). The form of the plot was very similar to $v - q$ plot as indicated in Fig. 2.4 (b). Using the form of Fig. 2.4 Woxen proposed the following tool life equation:

$$v_T = \dot{G}_T (q_0 + q) \quad (2.36)$$

Where \dot{G}_T , q_0 are constants determined by workpiece and tool.

Woxen found that in general, $v_T - q$ plots were not linear and introduced the factor $1/(1 + gq)$ to account for this fact and amended his equation to

$$v_T = \dot{G}_T \frac{(q_0 + q)}{(1 + gq)} \quad (2.37)$$

Where g is a constant.

Woxen introduced the tool life as a separate factor by adding the term $(T^*/T)^n$ and recognising that the Taylor exponent, n , could vary and added a further term to overcome this difficulty, thus

$$v = \left[\left(\frac{T^*}{T} \right)^n + g_1 T \right] G_s \left(\frac{q_0 + q}{1 + gq} \right) \quad (2.38)$$

Where G_s , g_1 are constants dependent on the workpiece and tool material and T^* - a certain tool life (e.g. 40 min).

Although the equation by Woxen seem to be valid for a wide range of cutting conditions they are rather complex and difficult to use.

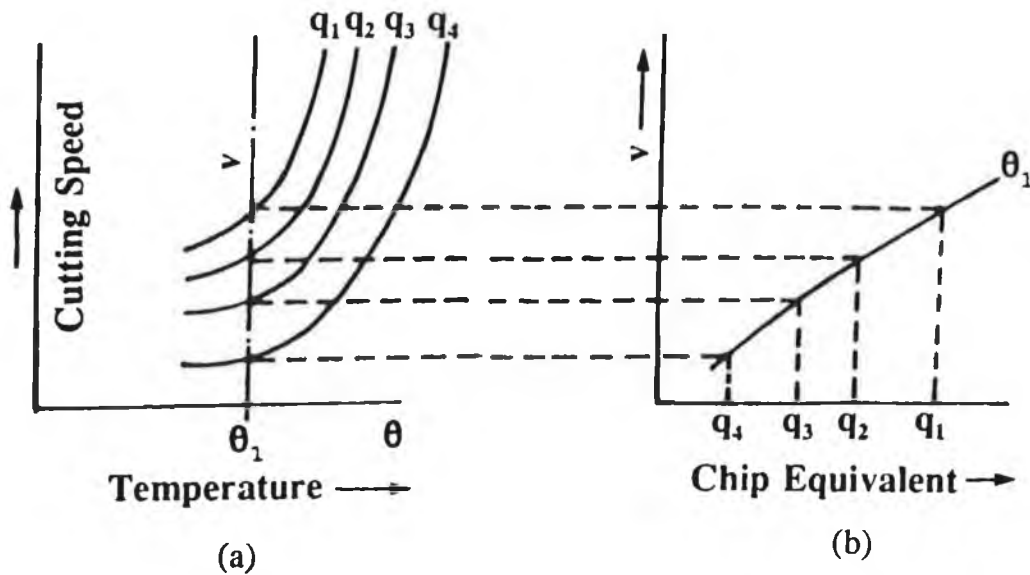


Fig.2.4: Influence of chip equivalent on cutting temperature

The complexity of the equations is chiefly because of non-linearities in the original $v_T - q$ plot, which was made in a linear manner. If $\log v_T$ is plotted against $\log q$, the resulting terms are often linear(nearly so), thus tool life can be expressed as:

$$v T^n = C_{14} q^j$$

or

$$v T^n q^\delta = C_{14} \quad (2.39)$$

Savhn and Colding [71] applied their findings from turning tests to slot milling in different way. In milling because of the non-linear and discontinuous nature of material removal, the simple chip equivalent q , was not directly applicable. Colding derived an alternative function termed "milling equivalent" by considering the work done to remove unit volume of stock, and using a "characteristic area" of undeformed chip thickness length of engaged edge. The milling equivalent for end milling, m_e is defined as:

$$q \approx m_e = \frac{\pi}{z * f_z * \cos \lambda_s} + \frac{1}{a_a * \cos \lambda_s} \quad (2.40)$$

Where z - number of teeth in the cutter, f_z - feed per tooth, λ_s - helix angle and a_a - axial depth of cut.

Colding [64] and Brewer and Rueda [72] used relationships of the form of equation (2.39) and showed that the exponents n and δ are not necessarily constant.

Using dimensional analysis, Colding [64] proposed an equation of the form:

$$C_{15} + a\dot{X} + b\dot{X}^2 + c\dot{Y} + d\dot{Y}^2 - \dot{Z} + e\dot{Z}^2 + f\dot{X}\dot{Y} + g\dot{Y}\dot{Z} + h\dot{X}\dot{Z} = 0 \quad (2.41)$$

Where $\dot{X} = \log q$, $\dot{Y} = \log v$, $\dot{Z} = \log T$ and C_{15} , a , b , c , d , e , f , g , h are constants.

This equation is valid over a wide range of cutting conditions and can cope with tool life curves with considerable curvature, but the evaluation of the constants, to a reasonable degree of accuracy involves a large number of machining tests. However, Barrow [62] reports that "extensive tool life testing at UMIST has shown that although curved plots do occur when using the chip equivalent rather than the individual variables, the amount of curvature is considerably reduced.

Tool life Equation by Response Surface Methodology

Wu [73] derived the following first-order tool life equation in terms of machining variables like speed, feed and depth of cut for turning using response surface methodology:

$$\hat{y} = b_0x_0 + b_1x_1 + b_2x_2 + b_3x_3 \quad (2.42)$$

The first-order tool life equation is only accepted over a narrow range of variables. In order to predict the tool life reliably over a wide range of variables, a second-order equation is needed in some cases. The second-order equation is of the form:

$$\begin{aligned} \hat{y} = & b_0x_0 + b_1x_1 + b_2x_2 + b_3x_3 + b_{11}x_1^2 + b_{22}x_2^2 \\ & + b_{33}x_3^2 + b_{12}x_1x_2 + b_{13}x_1x_3 + b_{23}x_2x_3 \end{aligned} \quad (2.43)$$

\hat{y} - predicted tool life on natural logarithmic scale, while x_1, x_2, x_3 are coded values (logarithmic transformations) of speed, feed and depth of cut respectively and b 's are model parameters estimated using experimentally measured tool life data.

Konig-Depiereux equation

Konig-Depiereux developed an equation which can accommodate non linearities in the $\log T - \log v$ and $\log T - \log f$ plots. The equation is shown in reference [62] as:

$$T = \exp\left(-\frac{k_v}{m} v^m - \frac{I_s}{m_1} f^{m_1} + C_{17}\right) \quad (2.44)$$

Where k_v, I_s, m, m_1 are experimentally determined constants (machinability exponent) and C_{17} is a parameter depending upon the tool life and the exponents K_v, L_s, m and m_1 .

If the slope of $\log T - \log v$ curve is constant the equation is modified to

$$T = \exp\left(-\frac{I_s}{m_1} f^{m_1} + C_{18}\right) v^{-k} \quad (2.45)$$

Where k - the slope of the $\log T - \log v$ plot.

Equation based on thermal stress (cycling)

In recent work Yellowley and Barrow [74] have shown that active tool life of a end mill cutter varies non-proportionately with different immersion ratios. To characterize this behaviour, a thermal fatigue parameter was proposed which accounted for the thermal straining experienced by the tool during each heating and cooling cycle. To account for

this, an empirical thermal fatigue parameter (X_T) was proposed to characterize the range of thermal strain and the number of plastic strain cycles. The authors developed a comprehensive tool life equation for the end milling process as:

$$T = \frac{C_{19}}{(X_T)^{\alpha_1} f_{zeq}^{\beta_1} V^{\gamma_1} a_a^{\delta_1}} \quad (2.46)$$

Where X_T - thermal fatigue parameter, f_{zeq} - equivalent feed, v - peripheral cutting speed of the cutter and a_a - axial depth of cut and α_1 , β_1 , γ_1 and δ_1 are constants.

This equation makes allowance for the following practical variables:

- (a) peripheral cutting speed of the cutter.
- (b) feed per tooth
- (c) radial depth (width) of cut (immersion ratio)
- (d) axial depth of cut
- (e) cutter diameter

This equation is limited to one mode of milling and should not be applied when chip sticking conditions prevail. It is not valid when angle of lag between leading and trailing edges of the cutter becomes appreciable compared to the swept angle of cut.

Tool life equation for milling by PERA

The relationship between tool life and machining parameters which adequately represent the milling process has been found [75] to be of the following form:

$$T = C_{20} v^n t_{ca}^{n_1} a_a^{n_2} H^{n_3} X_T^{n_4} VB \quad (2.47)$$

Where

T = Tool life (effective cutting time to failure)

v = peripheral cutting speed

t_{ca} = average undeformed chip thickness

a_a = axial depth of cut

H = work material hardness

X_T = thermal fatigue parameter (incorporating the radial depth of cut)

VB = flank wear

n, n_1, n_2, n_3 and n_4 are exponents representing the relationship between tool life and the corresponding machining parameters.

It can be seen that the equation (2.47) is a development of F.W Taylor's original equation (2.26). Each parameter in the equation (2.47) is assumed to be independent of the other and its effect can be analyzed by selecting from a group of proven data sets in which T varies as a function of one parameter such as cutting speed (v), $\log v$ is plotted against $\log T$ and the best straight line is drawn through the points. The gradient of this line gives the value of exponent 'n'. Having evaluated n, n_1, n_2, n_3, n_4 the value of the constant C_{20} is calculated which is representative of the whole group.

ISO [44] recommended that tool life values obtained can be plotted against any independent factor (i.e cutting speed, feed, depth of cut etc.). It is common to plot $v_T - T$ diagram (Fig. 2.2) with logarithmic scales. The $v-T$ curve thus obtained will, under normal conditions be represented by a straight line. This line should be fitted to the data points in such a manner that the sum of the squares of the vertical distances between the line and the actual points is as small as possible.

Usually when dealing with material cutting data, it is liable to an appreciable amount of scatter. This may be due to non-homogeneity of material being cut and its effect on the measurement of machining response data, as well as due to the errors in the measuring technique itself. So, if one considers the intrinsic scatter in tool life results (even with closely controlled tool and workpiece material), it is doubtful whether the more sophisticated tool life equations (catering for non-linearities) are really necessary, or indeed, applicable at present, except, of course, in cutting conditions in which non-linearities are expected. In other words, when evaluating constants in equations (2.31), 2.32) and (2.39) a reasonable amount of non-linearity can be accommodated when applying the necessary 'safety factor' or confidence limit by using statistical techniques.

Table 2.3: Summary of Tool life equations

Source	Equation	Advantage	Disadvantage
Reference[58], before 1907	$vT^{\frac{1}{3}} = C_7$	Uncomplicated	Does not hold good under all conditions.
Taylor[57],1907	$vT^n = C_8$	Uncomplicated & easy to use	Assumes logv-logT to be linear; all important cutting variables not considered.
Taylor	$v = \frac{C_9[1 - \frac{3}{7}(32r_a)^2]}{[r^{\frac{1}{3}} + 5 + (\frac{2.12}{32r_a})(\frac{48a}{32r_a})^{\frac{1}{3}} + 0.16(32r_a)^{\frac{1}{2}} + \frac{0.8(32r_a)}{16(32r_a)+48a}]^3}$	Takes important machining variables into account.	Complicated and difficult to use.
Reference[42],1930	$T\theta^{n_1} = C_{13}$	uncomplicated	Accurate determination of cutting temperature is difficult.
Woxen,1931	$v = [(\frac{T^*}{T})^n + g_1 T] G_s (\frac{q_0 + q}{1 + gq})$	Accounts for variables; non-linearities accounted for.	Extremely complicated
Savhn & Colding [71],1948	$vT^n q^8 = C_{14}$	Easy to use and accounts for variables.	Does not cater for non-linearities.
Colding[64],1959	$C_{15} + aX + bX^2 + cY + dY^2 - Z + eZ^2 + fXY + gYZ + hXZ = 0$	Accounts for variables	Evaluation of constants laborious.
WU[73],1964	$\hat{y} = b_0 x_0 + b_1 x_1 + b_2 x_2 + b_3 x_3$	require small number of experiments to determine constants.	Pure error determine the adequacy of the model.
Kronenberg[66], 1966	$v = \frac{C_{10}(\frac{G}{5})60^n}{1000A^{2.1}}$	feed and depth of cut considered	all important variables not considered
Konig-Depiereux 1969	$= \exp(-\frac{k_v}{m} v^m - \frac{I_s}{m_1} f^{m_1} + C_{17})$	feed is accounted for; accomodates non linearities	Depth of cut not considered; complicated to use.
Yellowley & Barrow[74],1972	$T = \frac{C_{19}}{X_T^{a_1} f_{teq}^{b_1} v^{c_1} a_s^{d_1}}$	immersion ratio of the cutter considered.	Evaluation of thermal fatigue factor not easy.
Extended Taylor equ.[60],1973	$T = \frac{C_{12}}{v^{\frac{1}{n}} f_s^{\frac{1}{n_1}} a_s^{\frac{1}{n_2}} a_r^{\frac{1}{n_3}} z^{\frac{1}{n_4}}}$	number of teeth, width of cut included	evaluation of constants laborious
PERA[75],1978	$T = C_{20} v^n t_{ca}^{n_1} a_s^{n_2} H^{n_3} X_T^{n_4} VB$	Hardness of work material considered.	Evaluation of constants laborious.

2.4 SURFACE FINISH IN MILLING

In engineering design and production, it is important to be able to specify the degree of surface roughness desired. Before 1929 this was done by the use of tactual standards. This involved the use of a series of specimens that had different finishes. The "man in the shop" used these specimens by running his fingernail first across a standard tactual surface and then across the surface he was producing. When the two surfaces were felt to have the same roughness, the workpiece was considered to be smooth enough. In 1929 one researcher published details of his surface recorder which operated by traversing a stylus across the surface to be measured and magnifying the stylus motion by means of an optical lever [76,77]. Other investigator developed further the stylus instrument in the thirties(1930) and could achieve magnifications of the vertical components of the surface of up to 1000X by making use of a projector and recording on a smoked glass screen. Since this time several private companies have developed stylus instruments, the best known being from Rank Taylor Hobson, Hommel, Perthen, Mitusu etc.

Perhaps the first definitive work on the surface roughness of the milling process has been done by Martelloti [9,10]. He considered the milling path as tracheidal and derived the following formula for surface roughness in slab milling:

$$R_a = \frac{f_z^2}{32 \left(R \pm \frac{f_z * z}{\pi} \right)} \quad (2.48)$$

Where R_a - surface roughness in CLA, f_z - feed per tooth, R - radius of the cutter and z - number of teeth in the cutter.

The author [78] has shown that the cycloidal motion of plain milling cutter teeth in relation to the cause of the appearance of surface irregularities:

$$R_a \approx 62.5 \frac{f_z^2}{D} \quad (2.49)$$

Where D - diameter of the cutter

But measured milled surface roughness value was greater than that of theoretical surface roughness value obtained by the above formula (2.49). So, he [78] modified the above formula to take cutter runout into consideration as:

$$R_a = \frac{f_r^2}{16(D+e_r)} \quad (2.50)$$

Where f_r - feed rate in mm/rev.(= $z * f_z$) and e_r - cutter runout

National Twist Drill & Tool Co. carried out extensive works on surface irregularities in plain and end milling processes. They have studied the effect of cutter diameter, number of teeth, runout, feed and depth of cut, mode of milling etc. on surface irregularities. Detailed studies are found in the references [79-81]. These studies offer solutions to problems such as using the shortest possible end mill for greatest rigidity and reducing feed for finish cut. They simplified the surface roughness formula for plain milling operations considering the circular tooth path as:

$$R_a = \frac{f_z^2}{32R} \quad (2.51)$$

Where R - radius of the cutter.

The surface roughness in face milling operations by end mill can be shown from the reference [82] as:

$$R_a = \frac{f_z}{4 * \cot \alpha_{o1}} \quad (2.52)$$

α_{o1} - tool orthogonal clearance, first flank.

Kline et al.[83] have studied the surface error generated during end milling based on mechanistic cutting force. They have shown that in the end milling process, the cutting forces during machining produce deflection of the cutter and workpiece which result the surface taper and surface error on the finished component. They combined the models for cutting forces, cutter deflection and workpiece deflection to predict surface error. They developed a simplified model for the deflection of the workpiece by considering

the thin walled section to be an elastic plate of varying thickness clamped on three sides with a static point force loading. The finite difference method was used to generate a data base of static flexibility co-efficient at particular points on the plate, hence the deflection of the plate was determined. For the deflection of the cutter itself it is assumed usually that the end mill acts as a cantilever circular beam rigidly supported by the tool holder.

Ema and Davies [84] have investigated the effects of machining conditions on surface roughness using end mill cutters with different helix angles. They have shown that the effect of speed, feed and axial depth of cut on surface roughness. They have also shown that end mills with small helix angles develop greatest surface roughness due to chatter and reduction of the period when the cutting inserts engage with the work piece material in down milling.

The authors [85] have studied the effect of vibration on surface error in end milling. In the finish end milling of thin walled sections, the possible rate of metal removed for a given tolerance is often limited by the onset of machining vibration. This vibration can be either forced or self excited(chatter). The surface errors are the result of both the static and dynamic deflection of the workpiece and tool, the deflection being due to both D.C and A.C components of the cutting force that is exciting the vibration of the workpiece/tool system. The authors [85] investigated the surface error in end milling by considering:

- (a) a regenerative force model
- (b) a dynamic cutter-deflection model
- (c) a dynamic workpiece deflection model.

The resulting surface error profile has been examined for variation of cutting parameters such as the width of cut, the depth of cut and rotational speed etc.

The workpiece surface generation in dynamic end milling has been developed in the reference [40,86]. Surface generation in milling is shown as a function of tooth passing and vibration frequencies. The model can simulate frequency of dynamic milling. The

surface finish form is predicted by identifying the relative positions and velocities of the vibrating tool and workpiece. The model can help in selecting spindle speeds to obtain a smoother surface finish when dominant vibration frequencies are known.

Table 2.4: Summary of surface roughness equations.

Source	Equation	Advantage	Disadvantage
Martelloti[9], 1941	$R_a = \frac{f_z^2}{32(R \pm \frac{f_z * z}{\pi})}$	Feed and tool geometry is considered: tracheidal milling path is considered.	Speed, depth of cut not considered.
National Twist Drill & Tool Co.[80],1961	$R_a = \frac{f_z}{32R}$	uncomplicated	Milling path is assumed circular
Reference[82], 1976	$R_a = \frac{f_z}{4 * \cot\alpha_{ol}}$	Simple	Actual surface finish is greater than the theoretical surface finish estimated by the formula
Reference[78], 1976	$R_a \approx 62.5 \frac{f_z^2}{D}$	Simple ; tracheidal milling path is considered.	Actual surface roughness is less than the measured roughness.
Reference[78], 1976	$R_a = \frac{f_r^2}{16(D + e_r)}$	Feed per revolution and cutter runout are considered.	speed and depth of cut are not considered.

2.5 MACHINABILITY OF ADVANCED MATERIALS

A literature survey on machinability of advanced materials is divided as:

- (1) Machinability of nickel base superalloys
- (2) Machinability of MMCs

2.5.1 Machinability of nickel base superalloys

Nickel base superalloys are tough high strength advanced materials which are generally difficult to machine. Such materials are sometimes also referred to as space-age materials or high strength temperature resistant (HSTR) materials or exotic materials or difficult to cut materials. Over the past forty years, high strength thermal resistant materials have been used in increasing quantities [4]. Application of these alloys include jet engines, cryogenic tankage, stationary power turbines, atomic power installation, gas and oil well tooling and some products of the defence industry etc.

These advanced materials are generally considered to have poor machinability [4, 52,56,87]. The basic reasons for the difficulty in machining nickel base superalloys are as follows:

- (a) work hardening rates at machining strain rates leading to high machining force.
- (b) abrasiveness
- (c) strong tendency for chip to weld to the tool and to form built up edge (BUE)
- (d) low thermal conductivity and specific heat leading to high temperature.
- (e) tendency for maximum tool-face temperature to be close to tool tip.

One investigator has shown that the relative machinability of high strength materials is directly proportional to their respective service temperatures. The relative machinability of Inconel 718, a nickel base superalloy is approximately 10% of the relative machinability of annealed AISI 4340 steel [87]. The power required for machining

Inconel 718 is approximately $0.056 \text{ Kw/cm}^3 \cdot \text{min}$ ($1.22 \text{ hp/ in}^3 / \text{min}$). It workhardens rapidly during machining. A surface hardness of $R_c 48$ may be reached under some conditions when dull tools are used. To avoid work hardening conservative cutting speeds and heavy chip loads should be maintained. Tools should be replaced at the first sign of dulling. Inconel 718 is relatively tough and gummy so, it is difficult to curl and break the chips. Positive rake angles are required to properly clear the chip from the work area.

Compared to most steels, nickel based alloys are more difficult to machine since they maintain a major part of their strength during cutting and high levels of heat are generated which gives rise to thermal stresses at the interface of the cutting tool and workpiece [52]. Nickel based work materials are commonly machined with uncoated tungsten carbide tools at low cutting speed, of the order of 10-30 m/min. At these low speeds, chip control is poor, the typical chip being continuous with abrasive "saw tooth" edges. The combination of high temperatures, high workpiece strength and abrasive chips causes depth of cut (DOC) notching to be a major problem. These superalloys which contain titanium, columbium (niobium) and aluminium are specially difficult to machine. In the case of nickel based hard alloys, the critical phase in the microstructure is the high volume fraction, micron sized coherent particles of $\text{Ni}_3(\text{Al},\text{X})$ (γ') embedded within a solid solution strengthened nickel (γ) matrix [56,88-90]. In the case of Inconel 718, within γ' phase X corresponds to the presence of columbium, titanium or tantalum whereas γ matrix contains varying amounts of chromium, molybdenum or cobalt. The increased difficulty of dislocation motion through the γ'/γ microstructure in Inconel 718 is responsible for retaining its high strength at elevated temperature.

Nickel based superalloys presently have the highest operating temperature and they are among the worst materials which tend to strain harden in the hot working region when strained at high rates. This strong tendency to strain harden gives rise to a deep groove at both edges of chips. These nickel based superalloys can be machined best in the solution treated condition since they then strain harden less. Also, wrought materials tend to be machined better than cast structure. Nearly all the reported works have been on premachined material in the solution treated and aged condition [52]. There is little published data available on the forged condition.

In reference [87], it is reported that the difference in machinability between the annealed and the age hardened condition is not significant. The temperature distribution in tools to machine nickel based alloys has been studied and compared with tools used to machine steels are found in reference [52]. The outstanding feature in machining nickel alloys is that tool temperatures are far higher than in conventional steel. An example is given in machining of cast iron and a nickel based superalloys (nimonics) at 10 m/min showing maximum temperatures of 320°C and 800°C respectively. The tip of the cutting edge was frequently the hottest location when machining nickel alloys, whilst the maximum temperature when machining steels was always on the rake face some distance back from the cutting edge. Kramer and Hasting noted the effect of temperature on the failure of cemented carbide tooling when machining Inconel 718, suggesting that a solution wear mechanism limits tool life. They observed that about 30 m/min carbide tools failed due to thermal softening of the cobalt binder phase and subsequent plastic deformation of the cutting edge. Wright and Chow attributed the break down of the cutting edge of carbide tools to the heat generated in the primary deformation zone. For any work material, elements enter the secondary deformation zone having been strain hardened in the primary deformation zone. Material in the secondary deformation zone is then subjected to very high rates of shear strain. For nickel based superalloys, the combination of a large primary deformation zone heat source and large secondary deformation zone shear stress applied immediately behind the cutting edge, gives rise to high temperatures and stresses in this region. In addition to the high temperature Wright and Chow observed that the normal stresses on the tool are roughly twice as high for machining steel at the same cutting speed.

Development of a "V" shaped groove or notch at the depth of cut(DOC) line is a common problem when machining nickel alloys. DOC occurs in cemented and some ceramic tools (single point) and governs tool life. Notching of the trailing edge may also govern tool life where a fine surface finish is required. Much work has been done to investigate notch formation but no common consensus of opinion exists as to its cause. However, one thing on which there is agreement is that notch formation results from a combination of factors and not from a single wear mechanism.

Focke et. al [53] carried out machining tests on Inconel 718 using single point carbide inserts. They observed that a plateau usually separates the crater from the cutting edge when machining steel AISI 4340, but in the case of machining Inconel 718 this plateau is totally absent even in a short 2 minute test. They also observed that increasing the speed above that recommended ≈ 30 m/min (100 sfpm) produces a drastic increase in flank wear. The position of the maximum depth of crater moves towards the cutting edge, only a thin wedge of carbide remains that either breaks off or deforms very rapidly, due to the increased local temperature because rake and flank sources of heat are so close together.

The amount of nickel in a nickel base high temperature alloy is very important [56]. For example, nickel alloy which has a nickel content of about 60% and a recommended carbide tool speed of 13 m/min, the speed would be increased to about 20 m/min for work containing about 50% nickel and to 26 m/min for work of 45% nickel.

A general recommendation about the tool geometry in machining nickel base alloys has been given in the reference [88-90]. Milling cutters should have the greatest possible number of teeth compatible with strength and chip clearance. Whenever possible, the set-up should permit milling with the periphery of the cutter rather than the end(face or end mill). Peripheral climb(down) cutting extend tool life. All milling cutters should have +ve rake angle. Face mills with HSS inserts should have +ve helix angles. A typical face mill for Inconel 718 has teeth set on a helix angle of 7° and a radial rake angle of 15° . The peripheral clearance on small end mills should correspond to that for all steels. Feed rates should be sufficiently high to prevent rubbing, which causes work-hardening and can shorten tool life.

Virtually any lubricant or coolant can be used in machining nickel base alloys [90]. Water base coolants(1:25 or 1:30) are preferred for use in high speed operations. These may be soluble oils or a proprietary chemical mixture. In many cases, nickel base alloys respond well to ordinary sulphurised mineral oil. But in machining, if the temperature of the oil and workpiece becomes too high the sulphurized mineral causes brown sulphur staining. Besides, sulphur bearing compounds are not recommended for use with cemented carbide tools since the heat generated at the tip of the tool may cause the

sulphur to attack the binding agent contained in carbide tool material. Use of a high pressure air blast may assist when end milling nickel based alloys. Sometimes, gaseous coolants or mist can be used for certain machining operations. But it is reported [78] that in face milling with carbide tool using coolant hardly increases tool life due to thermal stress.

Most of the machining tests on nickel base alloys have been carried out by carbide tools particularly the uncoated carbide type. Though it has been reported that coating of the milling cutter increased tool life under certain conditions [91-92], still it is doubtful whether coated carbide inserts for milling cutters would be suitable for machining nickel base alloys! It is reported that coated tools are inherently more brittle than uncoated tools. Coated tools are generally not used for milling [56] and in general coated carbides are not useful for machining nickel-base alloys. Recently machining of Inconel 718 by single point ceramic tools like alumina, CBN and sialon are reported in the literature [52,93]. Besides, diamond coated tools gives poor performance on high temperature alloys [56] and are primarily used to machine non-ferrous alloys and non metallic material because of its affinity to steel. It is generally accepted that HSS and uncoated cemented carbide tools are suitable for milling nickel base alloys.

2.5.2 Machinability of Metal Matrix composites (MMCs)

Composites development began in 1960's with the introduction of boron, graphite and aramid fibre. The term advanced composite came into being more recently to designate certain composite materials having properties considerably superior to those of earlier composites [94]. According to the view of most production engineers current advanced composites are reinforced materials and in particular fibre reinforced materials [95]. The concept of reinforcement was known to and utilized by ancient Greece. The principle of fibre reinforcement is also very old. The Egyptians used chopped straw in bricks, the Incas and Mayas plant fibre in their pottery and most recently English builders, animals hair in household plaster [96].

MMCs are a relatively new range of advanced materials. Work on MMCs in the late 1960 resulted in numerous Boron/Aluminium MMCs parts. However, interest in MMC's diminished in the early 1970 as polymer matrix composites became the dominant material. The introduction of new fibre reinforcement materials in the late 1980's encouraged again the new development of MMCs [97].

Most MMC materials are not produced to a finished net shape, post production machining of the composite materials is necessary to produce different engineering components. However, MMCs are difficult to machine due to the use of hard abrasive materials as the reinforcing medium within a more ductile matrix materials. For example, the presence of hard SiC particles in Al-alloy-SiC presents difficulties when machining these materials using conventional methods i.e. turning, milling, drilling etc. In particular the presence of hard SiC particles leads to rapid tool wear. Consequently while the base material is easy to machine using these conventional methods it often results in frequent and expensive, tool changes and increased job completion times. Machining requires the use of carbide, diamond tools. Machining times tends to be 2-4 times longer than for unreinforced materials (aluminium), because of tool wear, reduced feed rates, and the need for a high surface finish. A high surface finish is required because MMC fracture behaviour is sensitive to surface finish [98]. Poor finish in continuous fibre reinforced MMCs results in longitudinal fracture and delamination.

Since MMCs are relatively a new range of materials their machinability has yet to be established and has aroused some research interests. For example, works by several authors [98] by non-traditional machining, i.e., laser machining, electro discharge machining, abrasive water jet machining are reported. In the field of traditional machining only limited data are available regarding the machinability of MMC materials [99]. Anderson et al.[100] have examined both the chip formation during machining and attendant surface characteristics of Al 9% Si alloys reinforced with short fibre Al_2O_3 . They measured the axial and tangential forces during machining, and showed that the cutting forces in alloys containing up to 20% Al_2O_3 were matrix dominated and decreased with increasing reinforcement. The authors [100] have carried out machining tests on a MMC material using single point carbide and PCD tools.

Milling is a difficult process due to the interrupted nature of the cutting process. Under these conditions the edge strength of the tool is critical. Face milling of the Du pont Fibre FP/Alum MMC using uncoated carbide or ceramic coated tools is reported in the literature [101]. The use of diamond tipped inserts for milling has been reported on by Walsdrop [102]. He cited two examples of the use of diamond cutters. The first involved the profile milling of a 250 mm diameter 40% $\text{Al}_2\text{O}_3/\text{Al}$ component during which a carbide end mill showed evidence of considerable wear after a single pass. The second related to the face milling of a 450 mm OD x 375 mm ID ring of 30% $\text{Al}_2\text{O}_3/\text{Al}$, MMC which exhibited 0.25 mm runout due to wear of the carbide inserts after one pass. In each case the use of PCD tipped inserts improved the situation. It is suggested that a compromise is possible in which the less expensive carbide tools can be used for the roughing operation and diamond tools used for the precision finishing cut. Diamond coated tools can also be used to mill B/Al MMC [103], however the process is slow, 25-50 mm/min, because high cutting rates result in tool overload and premature tool failure. Robertson and Maikish [103] have suggested that an oscillating motion applied to the end mill in addition to the usual rotary motion. This distributes the tool wear over a greater surface area and results in a cleaning action by removing machining debris from the cutting surfaces.

MMCs are now being manufactured in a variety of grades and forms. So, a generalization in machining could be very much in error due to the different reinforcement forms being enveloped in a varying percentage of a matrix metal.

CHAPTER 3

GENERAL DISCUSSION ON MACHINABILITY ASSESSMENT OF A MATERIAL

3.1 Introduction

Machinability of a material gives an indication of its adaptability to manufacture by a machining process. It is not easy to define, since the criteria for assessing it vary with the particular requirements. It has been suggested that the word "machinability" was first used in the 1920's and referred specifically to the speed/tool life relation [82]. Now, machinability is defined in various ways. It is broadly defined as the relative ease with which a material is cut. If tool life is the objective, then "good machinability" means long tool life. If high rates of cutting are required, rapid production allied to reasonable tool life presuppose good machinability. Another definition of machinability might be ease of obtaining good surface finish. However, in general machinability can be defined as an optimal combination of the following factors:

- (i) small cutting force
- (ii) high material removal rate
- (iii) low tool wear rate
- (iv) good surface integrity
- (v) accurate and consistent workpiece geometrical characteristics
- (vi) good curl or breakdown of chip

3.2 Machinability assessment

There is no standard scale or index of machinability, although some comparative measures have been produced with reference to turning [104]. For example, machinability can be given a numerical value expressing the ease or difficulty of measuring a particular workpiece material in comparison with AISI B1112 cold rolled free machining steel being turned at 60 m/min giving 60 minute tool life which is rated at 100%. From this figure it is possible to judge relative machinability and assess how much the cutting speed should be adjusted to maintain the same tool life. In milling, because of the complex nature of the relation between parameters it is difficult to establish quantitative relationships to define the machinability of a material.

However, in this study the machinability of the material by end milling process is assessed by investigating one or all of the following parameters:

- (i) cutting forces
- (ii) tool life
- (iii) surface finish

3.3 Factors influencing machinability

Factors that have an influence on machinability are shown in Fig.3.1. The factors are discussed below:

3.3.1 End milling process

Simplest of the milling processes is end milling process. It is the most widely used material cutting process in industry. Milling is a much more complex process than turning, and as might be expected the number of practical variables which are generally considered when assessing machinability of a material is much higher [74].

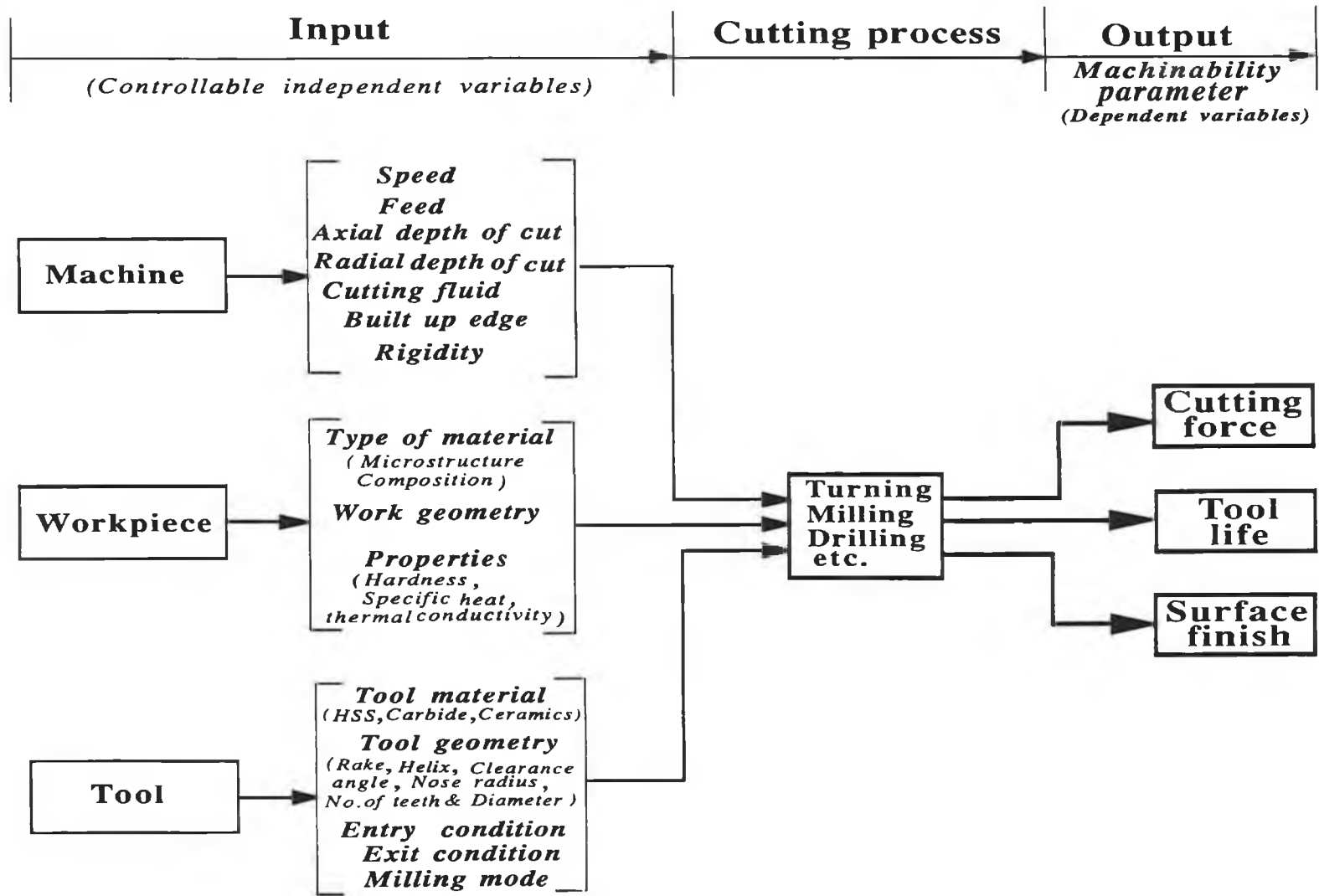


Fig.3.1: Factors influencing machinability of a material

In the past, the amount of effort which was directed towards the understanding of the milling process is small compared to that which has been expended in obtaining an understanding of turning. In milling both workpiece and cutter can be moved in more than one direction at the same time, so a surface having almost any orientation can be machined. Side milling, face milling and slot milling operations [84] can be performed by end mills. It is generally used for producing a flat surface and profile - frequently cornering, pocketing, die sinking etc. The basic geometry of end milling processes is shown in Fig. 3.2.

Mode of end milling

There are two modes of end milling depending on the relative motion of the cutter and workpiece as:

- up (or conventional) milling mode
- down (or climb) milling mode

Up milling mode: For a number of years, up milling, also known as "conventional milling and "milling against the feed" has been used almost exclusively in milling operation. In up milling mode, the workpiece is fed in the direction opposite to that of cutter rotation. Fig.3.3 (a) shows the up milling mode for right hand helix (RHH) with left hand cut.

Down milling mode: Conventional (up) milling mode was the most widely used method for many years until more modern and rigid machines were produced. Since the early 1880's when it enjoyed a considerable popularity. However, nowadays down milling has received a great deal of attention. In this method, the work is fed in the direction of cutter rotation shown in Fig.3.3 (b). down milling modes for left hand helix (LHH) with right hand cut. An end milling operation, where the immersion ratio is $a_p/D \leq 1/2$, can be in either an up or a down milling mode, while milling operations where the immersion ratio, $a_p/D \geq 1/2$, the mode of milling are combined since the feed motion is partly with, and partly against, the direction of cutter.

Classification of end milling Process: End milling processes by standard solid end mill cutter with straight shank may be classified according to ISO 8688-2 as:

- (i) slot milling ($a_r = D$, Fig. 3.4)
- (ii) end milling in which the tool periphery is used predominantly ($a_a > a_r$, Fig.3.5)
- (iii) end milling in which the end teeth of the tool are used predominantly ($a_a < a_r$, Fig.3.6)

ISO 8688-2 specifies the angular geometry of the standard solid end mill cutter for the above types of end milling process. The above classification may not hold good in the case of end milling with indexable inserts (i.e. inserts with sufficient end clearance angle).

End milling processes may also be classified with respect to immersion ratio, a_r/D [105-107]. In this case a_r/D determines the classification. The more commonly used end milling of this type are:

- (i) full immersion end milling or slot milling($a_r/D = 1$)
- (ii) three quarter immersion ($a_r/D = 3/4$)
- (iii) half immersion ($a_r/D = 1/2$)
- (iv) quarter immersion ($a_r/D = 1/4$)

Full, three quarter, half and quarter immersion milling are shown in the Fig. 3.7 (a), (b), (c) and (d) respectively.

Cutting geometry of end milling process: The first clear statements about milling were made by Professor Reuleaux [5, 108] in 1900. He was the first to draw attention to the fact that the paths of the teeth of the milling cutter are tracheidal. He was also the first to discuss the modes of feeding the material to a revolving cutter, namely in the direction of rotation of the cutter, and against it. Today these two processes are called up (conventional) and down (climb) milling mode. Solomon [5] assumed the path of the milling cutter to be an arc of a circle. The definitive work on the geometry of the

milling process has been done by Martellotti [9,10]. Results and models are shown for both up and down milling mode of plain milling processes. These results may with little extra effort be applied to all types of milling i.e., end milling and face milling. Martellotti showed that the true path of the milling cutter tooth is tracheidal and the equations describing the tooth path are given:

$$X = \mp \frac{f_m}{2\pi N_s} + R \sin \psi \quad (3.1)$$

$$Y = (1 - \cos \psi) R \quad (3.2)$$

Where X and Y - the coordinates of a point along the cutter path, f_m - feed per minute (mm/min), N_s - rotational speed of the cutter, ψ - the current angle of rotation of the cutter, R - radius of the cutter and the + and - signs apply to up and down milling respectively.

Martellotti has shown that the tooth path is longer for up milling and that the rake angle, clearance angle vary slightly during the cut. For light feeds, the tooth path is almost circular, and the circular tooth path approximation may be invoked if the radius of the cutter is much longer than the feed per tooth. This approximation simplifies the analysis of the process, and in practice, the necessary condition of the radius being larger than the feed is usually satisfied using this approximation.

Mechanics of cutting in end milling: An end mill has tooth/teeth on one end as well as on the periphery. In use, its axis of rotation is perpendicular to the surface produced. The basic geometry of cutting in end milling is shown in Fig. 3.2. Shaw [56] said that the term end milling cutter is misleading because in normal operation cutting is done on the periphery rather than by the teeth on the end of the cutter. But ISO 8688-2 has put forward suggestion for the criteria for end milling (standard solid end mill) tests as:

- (a) if $a_a > a_r$ then the teeth on the periphery are cutting predominantly(i.e., cutting edge on the periphery is the major cutting edge, Fig 3.5)
- (b) if $a_a < a_r$ then the end teeth are used predominantly (cutting edge on the end is the major cutting edge, Fig. 3.6)

But for end mills with indexable inserts which have sufficient end clearance angle then the above condition may not hold good. In this case the cutting edge of the insert set on the periphery is generally the major cutting edge.

Chip thickness: The geometric parameters of a chip in an end mill are shown in Fig. 3.8. Chip thickness at any instant, t_{ci} assuming the end mill path is circular can be found from Fig. 3.8 as:

$$t_{ci} = f_z \sin \psi \quad (3.3)$$

Where ψ - current angle of rotation of the cutter.

So, chip thickness depends on angle of rotation (ψ). It increases from zero to maximum and decreases to zero again. The maximum value of chip thickness occurs in end milling when $\psi = 90^\circ$. In some cases the middle chip thickness, t_m is used as:

$$t_m = \frac{f_z (\psi_2 - \psi_1)}{2} \quad (3.4)$$

Where ψ_2 - exit angle and ψ_1 - entry angle.

Use of middle chip thickness can lead to substantial errors and the use of average chip thickness is preferred. The average chip thickness, t_{ca} is given by:

$$t_{ca} = \frac{f_z}{\psi_s} \int_{\psi_1}^{\psi_2} \sin \psi \, d\psi \quad (3.5)$$

Where ψ_s - swept angle ($= \psi_2 - \psi_1$)

The cross-sectional area of the undeformed chip, A_{ci} for end mill teeth is expressed by:

$$A_{ci} = t_{ci} b \quad (3.6)$$

Where t_{ci} - chip thickness ($= f_z \sin \psi$) and b - undeformed chip width. For straight tooth, $b = a_a$ and for helical tooth

$$b = a_a \cos \lambda_s \quad (3.7)$$

where λ_s - helix angle of the cutter and a_a - axial depth of cut.

Usually for a small axial depth of cut, the helix angle is neglected.

The authors [20] have postulated that cutting action by peripheral cutting edge (Fig.3.6) is equivalent to an oblique cutting process (thin shear zone model) [21,56,82] with a straight edged tool shown in Fig. 3.9 (a). In an oblique cutting model, cutting speed, rake angle, depth of cut, inclination angle and width of cut are equivalent to the peripheral speed of the cutter v , radial rake angle γ_o (or α_n) of the cutting teeth, feed per tooth f_z , helix angle λ_s of the cutter and axial depth of cut a_a in end milling respectively. The author [82] also postulated that when the peripheral teeth are cutting predominantly then the end teeth of the cutter basically do not remove a significant amount of material from the workpiece, the cutting zone by the end teeth is considered equivalent to rubbing model (Fig.3.9 b). Oblique cutting is more complicated than orthogonal cutting in the sense that the deformation of material under cutting is not a plane strain case in the plane containing the cutting speed v and perpendicular to the machined workpiece surface. An effective cutting plane is defined here as the plane of the cutting speed v and the chip velocity v_c . The rake angle of the tool and the depth of cut measured in the effective cutting plane are called the effective rake angle α_e and the effective depth of cut t_e (feed per tooth or undeformed chip thickness) respectively as shown in Fig.3.10(a).

Chip thickness ratio: The chip thickness ratio or cutting ratio r_c can be shown from Fig.3.10(b) as:

$$r_c = \frac{t_e}{t_c} \quad (3.8)$$

Where t_e - effective depth of cut or undeformed chip thickness in oblique cutting (thin zone model) and t_c - chip thickness (measured).The chip thickness is usually less than unity and can be evaluated by measuring chip thickness. But it is very difficult to measure chip thickness precisely due to the roughness of the back surface of chip. The effective depth of cut (t_e) can be shown from Fig.3.9 (a), 3.10(a) and 3.10(b) [20] as:

$$t_e = \frac{t_n \cos \alpha_e}{\cos \alpha_n \cos \lambda_s} \quad (3.9)$$

Where t_n - normal depth of cut or feed per tooth (f_z), α_e - effective rake angle in oblique cutting, λ_s - helix angle of the cutter.

Shear angle: It is very difficult to measure the shear angle in milling because of varying chip thickness, still it can be assumed as equivalent to effective shear angle, ϕ_e in oblique cutting as the angle between the vectors v and v_s (shear velocity) (Fig.3.10 b and 3.10 c) as:

$$\tan \phi_e = \frac{\frac{v_c}{v} \cos \alpha_e}{1 - \frac{v_c}{v} \sin \alpha_e} \quad (3.10)$$

The resulting expression (3.10) is similar to that in orthogonal cutting which is:

$$\tan \phi_n = \frac{\left(\frac{t_n}{t_c}\right) \cos \alpha_n}{1 - \left(\frac{t_n}{t_e}\right) \sin \alpha_n} \quad (3.11)$$

Number of teeth cutting (z_c): The maximum number of teeth which can cut simultaneously, z_c in end milling can be determined as:

$$z_c \propto \frac{\psi_s}{\psi_t} = \frac{z * \psi_s}{360} \quad (3.12)$$

(helix angle neglected assuming axial depth of cut and milling cutter of uniform tooth pitch) and z - number of teeth in the cutter. Usually z_c is being rounded off to the nearest whole number.

The swept angle ψ_s can be found from Fig.3.2 and Fig.3.8 in terms of radial depth of cut and diameter of the tool as:

$$\cos \psi_s = \frac{\left(\frac{D}{2} - a_r\right)}{\frac{D}{2}} = 1 - \frac{2a_r}{D} \quad (3.13)$$

Feed/tooth f_z , feed/min f_m and cutting (peripheral) velocity v in end milling: The relationship between f_z and f_m (table speed) is given by:

$$f_m = f_z * z * N_s \quad (3.14)$$

Where z - number of teeth in the cutter and f_r ($= f_z * z$) - feed per rev. and N_s - rotational speed of the cutter.

Feed/tooth f_z is important for an end mill cutter which determines a particular load a cutter can withstand in a specific cutting. On the other hand feed in a milling machine usually is calibrated in term of feed/min f_m , hence one should have a knowledge of f_m for designing an experiment for a cut in a fixed feed (f_m) milling machine. The relationship between f_z and f_m is shown Fig 3.11. The cutting velocity (peripheral) v (m/min) is given by:

$$v = \frac{\pi * D * N_s}{1000} \quad (3.15)$$

Where D - diameter of an end mill.

The relationship among f_z , f_m and v of a milling machine is shown in Fig.3.12.

Material Removal Rate: The material removal rate (Q , cm^3/min) is given by:

$$Q = \frac{f_z * z * N_s * a_a * a_r}{1000} \quad (3.16)$$

Where the parameters have their usual meanings.

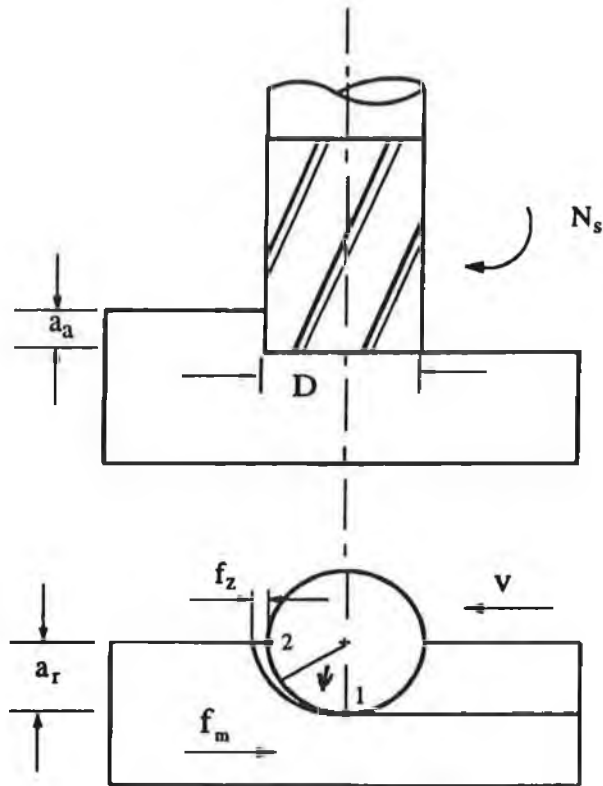
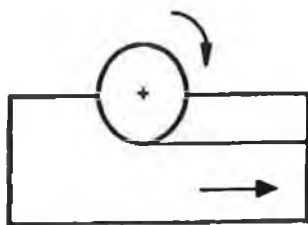
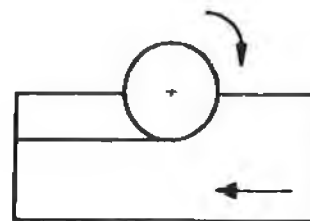


Fig.3.2: End milling process



Up milling



Down milling

Fig.3.3: Milling mode

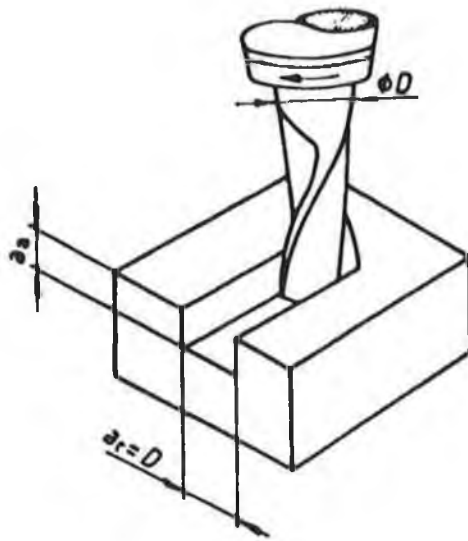
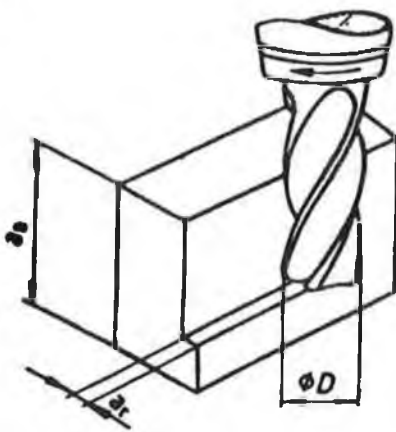
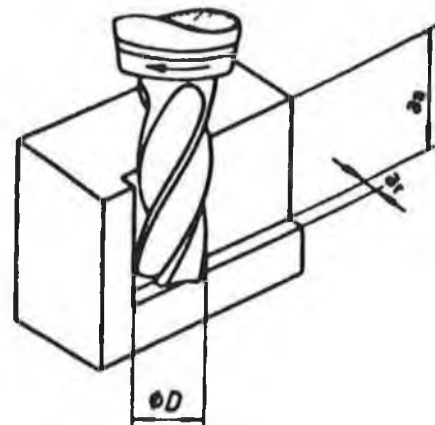


Fig.3.4: Slot milling

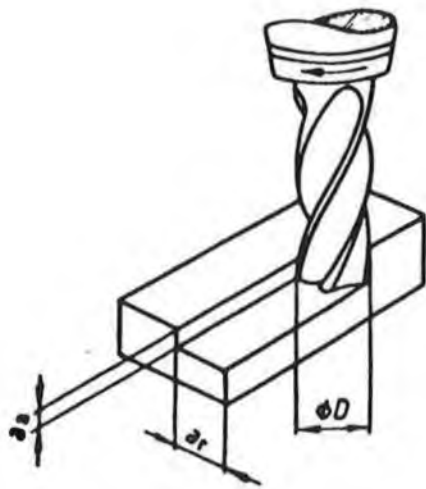


Up milling

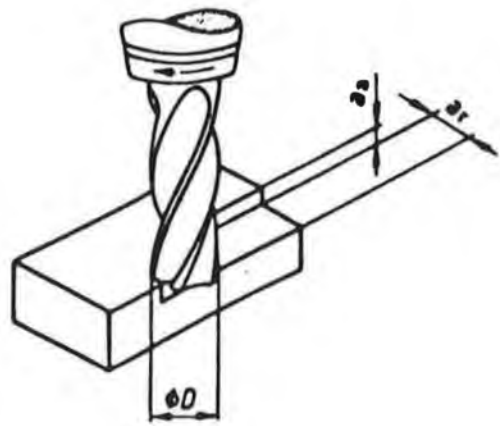


Down milling

Fig.3.5: End milling ($a_a > a_r$)

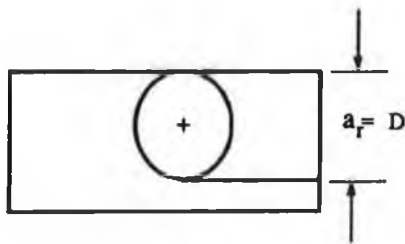


Up milling

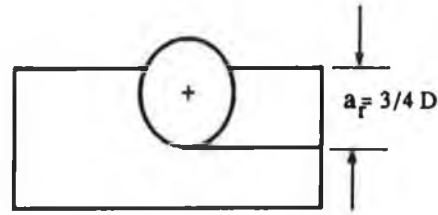


Down milling

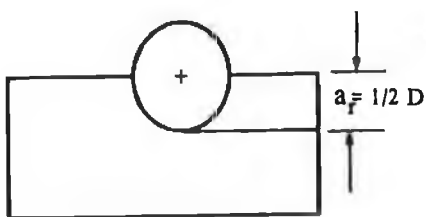
Fig.3.6: End milling ($a_a < a_r$)



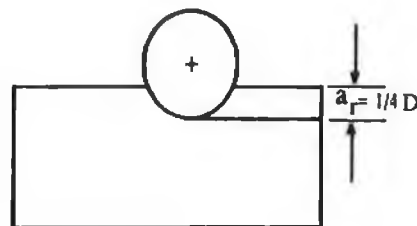
(a) Full immersion



(b) Three Quarter immersion

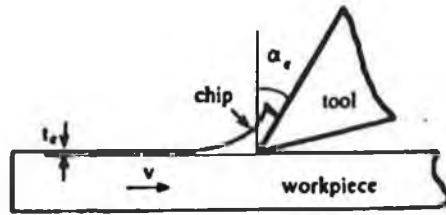


(c) Half immersion

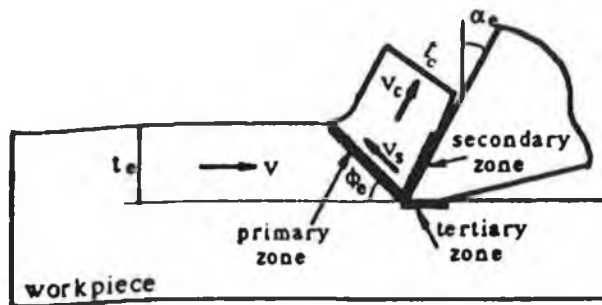


(d) Quarter immersion

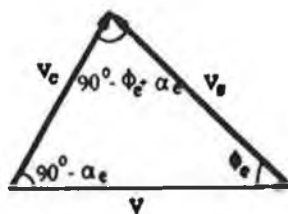
Fig.3.7: End milling processes



(a) The effective depth of cut (i.e. feed per tooth, f_z)



(b) The effective shear angle and cutting zones



(c) The velocity diagrams (hodograph)

Fig.3.10: Cutting processes in the effective cutting plane (simplified end milling process)

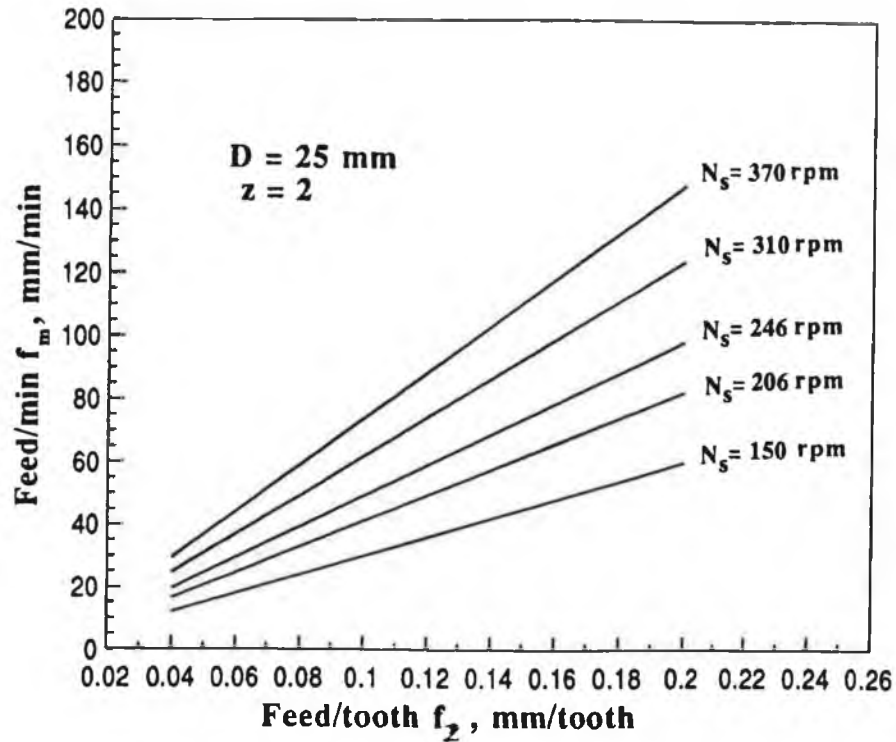


Fig.3.11: Relationship between feed/tooth (f_z) and feed/min (f_m) in end milling process

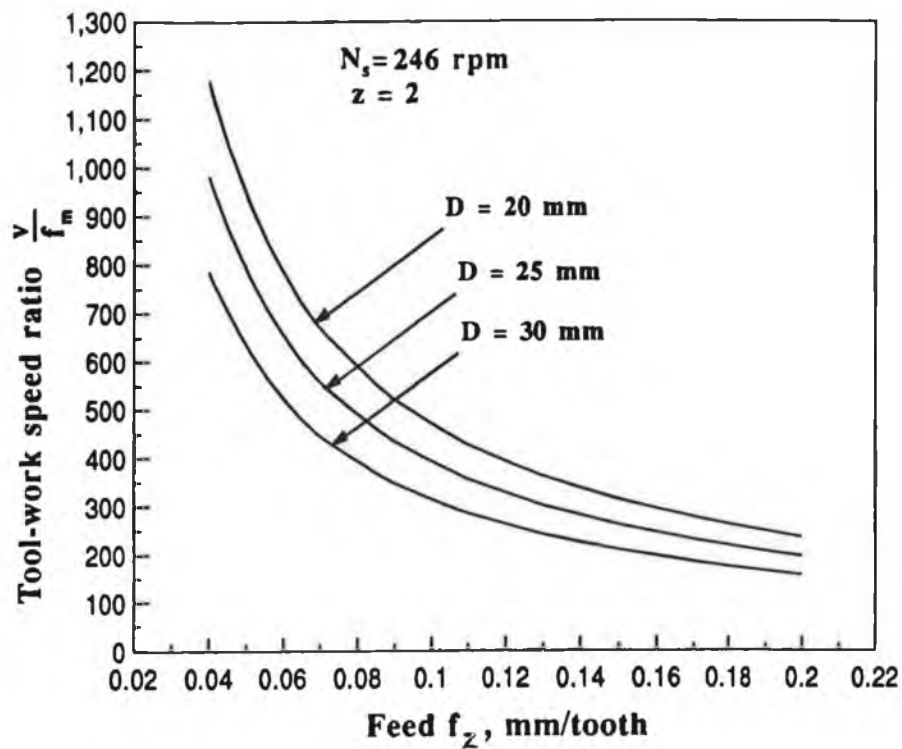


Fig.3.12: Relationship between feed/tooth (f_z) and speed ratio (tool work) in end milling process

3.3.1.1 Cutting force aspects in end milling

It is very difficult to predict accurately the cutting forces encountered in end milling operations due to the large number of independent variables involved. But the knowledge of magnitude of variation of the cutting forces is important for the use of the production engineer as well as the design engineer. Cutting forces generally increased from zero to maximum and again decrease to zero according to the variation of the rotational angle of the cutter within the workpiece. From this variation in cutting forces, average cutting forces can be measured. Though average cutting forces in milling do not indicate the maximum forces experienced by the cutter still it can help the design engineer to give an estimate in designing machine tool and drive systems. The actual cutting in end milling is dynamic in nature. The instantaneous cutting force in end milling operations varies not only with the variation of feed but also due to machine tools dynamics (deflection, vibration and chatter), chip segmentation process, cutting temperature etc.. So, cutting forces in unsteady state cutting are dynamic in nature. Knowledge of dynamic cutting forces is necessary for adaptive control machine tool or unmanned machining. But, in this study average cutting forces in end milling are investigated.

Cutting Force Components in end milling: In end milling two reference systems have been adopted to determine the components of the cutting forces:

- (i) table system of cutting forces
- (ii) cutter system of cutting forces

Table and cutter system of cutting forces from the action of one tooth of the end mill on the work piece is shown in Fig. 3.13.

(i) Table system of cutting forces

It consists of the following components:

- (a) **Feed or Horizontal (longitudinal) component of cutting force, F_x :** The projection of resultant cutting force in X direction.

(b) **Normal or Horizontal (traverse) component of cutting force, F_y :** The projection of resultant cutting force in Y direction.

(c) **Vertical component, F_z :** The projection of resultant cutting force in Z direction, perpendicular to both former axes. It usually passes through the axis of the spindle.

The table system of cutting forces (F_x , F_y & F_z) does not depend on the kinematics of the cutting and is, therefore stationary.

(ii) Cutter system of cutting force

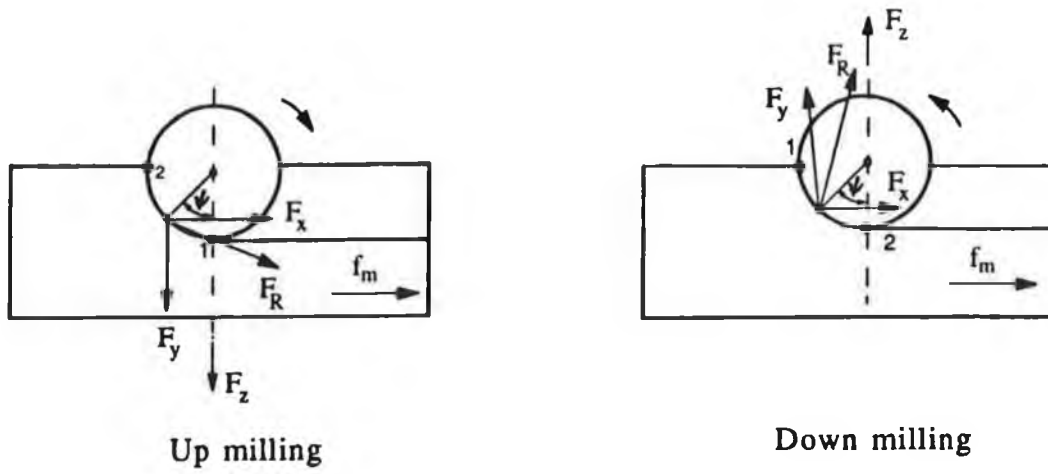
It consists of the following components:

(a) **Tangential component, F_t :** A force which passes through the tangent to the circle circumscribed on the contour of the cutter cross-section and represents the resistance to the rotation of the workpiece. This component of cutting force determines the torque which has to be applied to both the cutter and the spindle drive, consequently the almost net power required at the cutting edge. In a normal operation, tangential force is the highest of the three force components and accounts for 99% of the total power required by the operation.

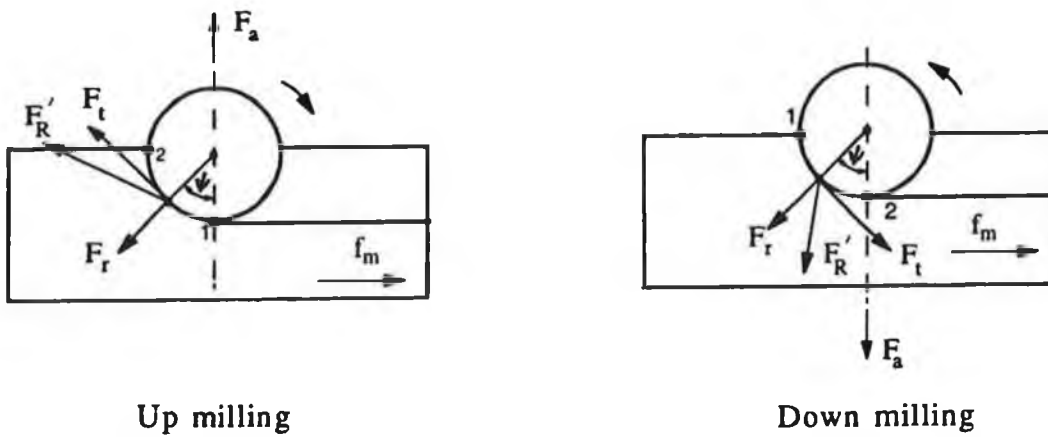
(b) **Radial component, F_r :** It is perpendicular to the cutter axis and acts along the radius of the cutter or tip of the tooth. This force attempts to push the cutter out of cut. Radial force is usually about 50% as great as tangential force but since radial velocity is very low in relation to the cutting velocity of the rotating cutter, radial force accounts for only about 1% of total power required.

(c) **Axial component, F_a :** This component of cutting force passes through the axis of the cutter and generally the smallest of three force components, often about 50% as large as the radial force. This force tends either to press the cutter against or pull it away from the spindle nose, depending on the hand of helix. Its effect on power requirement is very small because velocity in the axial direction is negligible.

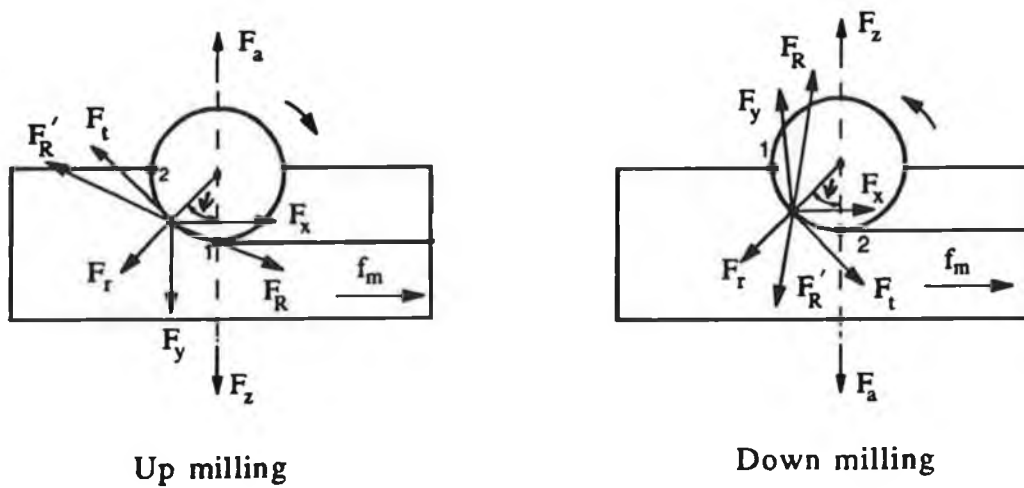
(When the cutter is correctly mounted, the cutter axis and spindle axis coincide, then $F_a = F_z$ is usually assumed).



(a) Table system of cutting force components



(b) Cutter system of cutting force components



(c) Combined table and cutter system of cutting forces

Fig.3.13: Cutting force components acting on one tooth of an end mill

Average or static (or D.C level) cutting forces

If the cutter is absolutely concentric i.e., each tooth is at exactly the same distance from the centre of rotation, the material removed per tooth and hence the magnitude of the force per tooth would be same. For multi-tooth milling if each tooth is not at exactly the same distance from the centre of rotation then the mean amplitude of the cutting forces per tooth is found by summing all the amplitudes per revolution and then dividing the sum by the total number of teeth, assuming that the material removed for each revolution is the same. Cutting forces in end milling vary due to the variation in chip thickness and specific cutting pressure. Variation in chip thickness is due to the rotational angle of the cutter. So the cutting forces in end milling do not remain constant. It will fluctuate around its average force. The cutting forces in milling are periodic in nature. They reach a maximum at regular intervals, depending upon the number of teeth and the revolutions per minute of the cutter. Actual shape of F_x component of cutting force acting on one tooth in slot milling by a end mill cutter is shown in Fig. 3.14. To obtain the average force per tooth, the area under the curve is to be determined and the value found is divided by the distance travelled per tooth. The cutting force signal is usually obtained by using a table type dynamometer under the workpiece. Average cutting force measurement has been discussed in chapter 5.

Cutting forces in multi-tooth milling: In multi-tooth milling if several teeth are cutting simultaneously then the cutting force components per cut (spindle) are:

$$F_{Xm} = \sum_{i=1}^{z_c} \delta(i) * F_{xi}(\psi_i) \quad (3.17)$$

$$F_{Ym} = \sum_{i=1}^{z_c} \delta(i) * F_{yi}(\psi_i) \quad (3.18)$$

$$F_{Zm} = \sum_{i=1}^{z_c} \delta(i) * F_{zi}(\psi_i) \quad (3.19)$$

$$\text{Where } \delta(i) = 1 \quad \text{if } \psi_1 \leq \psi_i \leq \psi_2$$

$$= 0 \quad \text{otherwise}$$

Where F_{Xm} , F_{Ym} and F_{Zm} are the mean value of the average cutting forces per cut in the

X, Y and Z direction respectively, and F_x , F_y and F_z are the average cutting force on an individual tooth in cut in the X, Y and Z direction respectively.

So, for multi-tooth milling cutter of uniform tooth pitch the mean value of the average cutting force per tooth are:

$$F_x = \frac{F_{xm}}{z_c} \quad (3.20)$$

$$F_y = \frac{F_{ym}}{z_c} \quad (3.21)$$

$$F_z = \frac{F_{zm}}{z_c} \quad (3.22)$$

z_c is the number of teeth cutting simultaneously; z_c is not being rounded off to nearest whole number(z_c is shown in equation 3.12).

In multi-tooth milling the average tangential cutting force, F_{tm} per cut(which is usually considered as the cutting force) and the average radial cutting force F_{rm} are:

$$F_{tm} = F_t * z_c \quad (3.23)$$

$$F_{rm} = F_r * z_c \quad (3.24)$$

Where F_t and F_r are the average tangential and radial cutting force per tooth of the cutter and z_c is not being rounded off to nearest whole number.

Relationship between table and cutter system of cutting forces: From Fig.3.13 the resultant cutting force, F_R acting on the workpiece can be shown as:

$$F_R = \sqrt{(F_x^2 + F_y^2 + F_z^2)} \quad (3.25)$$

Where F_x , F_y and F_z - the mean value of the measured average force per tooth over a few revolutions of the cutter in the X, Y and Z direction.

The resultant cutting force, \dot{F}_R acting on the cutter can be shown as:

$$\dot{F}_R = \sqrt{(F_t^2 + F_r^2 + F_z^2)} \quad (3.26)$$

Where F_t , F_r and F_a are the average tangential, radial and axial cutting force acting on the cutter.

For static equilibrium it is assumed $F_R = \dot{F}_R$

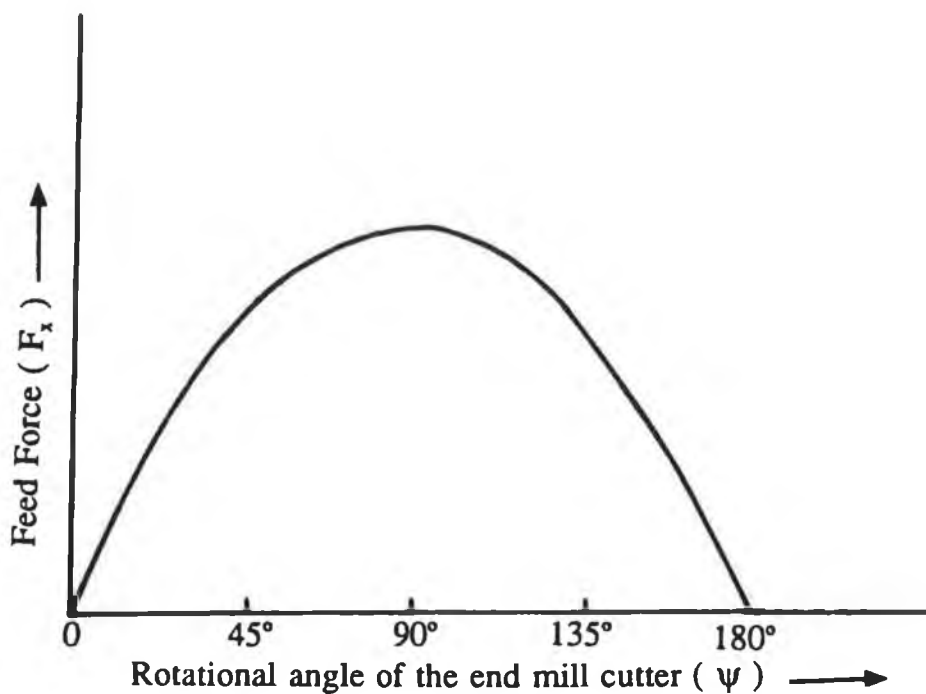


Fig.3.14: Variation of the feed force (F_x) on one tooth in slot milling operation

The resolution of the cutting forces in end milling with a cutter having straight tooth assumed as a plane system in which axial forces are equal to zero in both the up and down milling mode. Then from Fig.3.13 it is possible to relate the forces on the milling machine table to those on the cutter for both modes of milling as:

$$\left. \begin{aligned} F_t &= F_x \cos \psi + F_y \sin \psi \\ F_r &= F_x \sin \psi - F_y \cos \psi \end{aligned} \right\} \text{up milling} \quad (3.27)$$

$$\left. \begin{aligned} F_t &= F_y \sin \psi - F_x \cos \psi \\ F_r &= F_y \cos \psi + F_x \sin \psi \end{aligned} \right\} \text{down milling} \quad (3.28)$$

The resultant cutting force for (plane system) is:

$$F_R = \sqrt{(F_x^2 + F_y^2)} = \sqrt{(F_t^2 + F_r^2)} \quad (3.29)$$

Specific cutting pressure: As both the chip section and the specific cutting pressure vary during the milling operation, the cutting force rises periodically to a maximum value and then drops again. In end milling the chip section which lies in front of the tooth at any instant is the product of chip thickness, t_c and the axial depth of cut, a_a at any consideration. The chip section multiplied by the specific cutting pressure, k_s at any instant gives the instantaneous magnitude of the cutting force. The specific cutting pressure can be found from the magnitude of tangential force for the particular cut. The magnitude of tangential force can be determined from the table system of cutting force (F_x, F_y) measured by a dynamometer. The tangential cutting force divided by the area results in the specific cutting pressure.

The specific cutting pressure depends upon the workpiece material, shape of the cutter and the cutting conditions. Sabberwal [7] has shown that it is not a function of the chip-section but chip thickness. He has shown in a series of tests, the depth of cut and the chip thickness were varied in such a manner that the cross-sectional area of the chip remained constant. The cutting force was measured and corresponding specific cutting pressure, k_s calculated by dividing the force by the area of the chip section. k_s was not constant, but varied with chip section. For a given chip thickness, however, and varying axial depth of cut, the specific cutting pressure k_s remained constant. But it is seen that specific cutting pressure increases as chip thickness increases. Sabberwal [7] has also shown that the helix angle has no effect on the value of k_s . For a given material, therefore, the chip thickness and not the chip section must be taken a parameter to which k_s can be related, independent of other cutting parameters.

Mean cutting pressure: For determining the work done per tooth and the power requirements the concept of the mean cutting pressure may be considered.

The average area of the chip can be determined from the volume of material removed by the milling operation divided by the path of the cutter:

$$\text{Average area of chip} = \frac{f_m * a_a * a_r}{v} \quad (3.30)$$

where a_a - axial depth of cut (mm), a_r - radial depth of cut(mm), f_m - feed per minute (mm/min) and v - peripheral velocity of the cutter (m/min)

The average power consumed per cut is given by:

$$\text{Average Power} = \frac{k_m * a_a * a_r * f_m * v}{v * 60 * 1000 * 1000} = \frac{k_m * a_a * a_r * f_m}{60 * 1000 * 1000} \quad (3.31)$$

If the cutting is intermittent, i.e., if one tooth comes out of the workpiece before the following tooth has entered it, then the average energy consumed can also be determined from the average tangential force as:

$$\text{Average Power} = \frac{F_t * v * \phi_s * z}{2\pi * 60 * 1000} \quad (3.32)$$

From equation (3.31) and (3.32) mean cutting pressure k_m for intermittent cutting can be shown as:

$$k_m = \frac{F_t * v * \phi_s * z}{a_a * a_r * f_m * 2\pi} \quad (3.33)$$

$2\pi/z = \phi_t$ = angle between the consecutive teeth of the cutter

$$k_m = \frac{F_t * v * \phi_s}{a_a * a_r * f_m * \phi_t} \quad (3.34)$$

Where F_t - average tangential force per tooth.

If the cutting is continuous, i.e., if one tooth leaves the cut when the following one take over, or if more than one tooth is cutting at the same time:

$$k_m = \frac{F_t * v}{a_a * a_r * f_m} \quad (3.35)$$

Where F_t = average tangential force over a period which is ϕ_t

Dynamic cutting force: Milling is a non-steady cutting process which has complex geometry. The chip thickness in milling varies according to the angular rotation of the cutter. So, there is a variation of cutting force in milling according to the variation of chip thickness. This force increment causes the tool to deflect and vibrate. The vibration of the tool produces a wavy surface on the work-piece. When the generated wavy surface is removed by the tool in the subsequent revolution of the work-piece, the cutting forces again vary cyclically. If the nature of the cutting force variation is such that the maximum cutting force occurs sometime after the maximum chip thickness variation, then, some energy is available to maintain vibration between the tool and the work-piece. This vibration of the tool-workpiece system is known as regenerative chatter. Under the conditions of chatter, the cutting process is in a non-steady state of motion. Cutting forces in non-steady state of cutting is dynamic in nature.

The characteristics of dynamic forces are that the instantaneous value of the cutting forces in milling is dependent on a number of factors, predominant among which are:

- (i) the changing position of cutter tool in relation to the work
- (ii) cutting speed
- (iii) the incremental variation of the chip thickness and the rate of change of chip thickness.
- (iv) the effect of chip segmentation
- (v) the periodic variation of shear angle
- (vi) the non uniform physical and chemical composition of the tool and work- piece
- (vii) the uneven work surface

(viii) the deflection, vibration and chatter of machine tool and work piece fixture.

Mechanical forces and vibrations are transformed into electrical signals usually by piezo-electric transducers. For analysis of dynamic component of cutting forces these signals are stored in a multi channel magnetic tape recorder. The tape recorder signals are subsequently run to obtain the desired information. These signals may be allowed to pass through an A/D converter and data acquisition of the signal is done by a computer to know the desired information. By Fast Fourier Transformation (FFT) analysis it is possible to analyze the information in time domain and frequency domain.

Power required in End Milling: The most practical method of estimating power consumption in a end milling operation is based on the metal removal rate (Q). The approximate power to maintain a given rate of metal removal can thus be determined by the following formula:

$$P_s = P_u * Q \quad (3.36)$$

P_s - power (kW) required at the spindle and P_u - specific power unit(kW/cm³/min). Q - material removal rate (cm³/min).

For common materials the value for P_u are available in the literature[15].The specific power (unit power factor) at the spindle is the approximate power required at the spindle to remove 1 cubic centimetre per minute of a certain material. In practice, P_u is also dependent on the cutting speed, feed per tooth (insert), rake angle and tool wear land. If the formula shown above is used to calculate power requirements, the result should be increased by 50% to allow for the possible effects of these factors.

An estimate of power required at the motor of the milling machine, P_m can be made with the following formula:

$$P_m = \frac{P_s}{E} \quad (3.37)$$

Where E - efficiency of the power transmission system.

There is a definite fixed relationship between power consumed at the spindle and cutting force. When the value for power can be found from cutting force components as:

$$P_s = \frac{F_t * v_t}{60000} + \frac{F_r * v_r}{60000} + \frac{F_a * v_a}{60000} \quad (3.38)$$

Where F_t , F_r and F_a are the average tangential, radial and axial cutting force (N) per tooth of the cutter and v_t - tangential velocity of the cutter ($v = \pi DN_s/1000$), m/min.

v_r - radial velocity or milling table speed ($f_m = f_z * z * N_s$), mm/min. and v_a - axial velocity of the cutter, mm/min.

Since v_r and v_a are usually quite small in relation to v_t , this formula (3.38) can be simplified to:

$$P_s = \frac{F_t * v}{60000} \quad (3.39)$$

If the cutting is continuous i.e., if one tooth leaves the cut when the following one takes over, or more than one tooth cutting simultaneously then F_t of the equation (3.39) is the average force over one cycle (tooth), the period of which is ψ_t (angle between two consecutive teeth). F_t for multi-tooth can be found from the measured force component by the equations (3.17), (3.18), (3.23), (3.27) and (3.28).

If the cutting is intermittent, i.e., if one tooth comes out of the workpiece before the following tooth has entered it then F_t of equation (3.39) can be found as:

$$F_t = \frac{F_{tc} * 360}{\psi_s * z} \quad (3.40)$$

Where F_{tc} - average tangential force of the intermittent cut .

Factors influencing cutting forces in end milling

The factors which affect the cutting forces in end milling are shown Fig.3.15. A brief description of each factor is given below:

(i) Machine variables

(a) Cutting speed

Within the normal practical cutting range the cutting forces decrease as the cutting speed is increased, but after a certain speed the rate of decrease is not as great. At lower speeds the forces are influenced by the presence of a built up edge [109]. Cutting forces can vary in an unpredictable manner. It is shown in the reference [110] that as cutting speed decreases the shear angle decreases and friction coefficient increases. Both of these effects increase the cutting force. If cutting speed increases, the shear angle increases. When shear angle is high it gives a short shear plane. It is always desirable to obtain a shortest possible shear plane, because for a fixed shear strength, reduction in shear plane area reduces the shearing forces required to produce sufficient stress. If the cutting speed is high then the temperature in the tool-chip contact area is also high which affects the shear flow stress of material and this could reduce the friction force acting on the rake face. Thus the forces at higher speeds are reduced due to the disappearance of built up edge, reduced friction force and increased shear angle. But within realistic practical cutting speed range, cutting speed is known to have little effect on the cutting forces [111]. It is also reported at super high speed (over 300 m/min) cutting forces increase as the cutting speed increases due to high strain rate [112]. Cutting speed above 300 m/min shear angle still increases with increasing speed but the resulting reduction in area of shear plane is more than compensated by the increase in shear flow stress along the shear plane which increases approximately linearly with strain rate.

(b) Feed

As the feed rate is increased a thicker chip is produced and a larger shear plane is obtained. As chip thickness increases so cutting forces are increased. Experiments indicate that cutting forces increase exponentially with the increase of feed. At very small feed rates, the cutter is scraping rather than cutting.

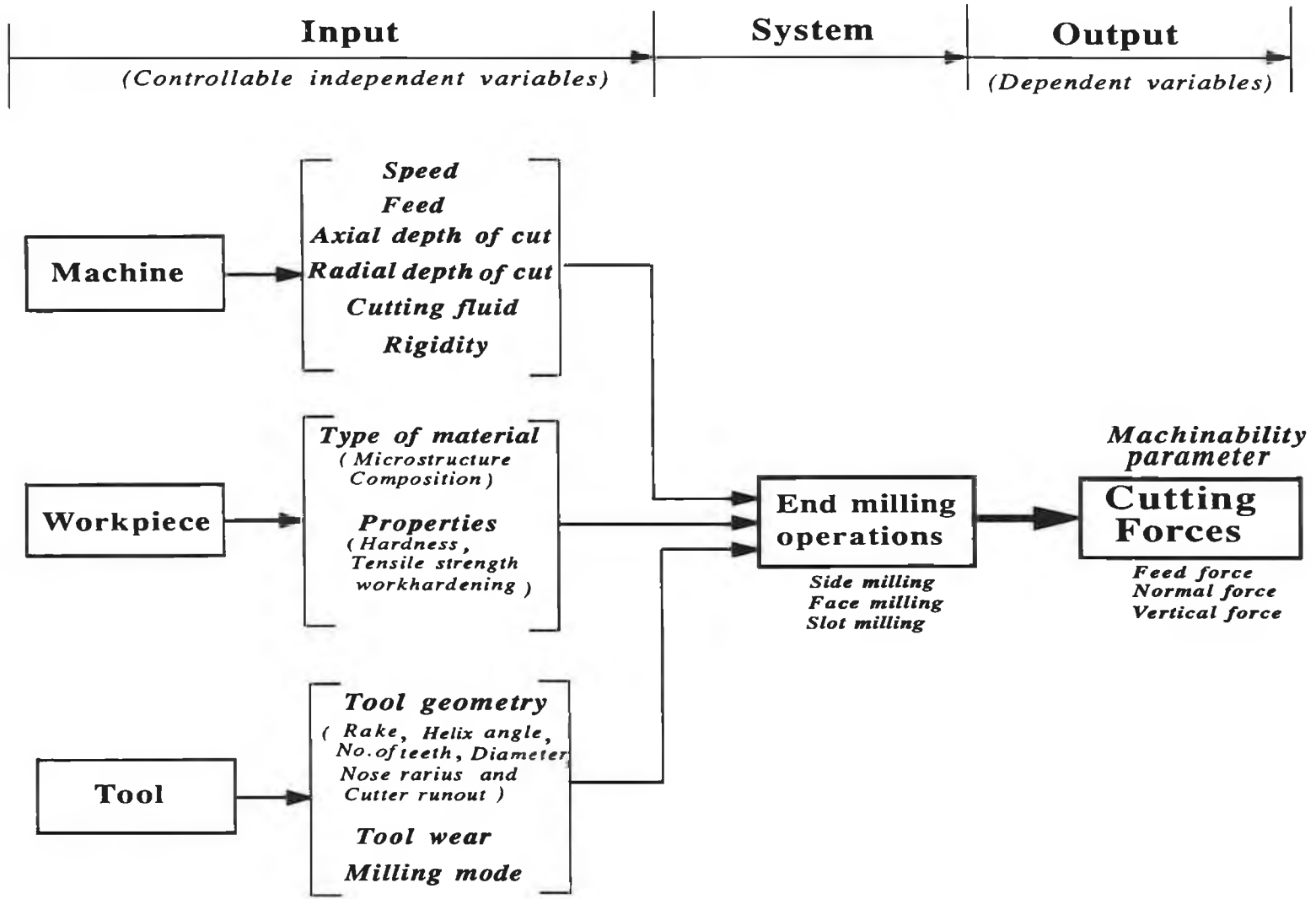


Fig.3.15: Factors influencing cutting forces in end milling processes

(c) Axial depth of cut

As the axial depth of cut increases the cutting forces also increase almost linearly. This is because of an increase in the size of cut. But for small depth of cut, where the thickness of the undeformed chip is very small, the cutter has a tendency to rub instead of cut. The influence of axial depth of cut in milling is usually greater than the influence of the feed per tooth for HSS cutter.

(d) Radial depth (width) of cut or immersion ratio (a_r/D)

Immersion ratio in end milling is defined by the ratio of radial depth of cut to diameter of tool. An increased radial depth of cut involves a rise in the number of teeth cutting simultaneously. In addition, increasing the radial depth of cut causes a growth of the undeformed chip surface which correspondingly increases total force. The magnitude and the direction of cutting forces vary with the rotational angle. The rotational angle depends on the radial depth of cut for constant diameter tool.

(e) Cutting fluid:

In general, at very low speeds the effect of cutting fluids is friction reduction. The major practical benefit from friction reduction effect is a decrease in the cutting force. Application of coolant to the conventional face mills resulted in some decrease in the values of the force components [113]. This could be due to the cutting fluid helping the formation of low shear strength film (metal sulphide) at the tool-chip interface. The tendency of reducing the contact area, which is created by the cutting fluid employed, may also have helped in the reduction of the cutting forces. But cutting at high speed, the cutting fluid causes a reduction in the temperature of the workpiece which may increase its shear flow stress, so that the cutting force and power consumption may be increased to some extent.

(f) Rigidity of machine tool

The dynamic cutting force is dependent on a number of factors: predominant among these are:

- deflection of the cutter
- vibration
- chatter of machine tools structure.

Force measurement becomes much more complicated even not reliable if vibration of machine tool prevails. The deflection of the cutter will also play a role in the computation of force. The deflection of the cutter only affects the parameter t_c (chip thickness). If the deflection of the cutter is considered, then the tangential force on a particular tooth as it passes through the cut is given by [17]:

$$F_t = k_s a_a \left(t_c - \frac{F_t}{K'} \right) \quad (3.41)$$

Where K' - stiffness of the cutter and F_t / K' - deflection of the cutter.

If the cutter is very stiff and axial depth of cut is low, the deflection will be very small and consequently the force will almost not be affected. On the other hand, if axial depth of cut is very large and the cutter is not very stiff, the ratio can become large, then the force system will be affected. It is obvious that the effect of deflection of the cutter becomes more important as the ratio of the cutting stiffness to system stiffness becomes large.

The deflection of the cutter plays another role. If the cutter deflects, then the thickness removed by the tooth is less than the nominal feed per tooth. As the next tooth passes, it will be required to remove that additional material, and the force will again be affected.

(ii) **Workpiece Variables**

(**microstructure, chemical composition, hardness, tensile strength, workhardening etc.**)

Microstructure refers to the arrangement of the crystals or grain structure of a material. The structure and mechanical properties of a material are determined basically by its chemical composition. In average workshop practice, scatter of cutting force may occur due to non-homogeneity of microstructure and chemical composition of workpiece material. Hardness of a material depends on many factors, for example its composition, its structure and the treatment it has undergone before machining. Hardness is usually defined as a material's resistance to indentation. Hardness is related to strength, and

therefore the hardness number also gives some indication of cutting pressure required. It is found that an increase in the work material hardness has a profound effect on cutting forces [114]. This is attributed to the increase in energy required to shear the harder material. Sometimes, due to improper cutting conditions(i.e., less than certain feed per tooth or dwelling of the cutter within work), workpiece material is workhardened due to interlocking of dislocations at the grain boundaries of crystal or at inhomogeneties within grain, so that further slip can only be produced by an increase in the external loads. So, if a work material has a tendency to workharden under certain condition then more cutting pressure is necessary to machine the workhardened layer.

(iii) Tool Variables

(a) Tool geometry

Rake angle: The rake angle exerts a distinct influence on cutting forces. The cutting force appeared to decrease with increasing radial rake (or true rake) angle. This is because the degree of plastic deformation of the chip is lower; the other reason for this decrease in force at high rakes can be ascribed largely to the greater shear angle at higher rakes and the consequent reduction in shear plane area.

Helix angle: A helix angle has no marked influence on the cutting forces. Studies carried out by Rozenberg [78] did not indicate the existence of such an influence within the range of helix angles (λ_s) = 20 - 25°. But Ema and Davies [84] have shown that end mills with a small helix develop the greatest cutting forces. The investigators [34] have shown that as the helix angle increases the cutting force decreases. They have also shown that smoother motion and vertical vibration of spindle may be expected if the helix angle is larger than 25° and up to 50°.

Number of teeth: An increase of the number of cutter teeth, if the feed rate (f_z - feed per tooth) remains constant, does not cause any changes in the specific cutting energy but it may increase the total cutting force if, as result of the reduction of the angle pitch of cutter teeth.

Diameter of the tool: Increasing the cutter diameter while all other cutting conditions remain unchanged, causes the cutting forces to diminish although the specific cutting energy is greater. This is explained by the fact that with growing cutter diameter the thickness of the undeformed chip decreases, but so also does its cross-sectional area. In the case of cutting simultaneously with more than one cutter tooth the increase of the cutter diameter while preserving the same number of teeth may reduce the number of teeth cutting simultaneously and thus, of course, reduce the resultant cutting force too.

Nose radius (tip radius of tool): This has a significant influence on the cutting forces. The larger the radius (i.e., the duller the tool) the higher the cutting force. Dull tools cannot remove thin layers of material. Dull tools may actually rub against the surface without removing any material. This type of tool could also impart compressive residual stresses on the surface.

(b) Tool wear

Cutting forces increase as the flank wear progressively develops. Usually a linear model is found between the flank wear and the cutting forces. The force components, due to the indentation or ploughing effect, should be added as a consequence of the roundness or bluntness of the cutting edge.

(c) Cutter runout

This is a common phenomenon in multi-tooth machining operations, particularly in milling operations. In milling, runout often referred to as radial and axial throw, may result from eccentricities related to the manner in which the cutter is held in the spindle. When insert type cutters are used, runout is more likely due to irregularities in the cutter pockets, cutter size, regrinding operations or the setting of the insert. The presence of runout causes chip load to vary over the rotation of a multi-tooth cutter. The varying chip load will alter average forces, peak forces and instantaneous force profile to varying degrees depending on the cutting conditions and cut geometry [13].

(d) Mode of milling

Mode of milling has influence on cutting force. In down milling the cutting forces are generally higher than in up milling [6]. But the rate of increase of the specific

cutting pressure for down milling from up milling is smaller for thin chips than it is for thick chip. This can be explained by Sabberwal [6] as squeeze effect. In up milling at the start of the cut, the cutter encounters an infinitely small chip thickness and thus the surface, which has already been cut by the previous tooth. This continues until a real cut starts. In case of down milling usually there is no squeezing effect . In realistic cutting the tangential force in down milling is similar to up milling except that, the reverse rotation of the cutter. The cutting force in down milling rapidly reaches a maximum and then decreases; with up milling the reverse is obtained. In down milling the cut achieves its maximum depth almost immediately and consequently there is no appreciable rubbing. The resultant force in up milling opposes the feed force, whereas in down milling it assists the feed force. For this reason an efficient backlash eliminator is essential in the case of down milling.

3.3.1.2 Tool life aspects in end milling

In general a cutting tool may reach the end of its tool life by any of the following major classes of tool deterioration:

- (i) tool wear
- (ii) chipping
- (iii) cracks
- (iv) plastic deformation
- (v) catastrophic failure

In practice, different types of deterioration will occur together during machining. A detailed discussion on the above tool deterioration phenomena in milling cutter or inserts is shown in references [43,44]. The cutting conditions in end milling may be considered under two categories as follows:

- (a) conditions as a result of which tool deterioration is due predominantly to wear
- (b) conditions under which tool deterioration is due mainly to other phenomena such as edge fracture or plastic deformation.

As ISO 8688 covers only conditions as a result of which tool deterioration is due predominantly to wear, and does not consider tool deterioration due to other phenomena such as edge fracture or plastic deformation. In this work, the recommended procedure specified by ISO 8688-1 and 8688-2 for tool life testing (end milling) will be followed whenever possible. It is found that flank wear phenomenon is common to end mill cutter hence, end mill tool life end point criterion based on flank wear will be considered in this work.

Flank wear

Loss of tool material from the tool flanks (clearance faces) during cutting, results in the progressive development of a flank wear land. Flank wear starts at the cutting edge and then starts widening along the clearance face. ISO 8688 specifies different forms

of flank wear for HSS solid end mill cutting edges and carbide inserts. Flank wear on a solid HSS end mill cutter is illustrated in Fig. 3.16 according to ISO 8688-2.

Uniform flank wear (VB1): Wear land which is normally of constant width and extends over those portions of the tool flanks adjoining the entire length of the active cutting edge. The uniform flank wear of an end mill carbide insert is illustrated in Fig.3.17 (a).

Non-uniform flank wear (VB2): Wear land which has an irregular width and for which the profile generated by the intersection of the wear land and the original flank varies at each position of measurement. The non-uniform flank wear of a carbide end mill insert is illustrated in Fig. 3.17(b).

Localized flank wear (VB3): An exaggerated form of flank wear which develops at a specific part of the flank.

One special form of this type of flank wear is notch wear which develops on that part of the major flank adjacent to the work surface during cutting.

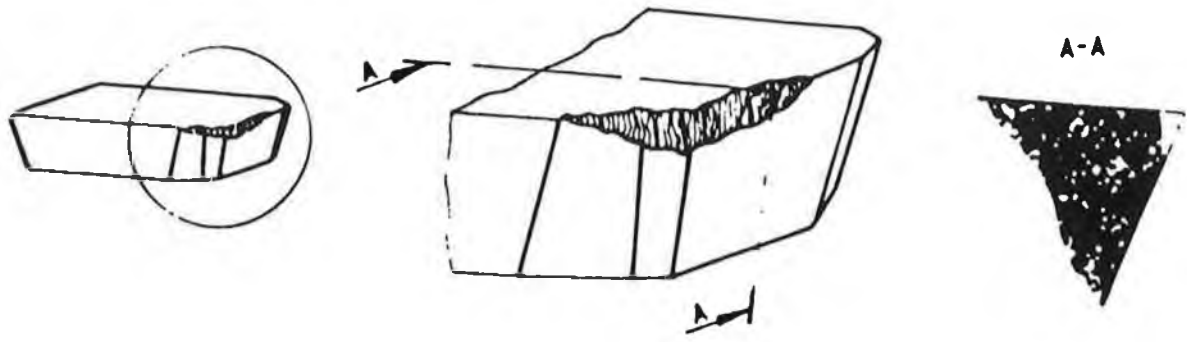
Another special form of this type of flank wear is groove wear which develops on that part of the minor flank adjacent to the machined surface during cutting.

A third special form of localized flank wear occurs sometimes at the point of intersection of two straight parts of the cutting edges. The localised flank wear of carbide insert is illustrated in Fig. 3.17(c).

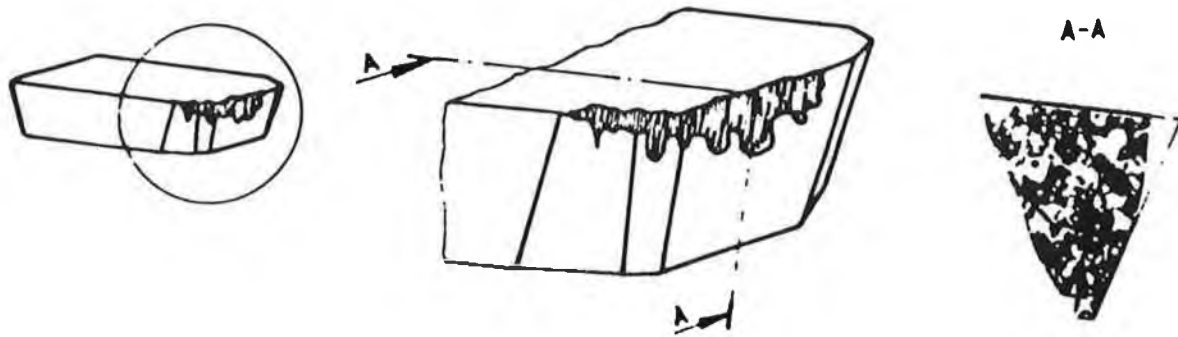
Tool wear and failure mechanism

There are two categories into which degrading processes associated with cutting tools can be placed:

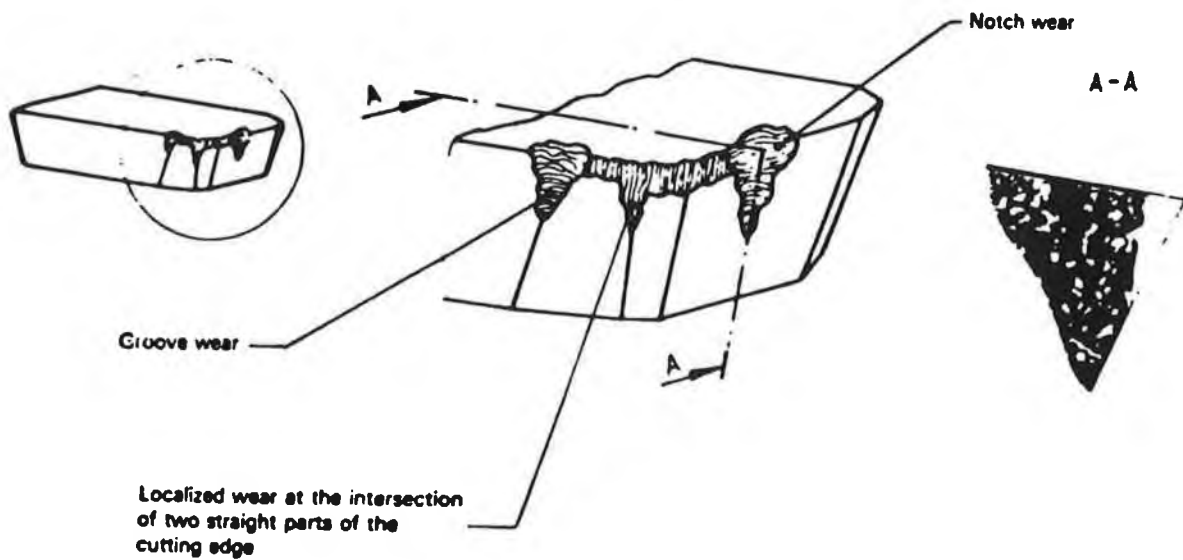
- (i) progressive wear of the tool
- (ii) mechanism causing an abrupt premature failure



(a) Uniform flank wear (VB1)



(b) Non uniform flank wear (VB2)



(c) Localized flank wear (VB3)

Fig.3.17: Flank wear of a carbide insert of an end mill

(i) Progressive wear of the tool

Wear means any process by which material is removed from tool surface in the form of very small particles. The four types of wear listed below are very broad subject areas. There are variations in the mechanisms of each type, depending on the nature of sliding systems and the environment. However, this discussion is primarily concerned with describing tool degradation. Thus the mechanisms of wear are only discussed briefly.

(a) **Adhesion wear:** When two surfaces are brought into intimate contact under moderate loads they form welded junctions (adhesive bonding) at the asperities (Fig.3.18). This phenomenon is known as "adhesion". When these welded junctions subjected to shearing loads are subsequently destroyed. Shearing can take place either at the original interface or along a path below or above it. The fracture path depends on whether or not the strength of the adhesive bond of the asperities is greater than the cohesive strength of either of the two bodies. The common mode of failure is shearing below this line. During material cutting it is accepted adhesion bonding (pressure welding) can occur between chip and tool and between workpiece and tool. Because of strain hardening the adhesive bonds are often stronger than the base material. As these junctions fracture small fragments of tool material are carried away by sticking either to the underside of the chip or to the newly generated workpiece surface. Adhesion is important at relatively low speeds as the process is both time and temperature dependent.

(b) **Abrasion (abrasive wear):** Abrasive wear is the result of a hard, rough surface, or a surface containing hard protruding particles, rubbing over a softer, more ductile surface. The mechanism of wear particle removal is basically one of formation of microchips, thereby producing groves or scratches on the softer surface. This is basically the cutting process. Consequently the amount of wear depends on the hardness of the contacting surfaces and elastic properties of the mating geometries. In material cutting, the hard particles responsible for abrasive wear are located on the underside of the chip and pass over the tool rake surfaces. The particles may be one or both of the following:

- (i) hard constituents present in the work material (carbide in case of Inconel 718 and MMC)
- (ii) fragments of a highly strain hardened and unstable built up edge.

In addition, fragments of the harder tool material may adhere to the underside of the chip early in the contact zone. Subsequently these fragments abrade additional tool material during the period of chip tool contact. Abrasive wear may occur on the tool flank. In some cases one may envisage these hard particles of the tool material becoming embedded in the softer workpiece material and causing wear by two body (Fig.3.19 a) or three-body abrasion (Fig.3.19 b).

(c) **Diffusion:** When a metal is in sliding contact with another metal and the temperature at their interface is high, conditions may become right for atoms from the harder metal to diffuse into softer matrix, thereby increasing the hardness and abrasiveness of the softer metal. On the contrary atoms from the softer metal may also diffuse into the harder medium weakening the surface layer of the latter to such an extent that particles on it are dislodged, torn (or sheared off) and are carried away by the flowing medium (Fig.3.20). The amount of diffusion wear occurring will depend on the following:

- bonding affinity of the tool and workpiece pair
- the level of atomic agitation (strongly temperature dependent)
- length of contact time at the elevated temperature

(d) **Fatigue wear:** Fatigue wear results when the surface of a material is subjected to cyclic loading such as in rolling contact. When two surfaces slide in contact with each other under pressure, asperities on one surface interlock with those of the other. Due to the frictional stress, compressive stress is produced on one side of each interlocking asperity and tensile stress on the other side (Fig. 3.21). After a given pair of asperities have moved over or through each other, the above stresses are relieved. New pairs of asperities are, however, soon formed and the stress cycle is repeated. Thus the material of the hard metal near the surface undergoes cyclic stress. This phenomenon causes surface cracks which ultimately combine with one another and lead to the crumbling of the hard metal. In addition to mechanical fatigue due to cyclic loading, another type of wear is by thermal fatigue. Here, cracks on the surface are generated by thermal stresses due to thermal cycling, such as in end milling tooth in cut (heating) and out of cut (cooling). Further, the hard metal may also be subjected to variable

thermal stress owing to temperature changes brought about by cutting fluid, chip breakage and variable dimensions of cut, again contributing to fatigue wear.

(ii) Mechanisms causing an abrupt premature failure

Premature tool failure mechanisms can be subdivided into two groups as:

- brittle failure
- plastic failure

Brittle failure: Brittle tool failure involves the development and propagation of micro cracks in the tool material. Micro cracks may develop when the tool surface is subjected to cyclic loading and thermal cycling (thermal stress due to heating and cooling of tool). Cutting tools are generally weaker in tension than compression. It is likely that brittle failure will occur when some portion of the tool is subjected to a tensile stress. In order to assess the true stress situation it is necessary to consider how the cutting forces are distributed on the tool face and also to take into account the thermal stress. Micro cracks will develop at dangerous points when the stress-state is such as to cause local rupturing of the interatomic bonds. The theoretical prediction of when cracks are likely to occur is extremely difficult due to the complex stress situation and the determination of reliable strength properties of brittle material.

Frequent chipping of cutting tools occurs due to the occurrence of cracks in the cutting part of a tool followed by the loss of small fragments of tool material. High positive rake angles can contribute to chipping due to a small included angle of the tool tip. It is also possible that crater wear may progress toward the tool tip and weaken it, thus causing chipping. Chipping or fracture can be reduced by selecting tool materials with high impact and thermal shock resistance with negative rake angle.

Plastic failure: During the material cutting process very high stresses and temperatures are generated within the tool material. The elevated temperatures that occur in the tool-chip workpiece contact zone can cause an initially sharp tool to lose some of its strength and hardness. The tool can then flow plastically, under the pressure developed

by the cutting forces. Edge depression and bulging cause the clearance angle to be reduced to zero for a portion along the tool flank. Thus, for some time the contact area between the tool and workpiece increases. During this period, layers of the tool material in contact with the workpiece gradually detach. The large area of contact results in substantial increases in friction between the cutting tool and workpiece. Consequently cutting temperature increases which causes the tool material to soften further and eventually fail. When plastic deformation occurs at the tertiary region of the wear land-time characteristic (curve) which is very short and can start at very low values of wear land.

Tool wear sensing and measuring techniques

Many attempts have been made and techniques suggested for the measurement of cutting tool wear. Several tool wear sensing models have been developed that correlate tool life with parameters that describe the machining environment, cutting condition, surface characteristics and cutting tool and workpiece material. The author [60] has discussed in detail various tool wear sensing techniques. Though more methods have been developed for tool wear sensing, none of these have achieved significant use in industry. Most of the authors [110,115-117] have classified the tool wear sensing techniques into two major classes:

- direct method
- indirect method

Direct method: These methods are usually concerned with measuring the actual tool wear and generally involve taking measurements associated with the volumetric loss of cutting tool material or changes in tool profile and, therefore, tend to be an " off line" techniques, since measurement can usually only be taken when the tool is out of cut. The two major disadvantages associated with off line techniques are that firstly, they can be very time consuming from a production rate standpoint, and secondly, the onslaught premature cutting edge failure, whilst the tool is actually in cut cannot be detected. Direct methods include the following main techniques:

- (a) optical scanning techniques(Microscope and other optic methods)
- (b) wear particle and radioactive technique

- (c) weighing method
- (d) electrical resistance method
- (e) Proximity sensors

Indirect methods: These methods are concerned with detecting some process born features from tool wear. These include measurement of cutting forces or torques, vibrations, roughness of machined surface, temperature and thermo-electric effects and acoustic emissions. These methods are considered as being 'on line' techniques. On-line techniques by their very nature, have the potential of eliminating the problems faced by direct methods. These methods are expensive due to the electronic circuitry and instrumentation needed and also there are problems involved concerning reliability and calibration. The indirect method (measurement) includes the following techniques:

- (a) acoustic emission signal measurement
- (b) cutting forces
- (c) roughness measurement
- (d) cutting temperature measurement
- (e) power/motor current
- (f) vibration measurement

The most common and reliable technique is the direct optical measurement. ISO 8688 also recommends to measure flank wear profile by tool makers' microscope. So, principle of tool wear measurement by optical technique is discussed below:

Optical technique: The use of optics to study the extent of a tool wear zone is a common technique. Optical tool-wear sensing devices utilise the light reflected from the wear land of a worn tool as a means of measuring tool wear. Generally, these methods rely upon the higher reflective properties of the wear-land compared with the unworn surface. The wear zone can be visually studied using tool maker's microscope or scanning electron microscope. The use of tool makers' microscope to determine the tool wear is a simple method which is commonly used on the shop floor. The tool makers'

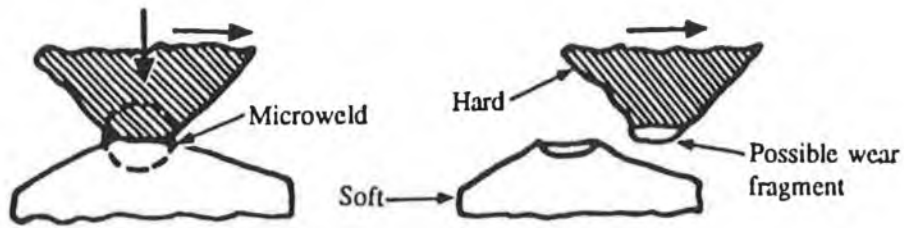


Fig.3.18: Schematic illustration of adhesion of material

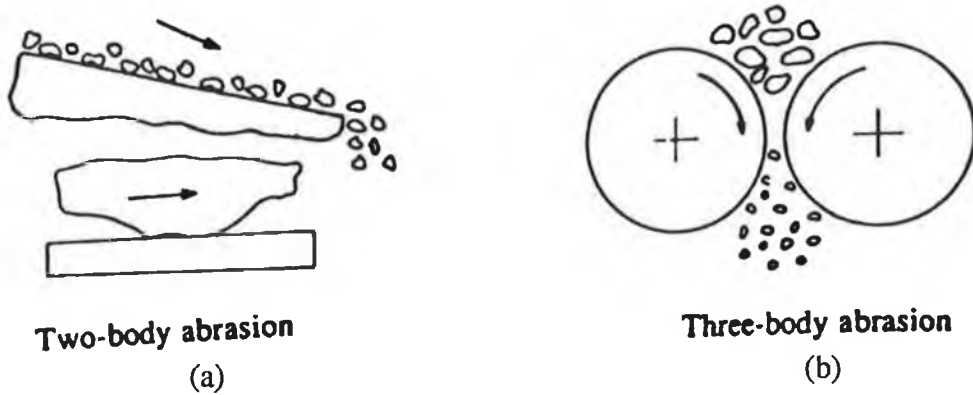


Fig.3.19: Schematic illustration of two body and three body abrasive wear

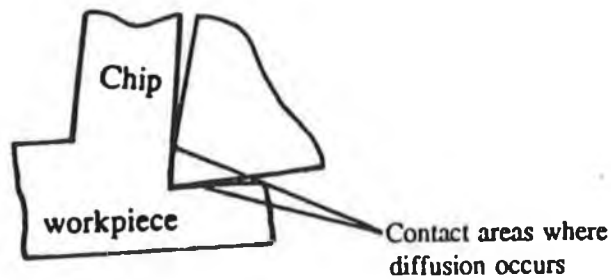


Fig.3.20: Wear by diffusion

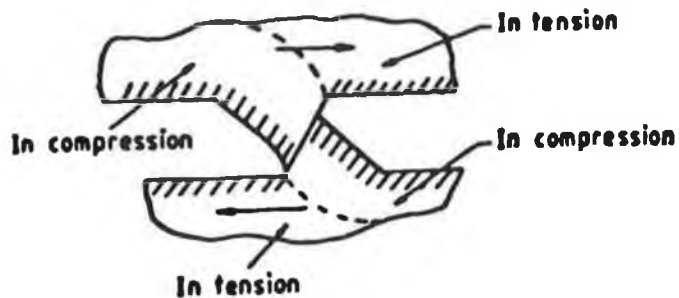


Fig.3.21: Stress distribution around the interlocking asperities

microscope is a precision optical measuring instrument. The tool is usually placed on the stage glass surface of the microscope. The stage glass surface is normal to the optical axis. The tool worn point is illuminated by light. The light can be adjusted so that the brightest image can be obtained. The object can be magnified by the objective and eyepiece of the microscope. Direct reading of the worn tool can be obtained by the counter or digimatic head installed in the microscope.

As there is no physical contact with the tool the same principle is used in many on-line methods, providing that the cutting tool is not permanently in contact with the workpiece. The tool is illuminated and the image formed by the reflected light is displayed on a TV screen or fed into an image analyzing computer. Optical and electro-optical methods analyze the image of the illuminated wear zone when the cutting tool is not continuously in contact with the workpiece. Consequently this proposed sensing set up can be only used in the cutting process such as milling where the cutting edge does not contact the workpiece during more than half rotation of the cutter, and can be exposed to a light beam.

Tool life criteria

To increase reliability and comparability of test results it is useful that tool life be defined as the effective cutting time of the tool to reach a specified value of tool life criterion. Flank wear of the cutting tool is common in a material cutting operation. So, in this work tool life end point criteria is considered on the basis of the effective cutting time to reach a certain width of flank wear as :

(a) Tool life criteria for solid HSS end mill cutter

(i) if the flank wear (on the major cutting edge) is uniform then 0.3mm averaged over all teeth can be used as criterion for tool life i.e.,

$$\text{Average } VB1 = \frac{1}{z} \sum_{i=1}^z VB1(i) = 0.3mm \quad (3.42)$$

Where VB1- uniform flank wear and z - number of teeth.

(ii) if the flank wear land (major cutting edge) is non-uniform (VB2) and localized(VB3)

then $VB_{\max} = 0.5$ mm on any individual tooth can be used.

The above flank wear criteria for tool life end point has been recommended for solid HSS end mill when cutting mild steels. ISO 8688-2 also recommends that when chipping occurs it may be treated as localized wear using a VB3 value equal to 0.5 mm as a tool life end point.

(b) Tool life criteria for cemented carbide throw away inserts

(i) If the flank wear(major cutting edge) is uniform (VB1) then 0.30 mm averaged over all teeth.

(ii) If the flank wear(major cutting edge)is non uniform(VB2) and localized(VB3) then 0.75 mm averaged over all teeth or any individual tooth

The above flank wear criteria for tungsten carbide was considered when machining advanced materials i.e. Inconel 718. This conservative tool life criteria for a carbide cutter was considered because of the use of the advanced materials in the design of high strength and reliable components. Excessive flank wear may cause sub-surface change in the machined surface.

It may be noted that ISO 8688-2 recommends flank wear criteria for tungsten carbide inserts (**normal cutting operation**) when machining mild steel with a slight difference, as:

(a) $VB1 = 0.35$ mm

(b) $VB2 = 1.2$ mm

(c) $VB3 = 1.00$ mm

General tool life curve for an end mill cutter

ISO 8688 suggests the plotting of flank wear (VB) against effective cutting time in the following manner as shown in Fig. 3.22 and 3.23. It is normal for the curve to exhibit three distinct regions i.e.

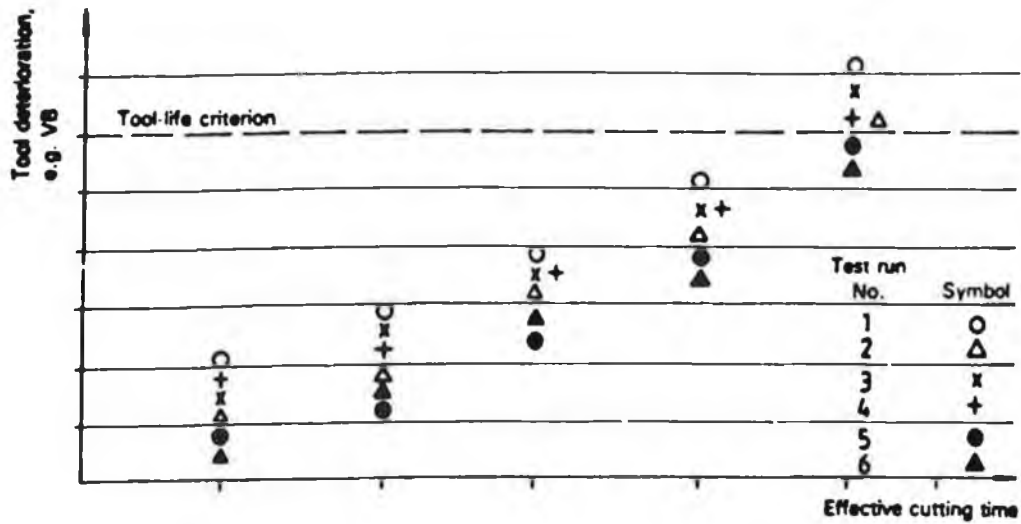


Fig.3.22: Tool deterioration values for a number of tests runs plotted against cutting time

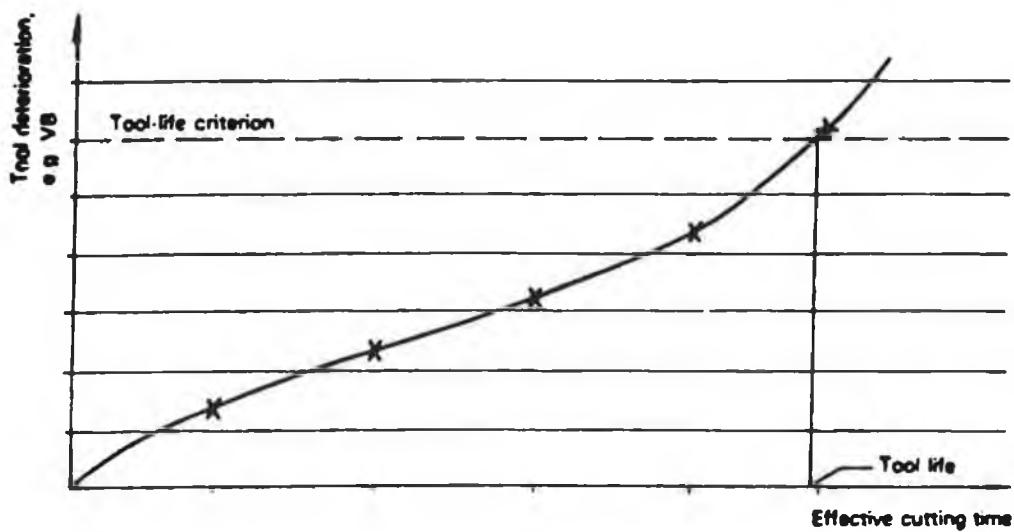


Fig.3.23: Arithmetic mean values of tool deterioration for a number of test runs against cutting time

- (i) an initial rapid wear rate
- (ii) an approximately constant wear rate
- (ii) a final zone of rapid wear leading to failure.

Factors effecting tool life in milling

The factors which are normally considered to influence the life of a cutting tools are shown in Fig.3.24. A brief description of each factor is given below:

(i) Machine Variables

(a) Cutting speed

The cutting speed has the maximum influence on tool life. Tool life decreases as the cutting speed increases. Higher cutting speed increases tool temperature and softens the tool material. It thereby aids abrasive, adhesive and diffusional wear and consequently the predominant wear may be flank wear and face wear. The cumulative effect is an exponential decrease in tool life as given by Taylor's [57] tool life equation. The effect of temperature in material cutting together with the dependence of tool wear on temperature, has been examined by several authors [42]. It has been suggested that tool life is directly influenced by temperature.

(b) Feed

The larger the feed, the greater is the cutting force per unit area of the chip-tool contact on the rake and work-tool contact on the flank face. Cutting temperatures and therefore the different types of wear are increased. An increase in cutting force as a result of larger feed also increases the likelihood of chipping of the cutting edge through mechanical shock.

(c) Axial depth of cut

If the axial depth of cut is increased, the size of the cut is also increased. Cutting temperature also increases as cutting forces are proportional to the size of the cut. Here the rise in tool temperature is relatively small because the area of the chip-tool contact increases roughly in equal proportion to the change in axial depth of cut (such is not

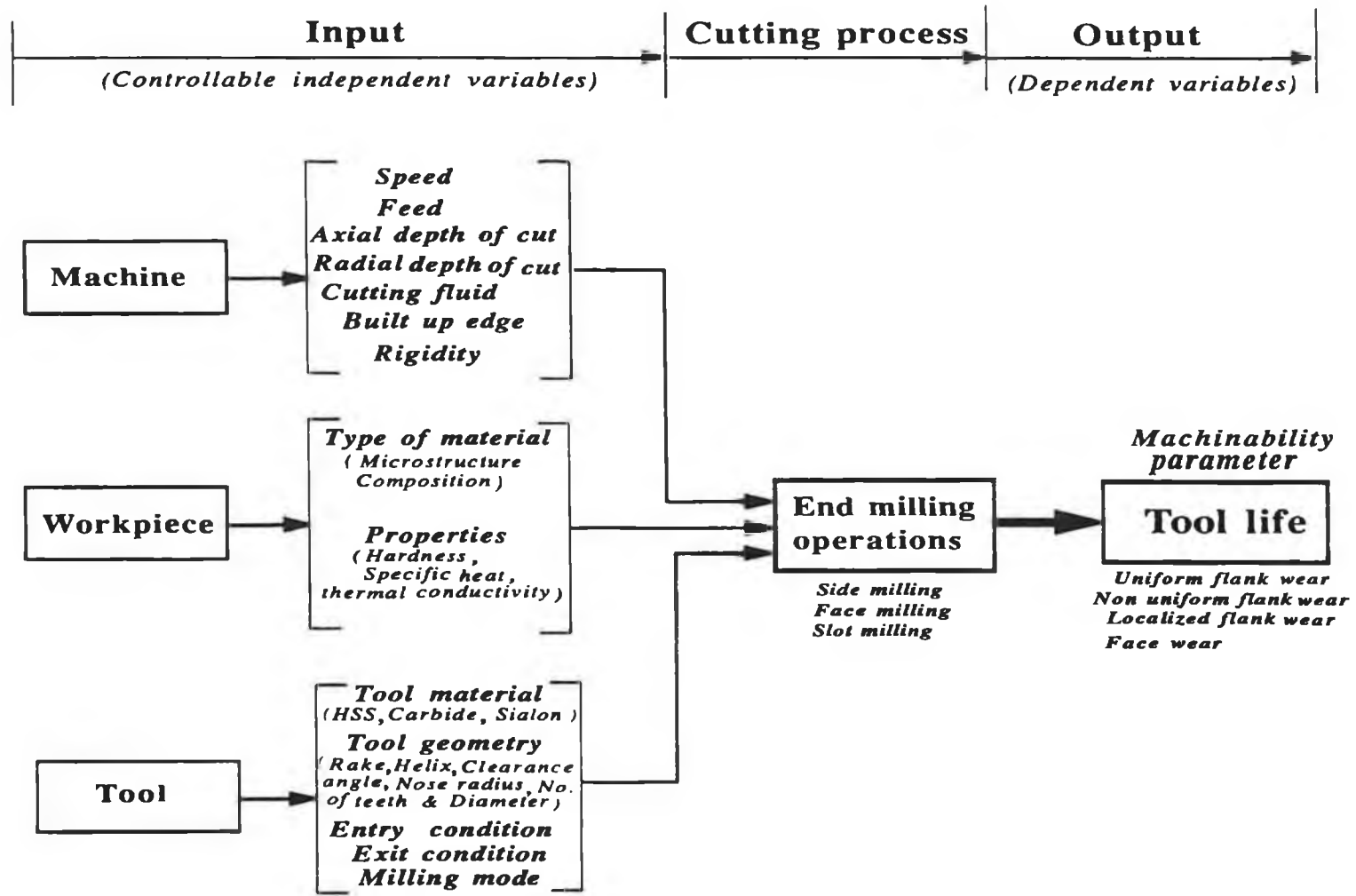


Fig.3.24: Factors influencing tool life in end milling processes

the case when feed is changed. In that case, the proportionate change in temperature is larger. This is on account of the fact that the area of chip-tool contact changes by a smaller proportion than the change in feed rate). Thus an increase in the axial depth of cut shortens tool life to some extent by accelerating the abrasive, adhesive and diffusional type of wear.

(d) Radial depth of cut (immersion ratio, a_r/D or width of cut)

Radial depth of cut generally has an influence of the same order of magnitude on tool life similar to axial depth of cut. Tool life varies non proportionately with immersion ratio [105]. Radial depth of cut does not influence the specific cutting energy. On the other hand, in proportion to greater radial depth of cut the cutting energy and heat rise. As, simultaneously, condition of heat abstractions deteriorates, a slight rise of temperature is observed when radial depth of cut is increased. The phenomenon is more pronounced with higher cutting speeds.

In general, the velocity has the greatest effect on tool life, followed by the feed and depth of cut.

(e) Built up edge

Under certain cutting conditions a built up edge is sometimes formed in the case of certain tool-work pairs. The built-up edge sticks to the actual cutting edge of the tool and being in a work hardened condition itself starts acting as a cutting edge. The built up edge increases the effective rake angle of the tool and, reduces the cutting forces, tool temperature and tool wear. However, the built up edge has a tendency to grow in size, becomes unstable and finally breaks up. The fragments of the built up edge get rolled away over the rake face and flank face. While doing so, these fragments severely abrade the respective surface. The net effect of the built up edge is flank wear and a decrease in crater wear.

(f) Cutting fluid

The effect of a cutting fluid over the lower range of cutting speed is smaller than at higher cutting speed. The cutting fluid cools the chip and workpiece and may reduce to some extent the friction at the tool-work and tool chip interfaces. Therefore, cutting

temperatures are decreased. Generally a reduction in temperature results in a decrease in wear rate and increase in tool life. This occurs because, first, the tool material is harder and so more resistant to abrasive wear at lower temperatures, secondly, the diffusion rate of constituents in the tool material is less at lower temperatures. Opposing the above effect, a reduction in the temperature of the workpiece will increase its shear flow stress, so that cutting force and power consumption may be increased to some extent. Under certain conditions this can lead to a decrease in tool life [82]. If a tool material has low value of hot hardness (HSS) there is a appreciable increase in tool life as a result of a copious supply of the coolant to the cutting zone. However in the case of carbides and ceramics which have a higher value of hot hardness, a cutting fluid has a negligible effect on tool forces or tool life. Attempts to apply cooling in face milling using sintered carbide teeth, with a view to extending tooth life were unsuccessful as the intermittent cutting of the tooth results in rapid periodical heating and cooling [78]. This, in turn causes or accelerates the cracking of an inserted tooth due to thermal cooling.

(g) Rigidity of machine tool-work system

The machine, tool and work constitute a vibratory system having several significant modes of vibration with corresponding modal stiffness and damping. The larger the individual stiffness of machine, tool and work, and larger the inherent or inbuilt damping, the greater is the dynamic rigidity of the system and less prone is it to large amplitude of vibration and chatter. On the other hand if the machine is not properly designed, if the workpiece is long and thin, or if the tool overhang is excessive, chatter may occur during cutting. It is known that chattering may cause fatigue failure or catastrophic failure of the tool due to mechanical shock.

(ii) Workpiece variables

The common variables considered are work material composition and microstructure (heat treatment), its hardness (or tensile strength) and work hardening properties. It may be expected that the harder the work material, the lower the tool life. It has been shown that cutting temperature is increased with workpiece material hardness. A number of investigators [82] have shown that the cutting speed for fixed tool life is related to the hardness by an equation of the type:

$$v = \frac{C_{21}}{(BHN)^\delta} \quad (3.43)$$

Where v - cutting speed for a fixed tool life T , and BHN - Brinell hardness number and C_{21} - a constant will depend on the work material and tool material. The exponent " δ " will vary with tool material.

The hardness of a material depends on many factors, for example its composition, its structure and any treatment it has undergone related to tensile strength. It is well known that the mechanical and thermal properties (specific heat and thermal conductivity) of the work material have a considerable effect on tool life. Workhardening tendencies usually reduces the tool life. When insufficient allowance is left on a component for the finish pass, the tool may cut a layer of work hardened material with a resulting decrease in tool life.

Inclusion of small proportions of various additives intentionally or as impurities does not always improve tool life. Slag and sand particles are abrasive and tend to reduce tool life; surface scale on casting has a similar effect. It is generally useful to check the hardness as well as the microstructure when inspecting a work material. Sometimes for a given hardness the tool life will vary over a wide range by having a different microstructure.

The properties of a work material that tend to increase the life of the tool include the followings:

- (a) softness (or lack of hardness) to reduce cutting forces, cutting temperature and abrasive wear
- (b) absence of abrasive constituents such as surface scale, sand and slag inclusions
- (c) presence of desirable additives like lead to act as boundary lubricants and sulphur to reduce cutting forces and temperature
- (d) lack of work hardening tendency that tends to reduce cutting forces and temperature and also abrasive wear

- (e) occurrence of favourable microstructure; tool life varies with nature of pearlitic structure. Spheroidized pearlite is favourable to tool life whereas lamellar pearlite has harmful effect.

(ii) Tool variables

(a) Tool material

In general the properties of the tool material which enhance its life are the following:

- (a) high hot-hardness to resist deformation, adhesion and abrasion at the relatively high cutting temperatures occurring on the rake and flank faces of the tool, especially at high cutting speeds.
- (b) toughness to resist sudden loads in interrupted cutting.
- (c) wear resistance
- (d) lack of chemical affinity with work material
- (e) high thermal conductivity and specific heat (combined with low co-efficient of thermal expansion).

Little is known as to the properties of carbides which influence their wear rate when used as cutting tools. Moreover, it is, in general difficult to directly compare widely different grades because of the constraint on their tool life, i.e., the use of straight grades at high speed will lead to their failure due to cratering, whilst the steel cutting grades will still fail due to flank wear. Conversely the use of steel cutting grades on high nickel alloys will almost invariably lead to their failure due to notching [49]. The properties of carbides are governed by the grain size and percentage of cobalt binder. The larger the tungsten carbide grain size and the greater the cobalt content, the lower the toughness and impact resistance. For longer tool life, the tool with the finest grain size and lowest cobalt content is preferred.

Ceramic tools like oxide, sialon have most of the desirable quantities for good cutting i.e., high hot hardness and wear resistance, but they are brittle and have poor shock

resistance. The use of ceramics in milling is limited. Large negative rake angle and chamfered cutting edges are recommended.

From the preceding discussion it is evident that the effect of a tool material is entirely complicated and it is impossible to use a straight scaling factor to arrive at the relative performance depending, to a great extent on the work material and the required value of tool life.

(b) Tool geometry

Clearance angle: The influence of a clearance angle is characterized, in the case of increasing angle, by diminishing friction, but also by simultaneous weakening of the tool corner. If the clearance angle is increased, the volume of wear required to reach a particular width of flank wear land is also increased. Therefore, larger tool life values are obtained in the case of larger clearance angle and vice versa. On the other hand, the larger the clearance angle, the smaller is the mechanical strength of the cutting edge and more liable to chipping or fracture. It may be supposed that a certain optimum value of clearance angle should exist for which tool life would attain its maximum.

Rake angle: The effective rake angle increases when the normal (back) rake angle is increased. The cutting forces decrease with the increase of rake angle because of small shear strain. Since the cutting forces are less, so temperatures and tool wear decreases. Consequently, tool life improves when rake angles are increased. However, larger rake angles make the cutting edge shorter. High rake angle in face milling results in a longer tool life due to less heat generation, less deformation and work hardening of tip [42]. Increasing a rake angle results in a decrease of natural contact length between tool and tip. The frictional forces on the rake face are directly proportional to the tool-chip contact area. However, larger rake angles make the cutting edge shorter and reduces its mechanical strength making the tool liable to chipping. Therefore, there is an optimum rake angle associated in every tool-work pair.

Helix angle: The helix angle affects the manner of chip flow and influences the rake chip contact pressure distribution and contact dimension. Thus the helix angle value is likely to influence significantly the temperature distribution at the rake face at right

angles to the edge in velocity direction and hence to affect the average temperature at the flank. So the amount and pattern of wear on tool face varies with helix angle. However the influence of helix angle on a tool tip has a similar character to that of clearance and rake angle [78]. The reduction of a helix angle causes a growth of tooth mass and thus heat resistance. On the other hand, a small helix angle results in rising friction and the number of teeth cutting simultaneously increases and unfavourably influence the resolution of cutting forces by increasing the tangential component (F_t) which in turn may cause the appearance of microchips in the teeth. The authors [118] have indicated that the larger the helix angle, the greater was the angle made in the plane of the rake face between the direction of chip flow and normal to the cutting edge thus increasing the length of rubbing between the chip and rake face. This shortens tool life. So, there exists also an optimum value of helix angle for a tool. Past researches on plain milling with a cutter with a helix angle within practically applied limits (20-45°) have shown that their effect on tool life is small [78].

Nose radius: Small nose radius results in excessive stress concentration and greater heat generation. Increase in nose radius increases the chip equivalent(q) and improves tool life. But increase in nose radius decreases the surface finish. So, there is a compromise between the two.

Cutter diameter: In general an increase in cutter diameter increases the tooth travel but at the same time the undeformed chip thickness decreases provided the cutting conditions remain the same. This causes an increase of work time and friction and simultaneously diminishes the resistance met by the cutter tooth, while the angular pitch of the teeth and the mass of the milling cutter increase. This phenomenon is accompanied by an improvement of cooling conditions, better heat extraction and lowering of tooth temperature. As a result, a larger diameter of cutter raises tool life with the same cutting conditions.

Number of teeth: The influence of the number of cutter teeth on tool wear is explained by the fact that with the growing number of teeth, and other cutting conditions remaining unchanged, there occurs;

- (a) an increase of mean value of tangential force and cutting power and therefore also of mean energy and cutting heat.
- (b) a reduction of space between teeth worsens the conditions of chip flow and heat abstraction
- (c) a reduction of volume and mass of particular teeth.

All these cause an increase of tooth temperature, and thus the acceleration of tooth wear. Wang et al. [119] and Kuljanic [48] have shown that an increase in the number of teeth results in higher tool temperature which increases diffusion rate.

(c) Entry condition

The influence of entry conditions on milling cutter life has been investigated by previous authors notably Kronenberg [49] and Optiz and Beckhaus [49]. Unfortunately, the work carried out has all been directed to an understanding of the face milling process which makes the results much more difficult to analyze. A change in cutter offset can change several variables simultaneously. Fig.3.25 shows the basic geometry of the process when a face milling cutter D is used to machine a blank width d_b , the offset of the cutter centre line with respect to the centre line of the blank d_b being the distance " e ". It is evident that a change in " e " leads to changes in the shape of chip, the equivalent feed rate, the time in and out of cut and the entry and exit conditions. If the secondary variables of chip shape, entry and exit conditions have no influence on the process, it is evident that a plot of tool life against distance offset should be symmetrical about the line $e = 0$ as shown in Fig.3.26 [49].

At the two extreme positions in face milling, given by the expression [49]:

$$e = \pm \frac{1}{2} (D + d_b) \quad (3.44)$$

the process of face milling becomes comparable to end milling, the two extremes representing the up and down milling modes. In many cases, especially when machining very hard or extremely work hardening materials, the relationship between tool life and distance offset is not symmetrical about the line $e = 0$ and takes the form in Fig. 3.27 [49]. This is explained from Fig. 3.28 [49] that initial contact between workpiece and

tool may occur as a point, line or full area of contact. Moreover, it would seem reasonable to consider that the impact should be kept away from the cutting point "S" in a tool so that tool breakage is to be avoided. The partial area of engagement is defined as the area which is crossed by the index line before the point " S " is reached (the index line being the line formed by the intersection of the plane "STUV" and the plane in which the rake face of the tool lies). The authors[46,75] then went on to show that the geometric relationships between the partial area of engagement and the distance offset were of the same form as the relationship between tool life and distance off-set, the higher the partial area of contact, the higher the resulting tool life.

(d) Exit condition

The fact that exit conditions influence the wear rate of milling cutters is well known and has been reported by Gilbert and Takeyama [49]. The mechanism which is normally suggested for this influence is the stress amplification produced at tool entry by the presence of deformed chip-material adhering to the tool. The type of tool degradation produced by this process is generally of a chipping nature and it is normally found that under conditions where chip sticking is prevalent then tool failure occurs remarkably quickly regardless of the cutting condition employed. It is generally found that the adhesion of chips to the tool cutting edge is the greatest with work-hardening work materials. It may be attributable to the formation of tensile cracks in the final shearing process as the tool point approaches the free surface. So, the influence of exit conditions through their influence on chip sticking can be tremendous. However, it would be seen that in most cases providing that chip adhesion is not observable then the influence of exit conditions may be neglected.

(e) Mode of milling

It is evident that the selection of one mode of milling as opposed to the other is likely to exert influence on the process which is not attributable to either entry or exit conditions [49]. The researcher [49] has tried to show the distinguishing process features i.e. shear angle and thermal strains experienced by both modes of milling. He [49] postulated that a shear angle at constant depth of cut(feed) will be lower in down milling than in up milling, thus one would expect the specific cutting pressure in down milling to be higher.

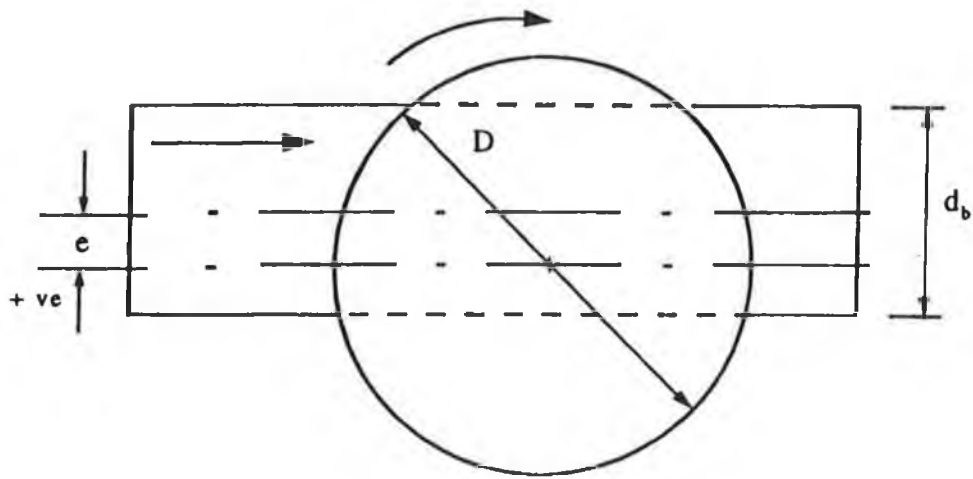


Fig.3.25: Face milling process

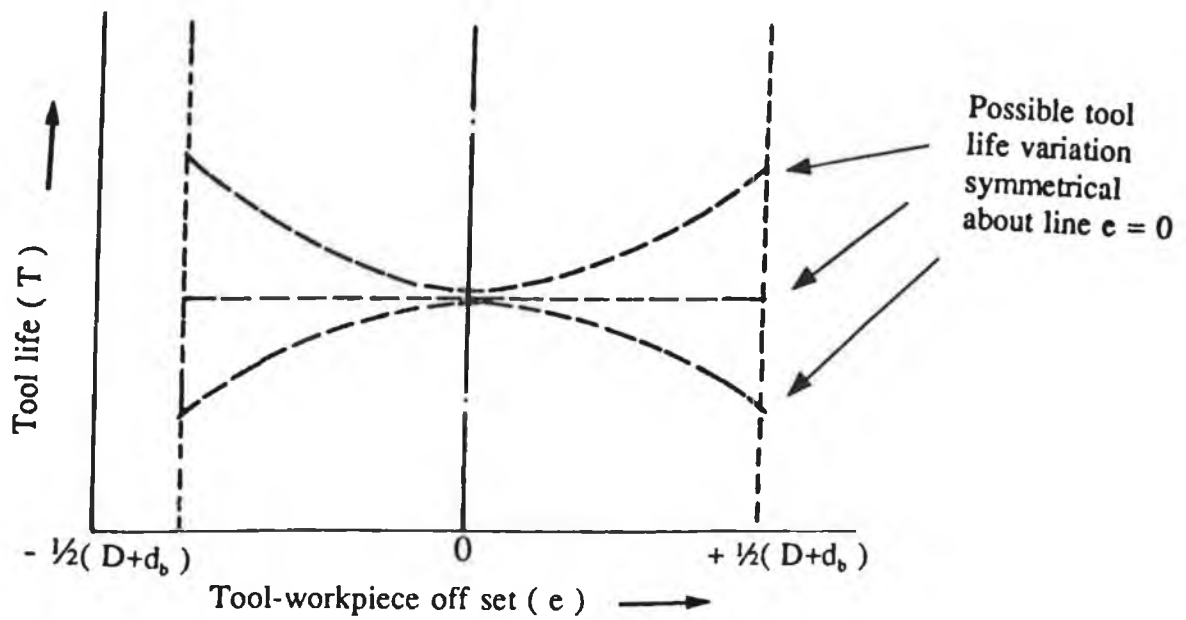


Fig.3.26: A typical plot of tool life (T) against off set (e)

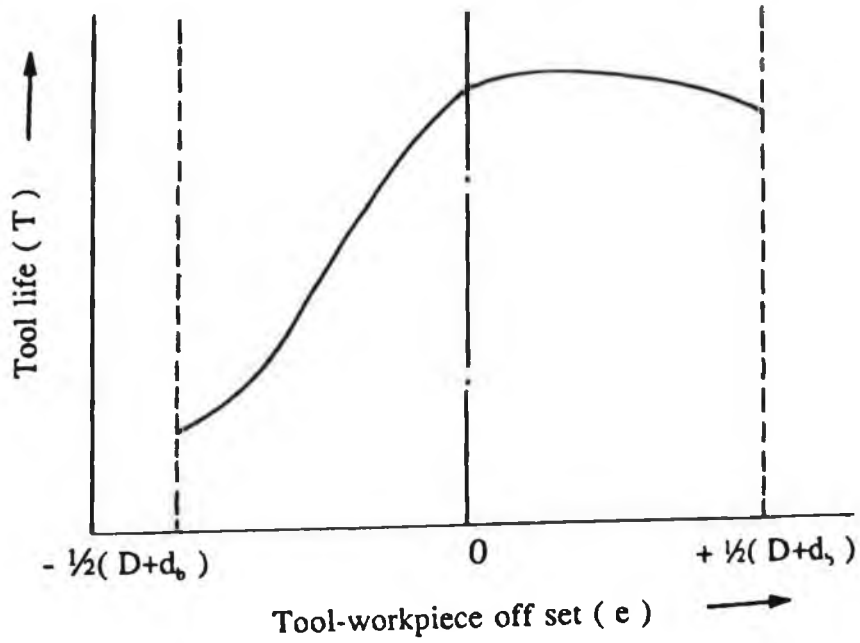


Fig.3.27: A plot of tool life (T) against distance off set in machining hard or extremely workhardening materials

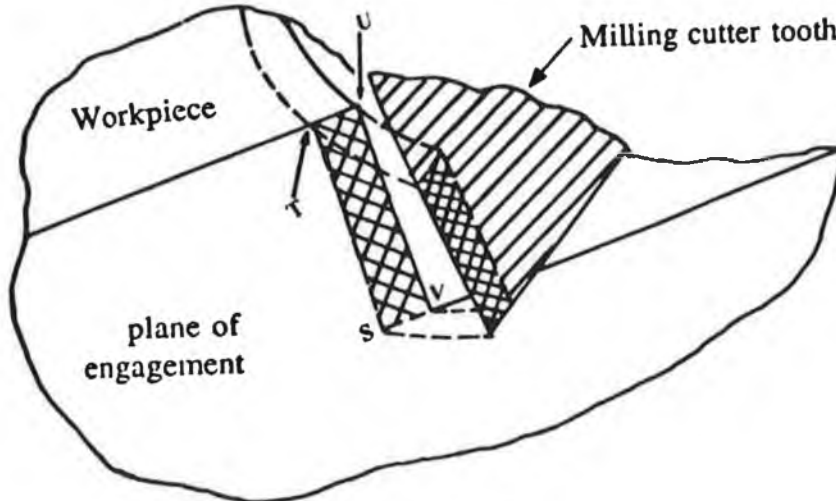


Fig.3.28: Schematic illustration of a tooth contact with workpiece in end (face) milling process

However, it was found that at low values of feed rate this trend was contradicted due to increased rubbing forces. The range of thermal strain will be higher in down milling. The authors mentioned that the above processes are extremely complex in nature and difficult to assess. However, it is well known that when machining most types of steel the differences in wear rate which occur when using the two modes of milling are small. On other materials, particularly those which significantly workharden then large differences do occur due to exit condition. The author [78] has shown that the tooth wear of a plain milling cutter in down milling mode proceeds slower than that of a cutter in up milling mode. The cause of faster wear in up milling is less advantageous condition of tooth entry into the material. As the cutting edge always has a certain roundness, in up cutting, the edge is exposed to greater pressure of friction on the flank while entering the material. This results in increased wear of the tooth.

3.3.1.3 Surface integrity aspects in end milling

In order to specify and manufacture surfaces having a high degree of integrity it has become essential to understand the need for the interdisciplinary application of metallurgy, machinability and mechanical testing to the production of surfaces. In meeting this special need the discipline known as " Surface Integrity " has come to be recognised as the inherent condition of a surface produced in a machining or other surface generating operation. The term has been widely adopted and is used to describe the nature or condition both at the actual and the sub-surface structure [120]. The more important elements which contribute to surface integrity can arbitrarily be classified under three main headings:

- topographical / surface finish
- mechanical / physical
- metallurgical / chemical

Before the advent of the term " surface integrity " the terms surface finish and surface roughness were most commonly used and these were taken to relate only to the topographical features of the surfaces. Before applying surface integrity technology, one must first decide whether a surface integrity problem actually exists or not. Surface integrity must be considered in the manufacture of highly stressed components used in applications involving human safety, high costs and predictable component life. If a surface integrity problem exists, then the pertinent surface characteristics and affected engineering properties of the material must be monitored. Surface integrity is concerned primarily with the host of effects a manufacturing process produces below the visible surface. The subsurface characteristics occur in various layer or zones. The sub-surface altered material zone (AMZ) can be as simple as a stress condition different from that in the body of the material or as a complex as a microstructure change interlaced with intergranular attack [16].

Surface finish (Surface topography)

All surfaces, regardless of their method of manufacturing and preparation, have unique characteristics referred to as surface finish or texture. Surface finish is a colloquial term widely used to denote the overall topography of a surface. Geometric properties of the machined surfaces are affected by surface irregularities and geometric structure of the surface. The surface to be shaped according to the drawing is called nominal surface or geometric surface. In practice it is usually not possible to have a nominal surface because of surface irregularities resulting from:

- (i) geometric and kinematic reproduction of tool point shape in the material being machined (taking into account vibration)
- (ii) external friction between tool point and workpiece material
- (iii) built up edge formation in the machining of certain material and within certain ranges of machining.

So the real surface differs from the nominal surface by deviations directed inward or outward interrelating to the latter. The real surface is perceived only approximately, since every observation, being a case of measurement, is weighted with certain error. Thus the observed or effective surface means an approximated image of the real surface. In order to obtain an image of the surface, a so called surface profile is used i.e., outline of a surface resulting in its intersection with a plane. Fig.3.29 shows the kinds of nominal, real and observed surface profile. So surface finish refers to the following properties of a machined surface:

- primary texture (roughness)
- secondary texture (waviness)
- errors of forms
- lay, flaws

Surface roughness: It consists of relatively closely spaced or fine surface irregularities mainly in the form of feed marks left by the cutting tool on the machined surface. Roughness is expressed in terms of mean height or depth of irregularities measured over a relatively small length or roughness sampling length.

Waviness: It includes all surface irregularities whose spacing is greater than the roughness sampling length (usually about 1 mm) and less than the waviness sampling length. It may result from machine or work deflection, chatter, vibration, heat treatment or cutting tool runout. Roughness may be considered superimposed on a wavy surface.

Errors of form: These are generally associated with deflection of the workpiece. Depending on the ratio of irregularities spacing, " S " to mean total height R_{tm} surface irregularities are distinguished as [78]:

- surface roughness when $S/R_{tm} < 50$
- surface waviness when $50 \leq S/R_{tm} \leq 1000$
- errors of form when $S/R_{tm} > 1000$

Lay: The machining (production) processes used will form a pattern on the surface. The predominant pattern of direction is known as lay. The lay depends upon the orientations of the workpiece and the cutting tool on the machine as well as the nature of the relative motion between the two. Measurements of a surface are normally made at right angle to the lay. Lay of end milling is curvilinear as shown in Fig.3.30.

Surface flaws: These are randomly spaced irregularities i.e., those which occur at some particular location on the surface or at varying intervals. Flaws could be due to inherent defects such as inclusions, cracks, blow holes etc. in the work piece that get exposed on machining or they could arise from machining process, e.g. shedding of built up edge fragments on the machined surface.

Surface finish is not specifically tied to the texture or characteristics pattern of the surface, nor it is tied to specific roughness values; however, a good finish implies low roughness and vice versa. In this work surface roughness is considered to mean surface finish.

Indices to measure surface roughness: The measurement and interpretation of surface roughness can be quite complex and even controversial. Two surfaces have the same roughness value, as measured by a profilometer, but their topography may be quite different. However, surface roughness can be measured by various indices (parameters) [16] as:

- R_a (centre line average)
- R_q (root mean square average)
- R_z (Ten point height)
- R_t (maximum peak to valley height within assessment length)
- R_{tm} (average peak to valley height)
- R_p (smoothing depth)

The various parameters which collectively help to build up an accurate picture of the surface is shown in Fig.3.31. In this work the index, R_a was used to measure the surface roughness of the machined surface which is described below:

R_a (centre line average): It is also known as the centre line average, CLA (British) and AA, arithmetic average (American). Based on the schematic illustration shown in Fig. 3.32. R_a is the arithmetic mean of the departures " Y " of the profile from the mean line. It is normally determined as the mean results of several consecutive sampling lengths " L_s ".

$$R_a = \frac{1}{L_s} \int_0^{L_s} |Y| dX \quad (4.40)$$

In practice, equation (4.40) is replaced by the approximately equivalent expression as:

$$R_a \approx \frac{1}{n_e} \sum_{i=1}^{i=n_e} Y_i \quad (4.41)$$

Because of simplicity, R_a has been recognised internationally and is widely used.

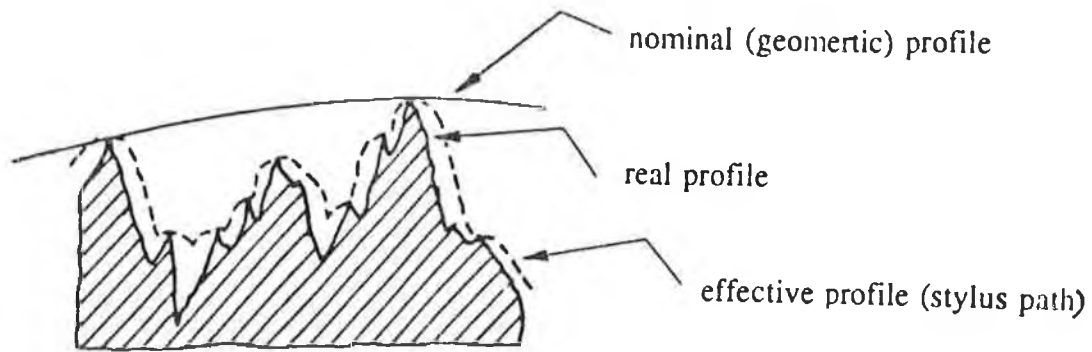


Fig.3.29: Kinds of surface profiles

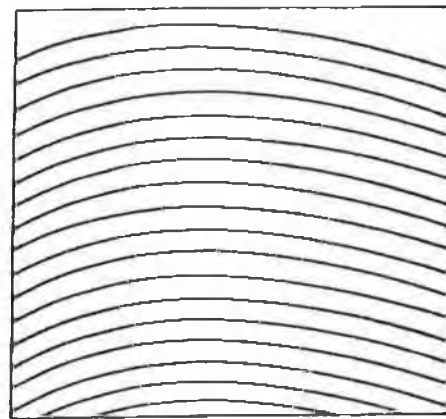


Fig.3.30: Lay direction in slot milling by an end mill insert

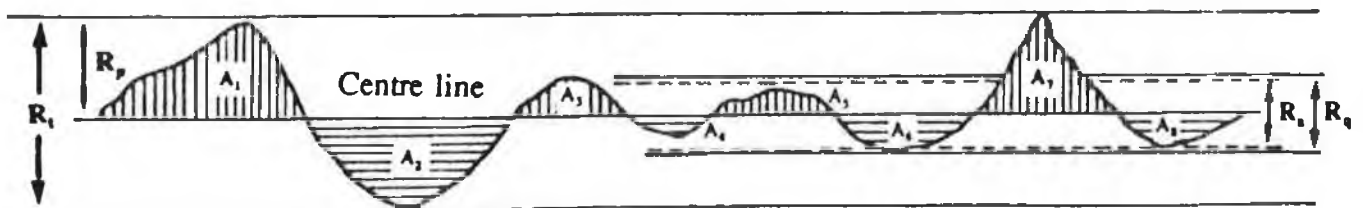


Fig.3.31: Common surface roughness parameters

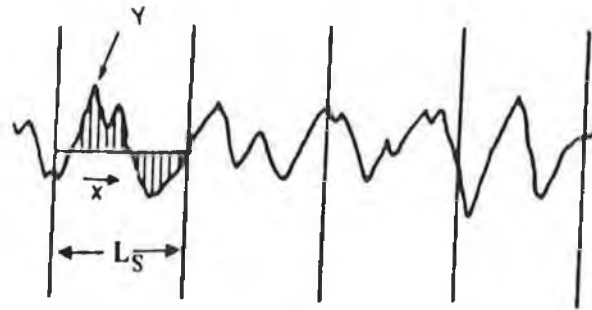


Fig.3.32: Definition of R_a

Factors influencing surface finish in end milling

Factors which influence surface finish in end milling are shown in Fig.3.33. A brief description of each factor is given below:

(i) Machine variables

(a) Cutting speed

At low cutting speeds, the shear angle is low and thus cutting forces are high. Further more, each section of the workpiece is in contact with the cutting tool for a relatively long period of time. Both these conditions encourage built up edge which leads to tearing and galling. So, surface finish decreases at low cutting speed. Due to increase in temperature and consequent decrease of frictional stress at the rake face at higher cutting speed, the tendency towards built up edge formation weakens. This effects is beneficial for surface finish. At a relatively small cutting speed, the built-up edge does not form on account of the cutting temperature being too low. As the speed is increased, conditions becomes more and more favourable for built-up edge formation. However when the cutting speed is increased further, the built-up edge size starts decreasing owing to increased tool temperature. Finally, at a sufficiently high speed, the built-up edge disappears altogether and surface finish becomes almost insensitive to cutting speed.

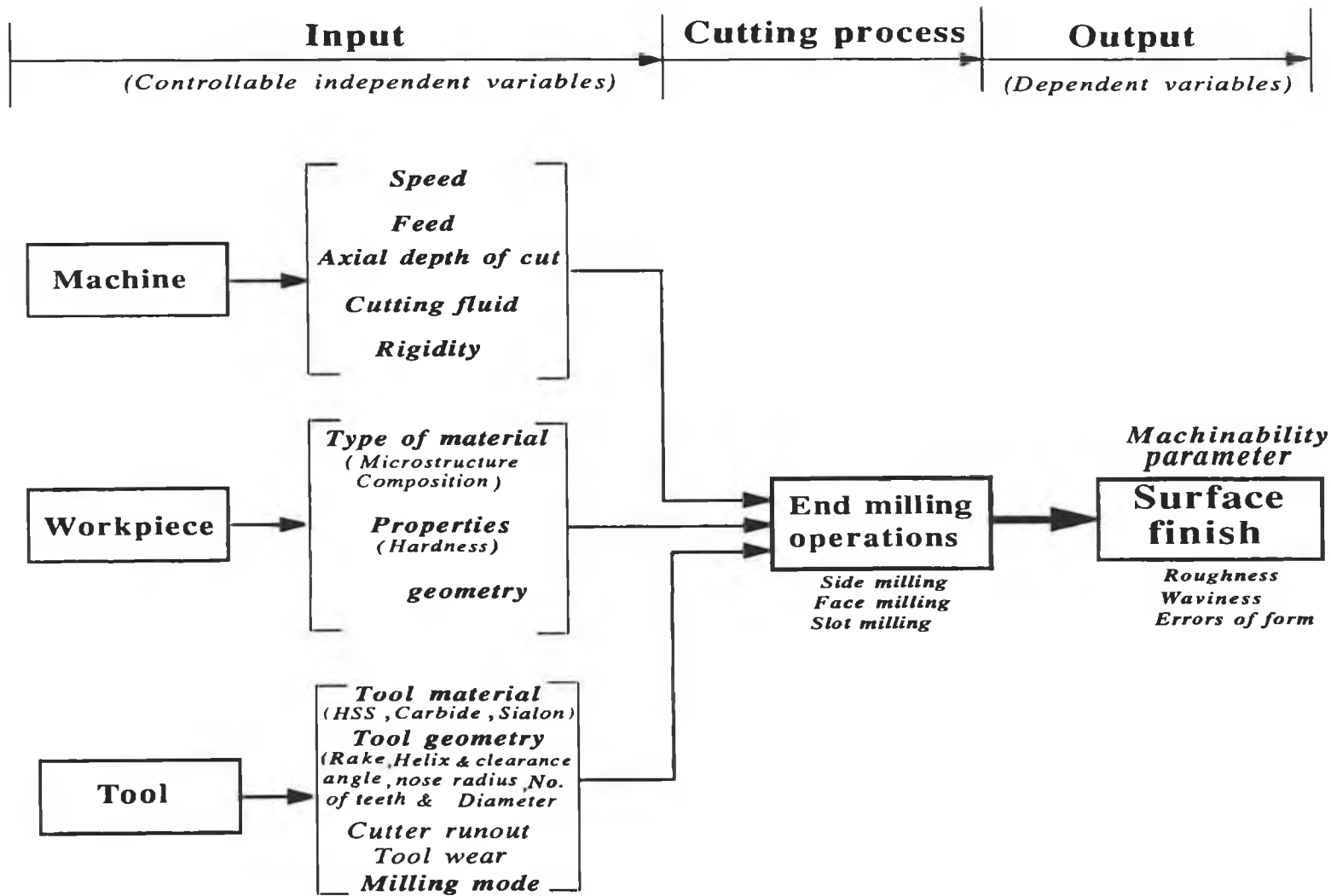


Fig.3.33: Factors influencing surface finish in end milling processes

(b) Feed

The ideal surface roughness is mainly dependent on feed. It is found that surface roughness increases with the increase of feed. Roughness height (height of the peaks and the depth of valleys of feed marks) are proportional to the square of the feed per insert. Thus, if feed per insert is cut in half, roughness will be reduced to $\frac{1}{4}$ of its previous value.

(c) Axial depth of cut:

It is well known that if axial depth of cut increases then cutting forces also increase and therefore, there is a tendency to deflection, vibration and chatter in the work-tool system. The authors[81] have shown that surface roughness increases as axial depth of cut increases. Surface error profiles have been studied in end milling as a function of axial depth of cut where it is shown that an increase in depth of cut causes a deflection of the cutter [80]. So, surface profile deteriorates due to deflection of the cutter. So, increase in axial depth of cut tends to increase surface irregularities.

(d) Cutting fluid

The use of cutting fluids during machining operations in many instances results in improvement in the reduction in the co-efficient of friction and a lessening in the size of built up edges. It is further explained that the cutting fluid penetrates into the chip tool interface by a capillary action. Following this penetration, the most effective cutting fluids reduce adhesion between chip and tool face by a chemical reaction with the newly formed chip surface resulting in the formation of a physically stable compound at the interface. The extent to which this reaction takes place is dependent on the time available for the formation of the new compound, and therefore, upon cutting speed. Besides, cutting fluid at medium to low speed reduces the formation of a built up edge. The cooling effect of a cutting fluid can also help in reducing thermal expansion and distortion of the workpiece. So, it may help to improve surface topography. A cutting fluid in some cases has an indirect effect on tool life. By acting as a coolant, it reduces tool wear and keeps the cutting edge in tact.

(e) Machine Tool- Workpiece rigidity

The machine tool affects surface finish mainly through the extent of its rigidity,

freedom from alignment errors and accuracy of motions. In general, the desirable characteristics of a machine tool are as follows:

- sufficient drive power to maintain the required cutting speed and feed without stalling
- adequate stiffness against static deflection
- rigidity and damping against vibration

Sometimes, under certain conditions cutting forces during machining produce deflection, vibration and chatter of the work tool system. In milling deflection, vibration and chatter lower the surface quality and destroy the tools. The appearance of vibrations is particularly connected with tooth wear and increase of cutting edge radius. So, in milling attention should be given for means to rigidly support the workpiece and cutting tool relative to each other.

(ii) **Workpiece variables**

(a) **Workpiece material and properties**

Chemical composition, microstructure and metallurgical consistency and hardness are known from experience to affect surface finish. For example in the case of steel, the carbon content is of great importance. Steels having 0.1% or less carbon produce built up edge during chip formation and thereby spoil surface finish. Addition of the so-called free machining elements like sulphur, selenium or lead to steel help reduce this tendency.

Very low hardness and ductility are not conducive to good finish because of the tendency of the tool to dig into a material having such properties. On the other hand, high hardness and strength and low ductility (high strain hardenability) result in good surface finish.

The nature and size of the micro-constituent (i.e., the microstructure) of a work material also affect surface finish. Fine grain size and high hardness of the microconstituents are favourable for obtaining good finish. Softer constituents may be fragmented or torn out by the cutting action and the machined surface may become pitted.

Metallurgical consistency determines the uniformity of finish of a machined surface. Often, a rod or casting is relatively softer at its core portions. Therefore, the surface finish is also relatively poor at those places.

(b) Workpiece geometry

Long slender or thin walled section have low stiffness both against static and dynamic forces. As a result waviness effects are more pronounced. On the other hand, if the workpiece is stiff (i.e. has a heavy cross-section) or is rigidly clamped on the machine, waviness height is small.

(iii) Tool variables

(a) Tool material

A material which permits high cutting speed will produce better surface finish. Different tool materials have different hot hardness, toughness and friction behaviour. High hot hardness enables the tool to be used at high cutting speed where built up edge practically disappears. Cemented carbides and oxides are superior materials, in this respect as compared to carbon steels and high speed steel (HSS). A tool material made of tough material can be given larger rake and clearance angles without endangering the cutting edge so far as chipping of cutting edges is concerned. HSS is a better tool material in this regard than cemented carbides and oxides.

In general, the smaller the friction between the tool and the work material, the better is the surface finish produced on the workpiece. Carbides and oxides are in this respect superior to HSS, although between carbides and oxides, there is not much difference.

(b) Tool geometry

Rake angle: In general, an increase in rake angle improves the surface finish considerably as it reduces the size of built-up edges. Besides, it is known that the larger the rake angles, the smaller are the cutting forces. And when the cutting forces are small, deflections and waviness height are also small.

Helix angle: The helix angle has relatively little effect on surface roughness. An increase in the helix angle reduces true feed and somewhat improves chip flow and surface finish. The investigators [84] have shown that end mills with small helix angles develop greater surface roughness due to deflection and chatter. However, large helix angles may prove harmful to surface finish by causing chatter. So, there is an optimum condition which produces a good surface finish.

Clearance angle: Clearance angles should be sufficient to prevent rubbing against the machined surfaces. The additional cutting forces due to the rubbing action causes harmful deflections. Also rubbing imprints the uneven wear profile of the cutting tool on the machined surface. Adequate clearance angles help the escape of the built up edge fragments and avoid their getting embedded in the machined surface.

Number of teeth: Experiments indicate that an increase of the teeth in the cutter favourably influences surface quality. In general, as the number of teeth in the cutter increases surface finish also increases. In the reference [79], it has been shown that in side milling operation at extremely high feeds a change from one to four teeth reduces generated surface irregularities by a factor of more than 18. However, for realistic feed, it is found from experience that surface roughness decreases not so significantly as number of teeth increases in the cutter. One should bear in mind that there is a limit on the number of teeth in the cutter. Since increasing teeth in the cutter increases cutting forces which in turn deflect the work-tool system. Besides, increasing the number of teeth causes an increase in temperature and thus an acceleration of tool wear. Surface roughness is influenced by a worn tool.

Nose radius: The major and minor (i.e. the side and end cutting) edges should be joined by a nose of sufficiently large radius to reduce the sharpness or pointedness of the tool. A large radius lessens the sawtooth effect of the feed marks and appreciably improves surface finish. An excessive nose radius, however, is harmful because it can cause vibration and chatter.

Diameter of the cutter: In general, as the cutter diameter increases surface irregularities decrease. The surface irregularities are seen to be approximately inversely proportional

to cutter diameter in side milling operation [79]. That means that if all other factors are held constant, the height of cusp(peak to valley) can be cut in half by doubling the cutter diameter.

(c) Cutter runout

Cutter runout influences surface generation on the milled surface. Cutter runout is due to the cumulative inaccuracies in the cutter, the spindle and the milling machine. The presence of runout increases the maximum forces on the cutter and changes the appearance of the finished surface. The effect of cutter runout on the appearance of the finished surface for a plain milling cutter with no helix angle has been discussed in reference [79, 121]. They have shown that at low feeds, the tooth mark spacing on the finished surface is the feed per revolution because the runout is larger than the tooth mark height, and the one high tooth obliterates the tooth marks left by the other tooth. The surface generation problem for a helical cutter is more complicated. With a helical cutter, the effect of runout cannot be associated with a particular tooth, but rather each tooth shifts from "low" to "high" as it wraps up the helix angle. Thus, the runout is equivalent to the variation in the radius of each tooth as a function of the axis of the cutter [121].

(d) Tool wear and rounding of cutting edges

Progressive wear of the mill tooth causes - after initial improvement of the quality of the surface - a steady growth in surface roughness. In general, rounding of cutting edges increases due to tool wear. A large radius on a cutting edge results in a greater compression of the material. The more ductile and deformable is the work material, the easier it is for surface irregularities to appear by burrs and cracks of the sub-surface layer. As tool wear increases cutting forces also increase which in turn causes deflection and vibration [85] of the cutting tool. So, surface irregularities increase due to deflection of the cutting tool.

(e) Mode of milling

The effect of mode of milling on surface roughness is contradictory. The author [79]

indicated that in plain milling (side milling) a greater compression occurs in the initial phase in the case of up milling mode. The more ductile and deformable are the workpiece material, the easier it is for surface irregularities to appear caused by burrs and cracks in the up milling mode. In down milling mode the influence of compression, particularly as the tooth enters the material, has no such significance for the finished surface, since cutting into the material occurs in the undeformed chip zone which is then removed by the following teeth. So, the final quality of a surface milled by a plain milling cutter is also influenced by the pressing in of the chips into the machined surface. This occurs particularly in up milling and to a greater extent if the material is ductile. The cause of this phenomenon is that some of the chips which become welded to the teeth or are carried away by the tooth, are " spread " over the material and pressed into it or else leaves scratches on the machined surface. For these reasons, the quality of down cut milled surfaces is generally higher than that of up cut ones. On the other hand, The National Twist Drills Co. [79] is of the opinion that the tooth path in plain milling in the case of down mode has a greater curvature than that of up cut milling. If these paths are considered to represent a single tooth cutter, then it would be expected that cusp height (peak to valley height) from down milling mode is higher than that from up milling.

The authors [84] have indicated that the surface produced in end milling at down milling mode is smoother than that of up milling mode.

3.4 The provision of machinability data to industry

3.4.1 Introduction

A knowledge of the relationships among cutting forces, tool life, surface finish and the machining condition for a particular work-tool combination enables one to investigate the economics of material cutting processes. In the past a great deal of effort has been directed towards the investigation of the machining. Still it is generally found that most medium sized and a high proportion of large industrial firms do not attempt

to optimize the machining processes in their factories. It is usually found that, the general levels of material removal rates which are usually based on practical experience are very low indeed when compared to those which may be achieved under laboratory test conditions. In a survey by PERA [122] it was estimated that the industrial rates of material removal rates are very low. It is evident that a large proportion of industry was working at material removal rates which are below the fringes of any optimization area. One method of increasing the awareness of production engineers to the capability of modern cutting tools and providing them with realistic cutting conditions is through the setting up of machinability data centres which collect, evaluate, store and disseminate cutting data and provide a service to industry. In the U S A the United States Air Force Centre (USAF) was established in 1948, mainly to satisfy some of the needs of the defence and aerospace programme. It was originally set up by a private company - Metcut Research Associates Inc., with U S Government funds. Metcut entered the field of information science and technology with the organisation of the Machinability Data Centre (MDC) in 1964. MDC serves both the American Government and Industry by providing material removal data and information. In the U K the Production Engineering Research Association (PERA) is the main agency involved in machining consultancy, development and information. The Institute for Industrial Research and Standards is the agent in Ireland for PERA.

3.4.2 Machining Data Handbook and Data Bank

A less sophisticated but worthwhile method of influencing industrial practice is through the provision of data handbooks to industry. The disadvantage of data handbooks lies in the fact that their very nature dictates a conservative approach and are often only intended as general guides, which sometimes do not even coincide with the particular product line and machine tool. Also, the use of handbooks is not compatible with the objective of many firms to automate the process planning function. Moreover, the feed back to the centre distributing handbooks is generally small and updating and redistribution of handbooks are sometimes difficult because firms will either copy them indiscriminately or just not order the updated information. So, the need for a computer based machinability data service arose. Metcut's Machinability Data Centre has a computerized bank of machining data and issues publications based on its activities. Perhaps, the best known of these is " Machining Data Handbook " [123].

In the U.K, a Computerised Machining Data Service [124] has been established with the objective of providing industry with reliable machining data. Initially, this involved developing a computerized bank of machining data and establishing a system which would enable industry to request data on specific operation/work material/cutting tool operations. This service was expanded with the introduction of machining data manuals into which the machining data bulletins could be filed. This coincided with the formation of the PERA Machining Data Club [125], which effectively combined the benefits of the Machining Data Service and the machining data manuals. Since, 1972, companies have received a regular supply of machining data bulletins containing proven data on a variety of operations using a wide range of work materials and cutting tools

Continuous development has taken place since the establishment of the data bank, including expansion of the bank itself and the development of mathematical models, based on an expanded form of Taylor's tool life equation, used in the production of computerized machining data bulletins for turning, drilling and milling [126-127,75]. The most recent activity has been the development of a fully computerized machining data processing procedure, which provides direct access to the data bank entry, retrieval, analysis and bulletin production.

Recent machinability data base systems use a different approach. Rather than storing recommended cutting conditions and simply retrieving them, the new system actually perform the engineering analysis necessary to determine the recommended cutting conditions. The recommendations are computed when they are needed and use a base set of raw machinability data.

Nowadays work is going on for the automatic selection of the optimized machining conditions for individual machining operations.

CHAPTER 4

RESPONSE SURFACE METHODOLOGY AND DEVELOPMENT OF MACHINABILITY MODELS

4.1 RESPONSE SURFACE METHODOLOGY

Response surface methodology (RSM) is a combination of mathematical and statistical techniques used in the empirical study of relationships and optimization where several independent variables (input) influence a dependent variable or response (output) [128]. In applying the RSM, the response is viewed as a surface [129,130] to which a mathematical model is fitted. Usually low order polynomials are used to represent the response surface. Only quantitative variables which are controllable can be included in the predictive models ; however, by building a number of models for each of the qualitative variables, their effect also could be studied. RSM is a sequential procedure. The eventual objective of RSM is to determine the optimum operating conditions for the system or to determine a region of the factor space in which operating specifications are satisfied.

RSM was initially developed and described by Box and Wilson [131] for the study of optimization problems in chemical processing engineering. Hill and Hunter [132] and Mead and Pike [133] reviewed the earlier work on RSM. It has also been used, due to its successful application, in tool life and surface roughness testing in turning, in ultrasonic grinding and prediction of frictional damping in machined joint [73, 134-138]]. It also assists in the understanding of the basic mechanism of the system under investigation.

4.1.1 The response function and the response surface

It is assumed that the independent variables are continuous and controllable by the experimenter with negligible error. The response is assumed to be a random variable. If all these variables are quantifiable, then the relation between the measured (observed) response and the independent variables can be expressed as:

$$y = f(x_1, x_2, x_3, \dots, x_k) + \epsilon'$$

Where y - the level of measured (experimental) response, f - the response function, $x_1, x_2, x_3, \dots, x_k$ - the levels of independent variables or factors and ϵ' - the experimental error.

A knowledge of the response function gives a complete summary of the results and enables the response for the values of factors that were not tested experimentally to be predicted [139]. The true or expected (predicted) response is denoted by \hat{y} , which would be obtained in the absence of experimental error and is given by:

$$\hat{y} = y - \epsilon' = f(x_1, x_2, x_3, \dots, x_k)$$

The surface generated by \hat{y} is called the response surface. The two dimensional response surface might be represented graphically by drawing the x_1 and x_2 axis in the plane of paper and visualizing \hat{y} as perpendicular to the plane of paper. A model of such surface, is shown in Fig. 4.1. A section of the solid bounded by the surface at any particular level of x_1 shows corresponding curve of \hat{y} against x_2 ; similarly a section for any particular x_2 shows the curve of \hat{y} against x_1 . The surface thus incorporates all such curves.

4.1.2 Representation of the response surface by contours

It is very instructive to see a pictorial representation of the relationship between a response and the independent variables. Just as the relationship between \hat{y} and a single variable x which may be represented by a two dimensional curve drawn on a sheet of paper, so the relationship between \hat{y} and two factors x_1 and x_2 may be represented by

a three dimensional surface called the Response Surface. A solid model of this surface may be constructed, but it is much simpler to draw lines of equal response on two dimensional graph whose co-ordinates denote the values of independent variables. These lines are termed the response contours. This type of representation is commonly used in maps to show rise and fall of land and in weather charts to show the distribution of atmospheric pressure. Contour lines which are close together in any region imply a rapid change in the response for relatively small changes in the independent variable or variables.

A first-order model yields a set of straight line contours; distances between these lines are proportional to difference in the response levels. For a quadratic relationship, contour lines generally consist of either concentric ellipses or concentric hyperbolas [140], although these figures may not be complete within the experimental region. When ellipses occur, the response has definite maximum or minimum, which may or may not be within the region plotted. The occurrence of hyperbolas implies that there is a saddle point (at which the response is a minimum for one direction and a maximum for other direction) somewhere on the response surface [141].

A quadratic regression relationship involving three variables is more difficult to appreciate; the direct equivalents to contours lines are three dimensional quadratic surfaces of equal responses. The simplest approach in this case is to obtain and compare separate two-variable contour diagrams at a number of fixed values of the third variable. The selected third variable should preferably be one which has the smallest and simplest effect on the response. The effect of four, five and so on may be displayed by micrographic method as discussed in the reference [140].

To appreciate the relationship between the surface represented in Fig. 4.1 (surface) and contour graph of Fig. 4.2 one might imagine a solid model of the surface in Fig. 4.1 (surface) enclosed in a tank. If water is poured up to the level 50% it will reach a line shown by the 50% contour in Fig. 4.2. The great advantage of the contour representation is that it focuses attention on the levels of the factors.

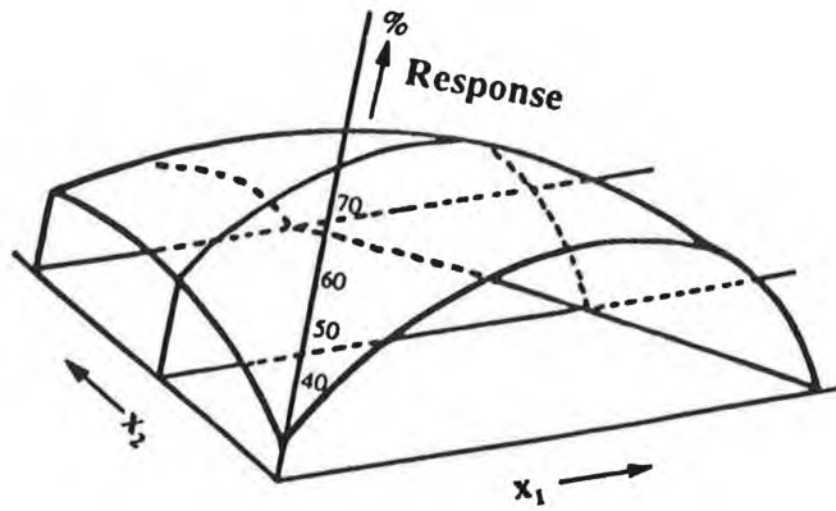


Fig.4.1: A response surface

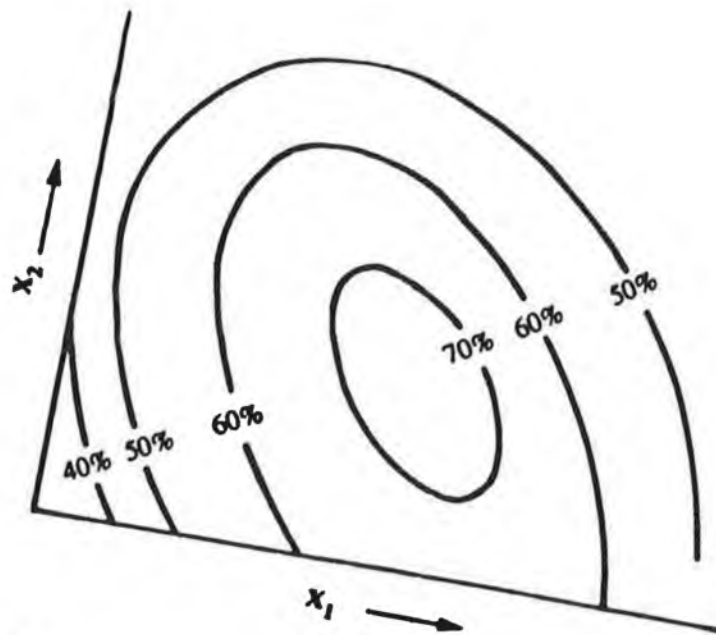


Fig.4.2: Response contours for the surface of Fig.4.1

4.1.3 General steps involved in the application of RSM

RSM involves the following steps:

- (i) Postulation of the mathematical model
- (ii) Experimental design
- (iii) Estimation of test regions (Coding) for independent variables
- (iv) Estimation of parameters in the postulated model
- (v) Analysis of results as:
 - (a) Checking the adequacy of the postulated model and the test for significance of individual variables
 - (b) Precision of prediction i.e. the estimation of confidence intervals.

(i) Postulation of mathematical model

The form of relationship between the response and the independent variables is unknown. The first step in RSM is to find a suitable approximation for the response surface and check whether or not this model is adequate by using data. The model proposed by many previous investigators [142,143] is a multiplicative non linear model which can be written in a general form as:

$$R_s = C_{40} \left(\prod_{j=1}^K \xi_j^{\beta_j} \right) \epsilon' \quad (4.1)$$

Where R_s - measured response, ξ_j - natural independent variables, C_{40} and β_j - model parameters, K - number of independent variables (factors) and ϵ' - multiplicative random error.

Of course, this equation (4.1) may be expressed in other non-linear forms. Taking natural logarithm converts the above intrinsically linear type non linear model into the standard linear form:

$$\ln R_s = \ln C_{40} + \sum_{j=1}^K \beta_j \ln \xi_j + \ln \varepsilon' \quad (4.2)$$

which can be written as

$$y = \beta_0 + \sum_{j=1}^K \beta_j x_j + \varepsilon \quad (4.3)$$

Where $y = \ln R_s$, $\beta_0 = \ln C_{40}$, β_j - model parameters, $x_j = \ln \xi$ and $\varepsilon = \ln \varepsilon'$

Based on the estimated parameters the equation (4.3) can be written in general form as:

$$y_i = b_0 x_0 + \sum_{j=1}^K b_j x_{ij} + \varepsilon_i \quad i = 1, 2, 3, \dots, n_e \quad (4.4)$$

Where b_0 and b_j - the estimated model parameters, x_{ij} - coded independent variables, n_e - the total number of data points and x_0 - the dummy variable which is always unity.

The equation (4.4) can be written as:

$$y_i - \varepsilon_i = b_0 x_0 + \sum_{j=1}^K b_j x_{ij} \quad i = 1, 2, 3, \dots, n_e$$

or

$$\hat{y} = b_0 x_0 + \sum_{j=1}^K b_j x_{ij} \quad i = 1, 2, 3, \dots, n_e \quad (4.5)$$

\hat{y} - the predicted (estimated) response on logarithmic scale.

The equation (4.5) is the predicted equation for the response. The right side of the equation (4.5) is called a first-order polynomial. This expression is the equation of a straight line. In terms of natural variables the predicted equation (4.5) becomes:

$$\ln \hat{R}_{st} = b_0 x_0 + \sum_{j=1}^K b_j x_{ij} \quad i = 1, 2, 3, \dots, n_e \quad (4.6)$$

Where $\ln \hat{R}_{si}$ - predicted response value, and n_e - total number of data points.

The first-order model in equation (4.5) can be fitted satisfactorily over narrow range of the independent variables. But the wider the range of independent variables the more terms will be necessary to obtain an adequate fit of a response. Experimental evidence indicates that the response surfaces often exhibit some curvature in the wide range of the independent variables. In order to cope with this, the polynomial model of higher degree are needed to provide a reasonable approximation to the response surface. Usually second-order polynomial are common and sufficient in many cases. The investigators [64,73] introduced and studied the polynomial of second-order model of the following form:

$$\hat{y}_i = y_i - \varepsilon = b_0 x_0 + \sum_{i=1}^K b_i x_i + \sum_{i=1}^K b_{ii} x_i^2 + \sum_i \sum_j b_{ij} x_i x_j \quad i < j \quad (4.7)$$

The general second-order predicted equation in terms of the natural variables is given by:

$$\ln \hat{R}_i = b_0 x_0 + \sum_{i=1}^K b_i x_i + \sum_{i=1}^K b_{ii} x_i^2 + \sum_i \sum_j b_{ij} x_i x_j \quad i < j \quad (4.8)$$

The constants b_0 , b_1 , b_2 etc. are sometimes called regression coefficients and the polynomial a regression function. x_1 , x_2 , x_{12} , x_2^2 , $x_1 x_2$ etc., would then be called the independent variables in the regression equation.

(ii) Experimental Design

A well designed experiment can substantially reduce the number of experiments. Many experiments involve a study of the effect of two or more factors. A response surface can be most efficiently fitted if proper attention is given to the choice of experimental design. The experimental designs which are useful in response surface methodology are discussed below:

(a) Designs for fitting the first -order Model

The most widely preferred class of design for fitting the first-order model is orthogonal first-order design. This orthogonal first-order design minimizes the variance of the co-efficient (b's) of the equation. A first-order design is orthogonal if the off-diagonal elements of the $(X_m^T X_m)$ matrix are all zero, where X_m is the calculated matrix or design matrix and X_m^T is the transpose of X_m . This implies that the cross-products of the columns of the X_m matrix sum to zero. This class of orthogonal first-order designs includes the 2^K factorial and fractional factorial designs. The response surface is assumed to be plotted in K (number of factor) dimensional space in which the units are chosen so that the levels of the factors are -1 and +1, that is , the origin " 0 " for the variables is taken at the mid-point of the design, and the Co-ordinates of the experimental points consists of -1's and +1's. As an example, suppose a 2^3 factorial design is used to fit the first-order model:

$$\hat{y} = b_0x_0 + b_1x_1 + b_2x_2 + b_3x_3 \tag{4.9}$$

The X_m matrix for fitting this model is as:

$$X_m = \begin{matrix} & x_0 & x_1 & x_2 & x_3 \\ \begin{matrix} 1 \\ 1 \\ 1 \\ 1 \\ 1 \\ 1 \\ 1 \\ 1 \end{matrix} & \begin{pmatrix} -1 & -1 & 1 \\ 1 & -1 & 1 \\ 1 & 1 & 1 \\ -1 & -1 & -1 \\ 1 & 1 & -1 \\ 1 & 1 & 1 \\ -1 & -1 & -1 \\ 1 & -1 & 1 \end{pmatrix} \end{matrix}$$

It is easy to verify that the off-diagonal elements of the $(X_m^T X_m)$ are zero for this design.

The 2^K factorial design does not afford an estimate of the experimental error unless some runs are repeated. A common method of including replication in the 2^K design is

to augment the design with several observations at the centre. The addition of centre points to the 2^K design does not influence the b_i for $i > 1$, but the estimate of b_0 becomes the grand average of all observations. Furthermore, the addition of centre points does not alter the orthogonal property of the design. The authors [137] added 5 centre points in the first order design for 2 factors shown in Fig 4.3. Box and Wilson [131] added 4 centre points in the first order design for 3 factors. Thus in a complete 2^3 factorial design the experimental points would be located at the vertices and 4 centre points, each repeated four times as illustrated in Fig. 4.4. This design provides three levels for each variable.

Sometimes, response surface designs are performed in blocks in such a way that the blocks are orthogonal to the model. Runs that would be repeat runs in an unblocked design are often divided amongst the blocks. In such a case, these runs are no longer repeat runs unless they occur in the same block, and the pure error must be calculated on that basis. Fig.4.4 shows the complete design consists of twelve experiments in two blocks, each block (half replicate) containing six experiments. The first block of experiments include numbers 1, 4, 6, 7, 9 and 10 and the second block of experiments include numbers 2, 3, 5, 8, 11 and 12.

(b) Design for fitting the second order Model

An experimental design for fitting a second-order model must have at least three level of each factor so that the model parameter can be estimated. The complete three-level factorial design (3^K) may be employed. Unfortunately, when K is greater than 2 the number of trials which such designs require often greatly exceeds the number of constants which it is desired to estimate. Consequently, when the experimental error is small and maximum economy in all experiment is essential, 3^K design are unsatisfactory. With four factors, for example, the factorial design involves $3^4 = 81$ trials, but the number of constant of second and lower order is only fifteen. Although the number of trials to be performed may be reduced by fractional replication, this device is much less effective in producing suitable arrangements with designs at three levels than with designs at two levels. For example, no satisfactory fractional replicate exists for four factors. For this reason alternative designs have been sought which will give estimates of all effects up to second order without necessitating a number of trials greatly in

excess of the number of constants to be determined. Designs of this sort which are particularly valuable for sequential experimentation are called central composite design. This design is the most widely used design for fitting a second-order model. The selection of experimental points, called a composite design, permits the experimenter to supplement experimental points of a first-order design, if a planer fit is found to be inadequate [144]. Composite designs to determine effects up to second-order are built up from complete two level factorials or fractional factorial. The procedure is first to choose a two level design so that all effects of order can be estimated. The design is then supplemented with further points which allow the estimation of quadratic effects. These composite designs consist of a 2^K factorial or fractional factorial (coded to the usual ± 1 notation) augmented by the axial points ($\pm \alpha, 0, 0 \dots\dots 0$), ($0, \pm \alpha, 0 \dots\dots 0$), ($0, 0, \pm \alpha, \dots\dots 0$).....($0, 0, 0 \dots\dots \pm \alpha$) and perhaps several centre points ($0, 0, 0 \dots\dots 0$).

One advantage of composite design is that they allow the work to proceed naturally in stages. The first-order design can first be completed, if it is found that the first-order model is not adequate it will be necessary to determine all second-order effects, the extra points may be added to complete the composite design. Central composite designs for $K = 2$ and $K = 3$ are shown in Fig.4.5.and Fig.4.6 respectively. A central composite design is made orthogonal by suitably choosing α . The manner in which these orthogonal complete design are built up when the number of factor (K) is equal to 2, 3, 4 and 5 is outlined in Table 4.1 [141].

Table 4.1: Orthogonal Composite Designs.

Number of factors (K)	2	3	4	5
Basic two level design	2^2	2^3	2^4	$\frac{1}{2} 2^5$
No. of extra points (2K+1)	5	7	9	11
Distance of axial points from centre(α)	1.0	1.215	1.414	1.547

In the fourth row the values of α are given which makes the corresponding composite designs orthogonal. But in the central composite design it is not essential to choose the α 's to fulfil the conditions for orthogonality or to have the α 's all equal. In order to get greater precision for the estimates of the quadratic effects larger values for the α 's may be taken, but it would be unwise to take them as large as 3, since the magnitude of possible bias would then become serious. In general case, when the α 's are not chosen to give orthogonality, the least square estimates of the b's and the standard errors are not found quite so readily.

A central composite design is made rotatable by choice of α . An experimental design is said to be rotatable if the variance of the predicted response \hat{y} at some point x is a function only of the distance of the point from the design centre, and not a function of direction. This implies that the variance contours of \hat{y} are concentric circles. Furthermore, a design with this property will leave the variance of \hat{y} unchanged when the design is rotated about the centre $(0, 0, 0, \dots, 0)$, hence the name rotatable design. The value of α for rotatability depends on the number of points in the factorial portion of the design; in fact, $\alpha = (n_c)^{1/4} = (2^K)^{1/4}$ yields a rotatable central composite design, where n_c is the number of points used in the factorial portion of the design. Thus the value of α for rotatability for three factors case is $\alpha = (2^3)^{1/4} = 1.682$. With proper choice of centre points (n_0) the central composite design may be made orthogonal (rotatable) or it can be made a uniform precision rotatable design. In a uniform precision rotatable design the variance of \hat{y} at the origin is equal to the variance of \hat{y} at unit distance from the origin. A uniform precision design affords more protection against bias in the regression co-efficient because of the presence of third order and higher terms in the true surface than does an orthogonal design. Table 4.2 [128] provides the design parameters for both orthogonal and uniform precision rotatable central composite design for various values of K .

From Fig. 4.5 the central composite design with 2 factors(K) consists of 9 experimental points of the first-order design (Fig4.3) and additional 4 axial points called augments. From Fig. 4.6 the central composite design with 3 factors(K) consists of 24 experiments.

The 24 experiments are shown in four blocks. The first and second blocks are shown to develop the first-order model of 3 factors in Fig. 4.4. The third block which consists of experiments 13, 14, 15, 16, 17 and 18 are added at the faces of the cube which can be chosen at a selected augment length.

Table 4.2 : Orthogonal and Uniform-Precision rotatable Central Composite Designs.

Factor K	Factorial point, n_c	Axial point, n_a	Centre point, n_0 (up)	Centre point, n_0 (orth)	Total point, $n(\text{up})$	Total point, n (orth)	Augment factor, α
2	4	4	5	8	13	16	1.414
3	8	6	6	9	20	23	1.682
4	16	8	7	12	31	36	2.000
5	32	10	10	17	52	59	2.378
6	64	12	15	24	91	100	2.828

The fourth block which consists of 19, 20, 21, 22, 23 and 24 were repeated experiments of the third block for increasing the model accuracy.

This central composite design provides five levels for each independent variable.

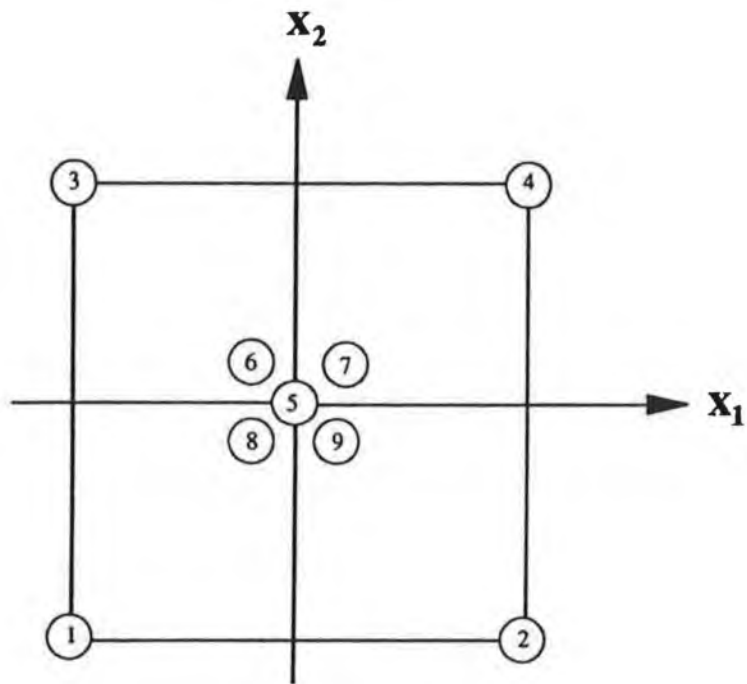


Fig.4.3: First-order orthogonal design for 2 factors ($K = 2$)

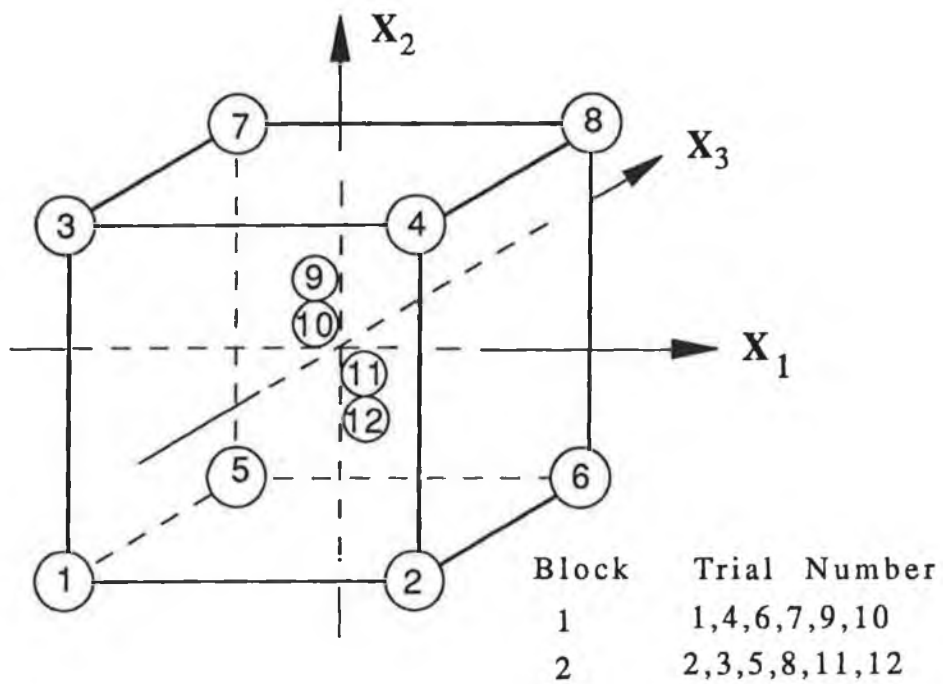


Fig.4.4: First-order orthogonal design for 3 factors ($K = 3$)

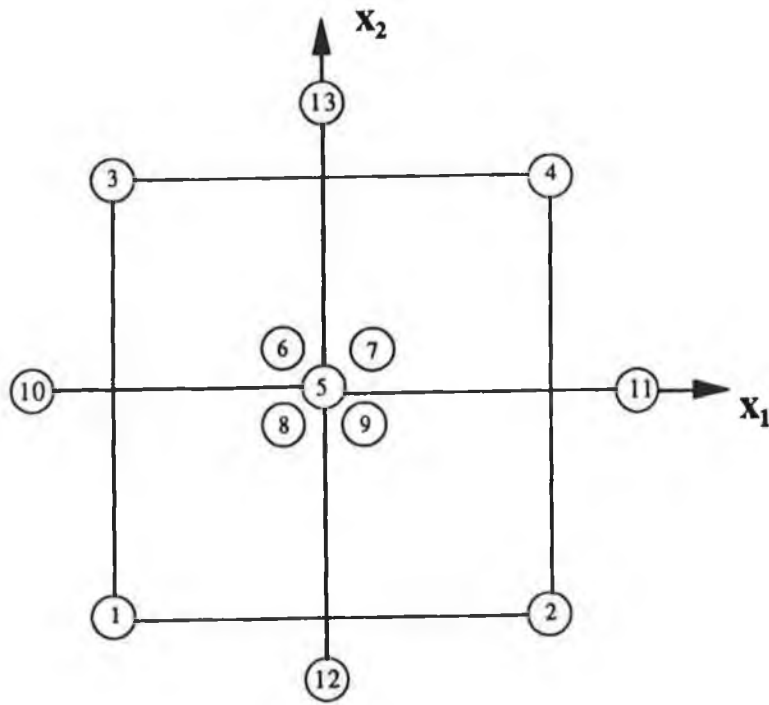


Fig.4.5: Central composite rotatable design for 2 factors ($K = 2$)

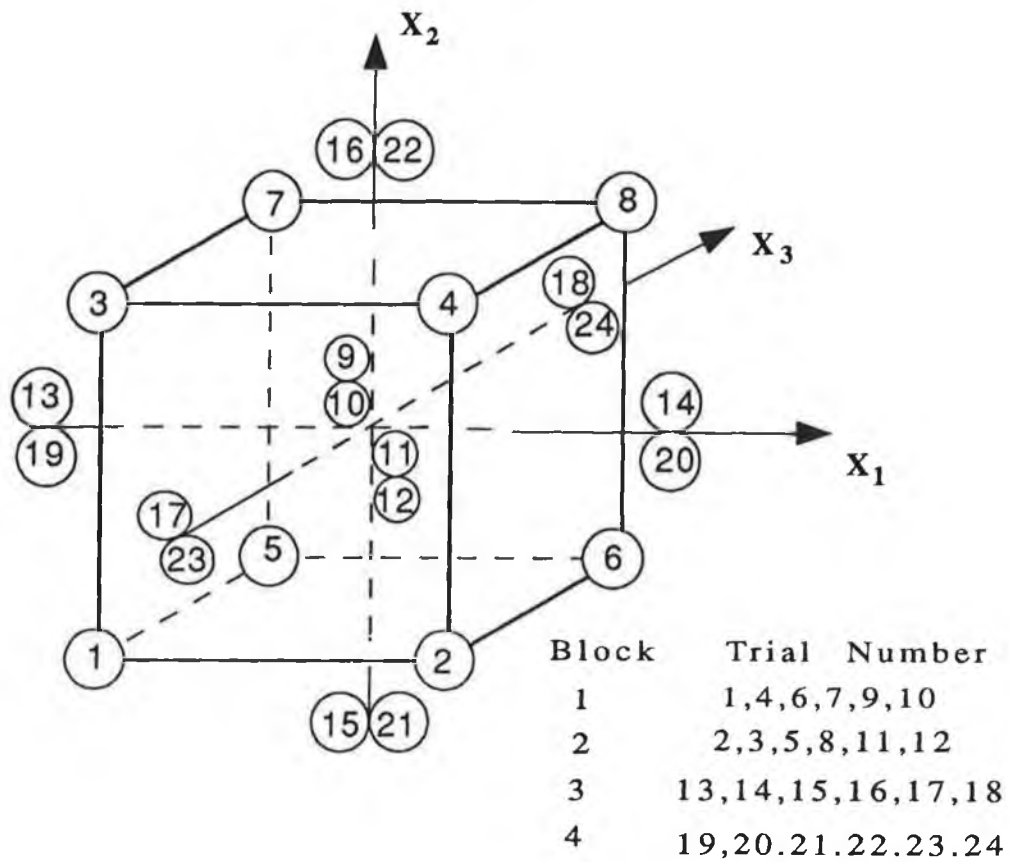


Fig.4.6: Central composite design for 3 factors ($K = 3$)

(iii) Estimation of test regions (Coding) for independent variables

The coded values (logarithmic transformations) of the variables for use in equations (4.5) and (4.7) are usually obtained from the following transforming equations [145]:

$$x = \frac{\ln X_n - \ln X_{n0}}{\ln X_{n1} - \ln X_{n0}} \quad (4.10)$$

Where x - the coded value of any factor corresponding to its natural value X_n , X_{n1} - the natural value of the factor at the +1 level and X_{n0} - the natural value of the factor corresponding to the base or zero level.

Other transformation equations for coding of independent variable are reported. Wu[73] coded the independent variables using the following transforming equation:

$$x = \frac{2(\ln X_n - \ln X_{n1})}{(\ln X_{n1} - \ln X_{-n1})} \quad (4.11)$$

Where x - the coded value of any factor corresponding to its natural value X_n , X_{n1} - the natural value of the factor at +1 level and X_{-n1} - the natural value of the factor at -1 level.

The authors [146,147] coded the independent variables using the following transforming equation:

$$x = C_{41} + d_1 \log X_n \quad (4.12)$$

Where x - the coded value of any factor corresponding to its natural value X_n , C_{41} and d_1 are chosen to satisfy the desired conditions at the end of the scale.

(iv) Estimation of model parameter

The model (regression) parameters can be estimated by the method of ordinary least squares (OLS) [148]. Other techniques are found in the literature [148,149] for selecting the best regression equation. Among these techniques which are currently popular are:

- (1) All possible subsets regression
- (2) Forward selection
- (3) Backward elimination
- (4) Stepwise regression

Computer programs available in commercial statistical packages [149,150] based on these techniques are used for selecting the best equation for the response. In this work, OLS method was used for estimating the model parameter. The basic formula of OLS is given by:

$$b_m = (X_m^T X_m)^{-1} X_m^T Y_m \quad (4.13)$$

Where b_m - the matrix of parameter estimates, X_m - the matrix of independent variables or design matrix, X_m^T - the transpose of X_m , $X_m^T X_m$ - the variance matrix, $(X_m^T X_m)^{-1}$ - the covariance matrix which is the inverse of $(X_m^T X_m)$ matrix and Y_m - the matrix of logarithms of measured responses (output).

(v) Analysis of results

(a) Checking the adequacy of the postulated model and the test for significance of individual variables

Adequacy of postulated models

The analysis of variance (ANOVA) technique [137,146,148] was used to check the adequacy of the developed models. As per this technique, the F ratio of the model is calculated and compared with the standard tabulated value of the F-ratio for a specific

level of confidence. If the calculated value of the F-ratio does not exceed the F-ratio obtained from the standard statistical tables [148], then with the corresponding confidence probability, the model may be considered adequate.

In order to perform a variance analysis the sum of the squares of the values of y ($\sum y^2$) is usually partitioned into contributions from the zero order terms, the first order terms, the second order (quadratic and interaction), the blocks, the lack of fit and experimental error. The detailed formulae [137,146,148] for variance analysis for the first and second-order model are given Tables 4.3 & 4.4 respectively.

Table 4.3 : Formulae for ANOVA for (First-order model)

Source	Sum of Square(SS)	Degree of freedom(df)
Zero-order terms(b_0)	$\frac{(\sum_{u=1}^{n_c} y_u)^2}{n}$	1
First-order terms(b_i)	$\frac{\sum_{i=1}^K b_i^2}{C_i}$	K
Lack of fit	Found by subtraction	$n_c - K$
Experimental error(pure error)	$\sum_u^{n_0} (y_{ou} - \bar{y}_o)^2$	$n_0 - 1$
Residual	$\sum_{u=1}^{n_c} (y_u - \hat{y}_u)^2$	$(n_c - K) + (n_0 - 1)$
Total	$\sum_{u=1}^{n_c} (y_u)^2$	n_e

Where n_0 - the number of centre points , n_c - the number of corner point, K - the number of factors, y_{u0} - the logarithmic value of observed response at central point with

mean \bar{y}_0 , n_e - the number of experimental points,, b_i - the co-efficient of the postulated model, C_i - the inverse of the sum of squares of ith column in X_m matrix and \hat{y} - the logarithm of predicted responses and y - the logarithms of the observed responses.

Table 4.4 : Formulae for ANOVA (Second-order model)

Source	Sum of Square(SS)	df.
Zero-order terms(b_0)	$\frac{(\sum_{u=1}^{n_e} y_u)^2}{n_e}$	1
First-order terms(b_i)	$\sum_{i=1}^K b_i (iy)$	K
Pure second-order(b_{ii}/b_0)	$b_0 (0y) + \sum_{i=1}^K b_{ii} (i iy) + \frac{(\sum_{u=1}^{n_e} y_u)^2}{n_e}$	K
Mixed second order(b_{ij})	$\sum_{i=1}^K \sum_{j=1}^K b_{ij} (ijy)$	$\frac{1}{2} K(K-1)$
Lack of fit	found by subtraction	$n_c + n_a - \frac{1}{2} K(K+3)$
Pure error	$\sum_{u=1}^{n_0} (y_{0u} - \bar{y}_0)^2$	$n_0 - 1$
Residual	$\sum_{u=1}^{n_e} (y_u - \hat{y}_u)^2$	$n - \frac{1}{2} K(K+3) - 1$
Total	$\sum_{u=1}^{n_e} y_u^2$	n_e

Where n_e - the total number of experimental points, K - the dimension of the design, n_a - the number of axial point, n_c - the number of corner point, y_{0u} - the logarithmic value of observed responses at centre points with mean \bar{y}_0 and

$$\begin{aligned}
(0y) &= \sum_{u=1}^{n_e} y_u \\
(iy) &= \sum_{u=1}^{n_e} x_{iu} y_u \\
(iiy) &= \sum_{u=1}^{n_e} x_{iu} x_{ju} y_u \\
(ijy) &= \sum_{u=1}^{n_e} x_{iu} x_{ju} y_u
\end{aligned}$$

All of these expressions being cross products of columns of the X_m matrix with the column of y values.

The formulae for analysis of variance shown in Tables 4.3 and 4.4. were for unblocked experimental designs. Often, however, response surface designs are performed in blocks in such a way that the blocks are orthogonal to the model. Runs that would be repeat runs in a unblocked design are often divided amongst the blocks. In such a case, runs are no longer repeat runs unless they occur in the same block, and pure error must be calculated on that basis. Also the analysis of variance must contain a sum of squares for blocks. For blocks orthogonal to the model, the appropriate sum of squares for blocks is usually found by the following formula:

$$SS(\text{blocks}) = \sum_{w=1}^m \frac{B_w^2}{n_w} - \frac{G_T^2}{n} \quad \text{with } (m-1) \text{ degrees of freedom} \quad (4.14)$$

Where B_w - the total of the n_w observations in the wth block (there are m blocks in all) and G_T - the grand total of all the observations in all of the m blocks.

Significance testing of individual variable

The main objective of RSM is to achieve an optimum condition in the system. Sometimes unnecessary variables decrease the model accuracy. So it is necessary to construct a model with significant terms only. It is necessary to test the effect of individual variables adjusted for all other variables [151].

To test the significance of X_i adjusted for all others variables, the variance ratio

$$F_{ratio} = \frac{b_i^2/C_{ii}}{s^2} \quad (4.15)$$

is compared with standard F-ratio for specified degree of freedom and level of confidence.

Where b_i - regression co-efficient, C_{ii} - the elements of $(X_m^T X_m)^{-1}$ matrix and s - standard deviation.

If the F-ratio for the individual variables calculated from the above formula is much less than the standard F-ratio obtained from the standard statistical table then the individual variable is insignificant. In this way insignificant variables in the equation can be eliminated.

(b) Precision of Prediction (Confidence Intervals)

The precision of the predicted model can be determined by calculating the appropriate confidence intervals and comparing them with the experimental value. The specific level of confidence interval for the predicted responses, \hat{y} are given by $(\hat{y} \pm \Delta\hat{y})$, where

$$\Delta\hat{y} = t_{df, \frac{\alpha}{2}} \sqrt{[V(\hat{y})]} \quad (4.16)$$

Where t - the value of horizontal co-ordinate of the t distribution corresponding to the specified degrees of freedom and level of confidence, $V(\hat{y})$ - the variance of the predicted responses \hat{y} and α - level of confidence interval. If the measured responses y are within the level of the predicted responses then that specified level of confidence is the precision of prediction of the model.

4.2 DEVELOPMENT OF MACHINABILITY MODELS BY RSM

The accelerated application of computer aided manufacturing(CAM) to machining operations by the use of DNC and CNC machine tools has focused on the desirability of developing reliable machinability data systems, to ensure optimum production from the expensive equipment involved. The machinability data system is essential for the selection of optimum cutting conditions during process planning and it has become an important component in the implementation of computer integrated manufacturing(CIM) systems.

Computerized machinability data systems have been classified into two general types[152]:

- (i) Conventional data retrieval systems
- (ii) Mathematical model systems

The conventional database systems are based on the collection and storage of large quantities of data from laboratory experiments and workshop experience and then simply retrieving recommended cutting speeds, feed rates and cost information for any specific cutting operations. The mathematical model systems attempt to predict the optimum cutting conditions for specific operation. Recent approaches to the problem of designing a suitable machinability data base system for CIM applications are to use mathematical model type systems, a strategy which has considerable advantages over simple data retrieval systems. The mathematical model systems attempt to predict the optimum cutting conditions for a specific operation. In mathematical model type systems, the machining response data such as cutting forces, tool life, surface finish etc. are used as primary data. Then mathematical models of these machining responses (dependent variables) as function of independent variables (i.e., cutting speed, feed and depth of cut etc.) can be developed using response surface methodology i.e.

$$R_{s \text{ (machining)}} = f (v, f_z, a_a)$$

Where R_s - responses (machining) or dependent variables (i.e. Cutting force, Tool life, Surface roughness etc.) and v, f_z, a_a - machining variables or independent variables(i.e.

cutting speed, feed and axial depth of cut respectively).To develop the mathematical models the relationship between the machining responses and the investigated independent variables is commonly approximated by polynomial function, while multiple linear regression analysis techniques are used for obtaining the model parameters. A well designed experiment is used to develop these mathematical models in order to minimize the amount of experimentation. In addition to development of mathematical models the RSM would provide a large amount of information with small amount of experimentation. The detailed discussion to apply RSM to develop mathematical models has been shown in section 4.1.3 of this chapter. Once these mathematical models are developed, they could be represented by response surfaces . Next, utilizing computer, section (contour) of these surfaces are obtained at different levels of the independent variables in planes of the other independent variables. By superimposing those contours, it is possible to select a proper combination of the investigated independent variables for optimum cutting condition. Such RSM differs from the common method, which investigates one variable at a time fixing the other variable at constant level. The common method is time consuming and expensive. The major weakness of mathematical model systems lies in the random errors contained in the machining response data and their effect on the validity of the predicted optimum cutting conditions. So, careful attention is needed to measure the measured data of the repeated points located at the centre of the experimental design.

CHAPTER 5

EXPERIMENTAL SET-UP AND PROCEDURE

5.1 Introduction

The experimental set-up and procedure for machinability assessment of the advanced materials can be divided as:

- (1) Apparatus, equipment and machine
- (2) Workpiece materials
- (3) Cutting tools
- (4) Measurement of average cutting forces
- (5) Measurement of flank wear of end mill cutter
- (6) Measurement of surface roughness index, R_a

5.2 Experimental Apparatus, Equipment and Machine

The following apparatus, equipment and machines were used in this study:

- (i) Three Component Dynamometer
- (ii) Charge Amplifiers
- (iii) Lightbeam Oscillograph (Recorder)
- (iv) A/D (Analog to Digital) Converter
- (v) Personal Computer(PC)
- (vi) Surface Profilometers (Roughness Tester)
- (vii) Toolmakers' Microscope

(viii) Scanning Electron Microscope(SEM)

(ix) Milling Machines

The specifications of the above apparatus, equipment and machine are shown in Appendix 1.

5.3 Experimental workpiece materials

The reference workpiece materials used in this study were:

- (i) Steel (\approx ISO C 22,)
- (ii) Inconel 718 (nickel base superalloy)
- (iii) 2618 Metal Matrix Composite

(i) Steel

The reference steel material was rectangular bar (150 mm x 50 mm) of cold rolled steel(as rolled condition). It was equivalent to steel C 22, in conformity with ISO/R 683-3 (\approx AISI 1020). It had the following properties:

Chemical composition

The chemical composition of steel 190 BHN is shown in Table 5.1.

Table 5.1: Chemical Composition of Steel (190 BHN)

Element	Symbol	%
Carbon	C	0.22
Manganese	Mn	0.90
Sulphur	S	0.050
Phosphorous	P	0.050
Iron	Fe	Balance

The hardness of the reference steel workpiece material was 190 BHN. The other properties of the steel workpiece material are shown in Appendix 1.

(ii) Inconel 718

Inconel 718 is a nickel-chromium based superalloy. This is essentially a face centred cubic or austenitic (non magnetic) and corrosion resistant advanced material. It can be used at - 217°C (- 423°F) to 700°C(1300°F). It is also called high strength thermal resistant material (HSTR) material because it can retain its high strength at elevated temperature(700°C). It contains a niobium(columbium) age hardening addition that provides increased strength without a decrease in ductility. Inconel 718 has good tensile, fatigue, creep and rupture strength which resulted in its use in a wide range of application. Example of these are, components for liquid rockets, parts for air craft turbine engine, cryogenic tankage, pump bodies and parts, nuclear engineering, gas and oil well tooling, defence industry products etc.

In most applications, Inconel 718 usually receives two kinds of heat treatment as:

- annealed (983°C for 20 min - air cool)
- Age hardened (720°C for 8 hrs, furnace cool to 622°C for 8 hrs - air cool)

In this study a block of Inconel 718 (200 mm x 150 mm x 50 mm) in the hot forged and annealed condition was used which had the following properties:

Chemical composition of Inconel 718

The chemical composition of Inconel 718 is shown in Table 5.2.

Table 5.2 : Chemical composition of Inconel 718

Element	Symbol	%
Carbon	C	0.10
Manganese	Mn	0.35
Silicon	Si	0.35
Titanium	Ti	0.60
Aluminium	Al	0.80
Cobalt	Co	1.00
Molybdenum	Mo	3.00
Niobium(Columbium)	Nb (Cb)	5.00
Iron	Fe	17.00
Chromium	Cr	19.00
Nickel	Ni	Balance

The hardness of the reference Inconel 718 workpiece material was 260 BHN. The other properties of the reference Inconel 718 workpiece material is shown in Appendix 1.

(iii) 2618 Metal Matrix Composite

Metal matrix composites (MMCs) are a relatively new range of advanced material. They are currently experiencing active development in many countries of the world. The benefit of using MMCs is the advantage of attaining property combinations that can result in a number of service benefits. Among these are; increased strength, decreased weight, higher service temperature and improved wear resistance. MMCs are manufactured in different grades and forms. They consist of a matrix and reinforcement. Metal acts as the matrix i.e. bonding element. Its main function is to transfer and distribute the load to the reinforcements. The matrix can be selected on the basis of oxidation and corrosion resistance or other properties [153]. Again selection involves not only desired properties but also which material is the best suited for composite manufacturing. Generally Al, Ti, Mg, Ni, Cu, Pb, Fe, Ag, Zn are used as the matrix material. However, Al, Ti and Mg are used widely. For good bonding and strength in the composite, metal alloy is used as the matrix element instead of pure metal. Reinforcement increases the strength, stiffness, temperature resistance capacity and lowers the density of MMC. The prime role of reinforcements is to carry load. The reinforcement material systems can be generally divided into five major categories i.e. continuous fibres, discontinuous fibres, whisker, particulate and wire [97]. With the exception of wires, which are metals, reinforcements are generally ceramics. Typically these ceramics are oxides, carbides and nitride. These are used because of their combinations of high strength and stiffness at both room and elevated temperatures. The common reinforcement elements are SiC, Al₂O₃, TiB₂, Boron and graphite. Particulate is the most common and cheapest reinforcement material. These present the isotropic property of MMC which shows a promising application in the structural field. The MMC material used in this study was high temperature MMC based on an aluminium alloy which has a high modulus which can retain at elevated temperatures. The trade name of this composite is 2618 MMC [1]. This MMC is lower cost than 7000 series based MMCs. It is thus more attractive for applications that are more cost sensitive, for example high performance automotive e.g., brake callipers (where high stiffness at

elevated temperatures can reduce distortion and improve braking performance), conrods and pistons (utilizing the reduced coefficient of thermal expansion and high stiffness at elevated temperatures to improve engine efficiency). The properties of the MMC material are given below:

Chemical composition of 2618 MMC (Al/12 Vf.SiC)

The chemical composition of matrix material of 2618 MMC is shown in Table 5.3.

Table 5.3 : Chemical composition of matrix of 2618 MMC

Element	Symbol	%
Copper	Cu	2.5
Magnesium	Mg	1.5
Nickel	Ni	1.1
Iron	Fe	1.1
Aluminium	Al	Balance

Reinforcement

- Particulate reinforcement
- SiC_p 12 % by volume

Fabrication technique

- Manufactured by spray deposition method [97] & subsequently extruded to 63 mm x 25 mm rectangular bar.

The hardness of the reference MMC workpiece material was 145 BHN. The other properties of the reference MMC workpiece material is shown in Appendix 1.

5.4 Experimental Cutting Tools

Tool Material

In this work the tool material is not itself a test variable. The tool materials were of two types :

- (a) Uncoated HSS (High Speed Steel), cobalt alloyed \approx S11 in accordance with ISO 4957 (AISI M42).
- (b) Uncoated tungsten carbide \approx ISO K20 or AISI M15 (Sandvik Grade H13A) with approximate Composition of WC 94% and Co 6%.

The tool geometries are shown in Appendix 1.

5.5 Measurement of cutting forces in end milling operations

Force measurement using a dynamometer is by far the most widely used technique for process monitoring in industry and research [155].The cutting force signals (table system of cutting forces) coming from the dynamometer were measured in two ways:

- (i) Cutting force data acquisition by the computer via A/D converter
- (ii) Cutting force oscillograph by the recorder

The second measuring system i.e., the force measurement by recorder was carried out as a check to confirm the results obtained by the computerised data acquisition system. In the recorder system, the force signal is visibly recorded by a light beam oscillograph and subsequently the force is measured. It was found that the results obtained by both systems were very close (i.e. 5-10% variation). In this study, cutting force data obtained by the computer were analyzed (note that throughout the experiment force data by the recorder were also collected simultaneously in order to compare the results with that of the computer). The experimental set up of the combined measuring system(i.e. computer and recorder) is shown in Fig 5.1.

5.5.1 Cutting force data acquisition system by the computer

The hardware configuration of the present data acquisition is shown in Fig.5.1. This consists of the following:

- (a) The transducer (piezo electric)
- (b) The distribution box
- (c) The charge amplifiers
- (d) The A/D converter
- (e) The personal computer (PC) with hard copy printout

(a) The transducer

The transducer is a three component piezoelectric dynamometer. The piezoelectric force measuring principle differs fundamentally from that of previous systems. Traditional dynamometers relied on the deformation produced on cantilevered elements by the cutting forces. These measuring systems had either high stiffness or high sensitivity. When using the piezoelectric system, it is not necessary to measure the actual deformation. Because, when a force acts on a quartz element, a proportional electric charge appears on the loaded surface. In such a system, the measured deflection amounts to no more than a few thousands of a millimetre at full load. With conventional systems, several tenths of a millimetre may be needed to produce a force reading. Furthermore, the piezoelectric properties of quartz are such that the elements are sensitive only to pressure in one axis. Therefore, the individual components are sensitive only to pressure in one axis.

Hence, the individual components of the cutting forces are measured directly. The force to be measured is introduced via the clamping surface and mounting plate and distributed between four 3-component transducers. The force transducers are arranged in a rectangle between the mounting plate and base plate. Resolution of the force applied into its three components takes place in the transducer.

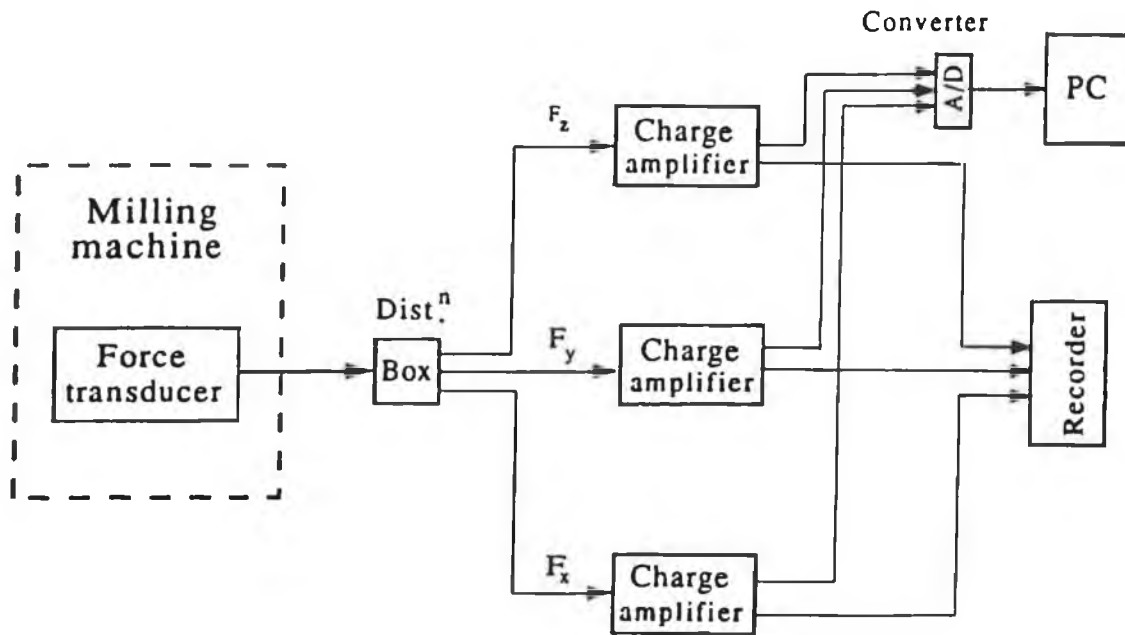


Fig.5.1: Schematic diagram of force measuring system

Calibration of the transducer

Kistler Instruments Ltd., the manufacturer of the three component dynamometer provided the calibration data [156] for the transducer. The out put of the transducer was checked by applying and measuring a known load on it.

(b) The distribution box

The F_x and F_y outputs of the transducer are led in pair and the F_z outputs singly to the Fischer flanged socket. The socket is then connected to the distribution box. The function of the distribution box is to distribute the individual components of cutting forces. Where, from the distribution box F_x , F_y , F_z components of the cutting forces are distributed to three charge amplifiers by special low noise cables. Depending on the direction of the force, positive or negative charges occur at these connections.

(c) The charge amplifier

The charge amplifier is an inverting amplifier. The charge amplifiers used in this study were one channel charge amplifiers which converts the electrical charge yielded by the piezoelectric transducer into a proportional voltage signal. Depending upon the direction of applied force, positive or negative charges occur at the connections coming from the transducer. Negative charges produce positive voltages at the charge amplifier output and vice versa.

Filtering of analog voltage signal

Since milling is a dynamic cutting process, the cutting force fluctuates as a result of chip thickness variation, vibration of the work tool system and the rate of penetration of the cutter teeth into the work etc. These fluctuations may cause instability when one tries to control the cutting force. To avoid dynamic cutting forces, a low pass filter was used. The concept of filtering is that it allows certain frequencies in a signal to pass and rejects the others. In other words, the filter transfer function forms a "window" in the frequency domain through which a portion of the input spectrum is allowed to pass. In this study, a low pass filter with Butterworth characteristic [157] switchable in 8 stages (10 Hz, 30 Hz, 100 Hz, 300 Hz, 1 KHz, 3 KHz, 10 KHz, 30 KHz) was utilised in the charge amplifier. The time constant of the amplifier was set at medium position. The frequency in the amplifier was set by synchronizing with the tooth passing frequency of the cutter (i.e available frequency in the amplifier \geq tooth passing frequency). For instance, when the spindle speed is 600 rpm and the number of teeth in the cutter is 2, then the tooth passing frequency is { i.e. $(2 * 600) / 60$ } equal to 20 Hz. In this case the frequency in the amplifier was set to 30 Hz (i.e, nearest but greater than the tooth passing frequency) which is much lower than the fundamental frequencies of the machine tool structure or of the feed mechanism.

Calibration of the charge amplifier

The calibration procedure of the charge amplifier is given in the reference [158].

(d) The A/D converter

The A/D converter which has been used in the present data acquisition system permits the personal computer(PC) to interface with the piezoelectric transducer. In practice, the A/D converter receives the analog signal from the piezoelectric transducer via the charge amplifier. All signals in the real world have to be converted into digital form for computer to read them. So, the A/D converter converts the analog signal to digital printed form signals. The DASH-8 , an 8 channel 12 bit high speed A/D converter and timer counter board was used in the present work. The full scale input of each channel of DASH-8 was ± 5 volts, A/D conversion time is typically 25 microseconds. The 8254 programmable counter timer embedded in the DASH-8 provides periodic interrupts for the A/D converter. The bus clock of the PC is used by the DASH-8 to drive the timer 8254. The DASH-8 board is 12.37 cm (5") long and can be fitted in a "half" slot of the motherboard of the PC. All connections are made through a standard 37 pin "D" male connector that projects through the rear of the computer. The base address of the DASH-8 has been set as &H300 through the microswitch.

Calibration of DASH-8

The calibration of the DASH-8 is shown in the reference [159].

Computer interfacing

With all the signals in the digital form it remains to connect to the computer and then read in. The connection point is what is traditionally regarded as an interface. Most operations involving computers have two types of interfaces : Parallel & Serial interface. There are also many intermediate forms, in many cases, combining serial and parallel. A/D conversion is no exception, the fastest converters are fully parallel, the cheapest are fully serial. Though the parallel transmission is speedy and require no special setting, the following problems will discourage the use of parallel interface [160].

- the data transmission distance is restricted to 1 & 2 meter
- the data transfer is only one way
- some intelligent commands cannot be used.

Thus, the serial interface was used in the present study. The serial interface was originally the standard for data communication equipment using telephone lines and has evolved into serial data transmission standard for the computer and their peripheral equipment.

(e) The Personal computer(PC)

This computer is a general purpose IBM-PC compatible that allows plug-in of the A/D to expand its compatibility. The PC feature is 640 Kbyte RAM with 42 Mbyte disk space with IBM compatible VDU. The process of converting the electrical signals of the transducer to the appropriate physical meaning has been carried out by this computer. This process has been performed after programming the A/D converter to collect, convert and store those electrical signals.

Software design

A basic program has been developed for PC to program the A/D converter and to facilitate measurements which involve analog to digital processing. The outline of programming has been discussed in the reference [159]. The program has been used to monitor the measurement of cutting forces in end milling. The program has been written in basic language and compiled with the I/O driver of the A/D converter using MetraByte's microsoftware compiler program. This is to translate the ASCII commands and instructions of the program to the computer code and store this in the memory of the computer. Therefore, the program can be executed from the prompt on the VDU. The I/O driver of the AD converter is a software routine containing the binary code of the operating system of the A/D converter. The routine can be accessed from "BASIC" using a simple " CALL " statement. Various operating modes of " CALL " routine select the function of the converter data formatting and error checking. The program is driven by a menu from which an option can be selected in order to collect a bulk of experimental data and display it in a printed form. The clock of the computer is used by the program to synchronize the measuring process. The Computer program is listed in Appendix 1.

5.5.2 Measurement of cutting force by the light beam oscillograph recorder

The experimental set-up for measuring cutting force by the recorder is shown in Fig. 5.1. The voltage signals which come out of the charge amplifiers were also measured simultaneously by the light beam oscillograph recorder. The voltage signals from the charge amplifiers is fed into the recorder by the 7 pin locking DIN connectors. The voltage signal deflect a tiny light source as a spot of light across the full width of the light sensitive paper, by the mirror of a miniature galvanometer. The resulting record becomes visible shortly after emergence from the recorder by the action of the ambient light on the recorded image. The calibration of the lightbeam Oscellograph Recorder has been discussed in the manual [161]. A section of the typical recorded signal of the cutting force is shown in Fig 5.2. This figure was obtained from the cutting condition when one tooth leaves the cut when the following one starts cutting.

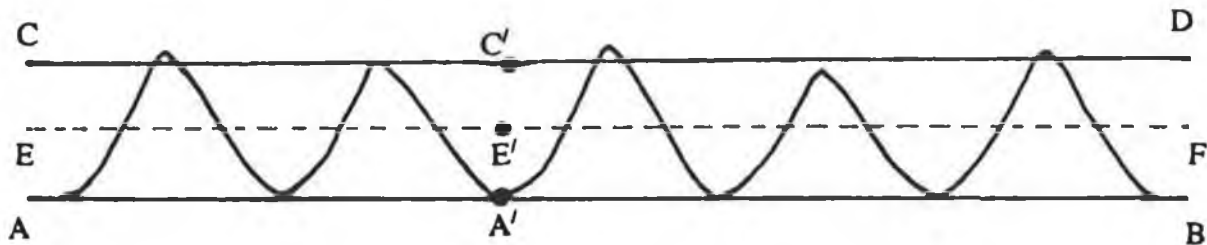


Fig.5.2: Measurement of average cutting force(F_x) of a section of cutting force signal from the light beam recorder

To measure the average cutting force from the above signal as shown in Fig.5.2 the following procedure was adopted:

- (a) A line CD is drawn parallel to the base line AB of the signal which touches almost all the periodic signals.

- (b) The distance between the two lines AB & CD is measured.
- (c) The line EF is drawn parallel to AB at a distance which is half of the distance between the two lines AB and CD i.e., $A'E' = A'C'/2$.
- (d) The distance $A'E'$ is the average cutting force encountered in the cutting system.

For multi-tooth cutting system to obtain the average force per tooth the area under the curve of force signals can be measured by planimeter and the value found is divided by the distance travelled per tooth. The procedure has been discussed in the reference [5]. In this work cutting was not multi-tooth cutting system.

5.6 Measurement of Flank wear of end mill cutter

Flank wear of the tools was measured by means of Toolmakers' Microscope. The glass stage attached to the microscope can be moved on two axes until the cutting tooth edge is parallel with the graticule (cross hair) of the microscope. The microscope tube is also sometimes necessary to bring the graticule parallel with the cutting edge. Flank wear measurement was carried out parallel to the surface of the wear land and in a direction perpendicular to the original cutting edge, e.g. the distance from the original cutting edge to the limit of wear land which intersect the original flank. Although the flank wear land on a significant portion of the flank may be of uniform size (VB1), there will be variations in its value (e.g.VB2 or VB3) at other portion of the flank. It is observed throughout the experiment that VB1 hardly occurs. In most cases, VB2 & VB3 are observed in this work.

5.7 Measurement of Surface Roughness

Generally, different surface roughness indices i.e. R_a , R_q , R_z etc. can be employed for expressing the surface roughness. Because of its simplicity, the arithmetic average R_a , has been adopted and is widely used. In this work, R_a value was used to measure the surface roughness. Surface Profilometers were used to obtain an enlarged tracing of the surface irregularities. The profilometers employ the travel of a diamond stylus along a

straight line over the surface. These instruments operate by amplifying the vertical motion of a stylus as it is drawn across the surface. Because of the finite radius of the stylus, its path is smoother than the actual surface roughness. The smaller the tip radius and the lower the surface roughness, the closer the path of the stylus to the actual surface profile. The profilometers produced a direct reading of the arithmetic mean surface roughness value. The arithmetic-mean surface roughness value was obtained by full wave rectifying. Waviness of the surface can be eliminated by a frequency cut-off device. A cut-off facility was built in to the profilometers. Cut-off is a filtering operation which is performed by a frequency dependent electronic filter. It may be noted that a misleading roughness height value could be obtained for the surface if proper value of cut-off(sampling length) is not selected [162]. In this work the cut-off values selected are shown in Table 5.4. The system was calibrated with a standard sample.

Table 5.4: Reference Cut-off values

Range of R_a (μm)	Cut-off (mm)
0.10 to 2.0	0.80
over 2.0	2.5

The R_a values of the machined surface were obtained by averaging surface roughness values at a minimum of three location points on the surface.

CHAPTER 6

INVESTIGATION OF CUTTING FORCES IN END MILLING STEEL (190 BHN) AND INCONEL 718

6.1 Introduction

Investigation of cutting forces in end milling steel (190 BHN) and Inconel 718 is divided as:

- (1) Development of cutting force model in end milling steel (190 BHN)
- (2) Influence of machining conditions (cutting speed, feed and axial depth of cut) on cutting forces in end milling Inconel 718.
- (3) Development of cutting force model in end milling Inconel 718

6.2 Development of cutting force model in end milling steel (190 BHN)

It is difficult to predict accurately the cutting forces encountered in milling operations due to large number of independent variables involved. In this work, an approach was undertaken to develop a mathematical model for predicting the average resultant cutting force in slot milling steel (190 BHN) by response surface methodology by taking into account primary machining variables like cutting speed, feed, and axial depth of cut. The cutting tool used was solid HSS slot drills. The adequacy of the model was tested by analysis of variance.

6.2.1 Development of the mathematical model by response surface methodology.

(i) Postulation of the mathematical model

Factors which influence cutting forces in end milling are shown in Fig.3.15 of chapter 3. But for a particular work-tool geometry cutting forces in end milling are assumed to be a function of primary machining conditions like cutting speed (v), feed (f_z) and axial depth of cut (a_a) i.e.:

$$\text{Cutting forces} = f (v, f_z, a_a)$$

From the equation (4.1) of chapter 4 the multiplicative model of the measured (experimental) resultant cutting forces can be written as:

$$F_{R(\text{steel})} = C_{40} v^{k_4} f_z^{l_4} a_a^{m_4} \epsilon' \quad (6.1)$$

Where F_R - measured (experimental) resultant cutting force (table system) for steel (N), v - cutting speed , m/min, f_z - feed per tooth, mm/tooth, a_a - axial depth of cut (mm) and C_{40} , k_4 , l_4 and m_4 - model parameters to be estimated using experimental data and ϵ' - experimental error.

From equation (4.5) of chapter 4, equation (6.1) can be written as:

$$\hat{y}_{(\text{steel})} = b_0 x_0 + b_1 x_1 + b_2 x_2 + b_3 x_3 \quad (6.2)$$

Where \hat{y}_{steel} - proposed predictive (estimated) response for steel on logarithmic scale, while $x_0 = 1$, and x_1 , x_2 and x_3 are coded values (logarithmic transformations) of v , f_z and a_a respectively. Decoding the equation (6.2), the multiplicative form can be written in terms of the cutting speed, v (m/min), feed, f_z (mm/tooth) and axial depth of cut, a_a (mm) as:

$$\hat{F}_{R(\text{steel})} = C_{40} v^{k_4} f_z^{l_4} a_a^{m_4} \quad (6.3)$$

Where $\hat{F}_{R(\text{steel})}$ - predicted (estimated) resultant cutting force (N) for steel.

(ii) Experimental Design

In order to estimate the model parameters of the equation (6.2) the first-order orthogonal design consisting of twelve experiments has been used to develop the predictive model. The first-order orthogonal design for 3 factors has been discussed in the section 4.1.3 of chapter 4. The complete design consists of twelve experiments in two blocks, each block consisting of six experiments. The first block of experiments includes trial numbers of 1,4,6,7,9 and 10. The four parameters (C_{60} , k_4 , l_4 and m_4) in the postulated model can be estimated using these six experiments. The second block of six experiments (2,3,5,8,11 and 12) has been added to provide more precise estimate of the parameters. The design provides three levels for each variable.

(iii) Coding of individual variables

The variables are coded by taking into account the capacity of the milling machine. The coded values of the variables shown in Table 6.1 for use in equation (6.2) were obtained from the following transforming equations:

$$x_1 = \frac{\ln v - \ln 30}{\ln 35 - \ln 30} \quad (6.4)$$

$$x_2 = \frac{\ln f_z - \ln 0.11}{\ln 0.20 - \ln 0.11} \quad (6.5)$$

$$x_3 = \frac{\ln a_a - \ln 0.60}{\ln 0.82 - \ln 0.60} \quad (6.6)$$

Where x_1 - the coded value of speed corresponding to its natural value v , x_2 - the coded value of feed corresponding to its natural value f_z and x_3 - the coded value of axial depth of cut corresponding to its natural value a_a

The above relationships were obtained from equation (4.10) of chapter 4.

Table 6.1 : Levels of the independent variables and coding identification for cutting force (steel)

Independent Variables	Levels in Coded form		
	-1 (low)	0 (centre)	+1 (high)
v , m/min (x_1)	26	30	35
f_z , mm/tooth (x_2)	0.06	0.11	0.20
a_a , mm (x_3)	0.44	0.60	0.82

(iv) Experiment

A slot milling operation was carried out on a vertical milling machine (Bridgeport). The milling machine was equipped with a Kistler piezo-electric dynamometer with three charge amplifiers. An average table system of cutting forces (F_x , F_y and F_z) was measured by a micro-computer via analog to digital (A/D) converter. The average force measuring system has been discussed in the section 5.4 of the chapter 5. The material selected was commercially available cold drawn bar of medium carbon mild steel. The detailed specification of the steel is shown in chapter 5. The hardness of the material was 190 BHN. Cutting tests were performed using commercially available HSS slot drills with a cobalt binder. The geometry of solid HSS slot drill is shown in chapter 5 and appendix 1. The first block of six tests (i.e., 1,4,6,7,9 and 10) were performed in random manner. After analyzing these results, the second block of six additional tests (i.e., trials 2,3,5,8,11 and 12) were also done in random manner. The results of twelve tests were listed in Table 6.2 together with actual cutting condition and code identification.

(v) Estimation of parameters in the postulated model

When the first block of six experiments was finished the parameters b 's in the equation (6.2) of the postulated model are estimated by the method of least square the basic formula of which is given by equation (4.13) of chapter 4. The solution of the above formula was done by computer using "Matlab" computer package (The calculation procedure to estimate parameter of the model is shown in appendix 2).

Table 6.2: Experimental Conditions and Results for cutting force (steel)

Trial No.	Block No.	Speed v m/min	Feed f_z mm/tooth	Axial depth of cut a_p , mm	Coding			Average Resultant cutting force F_R , N
					x_1	x_2	x_3	
1	1	26	0.06	0.44	-1	-1	-1	44.96
2	2	35	0.06	0.44	1	-1	-1	41.31
3	2	26	0.20	0.44	-1	1	-1	101.82
4	1	35	0.20	0.44	1	1	-1	103.68
5	2	26	0.06	0.82	-1	-1	1	77.45
6	1	35	0.06	0.82	1	-1	1	84.34
7	1	26	0.20	0.82	-1	1	1	220.25
8	2	35	0.20	0.82	1	1	1	185.20
9	1	30	0.11	0.60	0	0	0	102.80
10	1	30	0.11	0.60	0	0	0	105.07
11	2	30	0.11	0.60	0	0	0	93.51
12	2	30	0.11	0.60	0	0	0	97.42

(vi) **Analysis of results**

(a) **Development of the mathematical model**

The developed predictive cutting force model of the mean resultant cutting force for the first six experiments is given as:

$$\hat{y}_{(steel)} = 4.59 - 0.03x_1 + 0.45x_2 + 0.35x_3 \quad (6.7)$$

The combined results of 12 tests

To increase the precision associated with estimates of parameters of the model the second block of six trials (2,3,5,8,11 and 12) was conducted and the results are shown in Table 6.2. The developed cutting force model for the mean resultant cutting force for the second six experiments is found as:

$$\hat{y}_{(steel)} = 4.5050 - 0.0075x_1 + 0.4463x_2 + 0.3250x_3 \quad (6.8)$$

Combining the results of all twelve tests, the fitted mean resultant cutting force equation was found to be as:

$$\hat{y}_{(steel)} = 4.5475 - 0.02x_1 + .4463x_2 + 0.3262x_3 \quad (6.9)$$

The predicting equation (6.9) can be graphically represented in the 3 dimensional space of cutting speed, feed and axial depth of cut as depicted in Fig.6.1 (note that this figure is on a logarithmic scale). Equation (6.9) can be transformed using equations (6.4), (6.5) and (6.6) to provide the average resultant cutting force F_R (N) as function of cutting speed v (m/min), feed rate f_z (mm/tooth) and axial depth of cut a_a (mm) as follows:

$$\hat{F}_{R(steel)} = 1299.84 v^{-0.13} f_z^{0.74} a_a^{1.04} \quad (6.10)$$

The equation (6.10) is valid for slot milling of cold rolled medium carbon mild steel (190 BHN) using HSS slot drill under dry conditions and

$$26 \leq v \leq 35 \quad \text{m/min}$$

$$0.06 \leq f_z \leq 0.20 \quad \text{mm/tooth}$$

$$0.44 \leq a_a \leq 0.82 \quad \text{mm}$$

The equation indicates that an increase in the cutting speed decreases the mean resultant cutting force while an increase in the feed and axial depth of cut increases the mean resultant cutting force.

The predicting equation (6.9) can also be plotted in Fig.6.2 as contours for each of the response surfaces at three selected levels of feed rates (note that this figure is on a logarithmic scale). These selected levels were chosen as low ($f_z = 0.06$ mm/tooth), centre ($f_z = 0.11$ mm/tooth) and high ($f_z = 0.20$ mm/tooth). These contours were constructed by computer utilizing "Matlab" computer package.

(c) Adequacy of the postulated model

The analysis of variance (ANOVA) was used to check the adequacy of the developed model. As per this technique the calculated F_{rat} of the model was found to be 6.93 while the $F_{rat 5,2}$ for 95% confidence is 19.30 as obtained from statistical table. Hence the model is valid. The results for analysis of variance for the combined block of 12 tests are shown in Appendix 2.

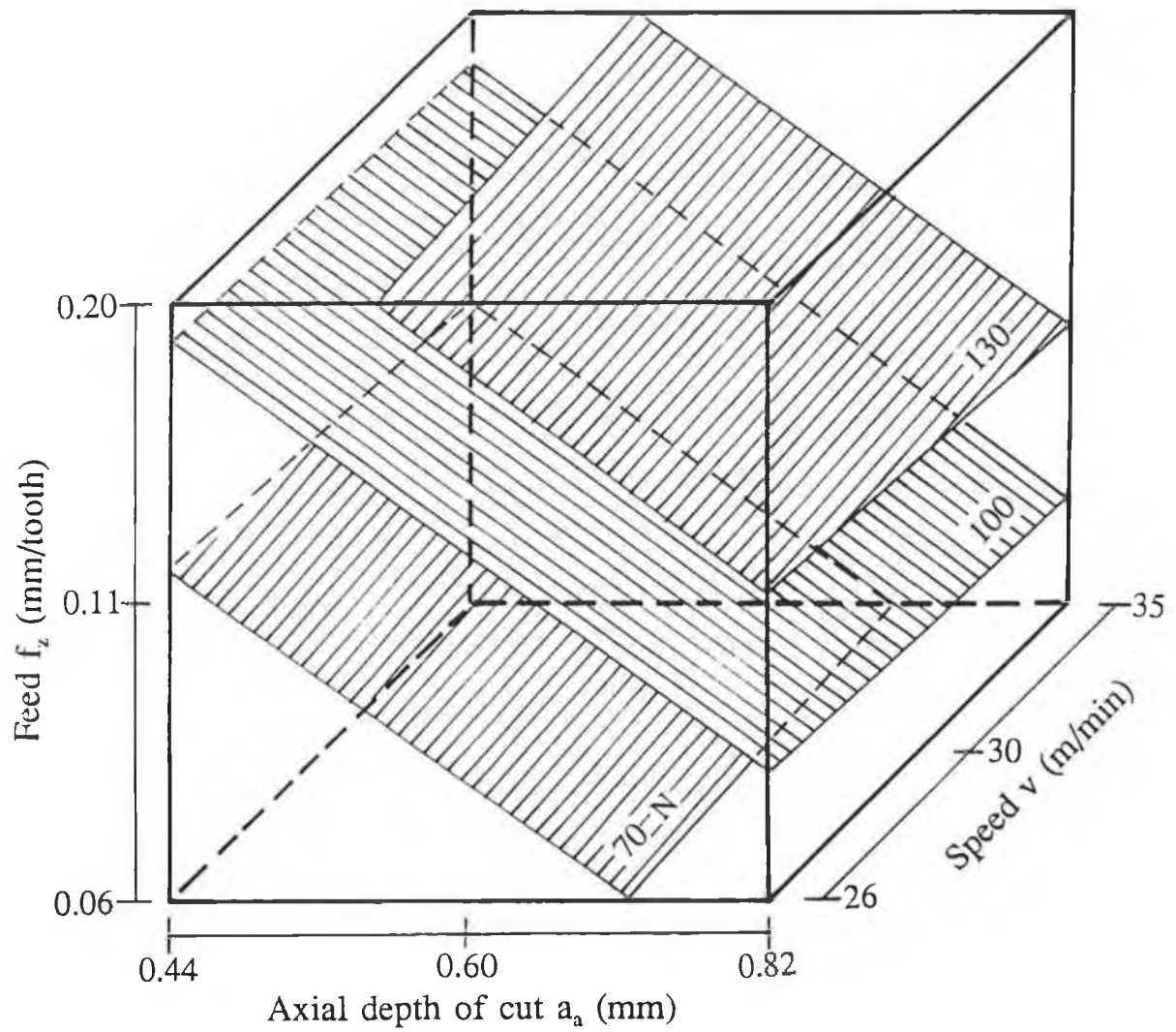


Fig.6.1: Contour surfaces for resultant cutting forces in end milling steel(190 BHN) in 3 dimensional factor space (log-scales)

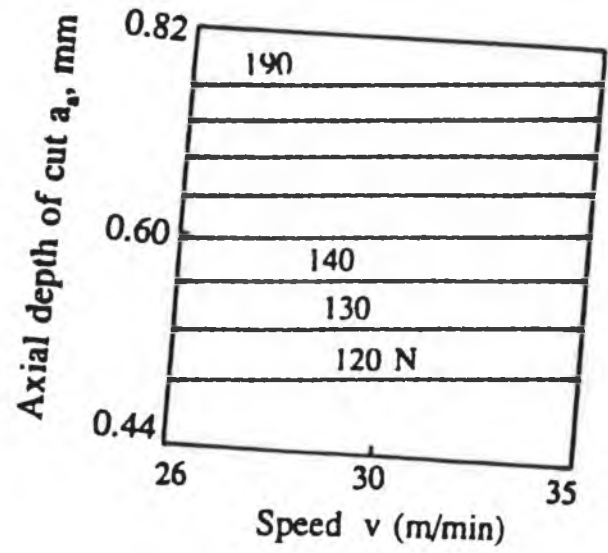
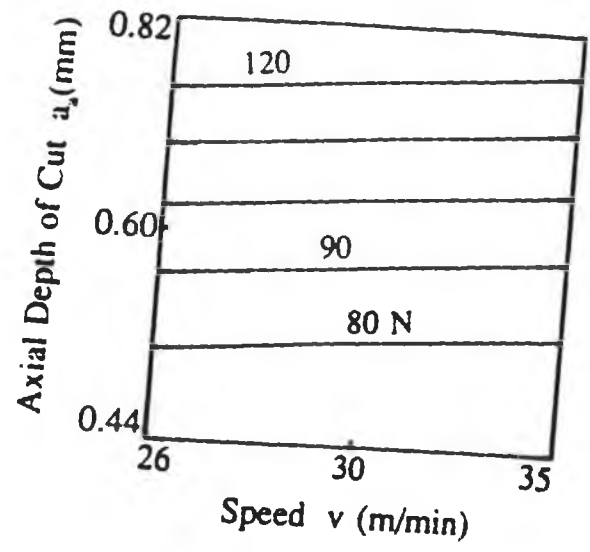
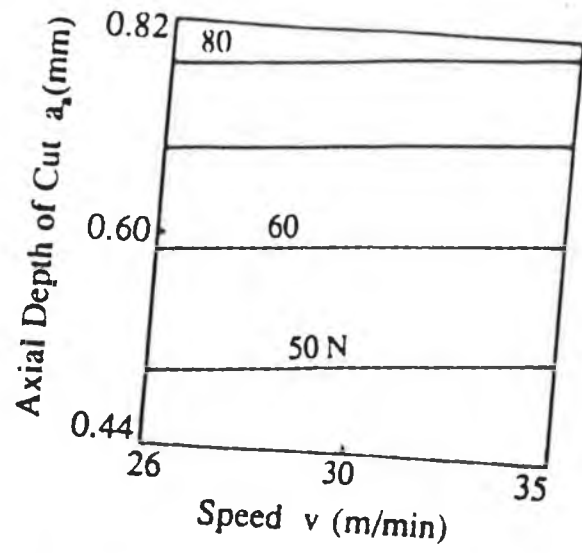


Fig.6.2: Resultant cutting force contours (first-order model) for steel (190 BHN) in speed-axial depth of cut planes at selected levels of feed (log-scales)

(c) Significance testing of individual variables (combined blocks)

The significance testing of the variables of the postulated model is performed using the formula (4.15) of chapter 4 and the results are shown in Appendix 2. From the significance testing it is seen that the calculated F_{rat} of the variables x_1 (speed), x_2 (feed) and x_3 (axial depth of cut) are 0.51, 291.84 and 155.91 respectively, while the F_{rat} for 95% confidence is 5.32 as obtained from statistical table. Hence, feed and axial depth of cut have a significant effect on the mean resultant cutting force while speed has no significant effect on the mean resultant cutting force. Though the effect of speed is not significant still it is included in the postulated model as it is an important variable in the material cutting operation.

(d) Precision of prediction (Confidence interval)

Due to the experimental error ϵ' , the estimated parameters and hence the estimated mean resultant cutting forces (\hat{y}) are subjected to uncertainty. Hence, the precision of these has been estimated by calculating confidence intervals on the mean resultant cutting force. The confidence intervals have been calculated using the formula 4.16 of chapter 4. The resulting 95% confidence interval for twelve tests are shown in Appendix 2.

(vii) Conclusions

- (a) A reliable predictive model for cutting forces can be estimated readily with a small number of tests.
- (b) Although the model has been developed and tested from very few experimental results, it can be used to predict the mean resultant cutting forces for any condition within the boundaries of research.
- (c) The predicting cutting force equation is valid within the speed range of 26 - 35 m/min., the feed range of 0.06 - 0.22 mm/tooth and the axial depth of range of 0.44 - 0.82 mm.
- (d) The cutting force is affected significantly by feed and axial depth of cut. It increases with the increase of feed and axial depth of cut. The cutting force is not affected significantly by the speed. It decreases slightly with the increase of the speed.

6.3 Influence of machining conditions on cutting forces in end milling Inconel 718.

The influence of machining conditions on cutting forces in end milling Inconel 718 is divided into 3 parts as:

- (1) Influence of machining conditions on cutting forces for full immersion end milling Inconel 718.
- (2) Influence of machining conditions on cutting forces for half immersion end milling Inconel 718 at up milling mode.
- (3) Influence of machining conditions on cutting forces for half immersion end milling Inconel 718 at down milling mode.

All cutting tests were conducted using uncoated carbide inserts under dry conditions.

6.3.1 Influence of machining conditions on cutting forces for full immersion end milling Inconel 718

The influence of machining conditions on cutting forces for full immersion end milling Inconel 718 is divided as:

- (1) Influence of cutting speed on cutting forces.
- (2) Influence of feed on cutting forces
- (3) Influence of axial depth of cut on cutting forces.

6.3.1.1 Influence of cutting speed on cutting forces for full immersion end milling Inconel 718.

The table system of cutting forces (i.e., F_x , F_y and F_z) measured at low ($f_m = 22$ mm/min), medium (i.e., $f_m = 45$ mm/min) and high (i.e., $f_m = 64$ mm/min) feed rates. The F_x components of cutting forces at low, medium and high feed rates are plotted

against the cutting speed at an axial depth of cut of 1.2 mm in Fig. 6.3. Similarly F_y at low, medium and high feed and F_z at low, medium and high feed is plotted Fig. 6.4 and 6.5 respectively.

The calculated tangential component of cutting forces (F_t) at low, medium and high feed rates is plotted against the cutting speed as shown in Fig.6.6 while the calculated resultant cutting force (F_R , table system) at low, medium and high feed is shown in Fig.6.7.

All the above figures show that the cutting forces increase as the cutting speed decreases. This may be attributed to the following reasons:

- (i) Since milling table speeds (f_m , feed per minute) at low, medium and high are kept constant against varying cutting speed, so the chip load (f_z , feed per tooth) or chip thickness increases as the cutting speed decreases. Consequently, cutting forces increase.
- (ii) It is usually observed that as cutting speed decreases shear angle (ϕ) also decreases. A small shear angle gives a long shear plane. For a fixed shear strength, an increase in shear plane area increases the shearing forces required to produce sufficient stress for deformation.
- (iii) At low cutting speed the friction co-efficient increases, hence, it increases cutting forces.

From all the above figures it is also observed that the cutting forces are higher for higher feed rates. This is due to the fact that as the feed rate increases, the chip load per tooth also increases, hence cutting force increases.

In Fig. 6.8, F_x , F_y and F_z are plotted against the cutting speed at medium feed ($f_m = 45$ mm/min). From Fig.6.8 it is seen that the F_y component of cutting forces is the highest of the table system of cutting forces. The intermediate and the lowest component of cutting forces are F_x and F_z cutting forces respectively.

In Fig.6.9 the measured cutting forces (F_x , F_y and F_z) are plotted against a varying cutting speed at constant chip load (i.e., f_m , feed per tooth - was kept constant at axial depth of cut 0.50 mm).

From Fig.6.9 it is seen that cutting forces decrease significantly up to a certain point (speed range 11 - 16 m/min) as the cutting speed increases. After a certain point (speed range 17 - 22 m/min) the increase of the cutting force with the decrease of cutting speed is not so significant. It may be attributed that the rate of decrease of shear angle and the rate of increase of the friction co-efficient (as mentioned in p.167) up to the speed range of 11 - 16 m/min are higher than that of 17 - 22 m/min.

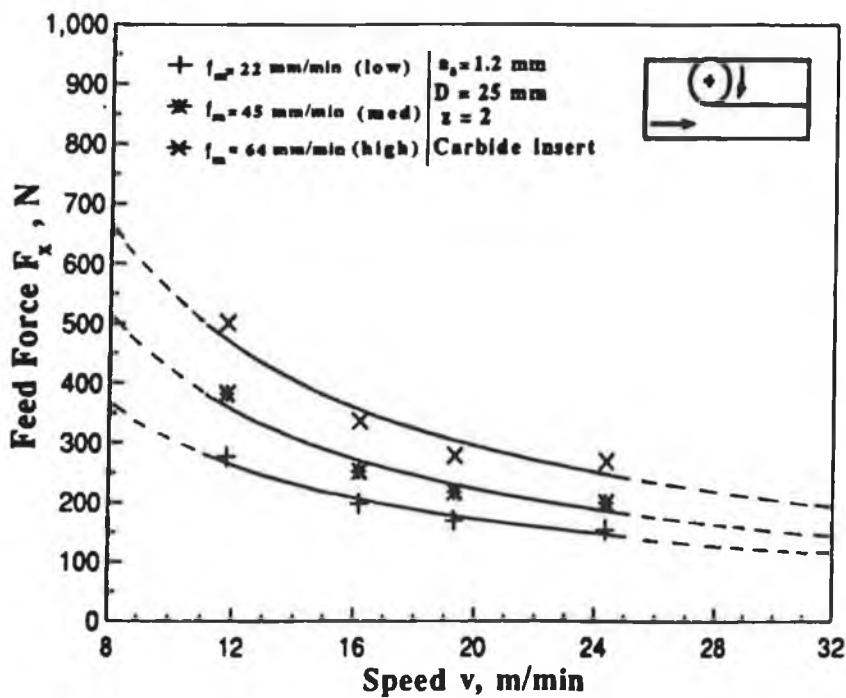


Fig.6.3: Effect of cutting speed on average feed force (F_x) in slot milling Inconel 718 at 3 selected levels of feed f_m (22, 45 and 64 mm/min)

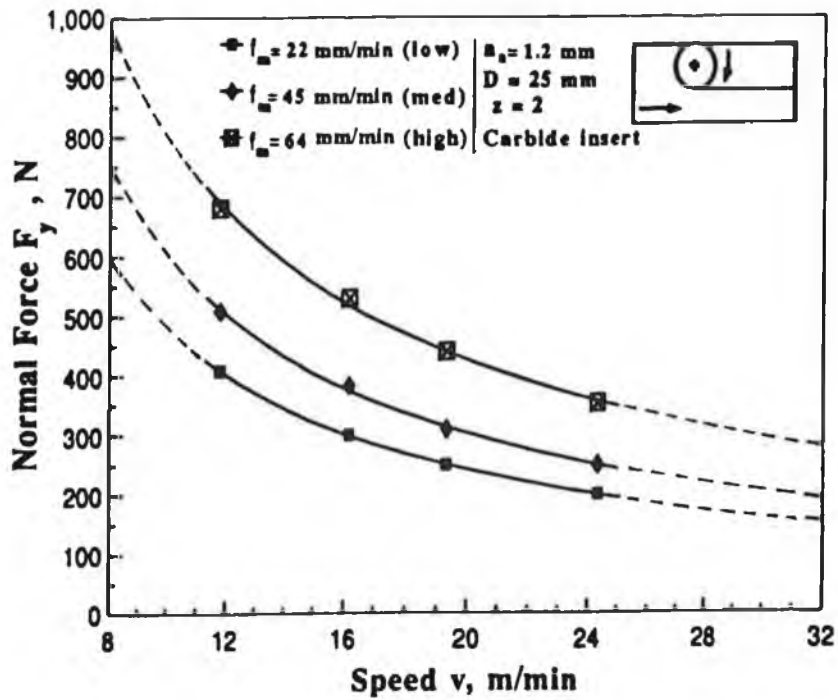


Fig.6.4: Effect of cutting speed on average normal force (F_y) in slot milling Inconel 718 at 3 selected levels of feed f_m (22, 45 and 64 mm/min)

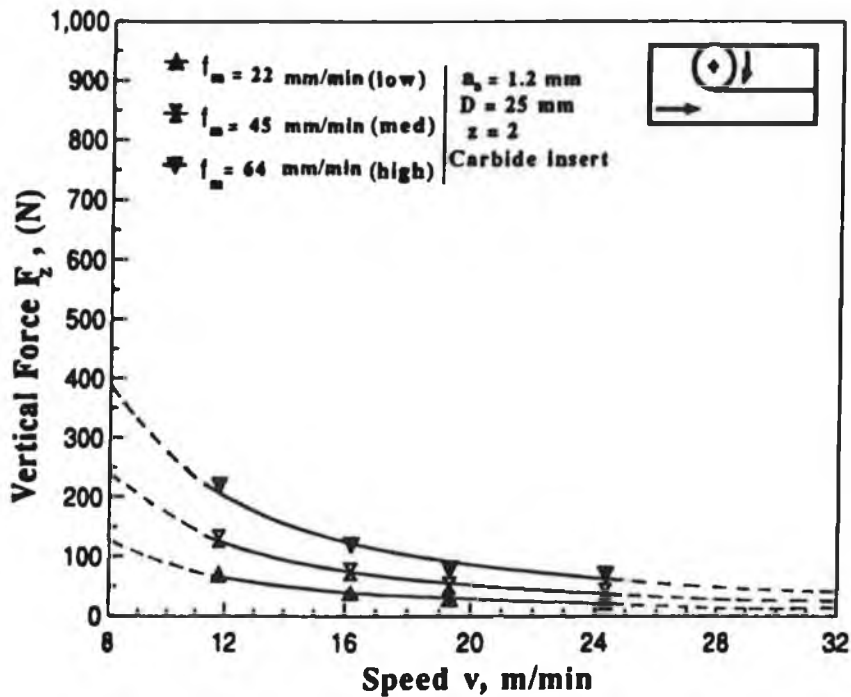


Fig.6.5: Effect of cutting speed on average vertical force (F_z) in slot milling Inconel 718 at 3 selected levels of feed f_m (22, 45 and 64 mm/min)

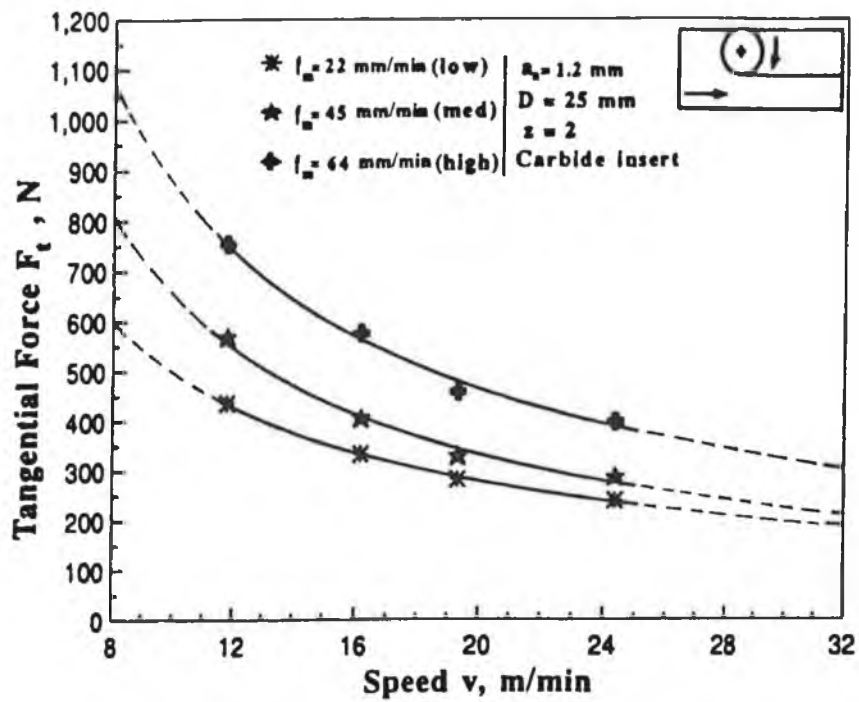


Fig.6.6: Effect of cutting speed on average tangential force (F_t) in slot milling Inconel 718 at 3 levels of feed f_m (22, 45 and 64 mm/min)

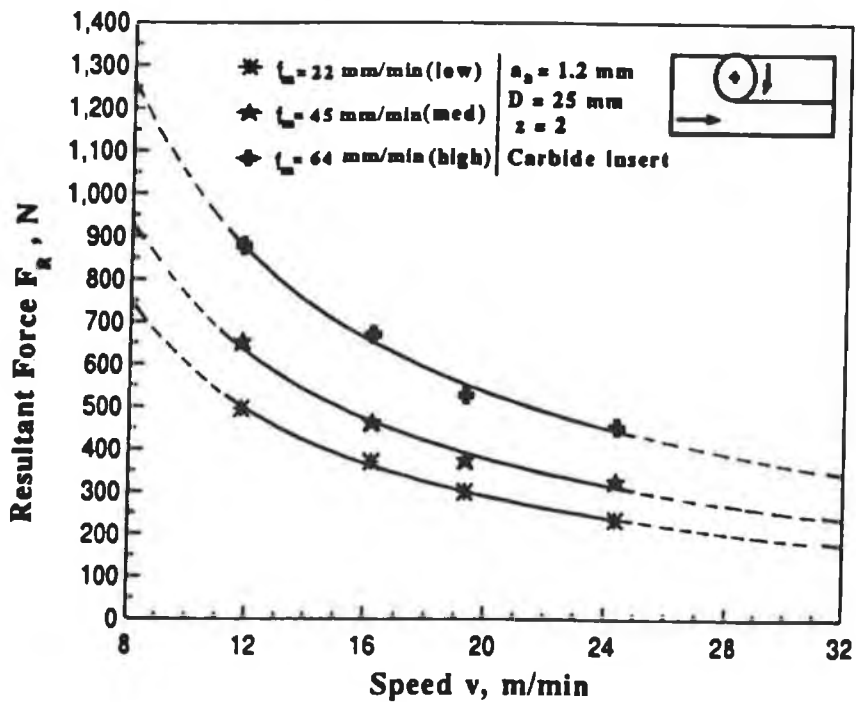


Fig.6.7: Effect of cutting speed on average resultant force (F_R) in slot milling Inconel 718 at 3 selected levels of feed f_m (22, 45 and 64 mm/min)

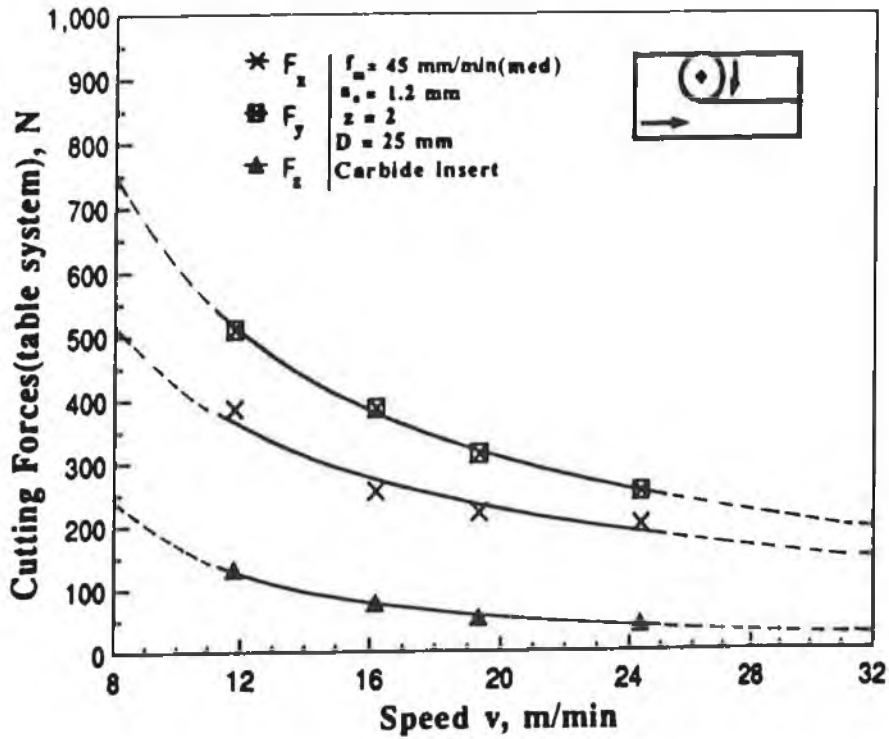


Fig.6.8: Effect of cutting speed on average table system of cutting forces in slot milling Inconel 718 at feed rate f_m (45 mm/min) and axial depth of cut a_1 of 1.2 mm

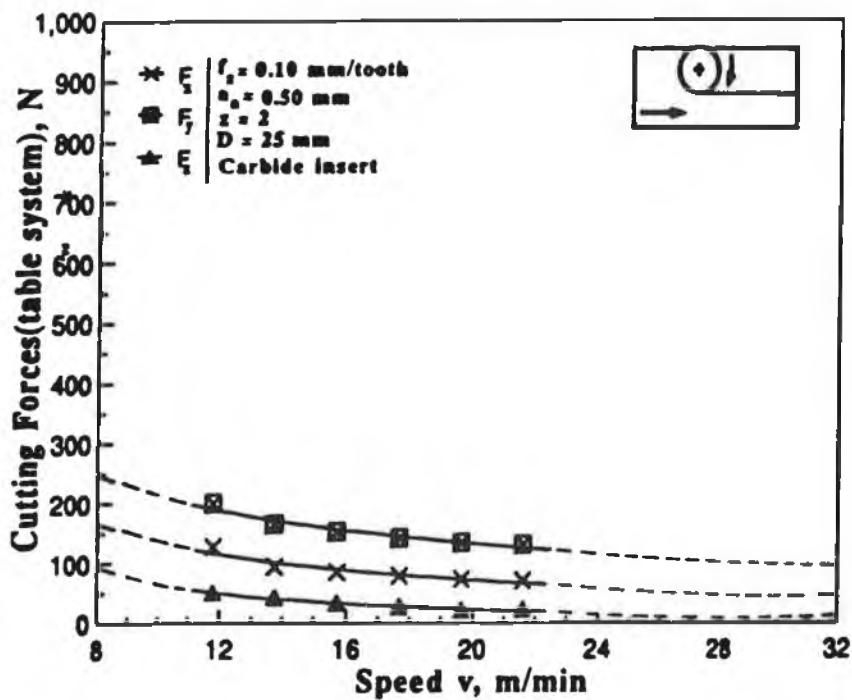


Fig.6.9: Effect of cutting speed on average table system of cutting forces in slot milling Inconel 718 at feed rate f_2 of 0.10 mm/tooth and $a_1 = 0.50 \text{ mm}$

6.3.1.2 Influence of feed rate on cutting forces for full immersion end milling Inconel 718

The F_x component of cutting forces obtained from low ($v \approx 11.78$ m/min), medium ($v \approx 16.17$ m/min) and high ($v \approx 24.34$ m/min) cutting speed are plotted against feed per minute (f_m) at an axial depth of cut of 1.2 mm in Fig.6.10. Similarly F_y at low, medium and high and F_z at low, medium and high cutting speed are plotted against feed per minute (f_m) in Fig.6.11 and 6.12 respectively.

The calculated tangential component of cutting forces (F_t) at low, medium and high cutting speed are plotted against feed per minute (f_m) as shown in Fig.6.13 while the calculated resultant cutting forces (F_R , table system) at low, medium and high speed are shown in Fig.6.14.

All the above figures show that:

- the cutting forces increase almost exponentially as the feed rate increases
- the cutting forces are highest for low cutting speed followed by the forces at medium and high cutting speed

This increase in cutting forces is due to an increase in chip thickness ($t_c = f_z \sin \phi$) with higher feed. Cutting forces are the highest for low cutting speed because for a fixed table speed (f_m), chip load (f_z) increases at low cutting speed.

In Fig. 6.15, F_x , F_y and F_z are plotted against feed per minute at medium cutting speed. From this figure 6.15 it is seen that F_y component is the highest of the table system of cutting forces and the intermediate and lowest components are F_x and F_z .

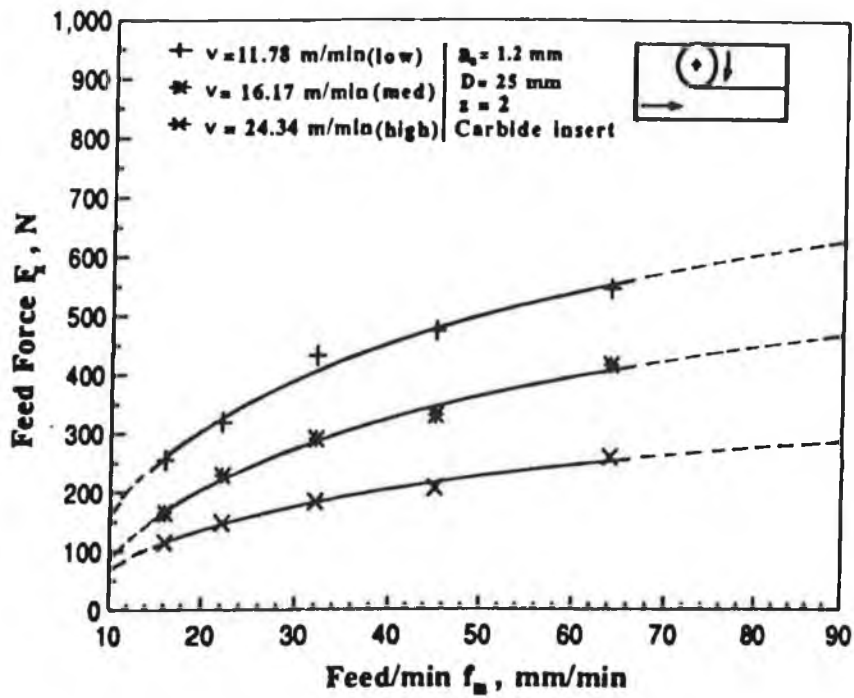


Fig.6.10: Effect of feed (f_m) on average feed force (F_x) in slot milling Inconel 718 at 3 selected levels of speed (11.78, 16.17 and 24.34 m/min)

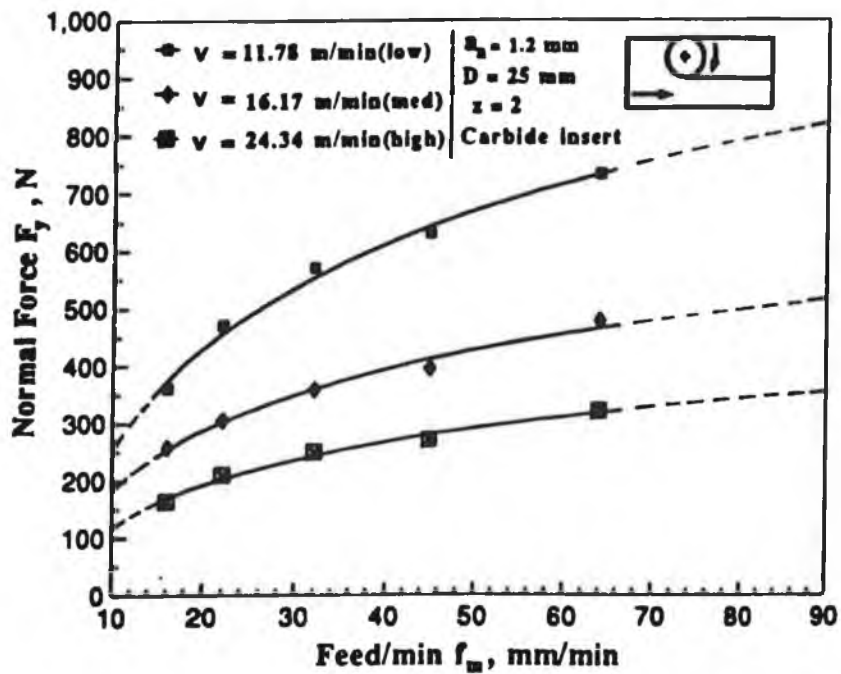


Fig.6.11: Effect of feed (f_m) on average normal force (F_y) in slot milling Inconel 718 at 3 selected levels of speed (11.78, 16.17 and 24.34 m/min)

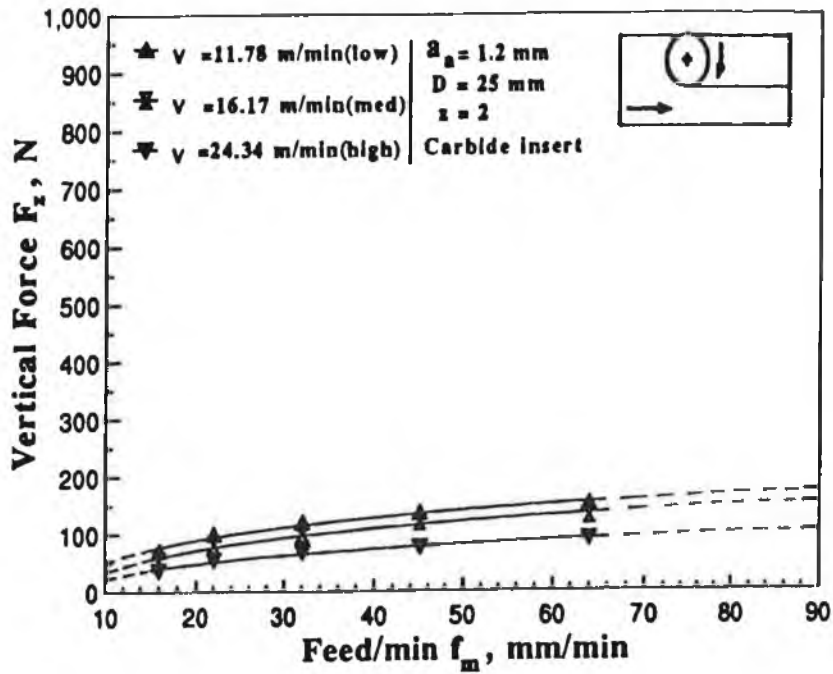


Fig.6.12: Effect of feed (f_m) on average vertical force (F_z) in slot milling Inconel 718 at 3 selected levels of speed (11.78, 16.17 and 24.34 m/min)

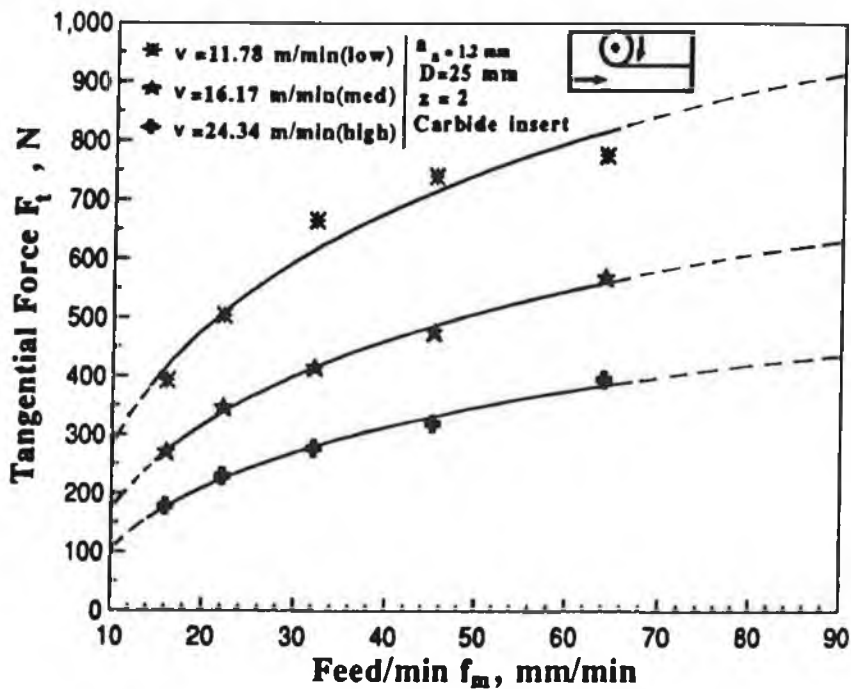


Fig.6.13: Effect of feed (f_m) on average tangential force (F_t) in slot milling Inconel 718 at 3 selected levels of speed (11.78, 16.17 and 24.34 m/min)

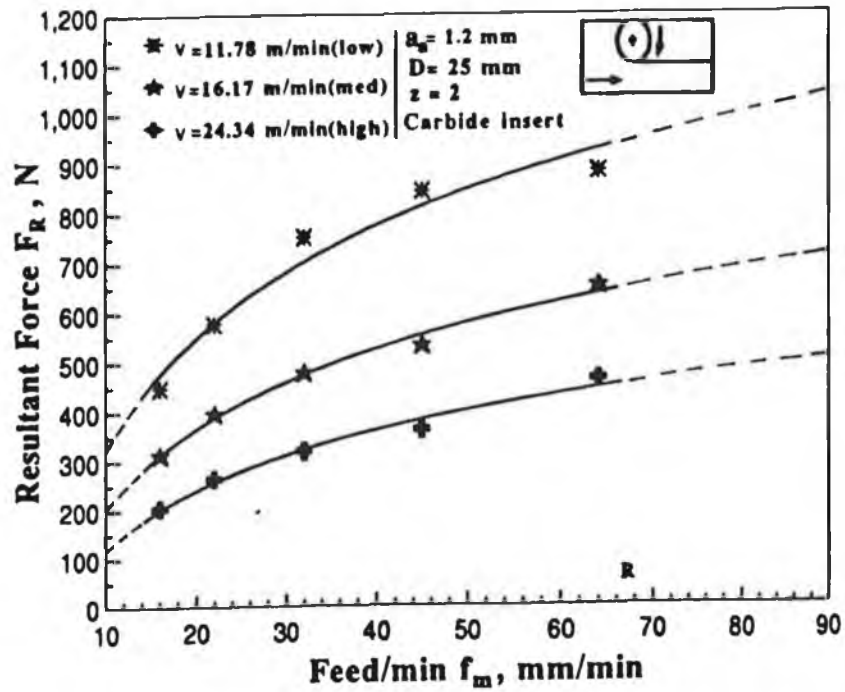


Fig.6.14: Effect of feed (f_m) on average resultant force in slot milling Inconel 718 at 3 selected levels of speed (11.78, 16.17 and 24.34 m/min)

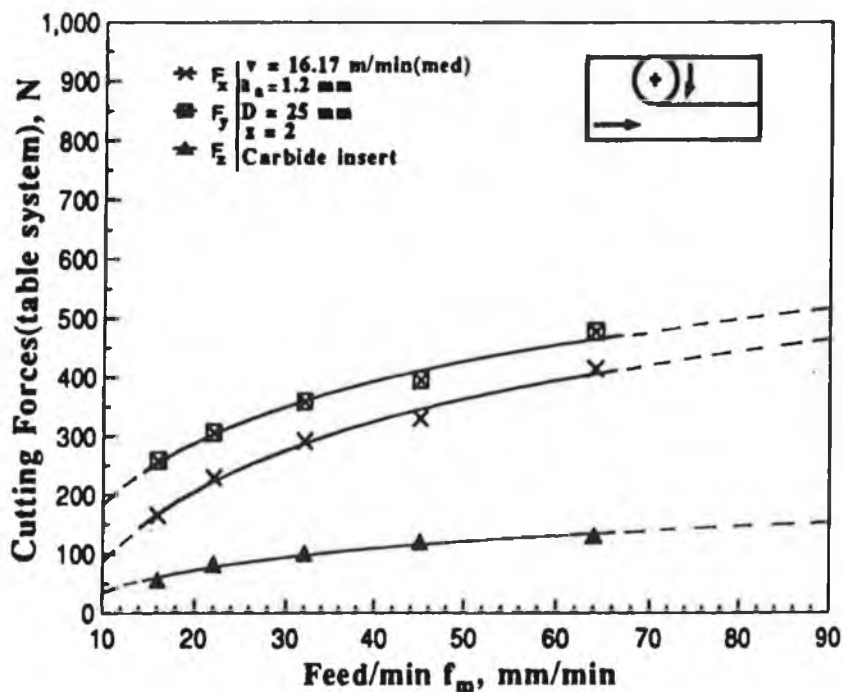


Fig.6.15: Effect of feed (f_m) on average table system of cutting forces in slot milling Inconel 718 at cutting speed of 16.17 m/min and axial depth of cut of 1.2 mm

6.3.1.3 Influence of axial depth of cut on cutting forces for full immersion end milling Inconel 718.

The F_x component of cutting forces at low ($v = 11.76$ m/min), medium ($v = 16.17$ m/min) and high ($v = 24.34$ m/min) cutting speed are plotted against axial depth of cut at feed rate (f_m) of 45 mm/min in Fig 6.16. Similarly the F_y at low, medium and high cutting speed and the F_z at low, medium and high cutting speed are plotted in Fig 6.17 and 6.18 respectively.

The calculated tangential component of cutting forces (F_t) at low, medium and high speed are plotted against axial depth of cut in Fig. 6.19 while the calculated resultant cutting forces (F_R) at low, medium and high speed are shown in Fig. 6.20.

From all the figures it is seen that cutting forces increase almost linearly with the increase of axial depth of cut. This is attributed to the increase of the size of cut with the increase of axial depth of cut. As the size of cut increases then the cutting force also increases. It may be mentioned here that the cutting forces at low and medium speed at an axial depth of cut of 2.00 mm is disproportionately high. The inserts were examined and found microchipped. Since the feed per minute (f_m) is constant, hence at low and medium cutting speed the chip load (f_z) is 0.15 mm/tooth and 0.11 mm/tooth respectively. So, at axial depth of cut 2.00 mm and chip load of 0.15 mm/tooth and 0.11 mm/tooth the cutting edge of the insert may not withstand compressive load of the cut, hence the insert may be microchipped. But at high speed, the chip load was 0.09 mm/tooth, which is lesser than that of the chip load at low and medium speed. So, at high speed the inserts are not microchipped.

In Fig.6.21, F_x , F_y and F_z are plotted against axial depth of cut at medium cutting speed. From this figure it is seen that F_y is the highest of the table system of cutting force and the intermediate and lowest components of cutting forces are F_x and F_z respectively.

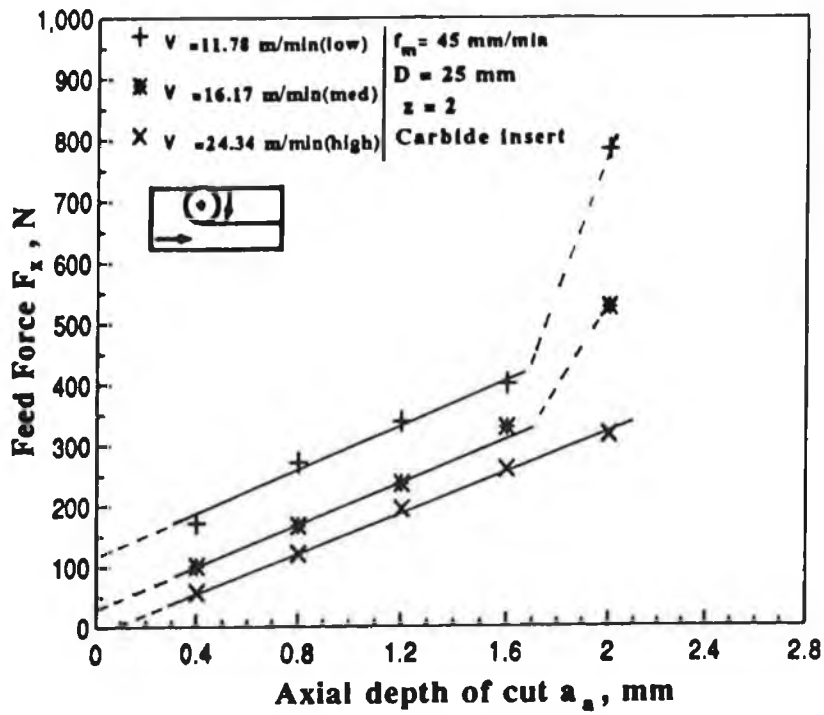


Fig.6.16: Effect of axial depth of cut on average feed force (F_x) in slot milling Inconel 718 at 3 selected levels of speed (11.78, 16.17 and 24.34 m/min)

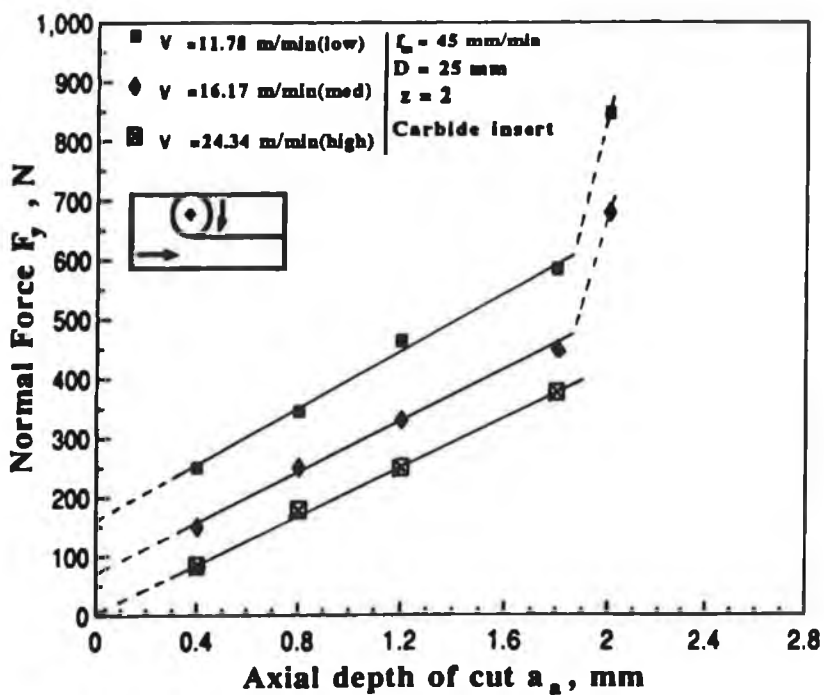


Fig.6.17: Effect of axial depth of cut on average Normal force (F_y) in slot milling Inconel 718 at 3 selected levels of speed (11.78, 16.17 and 24.34 m/min)

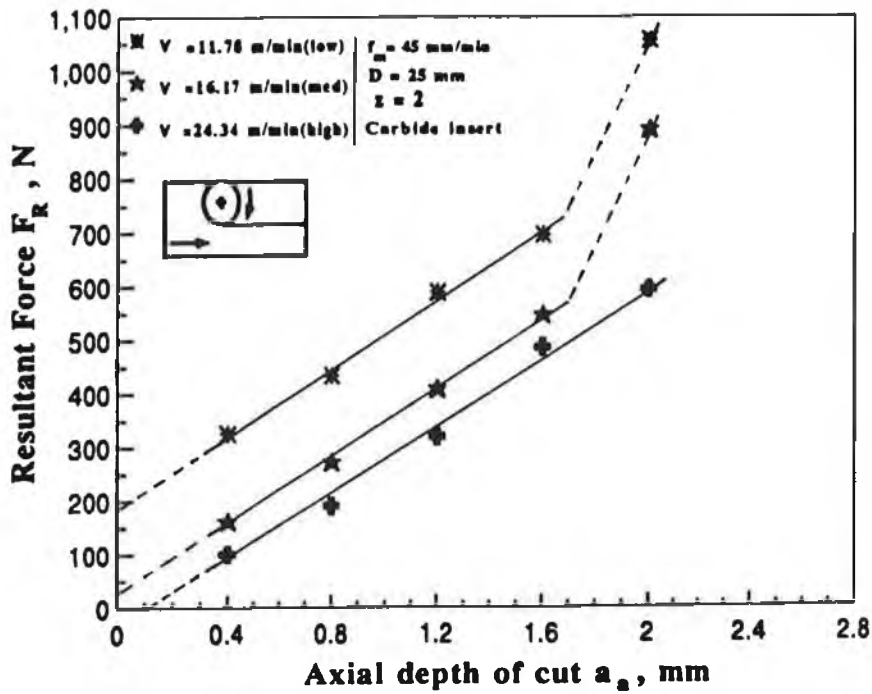


Fig.6.20: Effect of axial depth of cut on average resultant force (F_R) in slot milling Inconel 718 at 3 selected levels of speed (11.78, 16.17 and 24.34 m/min)

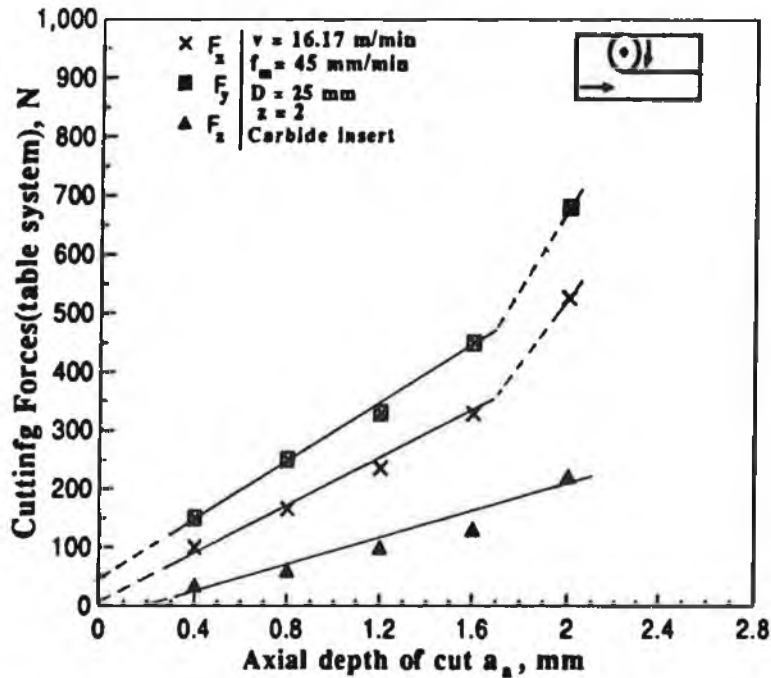


Fig.6.21: Effect of axial depth of cut on average table system of cutting forces in slot milling Inconel 718 at 3 selected levels of speed (11.78, 16.17 and 24.34 m/min)

6.3.2 Influence of machining conditions on cutting forces for half immersion end milling Inconel 718 at up milling mode

The influence of machining conditions on cutting forces for half immersion end milling Inconel 718 at up milling mode is divided into 3 parts as:

- (1) Influence of cutting speed on cutting forces
- (2) Influence of feed on cutting forces
- (3) Influence of axial depth of cut on cutting forces

6.3.2.1 Influence of cutting speed for half immersion end milling Inconel 718 at up milling mode

The measured (experimental) cutting forces (table system, F_x , F_y and F_z) are plotted against cutting speed at axial depth of cut of 1.2 mm in Fig.6.22. The calculated tangential component F_t and resultant cutting force are plotted against cutting speed in Fig.6.23 and 6.24 respectively. From these figures it is also seen that the force components decreases as the cutting speed increases. The reasons for this force decrease with the increase of cutting speed are discussed in section 6.3.1.1. From Fig. 6.23 it is seen that the F_x component is the highest in the table system of cutting forces. The F_y component is slightly greater than the vertical component. The F_x is much greater than F_y . The reason may be analyzed from the equation 3.27 of chapter 3. as that F_x is the sum of 2 resolved components of cutter system of cutting forces (i.e. $F_x = F_t \cos \psi + F_r \sin \psi$) while F_y is the subtraction of 2 resolved components of cutter system of cutting forces(i.e. $F_y = F_t \sin \psi - F_r \cos \psi$).

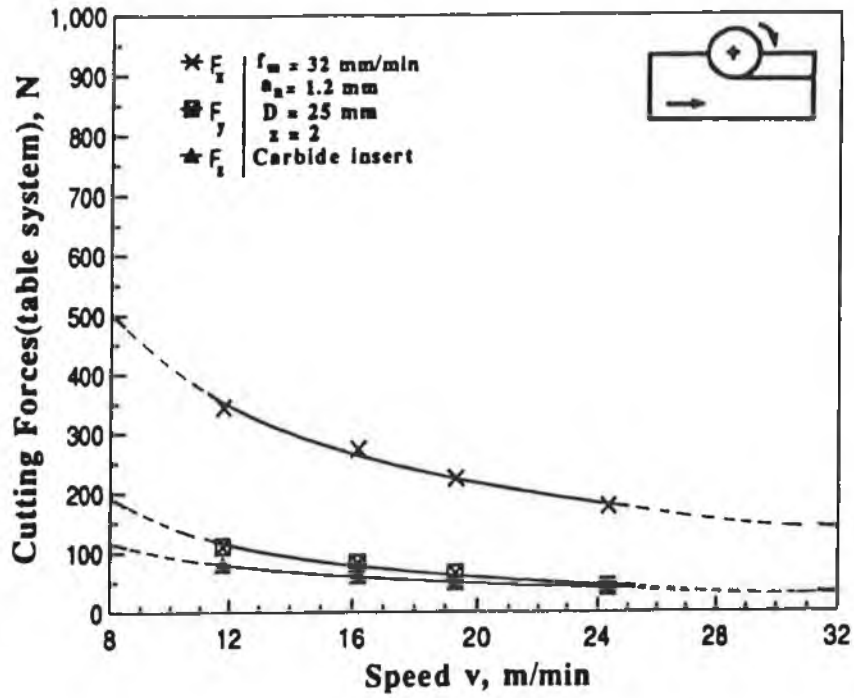


Fig.6.22: Effect of speed on table system of cutting forces in half immersion up end milling Inconel 718 at feed (f_m) rate of 32 mm/min

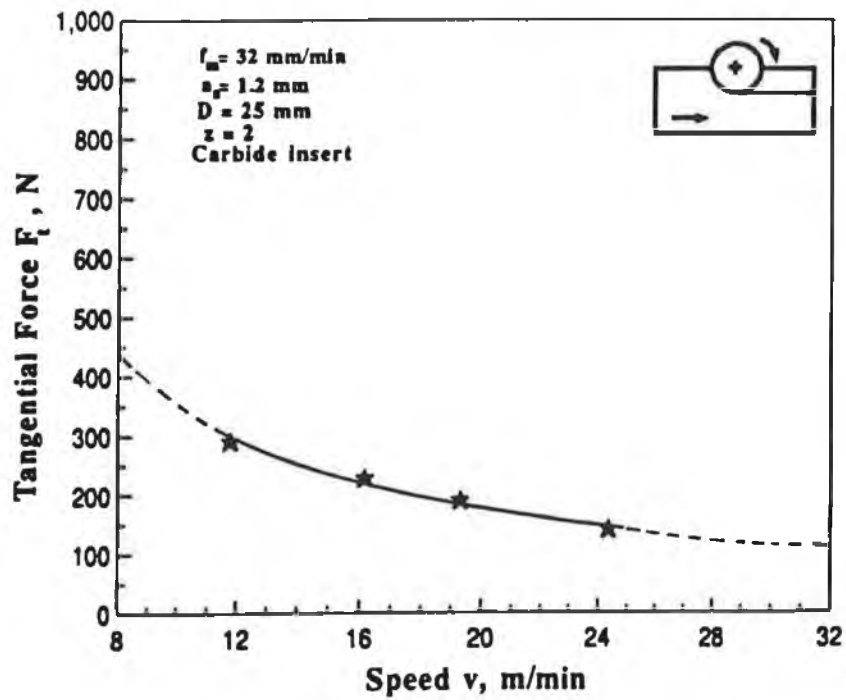


Fig.6.23: Effect of speed on average tangential force in half immersion up end milling Inconel 718 at feed (f_m) rate of 32 mm/min

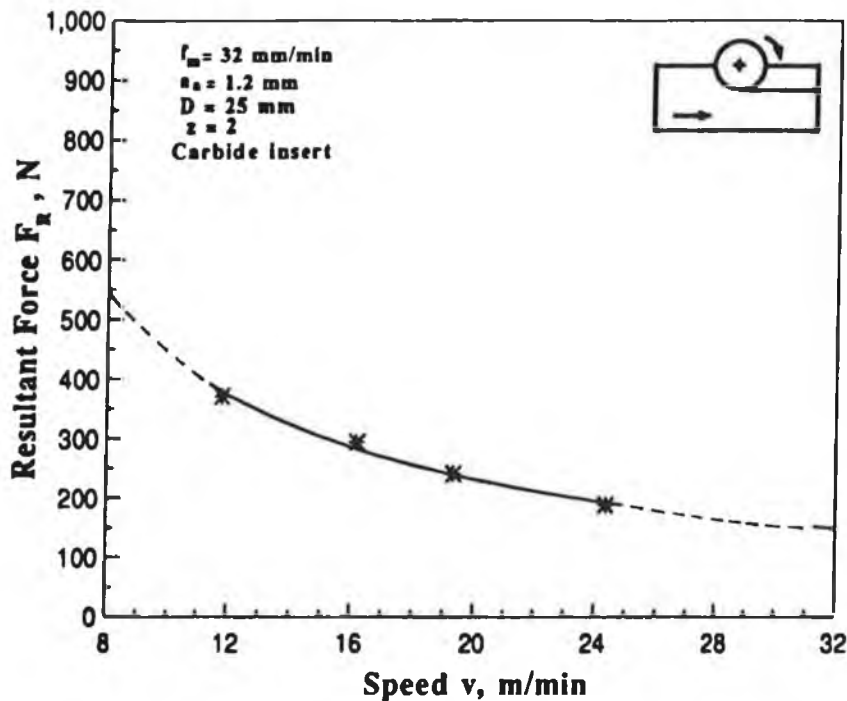


Fig.6.24: Effect of speed on average resultant force in half immersion up end milling Inconel 718 at feed (f_m) rate of 32 mm/min

6.3.2.2 Influence of feed (f_m) on cutting forces for half immersion end milling Inconel 718 at up milling mode.

The measured table system of cutting forces (F_x , F_y and F_z) are plotted against feed per tooth at axial depth of cut in Fig.6.25. The calculated tangential component F_t and resultant cutting force F_R are plotted against feed in Fig.6.26 and 6.27 respectively. From all the figures it is observed that the cutting forces increases as the feed rate (f_m) increases. The reasons for this increase of cutting force with the increase of feed are discussed in section 6.3.1.2. From Fig. 6.26 it is observed that the F_x component of cutting forces is the highest in the table system of cutting forces (the reason is mentioned section 6.3.2.1).

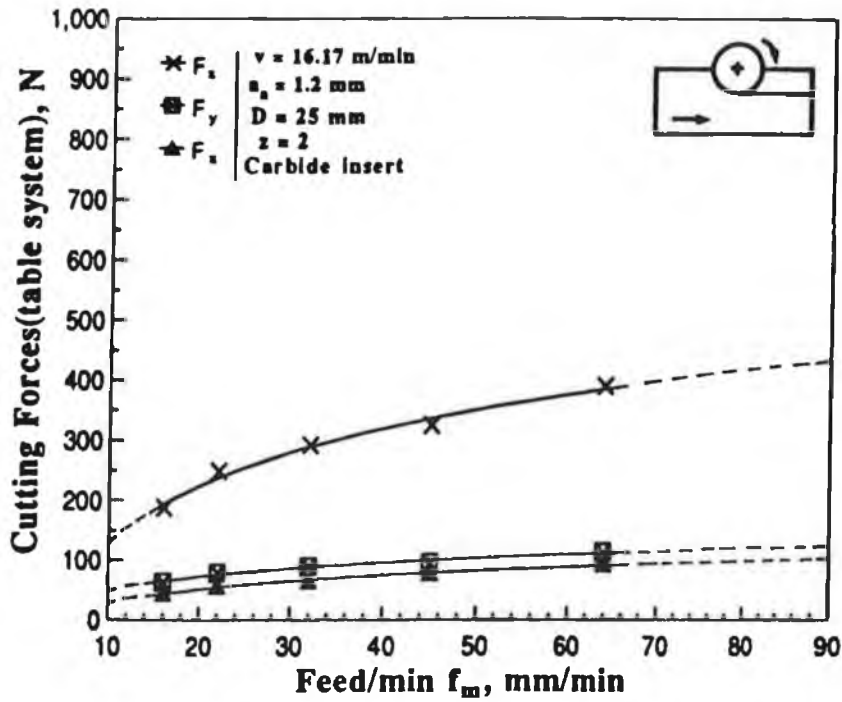


Fig.6.25: Effect of feed (f_m) on average table system of cutting forces in half immersion up end milling Inconel 718 at cutting speed of 16.17 m/min

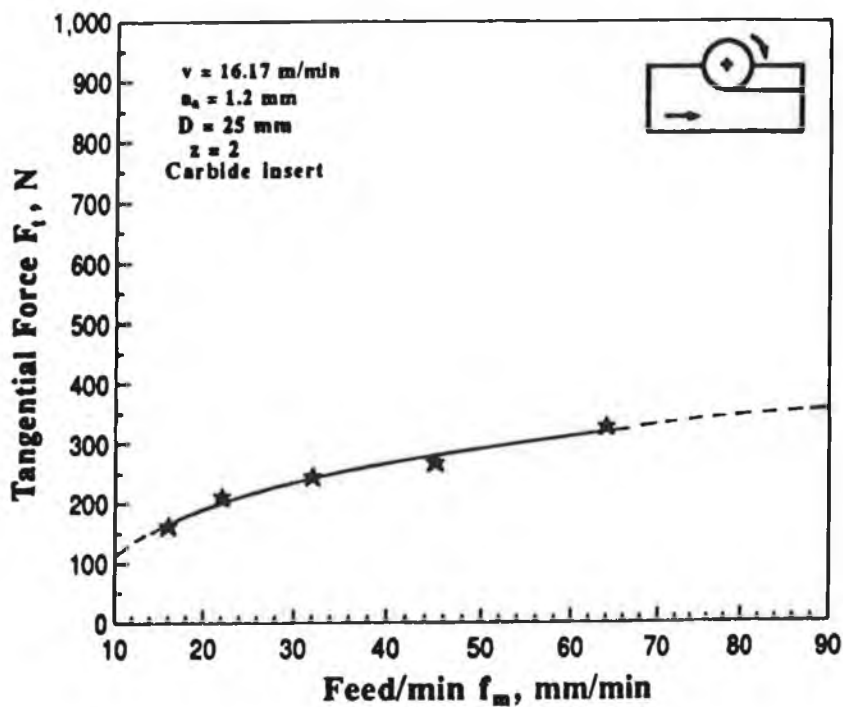


Fig.6.26: Effect of feed (f_m) on average tangential force in half immersion up end milling Inconel 718 at cutting speed of 16.17 m/min

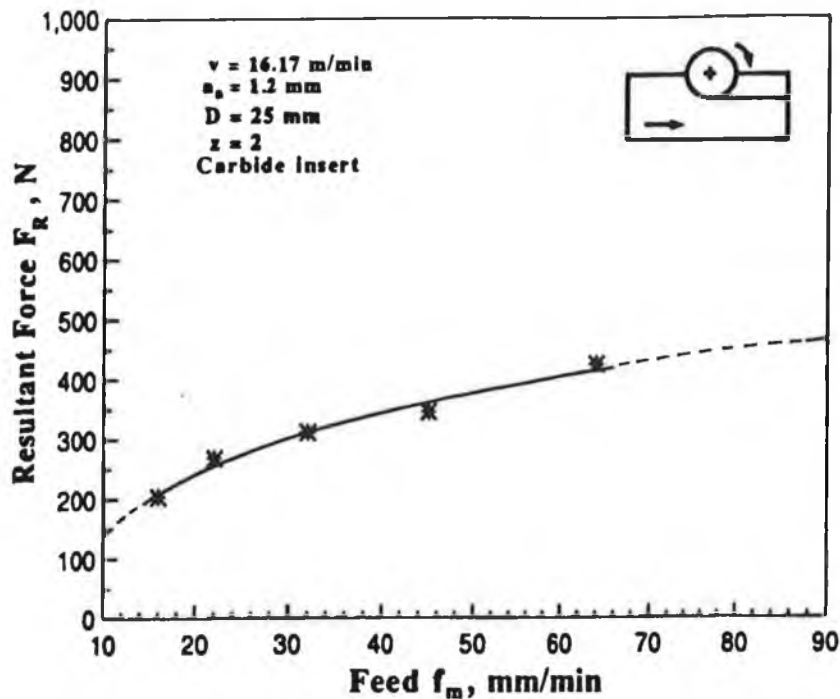


Fig.6.27: Effect of feed (f_m) on average resultant force in half immersion up milling Inconel 718 at cutting speed of 16.17 m/min

6.3.2.3 Influence of axial depth of cut on cutting forces for half immersion end milling Inconel 718 at up milling mode.

The measured table system of cutting forces (F_x , F_y and F_z) at a feed rate of 32 mm/min and speed of 16.17 m/min are plotted against axial depth of cut in Fig. 6.28 while the calculated tangential component F_t and resultant (table) cutting force is plotted in Fig.6.29 and 6.30 respectively. From all figures it is seen that cutting forces increase almost linearly with the increase of axial depth of cut. This is due to the fact that the size of cut per tooth increase as the axial depth of cut increase. From Fig.28 it is seen that F_x component of cutting forces is the highest in the table system of cutting forces (the reason is mentioned in section 6.3.2.1)

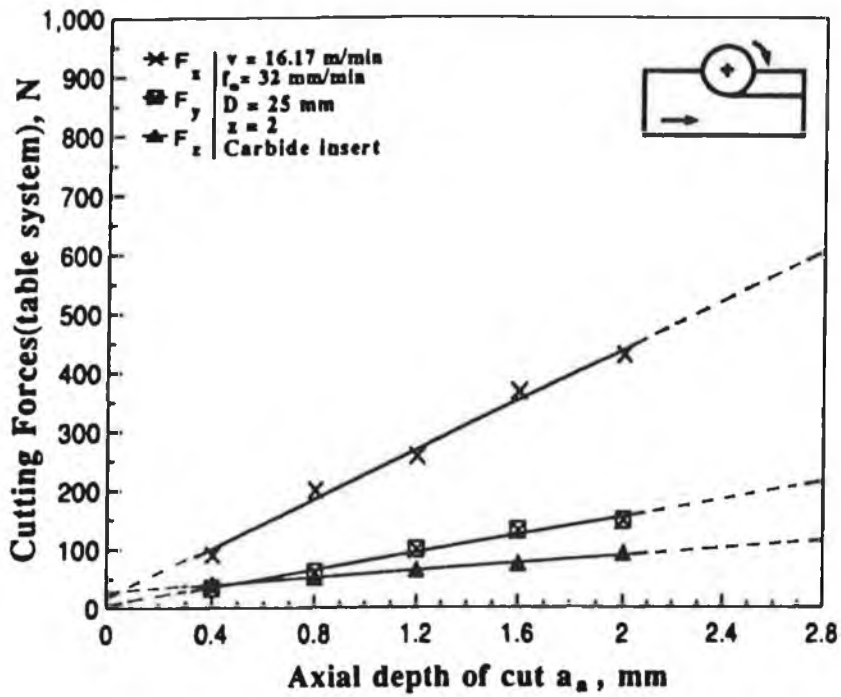


Fig.6.28: Effect of axial depth of cut on average table system of cutting forces in half immersion up end milling Inconel 718 at cutting speed of 16.17 m/min

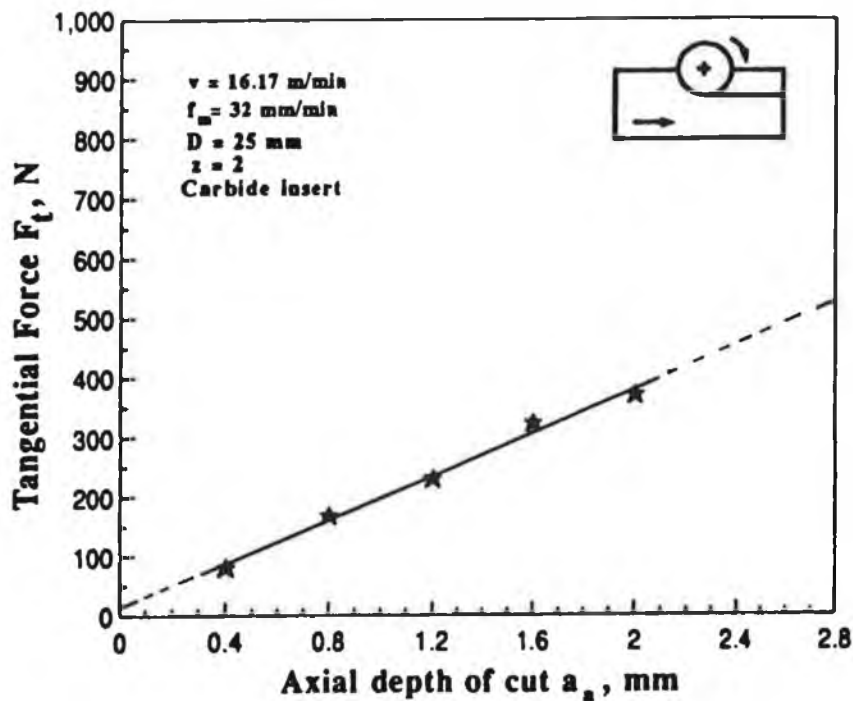


Fig.6.29: Effect of axial depth of cut on average tangential force in half immersion up end milling Inconel 718 at cutting speed of 16.17 m/min

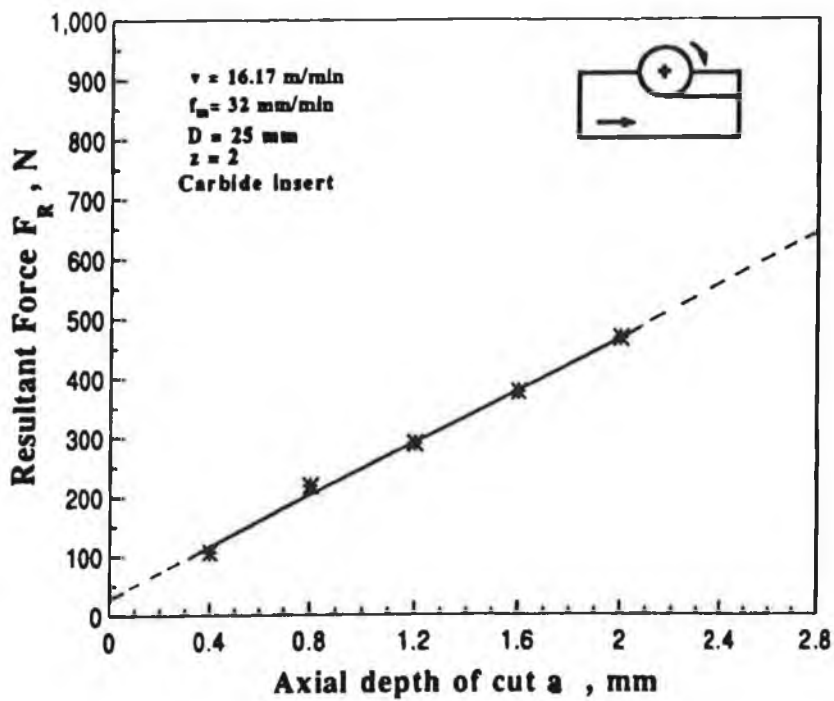


Fig.6.30: Effect of axial depth of cut on average resultant cutting force in half immersion up end milling Inconel 718 at cutting speed 16.17 m/min

6.3.3 Influence of machining conditions on cutting forces for half immersion end milling Inconel 718 at down milling mode

The influence of machining conditions on cutting forces for half immersion end milling Inconel 718 at down milling mode is divided into three parts as:

- (1) Influence of cutting speed on cutting forces
- (2) Influence of feed rate on cutting forces
- (3) Influence of axial depth of cut on cutting forces

6.3.3.1 Influence of cutting speed on cutting forces for half immersion end milling Inconel 718 at down milling mode.

The table system of cutting forces were measured at a feed rate of 32 mm/min and axial depth of cut of 1.2 mm and plotted against cutting speed as shown in Fig.6.31. The calculated tangential component F_t and resultant cutting force (F_R) are plotted against cutting speed as shown in Fig.6.32 and 6.33 respectively. From all the figures it is also seen that cutting forces decrease as the cutting speed increases. From Fig.6.32 it is seen that F_y is the largest among the table system of cutting forces. F_y is much greater than F_x component. The reason may be analyzed from equation 3.28 of chapter 3 as that F_y component is the sum of 2 resolved components of cutter system of cutting forces (i.e. $F_y = F_t \sin \psi + F_r \cos \psi$) while F_x component is the subtraction of 2 resolved components of cutter system of cutting forces (i.e. $F_x = F_r \sin \psi - F_t \cos \psi$).

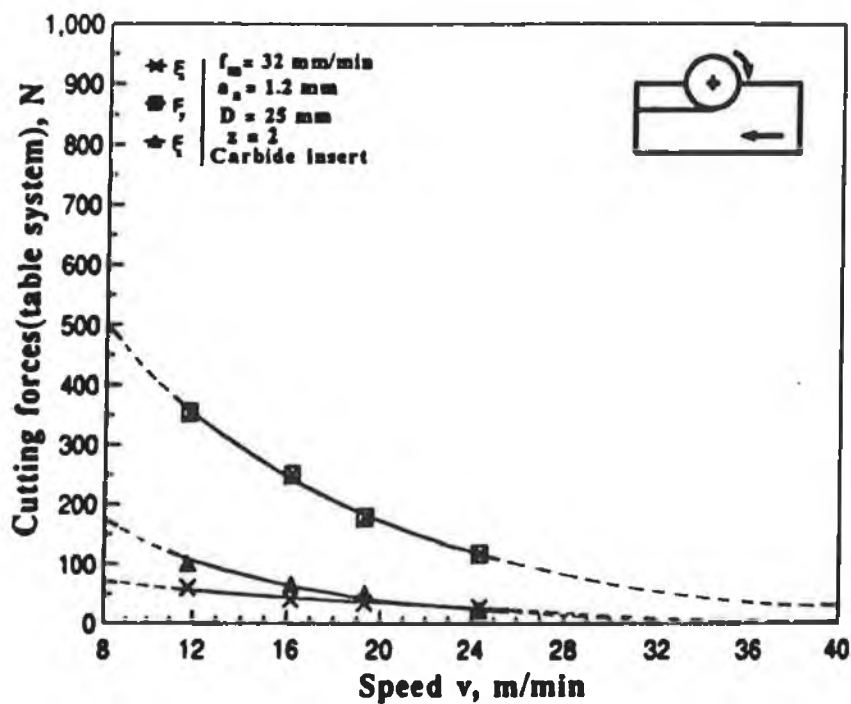


Fig.6.31: Effect of speed on average table system of cutting forces in half immersion down end milling Inconel 718 at feed (f_m) rate of 32 mm/min

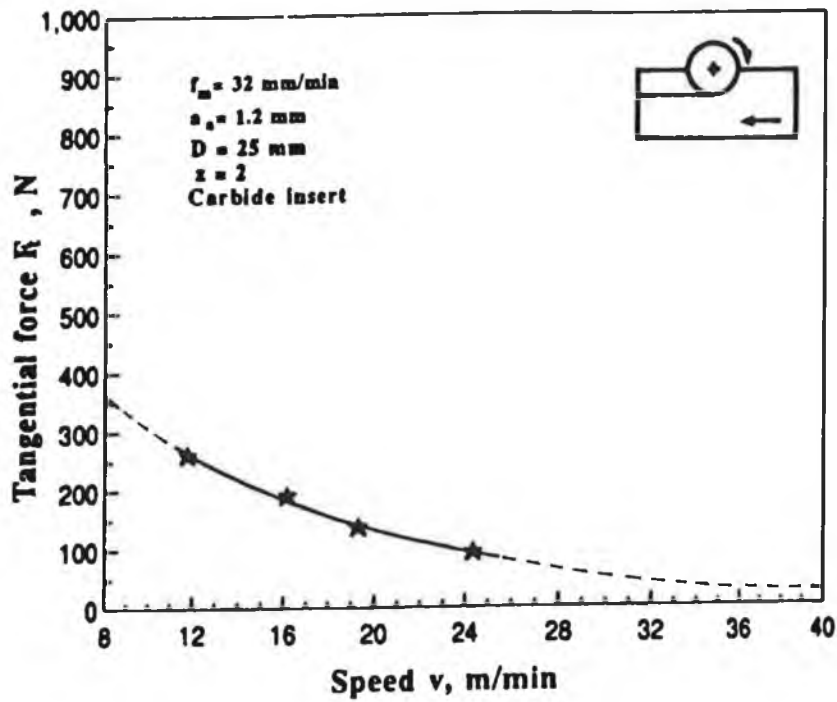


Fig.6.32: Effect of speed on average tangential force in half immersion down end milling Inconel 718 at feed (f_m) rate of 32 mm/min

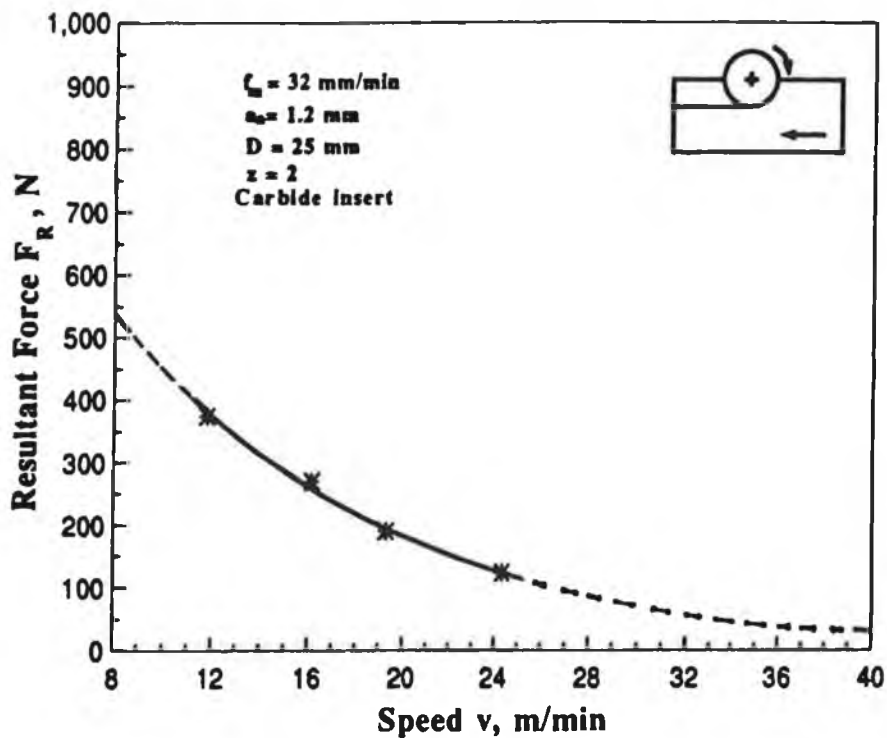


Fig.6.33: Effect of speed on average resultant cutting force in half immersion down end milling Inconel 718 at feed (f_m) rate of 32 mm/min

6.3.3.2 Influence of feed rate (f_m) on cutting forces for half immersion end milling Inconel 718 at down milling mode

The measured table system of cutting forces at a cutting speed of 16.17 m/min and axial depth of cut range of 1.2 mm are plotted against feed rate in Fig.6.34. The calculated tangential component and resultant cutting force (F_R) are plotted against feed (f_m) in Fig.6.35 and Fig.6.36 respectively. From all the figures it is seen that the cutting forces increase as the feed (f_m) increases. This is attributed to an increase of chip load per tooth as feed rate increases. From Fig.6.34 it is seen that F_y is the largest among the table system of cutting force. The reason is discussed in section 6.3.3.1.

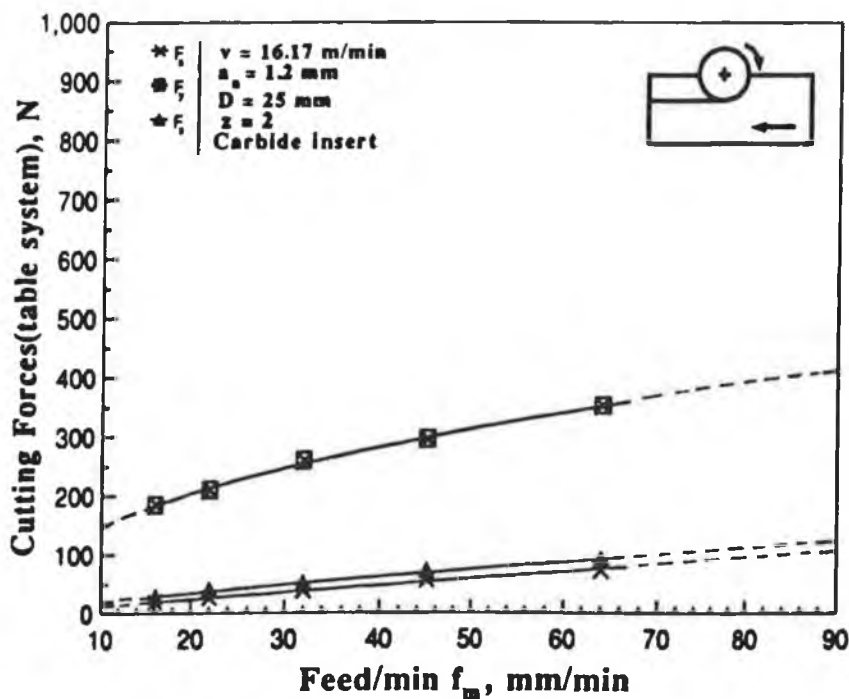


Fig.6.34: Effect of feed (f_m) on average table system of cutting forces in half immersion down end milling Inconel 718 at cutting speed of 16.17 m/min

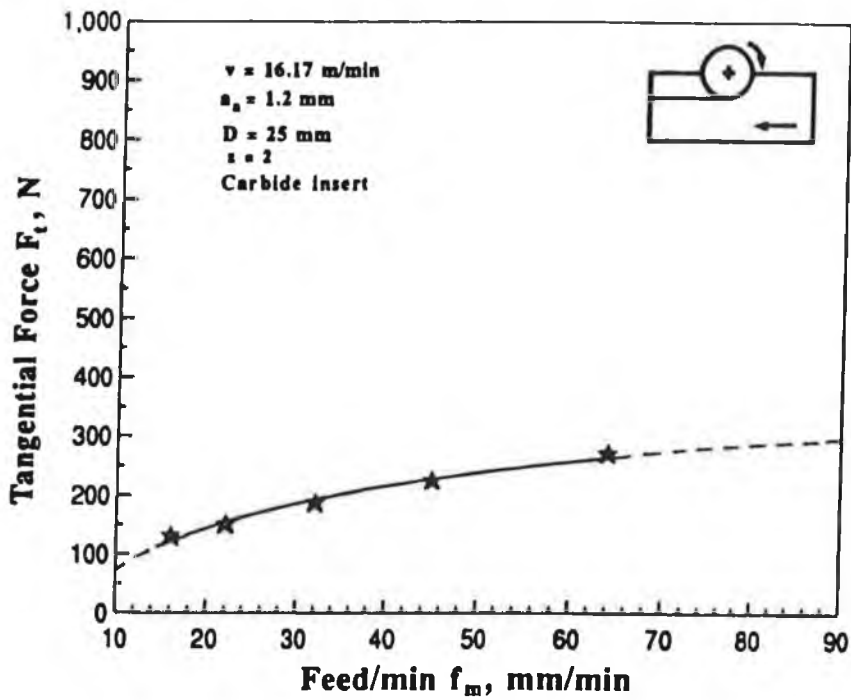


Fig.6.35: Effect of feed (f_m) on average tangential force in half immersion down end milling Inconel 718 at cutting speed of 16.17 m/min

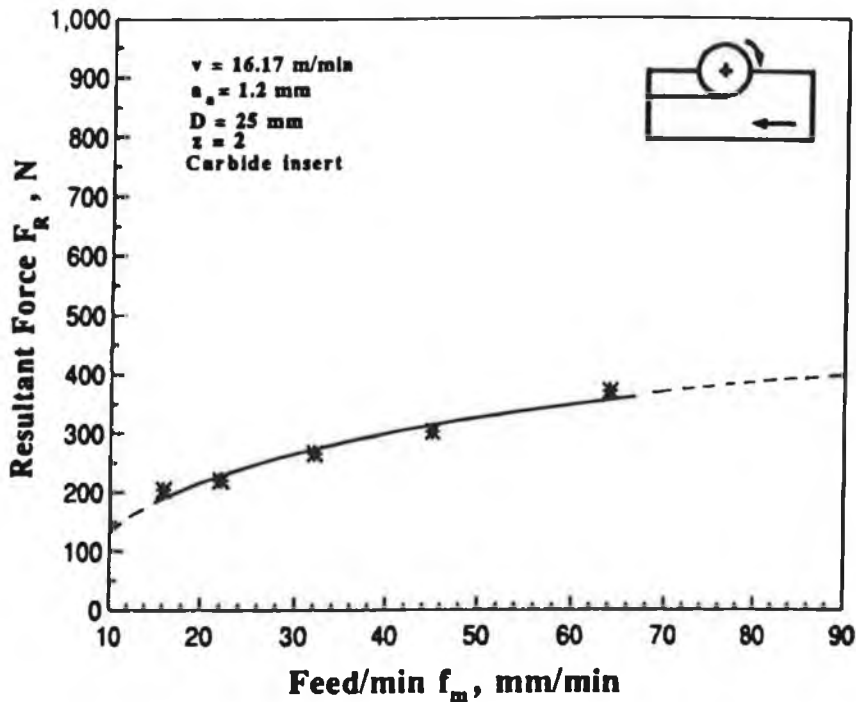


Fig.6.36: Effect of feed (f_m) on average resultant force in half immersion down end milling Inconel 718 at cutting speed of 16.17 m/min

6.3.3.3 Influence of axial depth of cut on cutting forces for half immersion end milling Inconel 718 at down milling mode

The measured table system of cutting forces at a cutting speed of 16.17 m/min and feed of 32 mm/min are plotted against axial depth of cut in Fig.6.37. The calculated tangential component F_t and resultant force (F_R) are plotted against axial depth of cut in Fig. 6.38 and 6.39 respectively. From all the figures it is seen that the cutting forces increase as the axial depth of cut increases. This is due to the fact that the size of the cut per tooth increases as the axial depth of cut increases. From Fig.6.37 it is observed that the F_y component is also the highest in the table system of cutting forces.

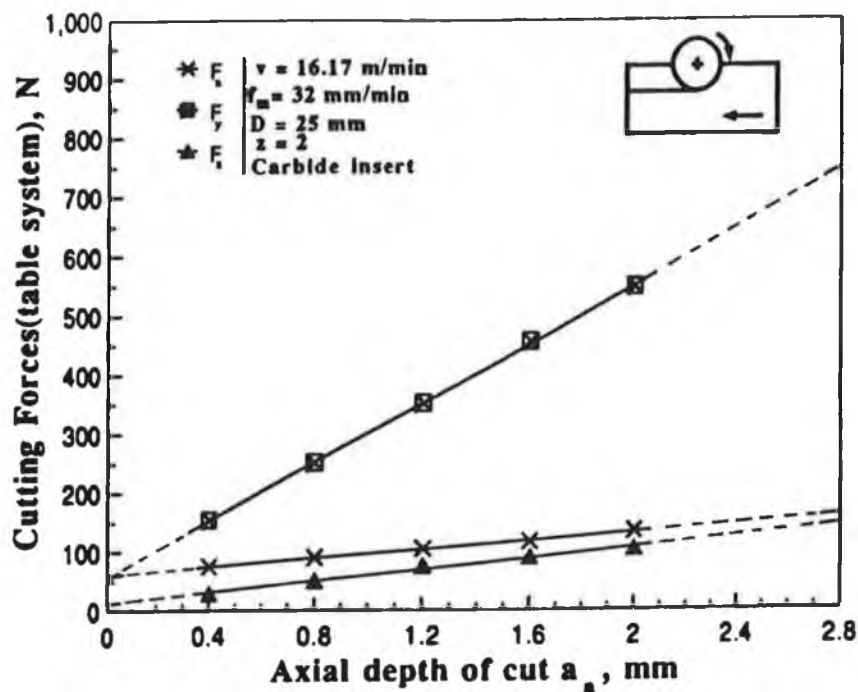


Fig.6.37: Effect of axial depth of cut on average table system of cutting forces in half immersion down end milling Inconel 718 at cutting speed of 16.17 m/min

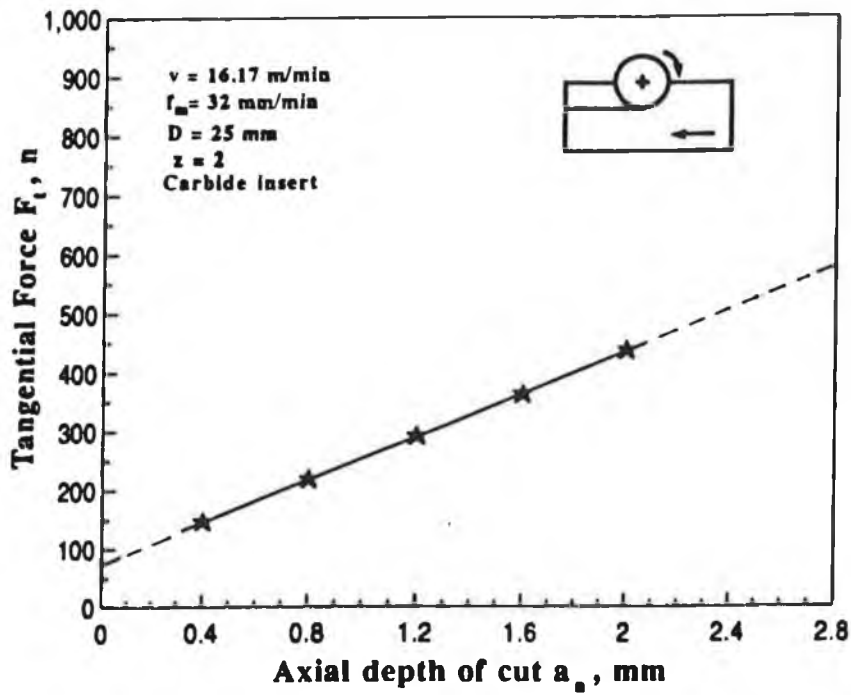


Fig.6.38: Effect of axial depth of cut on average tangential force in half immersion down end milling Inconel 718 at cutting speed of 16.17 m/min

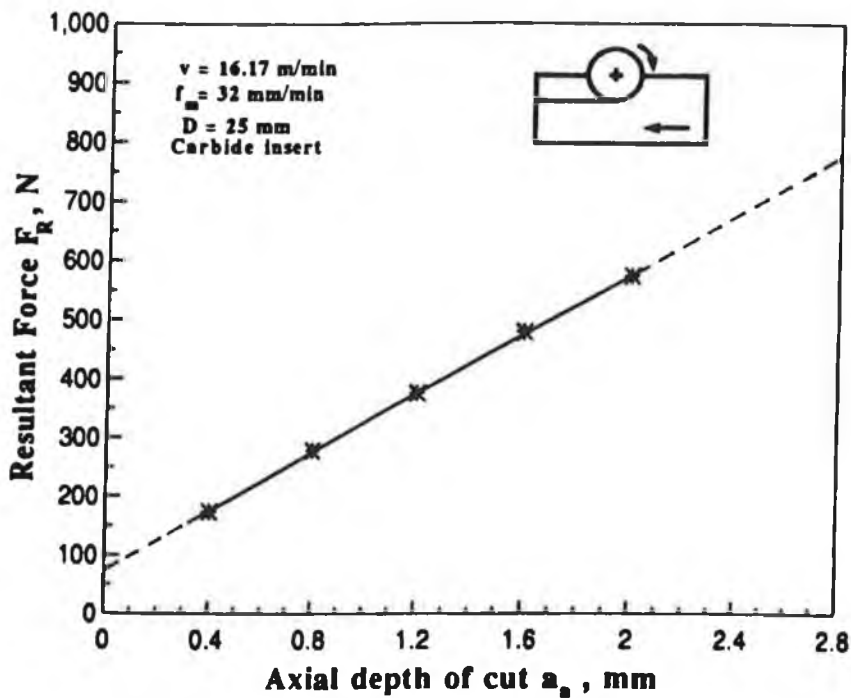


Fig.6.39: Effect of axial depth of cut on average resultant force in half immersion down end milling Inconel 718 at cutting speed of 16.17 m/min

6.3.4 Conclusions

- (1) Cutting forces decrease as the cutting speed increases (11 - 25 m/min) for full and half immersion end milling.
- (2) Cutting forces increase as the feed rate increases for full and half immersion end milling.
- (3) Cutting forces increases as the axial depth of cut increases for slot and half immersion end milling
- (4) Carbide inserts are microchipped while within the cutting condition of feed range (f_z) 0.11 - 0.15 mm/tooth with corresponding axial depth of cut of 2.00 mm and speed range of 11.78 - 16.17 m/min, while within a feed rate below 0.1 mm/tooth with corresponding axial depth of cut 2.00 mm and cutting speed 24.34 m/min inserts are not microchipped.
- (5) F_y component is the highest in the table system of cutting forces in slot milling.
- (6) F_x component is the highest in up milling mode and in down milling mode, F_y component is the highest in the table system of cutting forces.

6.4 Development of cutting force model in end milling Inconel 718

6.4.1 Introduction

In this work, a mathematical model for the average tangential cutting force for slot milling Inconel 718 was developed by response surface methodology. The cutting tool used was an end mill with uncoated carbide inserts. The adequacy of the developed model was tested by analysis of variance.

6.4.2 Development of cutting force model by response surface methodology

(i) Postulation of the mathematical model

For a particular work-tool geometry cutting forces in end milling are assumed to be a function of primary machining variables like cutting speed, feed and axial depth of cut. In machining steel, which is shown in section 6.2 of this chapter, within practical machining conditions, cutting speed has an insignificant effect on cutting force. So, in this postulation of the mathematical model the cutting forces are assumed to be a function of feed f_z (mm/tooth) and axial depth of cut, a_a (mm) i.e.

$$\text{Cutting forces} = f(f_z, a_a)$$

From equation (4.1) of chapter 4 the multiplicative model for the predictive tangential component of cutting forces, F_t can be written as:

$$\hat{F}_{t(\text{Inconel})} = C_{50} f_z^{l_5} a_a^{m_5} \quad (6.11)$$

Where $F_{t(\text{Inconel})}$ - average tangential component of cutting force(N) for Inconel, f_z - feed per tooth (mm/tooth), and a_a - the axial depth of cut (mm) and C_{50} , l_5 , m_5 - model parameters to be estimated using experimental data.

Equation (6.11) can be written using equation (4.4) of chapter 4 as first-order polynomial as:

$$\hat{y}_{(Inconel)} = b_0x_0 + b_2x_2 + b_3x_3 \quad (6.12)$$

Where $\hat{y}_{(Inconel)}$ - proposed predictive response (cutting force) on natural logarithmic scale, while $x_0 = 1$ and x_2, x_3 - the coded values (logarithmic transformations) of f_z and a_a respectively and b 's are model parameters to be estimated using experimentally measured cutting force data.

(ii) Experimental Design

In order to estimate the model parameters of the equation a first-order orthogonal design was used. This design consists of nine experiments which have been used to develop the first-order model. Four experiments represent a 2^2 (2^k) factorial design, where the experimental points are located at the corner of a square as shown in Fig 4.3 of chapter 4. Five experiments represent added centre points to the square, repeated five times to estimate the pure error. In this case the experiments are done in an unblocked manner.

(iii) Coding of individual variables

The variables are coded by taking into account the capacity of the milling machine and limiting cutting condition. The coded values of the variables are shown in Table 6.3. The coded values for use in equation (6.12) were obtained from the following transforming equations:

$$x_2 = \frac{\ln f_z - \ln 0.073}{\ln 0.088 - \ln 0.073} \quad (6.13)$$

$$x_3 = \frac{\ln a_a - \ln 1.00}{\ln 2.00 - \ln 1.00} \quad (6.14)$$

Where x_2 - the coded value of feed per tooth corresponding to its natural value f_z and x_3 - the coded value of axial depth of cut corresponding to its natural value of a_a .

The above equation is transformed from equation (4.10) of chapter 4.

Table 6.3: Levels of the Independent variables and coding identification for cutting force (Inconel 718)

Independent variables	Levels in Coded form		
	-1 (low)	0 (centre)	+1 (high)
f_z , mm/tooth (x_2)	0.06	0.073	0.088
a_a , mm (x_3)	0.50	1.0	2.00

(iv) Experiment

The process utilized for cutting forces was a slot milling operation, performed on a vertical milling machine (Cincinnati). The cutting tests were carried out with an end mill with carbide inserts. The specification of carbide inserts is shown in chapter 5 and appendix 1. The cutting tests were carried out under dry conditions. The average forces of the table system of cutting forces were measured and from this the tangential component of cutting forces were calculated by the formulae (3.27) and (3.28) of chapter 3. The results and conditions are shown in Table 6.4.

(v) Estimation of parameters

The regression parameters of the postulated model were estimated by the method of least squares. The basic formula of least square is shown in the section 4.1.4 of chapter 4.

(vi) Analysis of results

(a) Development of the mathematical model

The mathematical model for the cutting force is developed by substituting the estimated model parameters as:

$$\hat{y}_{(Inconel)} = 5.4996 + 0.1621x_2 + 0.7774x_3 \quad (6.15)$$

The predicting equation (6.15) can be plotted in Fig.6.40 as contours for each of the response surface at a selected level of cutting speed of 16.17 m/min (note that this figure is on a logarithmic scale) .

Table 6.4: Results and Cutting Conditions for cutting force (Inconel 718)

Trial No.	Feed f_z mm/tooth	Axial depth of cut a_a , mm	Coding		Calculated av. tangential cutting force, F_t , N
			x_2	x_3	
1	0.06	0.50	-1	<u>-1</u>	89.81
2	0.088	0.50	1	-1	141.40
3	0.06	2.00	-1	1	484.08
4	0.088	2.00	1	1	587.90
5	0.073	1	0	0	242.04
6	0.073	1	0	0	246.50
7	0.073	1	0	0	255.41
8	0.073	1	0	0	225.48
9	0.073	1	0	0	252.23

These contours were constructed by computer utilizing "Matlab" computer package. Equation (6.15) can be transformed using equations (6.13), (6.14) as:

$$\hat{F}_{t(Inconel)} = 2368.28 f_z^{0.8673} a_a^{1.1216} \quad (6.16)$$

Equation (6.16) indicates that an increase in either feed per tooth or axial depth of cut increases the cutting forces. This equation is valid for slot milling Inconel 718 using end mill with carbide inserts under dry conditions and

$$0.06 \leq f_z \leq 0.088 \quad \text{mm/tooth}$$

$$0.50 \leq a_a \leq 2.00 \quad \text{mm}$$

(c) Adequacy of the predictive model

The analysis of variance (ANOVA) was used to check the adequacy of the predicting model. As per this technique the calculated F_{rat} of the model was found to be 3.52 while the $F_{rat, 2,4}$ for 95% confidence is 6.94 as obtained from statistical table. Hence, the model is valid. The detailed formulae for the analysis of the variance has been shown in section 4.13 of chapter 4. The results of analysis of variance is shown in Appendix 2.

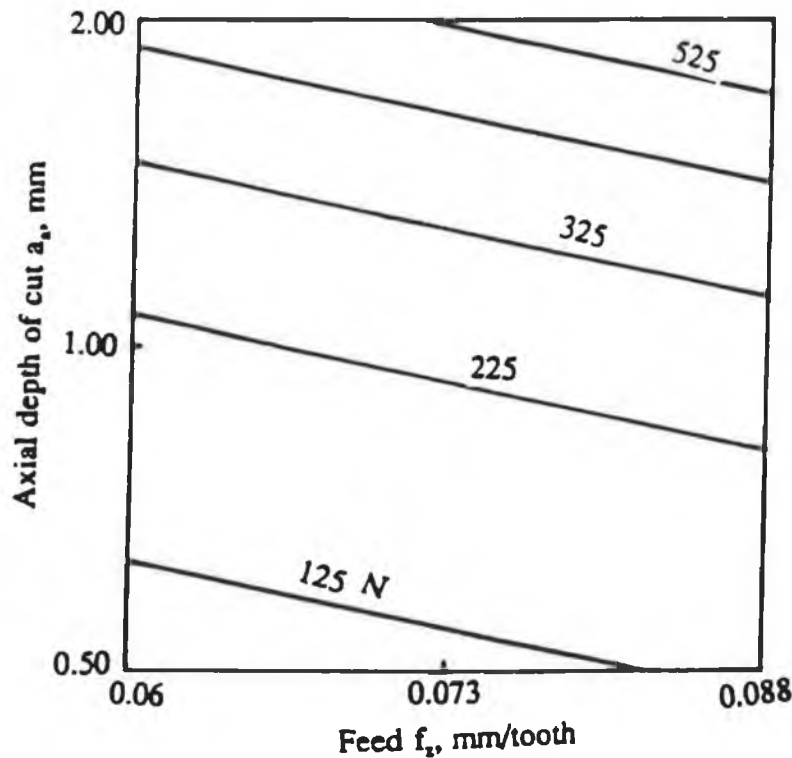


Fig.6.40: Tangential force contours (first-order model) in axial depth of cut-feed plane at a selected level of speed 16.17 m/min (log-scales)

(d) Significance testing of individual variables

The significance testing for the individual variable is done as per the procedure discussed in chapter 4 and the results are shown in Appendix 2. From the results of the significance testing it is seen that the calculated F_{rat} of feed and axial depth of cut are 23.78 and 547.07 whereas the corresponding F_{rat} for 95% confidence is 5.99 as obtained from statistical table. Hence, the effect of both feed and axial depth of cut are significant.

(e) Precision of prediction (Confidence intervals)

The precision of the predicting model is calculated by calculating the appropriate

confidence intervals. The basic formula for the calculation of confidence interval has been discussed in chapter 4. The resulting 95% confidence intervals for the nine tests are shown in Appendix 2.

(vii) Conclusions

- (a) A reliable predictive cutting force model for predicting the average tangential cutting force has been developed for end milling Inconel 718.
- (b) Although the cutting force model has been developed and tested from few experimental results, it can be used to predict the mean resultant cutting force for any condition within the boundaries of research.
- (c) Cutting forces increases as the feed or axial depth of cut increases.
- (d) The predictive model is valid within the feed range of 0.06 - 0.088 mm/tooth and the axial depth of cut range of 0.50 - 2.00 mm.
- (e) The effect of both the feed and axial depth of cut is significant.

CHAPTER 7

INVESTIGATION OF TOOL LIFE IN END MILLING

STEEL(190 BHN) AND INCONEL 718

7.1 Introduction

The investigation of tool life in end milling steel (190 BHN) and Inconel 718 is divided as:

- (1) Development of tool life models in end milling steel (190 BHN)
- (2) Tool deterioration with cutting time in end milling Inconel 718

It may be noted that due to limiting cutting conditions of the milling machine, experiments were not carried out to develop a tool life model in end milling Inconel 718.

7.2 Development of tool life models in end milling steel (BHN)

7.2.1 Introduction

It is very difficult to predict tool life with sufficient accuracy on the basis of controllable process parameters. But on the other hand it is an essential part of a machining system in the unmanned factory (fully automated) to change tools automatically due to wear or damage. Most tools fail either by gradual wear or fracturing. During gradual wear, the tool reaches its limit of life by either flank wear or crater wear. Fractures occur more readily in brittle tools under interrupted cutting conditions. Sometimes, the fracture does not cause a complete tool failure but small chipping of the cutting edge. But in this study, whenever possible tool life in end milling is considered on the basis of ISO 8688-2. The part of ISO 8688 considers only those recommendations concerned with testing which results predominantly in tool wear.

In this work, tool life predictive models have been developed by response surface methodology in terms of primary machining variables like speed, feed and axial depth of cut. Tool life contours were obtained utilizing a computer. These contours were used for determining the optimum cutting conditions for a required tool life.

7.2.2 Development of the tool life models in slot milling steel (190 BHN) by response surface methodology

(i) Postulation of the mathematical models

Factors which affect too life in end milling are shown in chapter 3. But for a particular work-tool geometry, the tool life in end milling is assumed to be a function of cutting conditions like cutting speed, feed and axial depth of cut. The multiplicative model for the predicted tool life in terms of the investigated independent variables can be expressed from equation (4.7) of chapter 4 as:

$$T_{(HSS)} = C_{60} v^{k_6} f_z^{l_6} a_a^{m_6} \quad (7.1)$$

Where $T_{(HSS)}$ - predictive tool life of HSS tool (min), v - cutting speed (m/min), f_z - feed per tooth (mm/tooth), a_a - axial depth of cut (mm) and C_{60} , k_6 , l_6 , m_6 - model parameters to be estimated using experimental data.

From equation (4.5) of chapter 4, the above equation (7.1) can be written as the first-order polynomial as:

$$\hat{y}_{(HSS)} = b_0 x_0 + b_1 x_1 + b_2 x_2 + b_3 x_3 \quad (7.2)$$

The first-order model is only accepted over a narrow range of the variables. In order to predict the response reliably over a wide range of machining variables, second-order polynomials are needed in some cases. From equation (4.7) of chapter 4 the second-order polynomial can be written as:

$$y_{(HSS)} = b_0 x_0 + b_1 x_1 + b_2 x_2 + b_3 x_3 + b_{11} x_1^2 + b_{22} x_2^2 + b_{33} x_3^2 + b_{12} x_1 x_2 + b_{13} x_1 x_3 + b_{23} x_2 x_3 \quad (7.3)$$

Where $\hat{y}_{(HSS)}$ - proposed predicted response (tool life of HSS tool)) on natural logarithm scale, while $x_0 = 1$ and x_1, x_2, x_3 - the coded value (logarithmic transformations) of v, f_z, a_p respectively and b 's are the model parameters to be estimated using experimentally measured tool life data.

(ii) Experimental Design

In order to determine the equation (7.2) and (7.3) of the response surface, the orthogonal first-order and central composite second-order designs were selected respectively. The orthogonal first and central composite second-order design for 3 factors is discussed in chapter 4.

(iii) Coding of independent variables

The variables were coded taking into account the capacity of the machine. The coded values of the variables shown in Table 7.1 for use in equations (7.2) and (7.3) were obtained from the following transforming equations:

$$x_1 = \frac{\ln v - \ln 30}{\ln 35 - \ln 30} \quad (7.4)$$

$$x_2 = \frac{\ln f_z - \ln 0.11}{\ln 0.20 - \ln 0.11} \quad (7.5)$$

$$x_3 = \frac{\ln a_p - \ln 0.60}{\ln 0.82 - \ln 0.60} \quad (7.6)$$

The above relationships were obtained from the equation (4.10) of chapter 4.

(iv) Experiment

The process utilized for tool life was a slot milling operation, performed on a vertical milling machine (Bridgeport). The reference work material was a bar of cold rolled steel. The specification of work material has been shown in chapter 5 and Appendix 1. The cutting tests were carried out using commercially available HSS slot drills under dry conditions. The specification of HSS slot drill is also shown in chapter 5 and appendix 1. The flank wear criteria were chosen for tool life end point which is shown in chapter 3.

Table 7.1: Levels of the Independent variables and coding identification for tool life (steel)

Independent Variables	Levels in Coded form				
	-1.5 (lowest)	-1 (low)	0 (centre)	+1 (high)	1.5 (highest)
v , m/min (x_1)	24	26	30	35	38
f_z , mm/tooth (x_2)	0.045	0.06	0.11	0.20	0.27
a_a , mm (x_3)	0.38	0.44	0.60	0.82	1.00

The flank wear of end cutting edge (major cutting edge) was measured by toolmakers' microscope. The measurement of flank wear is discussed in the section 5.4 of chapter 5. The results of tool life are shown in Table 7.2.

(v) Estimation of the model parameters

The regression parameters of the selected models were estimated by the method of least square. The basic formula has been shown in equation (4.13) of chapter 4. The calculation procedure is shown in Appendix 3.

(vi) Analysis of results

(a) Development of the first-order model

The first-order model of the tool life was developed using 12 test conditions of first and second blocks. The parameters in equation (7.2) were estimated, yielding the tool life predicting equation as:

$$\hat{y}_{(HSS)} = 4.2932 - 0.1954x_1 - 0.1622x_2 - 0.0440x_3 \quad (7.7)$$

The predicting equation (7.7) can be graphically represented in a 3 dimensional space of speed, feed and axial depth of cut as depicted in Fig.7.1. The predicting equation (7.7) can also be plotted in Fig.7.2 as contours for each of the response surfaces at a selected level of axial depth of cut of 0.60 mm (note that Fig.7.1 and Fig.7.2 are on a logarithmic scale). Equation (7.7) can be transformed using equations (7.4), (7.5) and (7.6) to provide the tool life (min) as a function of the cutting speed, v (m/min), feed, f_z (mm/tooth) and axial depth of cut, a_a (mm) as follows:

$$\hat{T}_{(HSS)} = 2210.55 v^{-1.20} f_z^{-0.25} a_a^{-0.15} \quad (7.8)$$

Equation (7.8) indicates that an increase in the cutting speed, feed and axial depth of cut decreases the tool life. This equation is valid for slot milling steel (190 BHN) using slot drills under dry conditions and $26 \leq v \leq 35$ m/min, $0.06 \leq f_z \leq 0.20$ mm/tooth $0.44 \leq a_a \leq 0.82$ mm

(b) Development of the second-order model

The second-order model was developed to extend the variable range to describe adequately the relationship between the slot milling output (tool life) and the investigated independent variables. The second-order model for tool life in its transformed state is given by:

$$\hat{y}_{(HSS)} = 4.3378 - 0.1640x_1 - .1337x_2 - 0.0476x_3 + 0.0083x_1^2 - 0.0311x_2^2 - 0.0005x_3^2 + 0.0028x_1x_2 + 0.0754x_1x_3 - 0.0274x_2x_3 \quad (7.9)$$

Equation (7.9) is plotted in Fig.7.3 as contours for each of the response surfaces at a selected level of axial depth of cut of 0.6 mm (note that this figure is on a logarithmic scale). These contours were constructed by computer utilizing "Matlab" computer package for determining the optimum cutting condition for a required tool life. From the contours shown in Fig.7.3 it is possible to select a combination of feed and cutting speed that reduces machining time without shortening tool life. This can be illustrated by further utilization of the model to include the rate of material removed. The rate of material removed Q (cm^3/min) is given by equation (3.16) of chapter 3. Equation of material removal rate (Q) can be written for slot milling using a cutter of diameter - 20 mm, the number of teeth in the cutter $z = 2$ and for a specified axial depth of cut $a_a = 0.6$ mm and using the transforming equations (7.4), (7.5) as:

$$\ln Q_{(steel)} = 0.2325 + 0.1530x_1 + 0.5978x_2 \quad (7.10)$$

For a constant rate of material removal, equation (7.10) can be represented by straight lines as illustrated in Fig.7.4.

Table 7.2: Cutting Conditions and Results for tool life (steel)

Tl No	Blk No.	Speed v , m/min	Feed, f_z mm/tooth	Axial depth of cut a_p , mm	Coding			Measured tool life, T, min
					x_1	x_2	x_3	
1	1	26	0.06	0.44	-1	<u>-1</u>	-1	117
2	2	35	0.06	0.44	1	-1	-1	64
3	2	26	0.20	0.44	-1	1	-1	84
4	1	35	0.20	0.44	1	1	-1	52
5	2	26	0.06	0.82	-1	-1	1	91
6	1	35	0.06	0.82	1	-1	1	77
7	1	26	0.20	0.82	-1	1	1	67
8	2	35	0.20	0.82	1	1	1	49
9	1	30	0.11	0.60	0	0	0	70
10	1	30	0.11	0.60	0	0	0	78
11	2	30	0.11	0.60	0	0	0	80
12	2	30	0.11	0.60	0	0	0	72
13	3	24	0.11	0.60	-1.5	0	0	96
14	3	38	0.11	0.60	1.5	0	0	63
15	3	30	0.045	0.60	0	-1.5	0	89
16	3	30	0.27	0.60	0	1.5	0	65
17	3	30	0.11	0.38	0	0	-1.5	82
18	3	30	0.11	0.96	0	0	1.5	76
19	4	24	0.11	1.00	-1.5	0	0	101
20	4	38	0.11	0.60	1.5	0	0	68
21	4	30	0.045	0.60	0	-1.5	0	84
22	4	30	0.27	0.60	0	1.5	0	60
23	4	30	0.11	0.38	0	0	-1.5	88
24	4	30	0.11	1.00	0	0	1.5	70

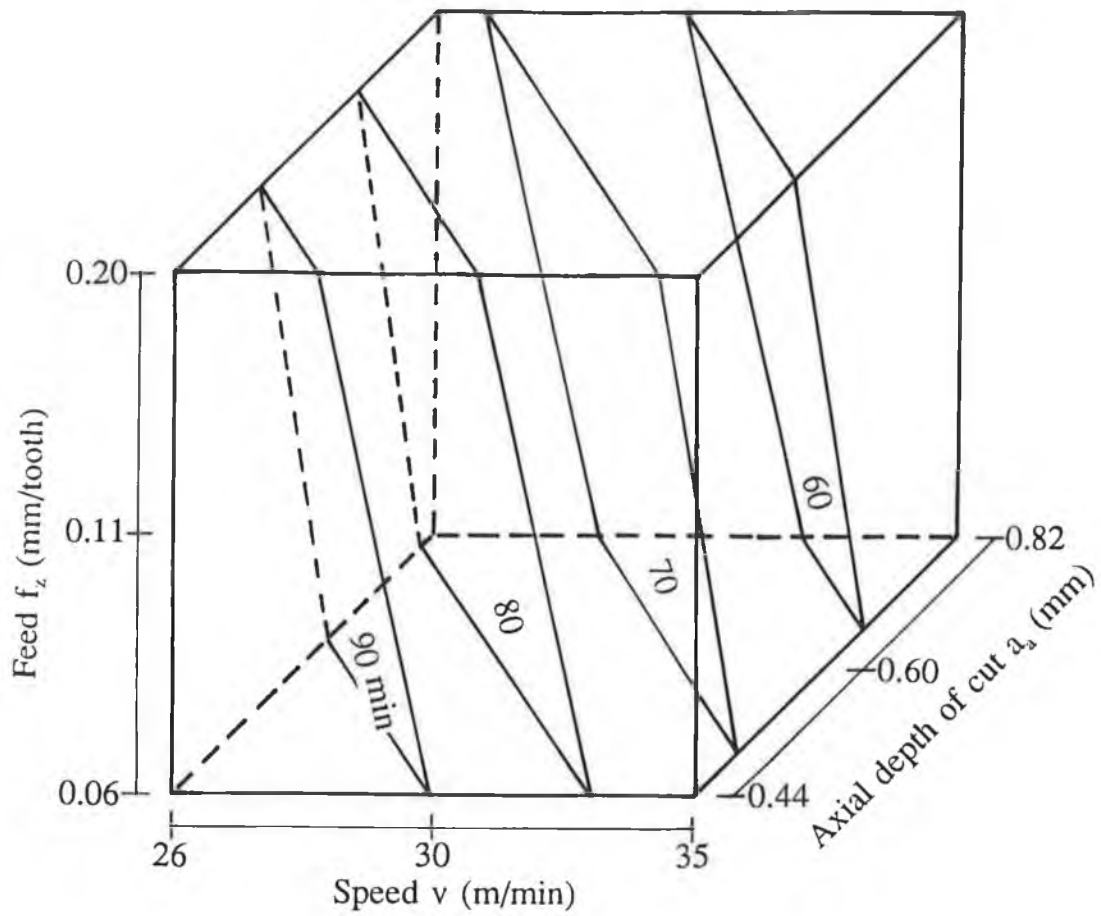


Fig.7.1: Contour surfaces for tool life in end milling steel (190 BHN) in 3 dimensional factor space (log-scales)

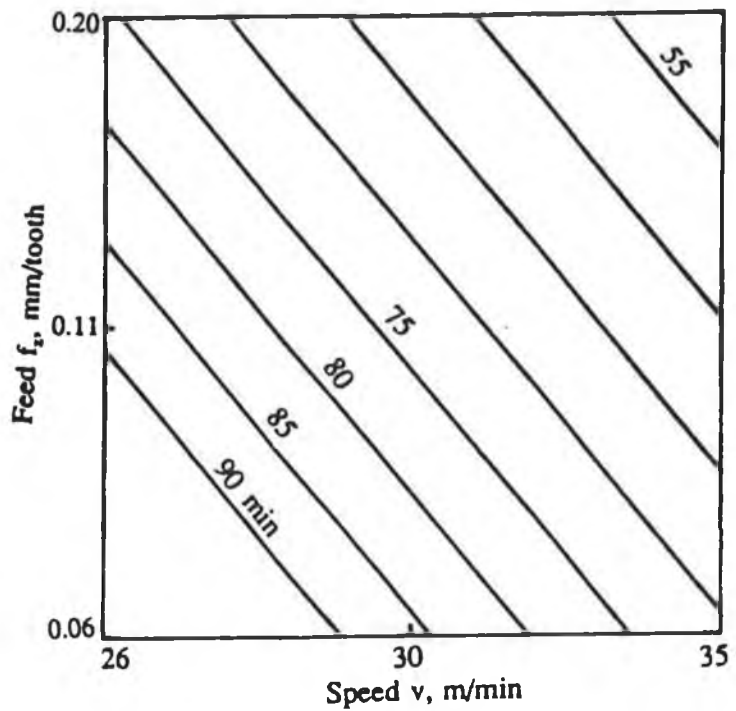


Fig.7.2: Tool life contours (first-order model) for steel (190 BHN) in speed-feed planes at 0.60 mm axial depth of cut (log-scales)

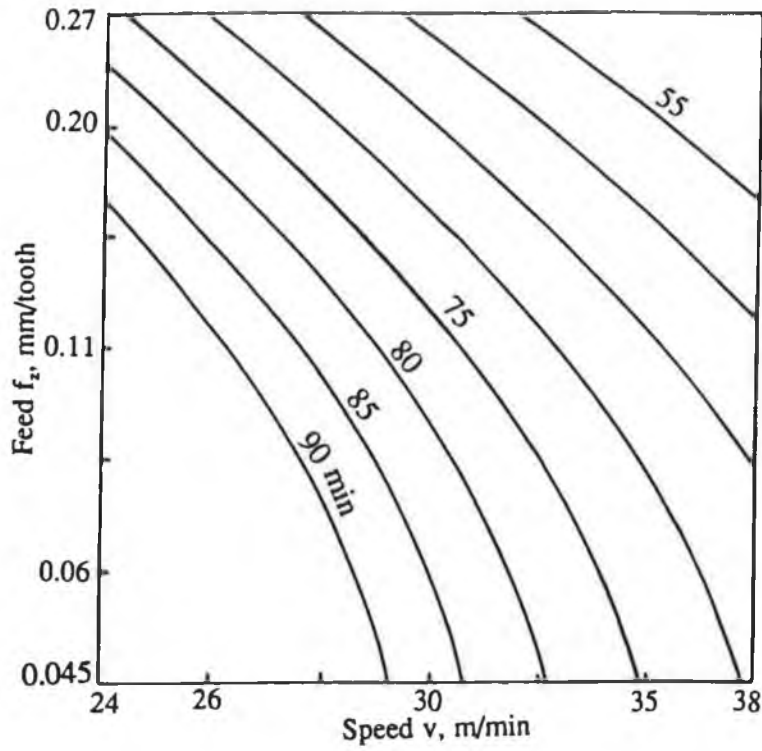


Fig.7.3: Tool life contours (second-order model) for steel (190 BHN) in speed-feed planes at 0.60 mm axial depth of cut (log-scales)

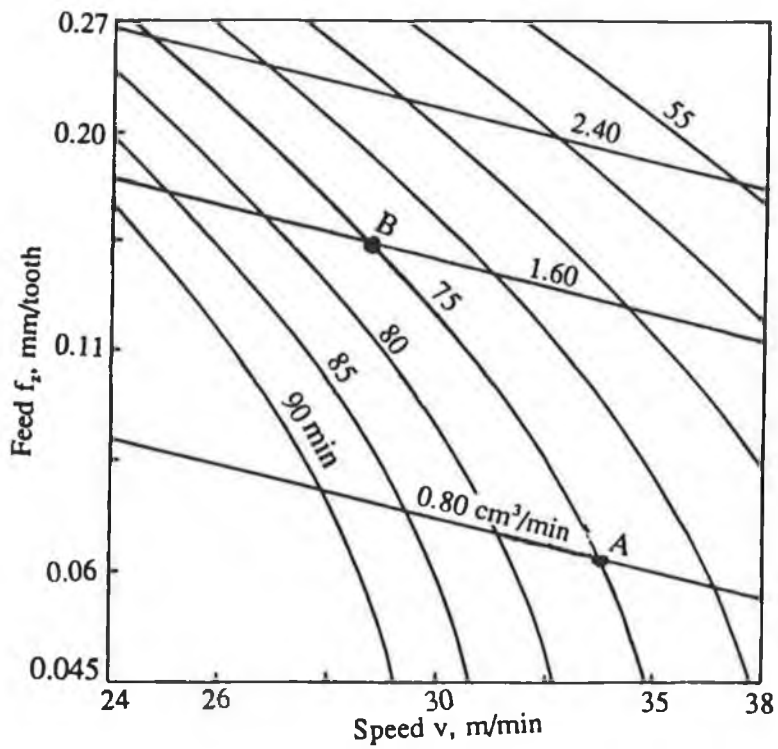


Fig.7.4: Contours of tool life (second-order model) and material removal rates for steel (190 BHN) in speed-feed planes at 0.60 mm axial depth of cut (log-scales)

This figure was obtained by superimposing the constant Q lines on the tool life contours in the speed-feed plane, for an axial depth of cut $a_a = 0.60$ mm. Fig.7.4 shows that the rate of material removed can be doubled without shortening the tool life $T = 85$ minute. It can be shown that the selection of the cutting condition represented by the point "B" is better than that represented by the point "A". This 100% increase in material removal rate is obtained without shortening the tool life.

(c) Adequacy of the postulated model

The analysis of variance (ANOVA) was used to check the adequacy of the developed model. As per this technique the calculated F_{rat} of the first and second-order models were 2.12 and 2.39 respectively while the corresponding $F_{rat 5,2}$ (first-order) and $F_{rat 3,8}$ (second-order) for 95% confidence are 19.30 and 4.07 as obtained from statistical tables. Hence, both the first-and second-order models are valid. Detailed formulae for the variance analysis used here are given in chapter 4. The results of the variance analysis are shown in Appendix 3.

(d) Significance testing for Individual variables

The significance of the individual variables were tested using the formula (4.16) of chapter 4. The results of significance testing for the individual variables for the first-and second-order model are shown in Appendix 3. The calculated F_{rat} of the speed, feed and axial depth of cut for the first-order model are 23.94, 15.61 and 1.56 respectively while the corresponding $F_{rat 1,8}$ for 95% confidence is 5.32 as obtained from standard statistical table. The calculated F_{rat} of the speed, feed and axial depth of cut for the second-order model are 67.75, 51.72 and 7.90 respectively while the corresponding $F_{rat 1,14}$ for 95% confidence is 4.60 as obtained from statistical table. Hence, it is observed that the effect of speed and feed on tool life are significant in the first-order model (the narrow range of the variables) while the effect of axial depth of cut in the second-order model (the wide range of the variables) is not so significant. But the first-order effect of all cutting parameters i.e. speed, feed and axial depth of cut are significant.

(e) Precision of prediction (Confidence intervals)

Due to experimental error, the estimated parameters and hence the estimated tool life \hat{y} is subjected to uncertainty. The precision of the predicted model can be determined by calculating the appropriate confidence intervals using formula (4.16) of chapter 4. The resulting 95% confidence intervals for the first and second-order models are shown in appendix 3.

(vii) Conclusions

- (a) Reliable tool life models have been developed and utilized to enhance the efficiency of slot milling steel (190 BHN) when using HSS slot drills.
- (b) The first-order tool life prediction equation is valid within the speed range of 26 - 35 m/min, the feed range of 0.06 - 0.20 mm/tooth and the axial depth of cut range of 0.44 - 0.80 mm.
- (c) By utilizing the second-order model, it is possible to extend the variable range. The predicting equation is valid within the speed range of 24 - 38 m/min, the feed range of 0.045 - 0.27 mm/tooth and the axial depth of cut range of 0.38 - 1.00 mm.
- (d) The speed and feed effect are significant in both the first and the second-order models while the effect of the axial depth of cut is significant only in the second-order model. In the first-order model the effect of axial depth of cut is not so significant. The speed effect is dominant in both the first and the second-order models then followed by the feed and the axial depth of cut.
- (e) An increase in the speed, feed and the axial depth of cut decreases the tool life.
- (f) Contours of the tool life outputs were constructed in planes containing two of the independent variables. These contours were further developed to select the proper combination of cutting speed and feed to increase the material removal rate without shortening the tool life.

7.3 Tool deterioration with effective cutting time in end milling Inconel 718

The cutting tests were performed on a Cincinnati milling machine using uncoated carbide inserts under dry conditions. Due to limiting cutting conditions of the milling machine only tool deterioration with the effective machining time in end milling Inconel 718 at selected level of cutting conditions was investigated. So, the tool deterioration in end milling Inconel 718 is divided as:

- (1) Tool deterioration with effective cutting time in full immersion end milling Inconel 718
- (2) Tool deterioration with effective cutting time in half immersion end milling Inconel 718

7.3.1 Tool deterioration with effective cutting time in full immersion end milling Inconel 718

Tool deterioration with effective cutting time in full immersion end milling Inconel 718 is divided into 2 cutting conditions as:

- (a) Tool deterioration with effective cutting time at cutting speed $v = 19.32$ m/min, feed $f_z = 0.091$ mm/tooth and axial depth of cut $a_a = 1.00$ mm
- (b) Tool deterioration with effective cutting time at cutting speed $v = 29.05$ m/min, feed $f_z = 0.086$ mm/tooth and axial depth of cut $a_a = 1.00$ mm

- (a) **Tool deterioration with effective cutting time in full immersion end milling at cutting speed $v = 19.32$ m/min, feed $f_z = 0.091$ mm/tooth and axial depth of cut $a_a = 1.00$ mm**

The full immersion end milling operation was conducted at cutting speed $v = 19.32$ m/min, feed $f_z = 0.091$ mm/tooth and axial depth of cut $a_a = 1.00$ mm using carbide

inserts. Tool deterioration in the form of flank wear (VB1, VB2 and VB3) was measured with tool makers' microscope at an interval of an effective cutting time of 1 minute . It was observed that VB2 and VB3 flank wear were dominant while VB1 flank wear was hardly found. The flank wear values (if the VB2 or VB3 values of both the inserts < 0.75 mm or > 0.75 mm, of the average flank wear value of both the inserts; if the VB2 or VB3 value of only one insert ≥ 0.75 mm, of the flank wear value of the individual insert only) obtained in five test runs for the above cutting condition was plotted against effective cutting time in Fig.7.5. The tool life is obtained from the point or the field of intersection of the curves by the horizontal line representing the limiting deterioration value determined as the " tool life criterion " (as discussed in chapter 3). Arithmetic mean value of flank wear for the above test runs (Fig.7.5) was plotted against effective cutting time in Fig.7.6. The SEM (Scanning Electron Microscopy) photograph of carbide inserts is shown in Appendix 3. The tool wear mechanism is due to a combination of adhesion, abrasion, diffusion and fatigue wear mechanism. From the Fig.7.6 it is observed that the tool life is 9.50 minutes.

(b) Tool deterioration with effective cutting time in full immersion end milling

Inconel 718 at cutting speed $v = 29.05$ m/min, feed $f_z = 0.086$ mm/tooth and axial depth of cut $a_a = 1.00$ mm

The full immersion end milling at cutting speed $v = 29.05$ m/min, feed $f_z = 0.086$ mm/tooth and axial depth of cut $a_a = 1.00$ mm was carried out using carbide inserts. Tool deterioration in the form of flank wear (VB1, VB2 and VB3) was measured by tool makers' microscope after an interval of an effective cutting time of 1 minute. In this case also VB2 and VB3 flank wear were found in most cases while VB1 flank wear was hardly found. The SEM image of the flank wear of the carbide insert is shown in Appendix 3. The flank wear values obtained in five test runs for the above cutting condition were plotted against effective cutting time in Fig.7.7. Arithmetic mean value of the flank wear for the above test runs (Fig. 7.7) was plotted against effective cutting time in Fig.7.8. From the Fig.7.8 it is observed that the tool life is 5 minutes which is much less than that of the tool life in cutting conditions at cutting speed $v = 19.31$ m/min. This decreased tool life is due to the effect of the increased cutting speed of the cutter.

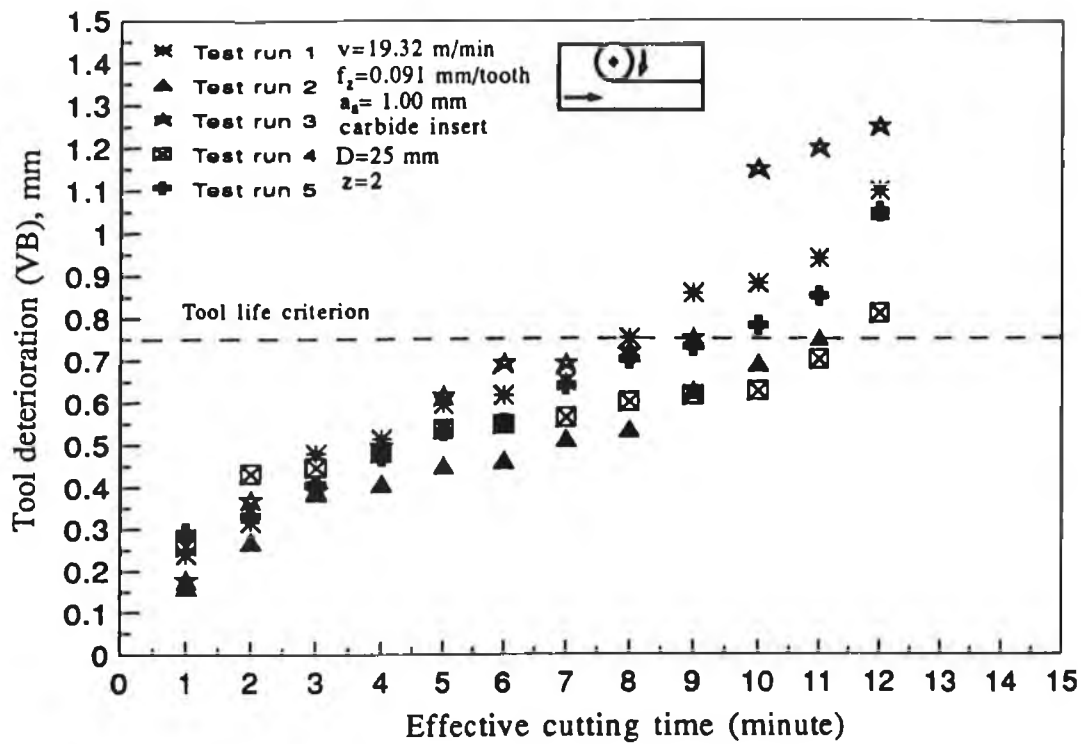


Fig.7.5: Tool deterioration (flank wear) values for a number of test runs plotted against cutting time in full immersion end milling Inconel 718 at $v = 19.32$ m/min, $f_z = 0.091$ mm/tooth and $a_p = 1.00$ mm

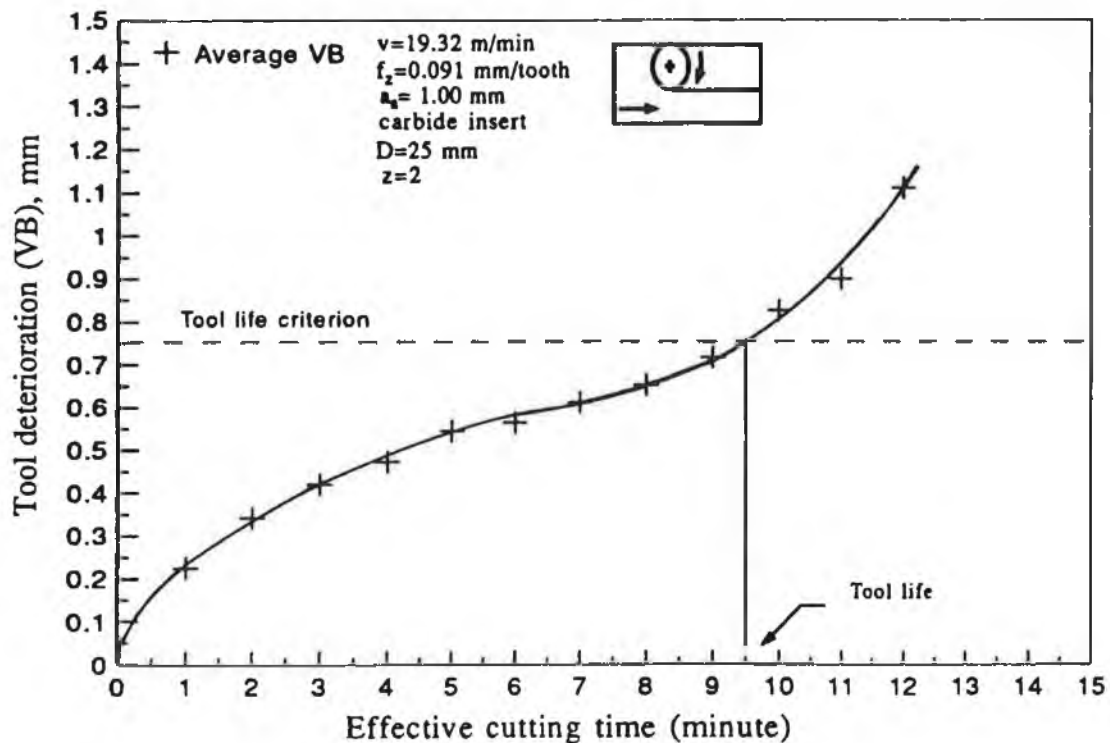


Fig.7.6: Arithmetic mean values of tool deterioration which is obtained from Fig.7.5 plotted against cutting time

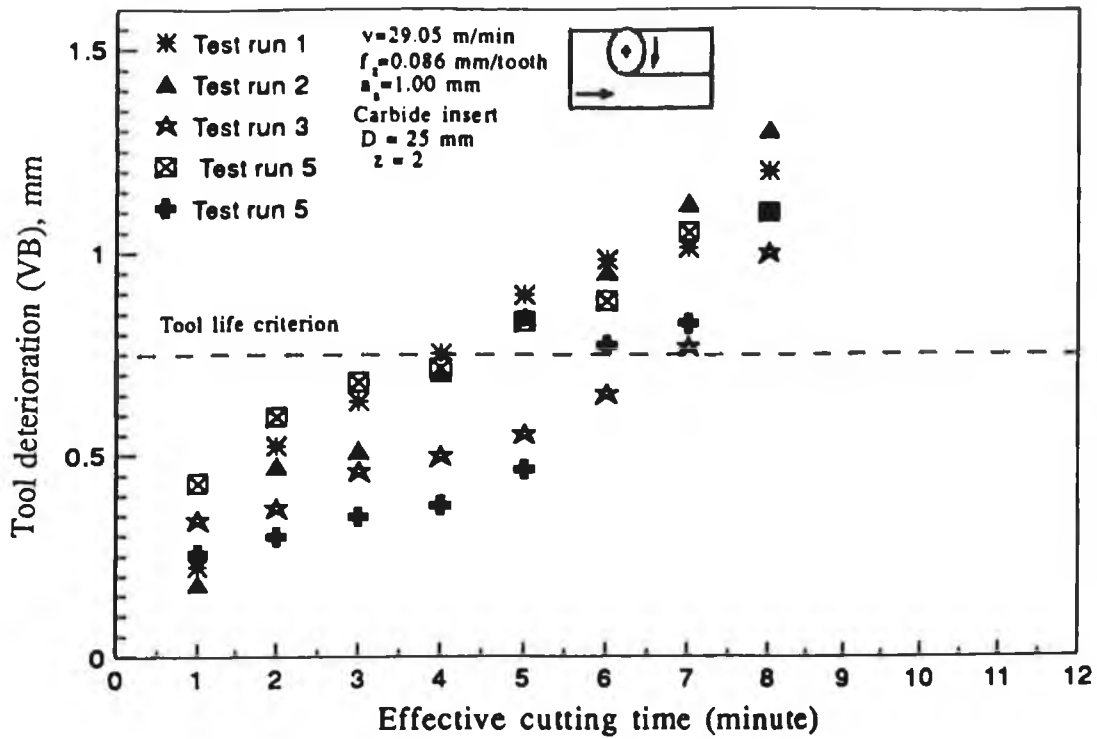


Fig.7.7: Tool deterioration (flank wear) values for a number of test runs plotted against cutting time in full immersion end milling Inconel 718 at $v = 29.05$ m/min, $f_z = 0.086$ mm/tooth and $a_p = 1.00$ mm

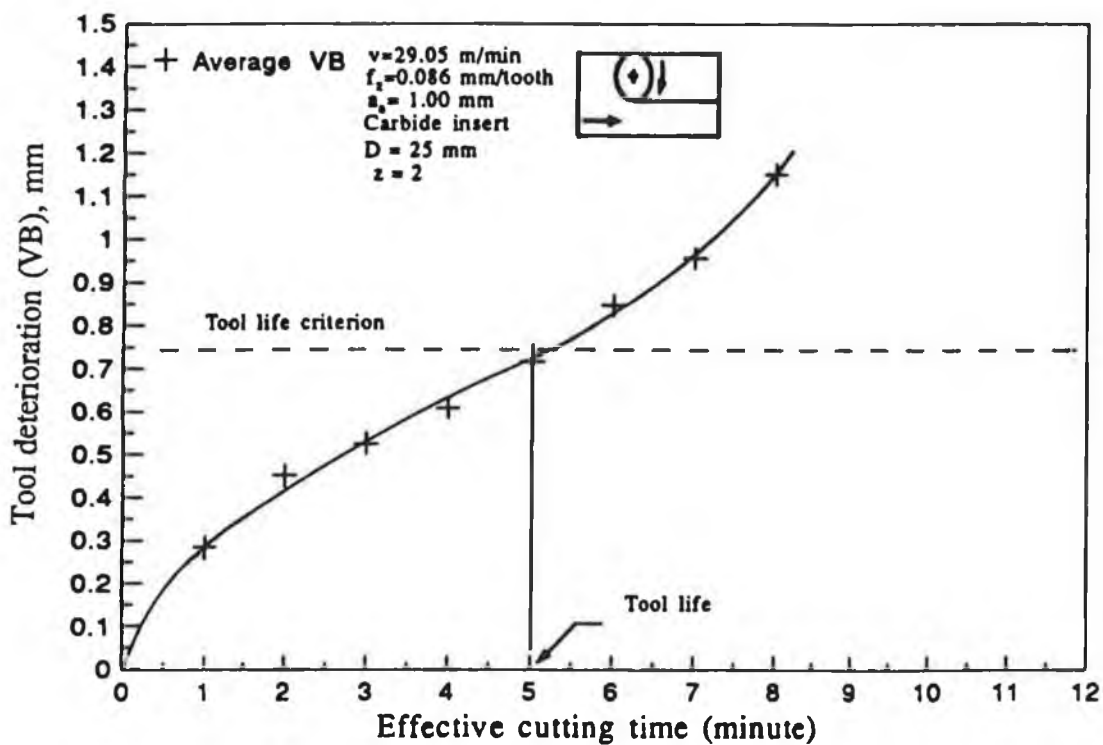


Fig.7.8: Arithmetic mean values of tool deterioration which is obtained from Fig.7.7 is plotted against cutting time.

7.3.2. Tool deterioration with effective cutting time in half immersion end milling Inconel 718

Tool deterioration in half immersion end milling Inconel 718 is divided as:

- (1) Tool deterioration with effective cutting time in half immersion up cut end milling at cutting speed $v = 19.32$ m/min, feed $f_z = 0.091$ mm/tooth and axial depth of cut $a_a = 1.00$ mm

- (2) Tool deterioration with effective cutting time in half immersion down cut end milling at cutting speed $v = 19.32$ m/min, feed $f_z = 0.091$ mm/tooth and axial depth of cut $a_a = 1.00$ mm

7.3.2.1 Tool deterioration with effective cutting time in half immersion up cut end milling Inconel 718 at cutting speed $v = 19.32$ m/min, feed $f_z = 0.091$ mm/tooth and axial depth of cut $a_a = 1.00$ mm

The half immersion end milling at up milling mode was conducted at the above cutting conditions using carbide inserts. Tool deterioration in the form of flank wear was measured with tool makers' microscope after an interval of an effective cutting time of 30 seconds. Flank wear such as VB2 and VB3 are observed in most cases. Average flank wear obtained in five test runs for the above cutting conditions was plotted against the effective cutting time in Fig.7.9. The tool life is obtained from the point or the field of intersection of the curves by the horizontal line representing the limiting deterioration value determined as the " tool life criterion ". Arithmetic mean value of the flank wear of the above test runs (Fig.7.9) was plotted against effective cutting time in Fig.7.10. The SEM photograph of the tool wear in the carbide inserts are shown in Appendix 3. From Fig.7.10, it is observed that the tool life value is 1.5 minutes.

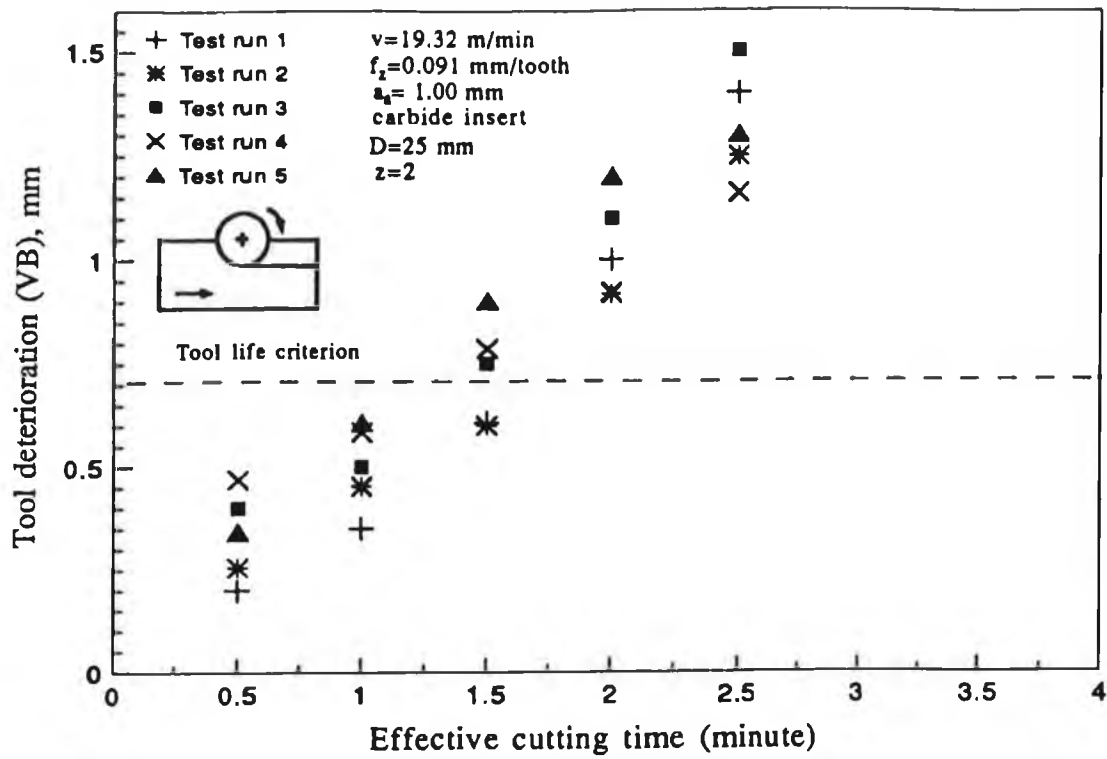


Fig.7.9: Tool deterioration (flank wear) values for a number of test runs plotted against cutting time in half immersion up cut end milling Inconel 718 at $v=19.32$ m/min, $f_z=0.091$ mm/tooth and $a_p=1.00$ mm

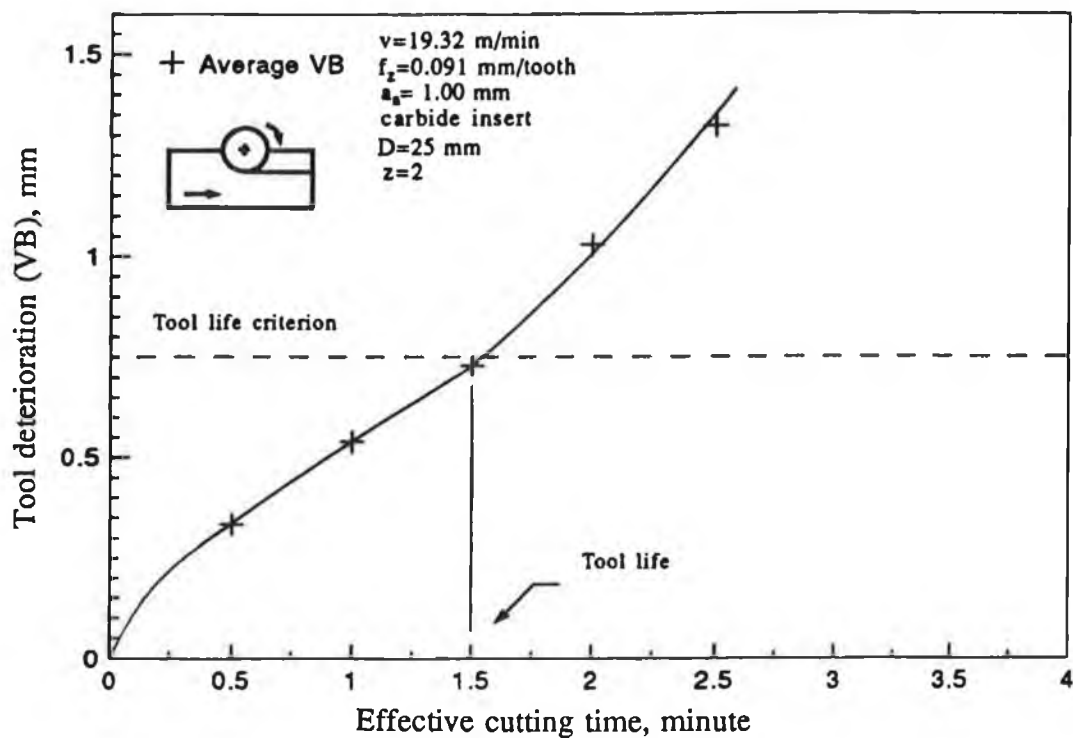


Fig.7.10: Arithmetic mean values of tool deterioration which is obtained from Fig.7.9 plotted against cutting time

**7.3.2.2 Tool deterioration with effective cutting time in half immersion end milling
Inconel 718 at down milling mode at cutting speed $v = 19.32$ m/min, $f_z =$
 0.091 mm/min and axial depth of cut $a_a = 1.00$ mm**

The half immersion end milling operation in down milling mode was conducted at a selected level of cutting condition of $v = 19.32$ m/min, $f_z = 0.091$ mm/tooth and $a_a = 1.00$ mm. Flank wear was measured with tool makers's microscope after an interval of 1 minute. VB1 flank wear was dominant in the cutting operation, but the cutting operation is continued until VB2 or VB3 flank wear appears. Flank wear obtained in four test runs for the above cutting conditions was plotted against the effective cutting time in Fig.7.11. From Fig.7.11 it is observed that tool deterioration value after a cutting time of 6 minutes is disproportionately high. This is due to the fact that up to a cutting time of 6 minutes the tool deterioration was as result of uniform flank wear. After a cutting time of 6 minutes the tool deterioration is due to VB2 or VB3 flank wear. The tool life obtained from the point or field of intersection of the curves by the horizontal line representing the limiting deterioration value is determined as the " tool life criterion ". The arithmetic mean value of the flank wear of the above test run was plotted against the effective cutting time in Fig.7.12. The SEM photograph of the tool wear in the carbide insert is shown in Appendix 3. From Fig.7.12 it is observed that the tool life is about 7 minutes.

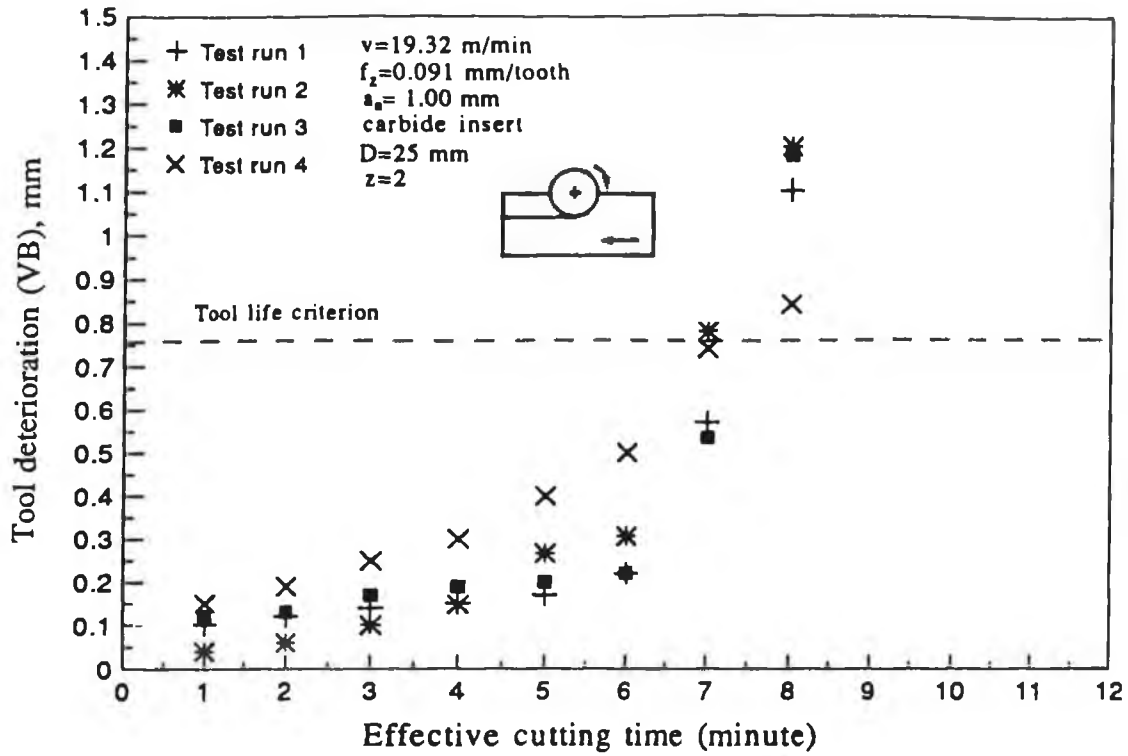


Fig.7.11: Tool deterioration (flank wear) values for a number of test runs plotted against cutting time in half immersion down cut end milling Inconel 718 at $v = 19.32$ m/min, $f_z = 0.091$ mm/tooth and $a_p = 1.00$ mm

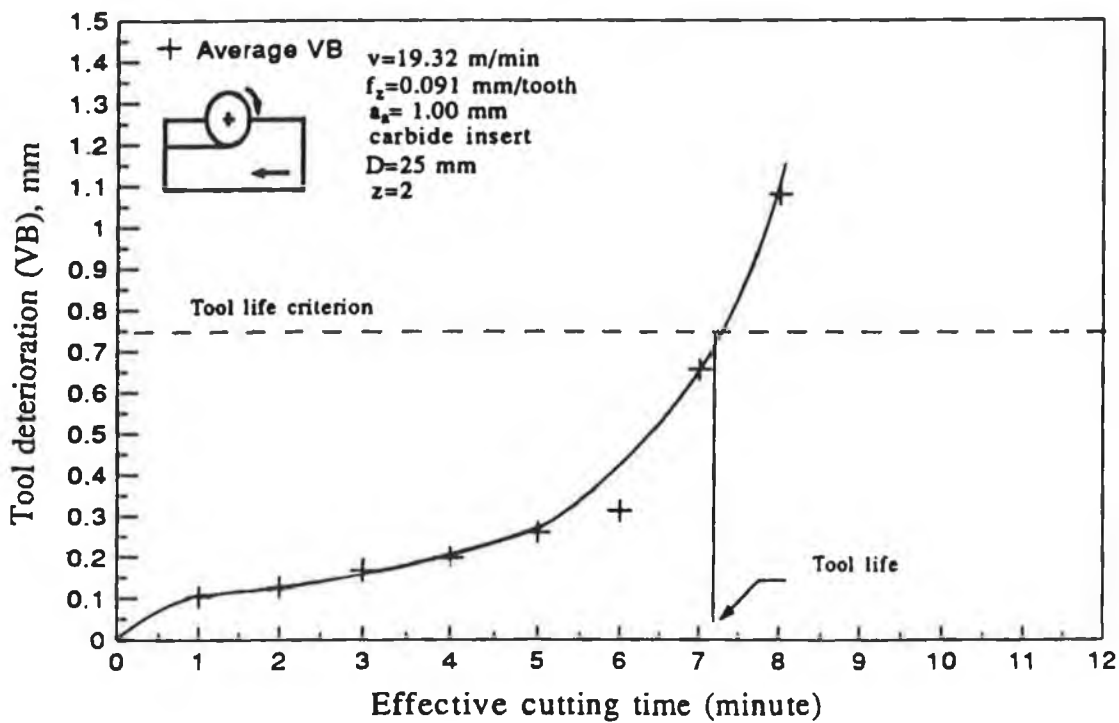


Fig.7.12: Arithmetic mean values of tool deterioration which is obtained from Fig.7.11 plotted against cutting time

7.3.3 Comparison of tool life between half immersion and full immersion end milling Inconel 718

Fig.7.13 shows the difference in tool life between half immersion and full immersion end milling Inconel 718 at cutting speed $v = 19.32$ m/min, feed $f_z = 0.091$ mm/tooth and axial depth of cut $a_a = 1.00$ mm. The half immersion tests were carried out for both up and down milling mode. From this figure it is observed that full immersion (slot) tests give a considerable increase in tool life. This may be due to the difference in heating and cooling time during cutting which induces a thermal stress and consequently influences the tool life. The difference in tool life in up and down milling mode is more significant. Up milling mode gives the least tool life. This is because in up milling, the cutter is somewhat guided by the portion already machined. Hence, in up milling there is a strong rubbing action before the cutter actually starts cutting and the rubbing action dulls the cutter quickly. It is also reported that in up milling, the cutting edge initially rubs the surface cut by the previous tooth, and only when the elastic limit of the workpiece has been reached does the cutting edge penetrate the surface. This causes a peak value of radial force to occur before it settles down to a fairly steady value. In machining work hardening materials, this radial force can be very high leading to failure of cutting edge. Besides, in up milling, the chips accumulate ahead of the cutting region where they can be picked up by the cutter. Also the chip thickness being highest at the end, the temperature is highest there also and there is a greater tendency for the chip to weld to the cutter which decreases the tool life.

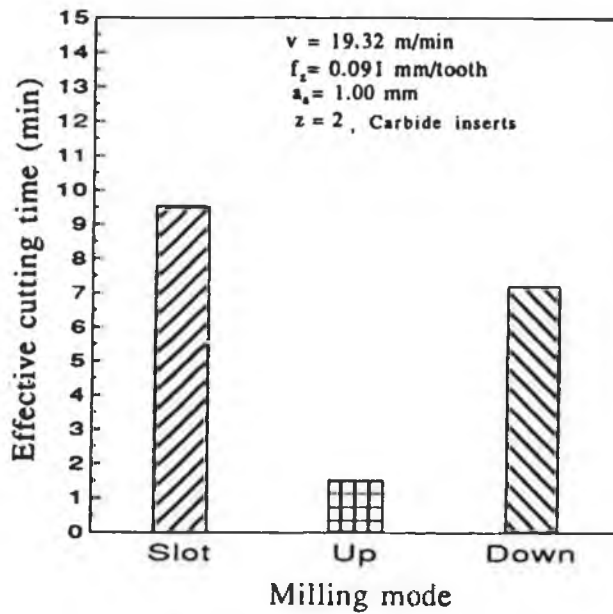


Fig.7.13: Comparison of tool life between half immersion (up and down) and full immersion (slot) end milling Inconel 718

7.3.4 Conclusions

- Full immersion end milling (slot) has an increased tool life than that of half immersion (up and down) end milling.
- Tool life in down cut end milling is higher than that of up cut end milling.
- Cutting speed decreases tool life significantly in full immersion end milling.

CHAPTER 8

INVESTIGATION OF SURFACE FINISH IN END MILLING STEEL(190 BHN), INCONEL 718 AND 2618 MMC

8.1 Introduction

The investigations of surface finish in end milling steel (190 BHN), Inconel 718 and 2618 MMC are divided as:

- (1) Development of surface roughness models in end milling steel (190 BHN)
- (2) Influence of machining conditions on surface roughness in end milling Inconel 718
- (3) Development of surface model in end milling Inconel 718
- (4) Development of surface roughness model in end milling 2618 MMC

8.2 Development of surface roughness models in end milling steel (190 BHN)

8.2.1 Introduction

The theoretical surface roughness in end milling can be estimated with the formulae [9,78,80,82] which are usually a function of feed and tool geometry. But the actual surface roughness is usually larger than the theoretical roughness values estimated by those formulae. This is because the formulae for estimating surface roughness in end milling do not take into account vibration, deflection of the work-tool system, chatter and built up edge embedded in the machined surface which are generally a function of cutting speed and depth of cut. Hence, it is necessary to develop the mathematical

models (empirical equations) which relate surface roughness and the machining variables. In this work, RSM is used to develop the mathematical models in terms of the investigated primary machining variables. Response surface contours were constructed by computer for determining the optimum cutting conditions.

8.2.2 Development of surface roughness models by Response Surface Methodology

(i) Postulation of Mathematical Models

Factors influencing surface roughness in end milling operations are shown in chapter 3. For the sake of simplicity, the factors arising out of workpiece, tool and other qualitative factors like coolant, mode of milling are kept constant. Only quantitative primary machining variables like speed, feed and axial depth of cut which are easily controllable were used to predict the proposed mathematical models. Hence, for a particular work-tool geometry the surface roughness in end milling is assumed to be a function of cutting speed, feed and axial depth of cut, i.e.

$$\text{Surface roughness} = f (v, f_z, a_a)$$

The multiplicative model for the predicted surface roughness (response surface) in end milling in terms of the investigated independent variables can be expressed from equation (4.6) of chapter 4 as:

$$\hat{R}_{a(\text{steel})} = C_{70} v^{k_7} f_z^{l_7} a_a^{m_7} \quad (8.1)$$

Where $\hat{R}_{a(\text{steel})}$ - predictive surface roughness for steel CLA (μm), and C_{70} , k_7 , l_7 , m_7 - model parameters.

Equation (8.1) can be written from equation (4.5) as first-order polynomial:

$$\hat{y}_{(\text{steel})} = b_0 x_0 + b_1 x_1 + b_2 x_2 + b_3 x_3 \quad (8.2)$$

The first-order model is only accepted over a narrow range of the variables. In order to predict the response reliably over a wide range of machining variables, second-order

polynomial models are needed in some cases. From equation (4.7) of chapter 4, equation (8.2) could be extended to a second-order model as:

$$\hat{y}_{(steel)} = b_0x_0 + b_1x_1 + b_2x_2 + b_3x_3 + b_{11}x_1^2 + b_{22}x_2^2 + b_{33}x_3^2 + b_{12}x_1x_2 + b_{13}x_1x_3 + b_{23}x_2x_3 \quad (8.3)$$

Where \hat{y}_{steel} - predictive response (surface roughness) on natural logarithmic scale, while $x_0 = 1$, and x_1, x_2, x_3 - the coded value(logarithmic transformations) of speed, feed, axial depth of cut respectively and b's - model parameters to be estimated using experimentally measured surface roughness (R_a) data.

(ii) Experimental Design

In order to determine equations (8.2) and (8.3), the first-order orthogonal and central composites designs were selected respectively. The first-order orthogonal design for 3 factors is shown in Fig.4.4 of chapter 4. This design consists of 12 experiments which are divided into 2 blocks (Blocks 1 & 2) of 6 tests each. As the first-order model is only accepted over a narrow range of variables, the experiments were extended to obtain a second-order model. Six experiments were added at the faces of the cube where each was chosen at a selected augment length of $\sqrt{2}$. These six experiments were repeated to increase the model accuracy. The resulting 24 experiments form a central composite design for 3 factors are shown in Fig.4.6 of chapter 4. The 24 experiments were performed in four blocks (Blocks 1, 2, 3 and 4). The central composite design with 24 experiments provided five levels for each independent variable.

(iii) Coding of independent variables

The coded values of the variables shown in Table 8.1 for use in equations (8.2) and (8.3) were obtained from the following transforming equations:

$$x_1 = \frac{\ln v - \ln 30}{\ln 37 - \ln 30} \quad (8.4)$$

$$x_2 = \frac{\ln f_z - \ln 0.10}{\ln 0.20 - \ln 0.10} \quad (8.5)$$

$$x_3 = \frac{\ln a_a - \ln 1.00}{\ln 1.40 - \ln 1.00} \quad (8.6)$$

Where x_1 - the coded value of the cutting speed of the cutter corresponding to its natural value v , x_2 - the coded value of the feed per tooth corresponding to its natural value f_z and x_3 - the coded value of the axial depth of cut corresponding to its natural value a_a .

The above relations were obtained from the transforming equation (4.10) of chapter 4.

Table 8.1: Levels of the Independent Variable and Coding Identification for surface roughness (Steel)

Independent Variables	Levels in Coded form				
	$-\sqrt{2}$ (lowest)	-1 (low)	0 (centre)	+1 (high)	$+\sqrt{2}$ (highest)
v , m/min (x_1)	22	24	30	37	40
f_z , mm/tooth (x_2)	0.04	0.05	0.10	0.20	0.26
a_a , mm (x_3)	0.62	0.72	1.00	1.40	1.60

(iv) Experiment

The process utilized for surface roughness was a slot milling operation, performed on a vertical milling machine (Bridgeport). The cutting tests were conducted under dry conditions using commercially available HSS solid slot drills. The specification of the HSS slot drill is shown in chapter 5 and Appendix 1. The workpiece material was steel 190 BHN. The properties of the material are shown in chapter 5 and Appendix 1. The bottom surface roughnesses (R_a) produced in the slot were measured by a stylus type instrument (Taylor Hobson's Talysurf 5-120). Table 8.2 shows the cutting conditions and the surface roughness results. The measured surface roughness values were obtained by averaging the surface roughness values at a minimum of three location points on the bottom surface of the slot.

Table 8.2: Experimental Conditions & Results for surface roughness (Steel)

Tl. No.	Blk. No.	Speed v m/min	Feed f_z mm/tooth	Axial depth of cut a_p , mm	Coding			Experimental av. surface roughness $R_a, \mu\text{m}$
					x_1	x_2	x_3	
1	1	24	0.05	0.72	-1	-1	-1	2.73
2	2	37	0.05	0.72	1	-1	-1	1.41
3	2	24	0.20	0.72	-1	1	-1	2.94
4	1	37	0.20	0.72	1	1	-1	6.31
5	2	24	0.05	1.40	-1	-1	1	2.94
6	1	37	0.05	1.40	1	-1	1	1.53
7	1	24	0.20	1.40	-1	1	1	8.07
8	2	37	0.20	1.40	1	1	1	7.13
9	1	30	0.10	1.00	0	0	0	2.31
10	1	30	0.10	1.00	0	0	0	2.88
11	2	30	0.10	1.00	0	0	0	2.89
12	2	30	0.10	1.00	0	0	0	2.11
13	3	22	0.10	1.00	$-\sqrt{2}$	0	0	6.71
14	3	40	0.10	1.00	$\sqrt{2}$	0	0	2.22
15	3	30	0.04	1.00	0	$-\sqrt{2}$	0	1.39
16	3	30	0.26	1.00	0	$\sqrt{2}$	0	5.60
17	3	30	0.10	0.62	0	0	$-\sqrt{2}$	1.86
18	3	30	0.10	1.60	0	0	$\sqrt{2}$	3.15
19	4	22	0.10	1.00	$-\sqrt{2}$	0	0	4.88
20	4	40	0.10	1.00	$\sqrt{2}$	0	0	2.13
21	4	30	0.04	1.00	0	$-\sqrt{2}$	0	1.42
22	4	30	0.26	1.00	0	$\sqrt{2}$	0	6.83
23	4	30	0.10	0.62	0	0	$-\sqrt{2}$	1.86
24	4	30	0.10	1.60	0	0	$\sqrt{2}$	2.30

(v) Estimation of the model parameters

The regression parameters of the selected models were estimated by the method of least squares. The basic formula of the least square is shown in equation (4.13) of chapter 4.

(vi) Analysis of results

(a) Development of the first-order model

The first-order model of the surface roughness was developed using 12 tests of the first and second blocks. The parameters in equation(8.2) were estimated, yielding the surface roughness predicting equation as:

$$\hat{y}_{(steel)} = 1.1272 - 0.0832x_1 + 0.5151x_2 + 0.1608x_3 \quad (8.7)$$

This predicting equation (8.7) can also be graphically represented in the 3 dimensional space of cutting speed, feed and axial depth of cut as depicted in Fig. 8.1 The predicting equation (8.7) can also be plotted in Fig. 8.2 as contours for each of the response surfaces at three selected levels of axial depth of cut (note that Fig. 8.1 and 8.2 are on a logarithmic scale). These selected levels were chosen as low($a_a = 0.72$ mm), centre($a_a = 1.00$ mm) and high($a_a = 1.40$ mm) Equation (8.7) can be transformed using equations (8.4), (8.5) and (8.6) to provide the surface roughness R_a (CLA, μm) as a function of the cutting speed v (m/min), f_z (mm/tooth) and axial depth of cut a_a (mm) as follows:

$$\hat{R}_{a(steel)} = 65.87 v^{-0.40} f_z^{0.74} a_a^{0.48} \quad (8.8)$$

This equation is valid for slot milling steel (190 BHN) using slot drills under dry conditions and

$$24 \leq v \leq 37 \quad \text{m/min}$$

$$0.05 \leq f_z \leq 0.20 \quad \text{mm/tooth}$$

$$0.72 \leq a_a \leq 1.60$$

Equation (8.8) indicates that an increase in either the feed and axial depth of cut increases the surface roughness while an increase in the cutting speed decreases the surface roughness.

(b) Development of the second-order Model

The second-order model was developed to extend the variables range to describe adequately the relationship between the slot milling operation output (surface roughness) and the investigated independent variables.

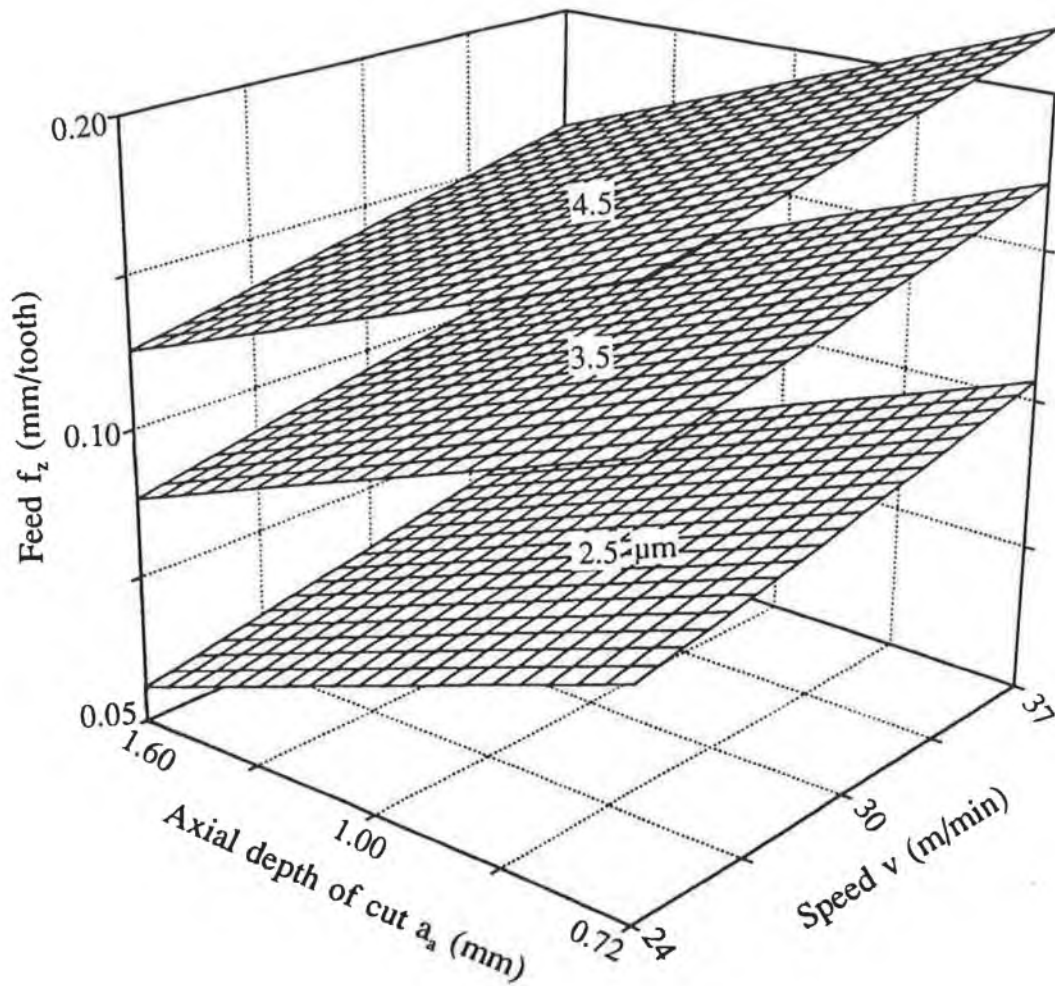
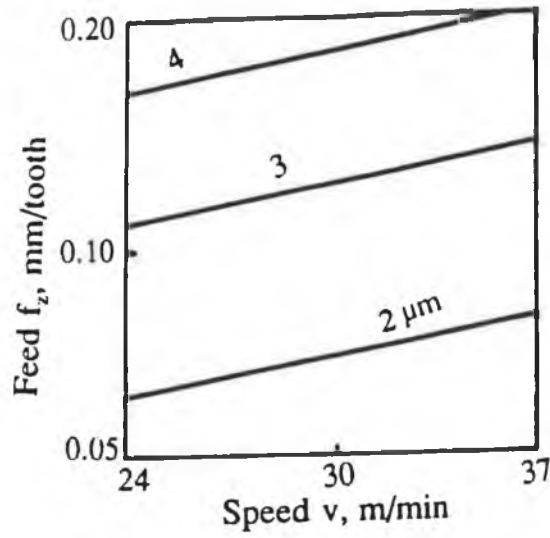
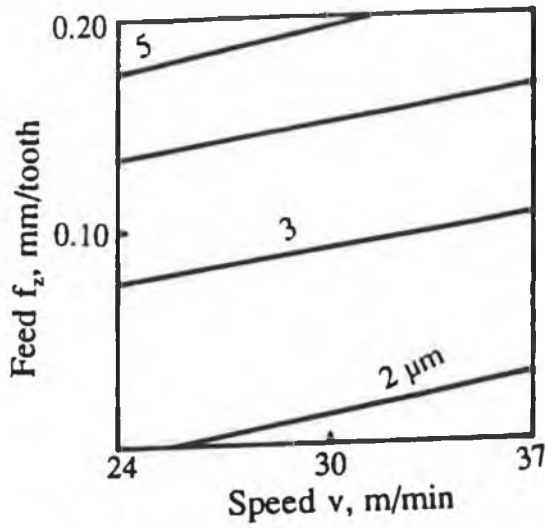


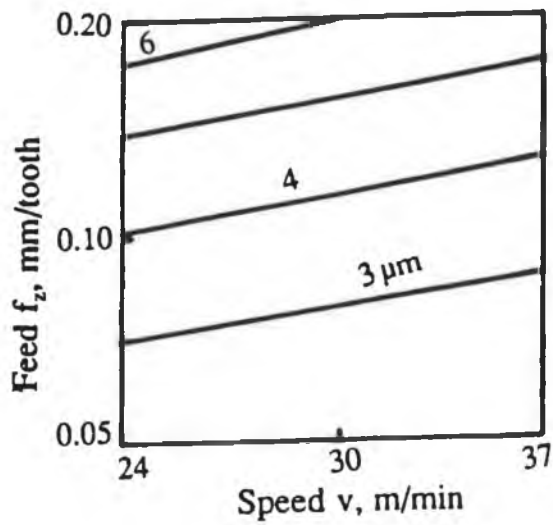
Fig.8.1: Contour surfaces for surface roughness in end milling steel (190 BHN) in 3 dimensional factor space (log-scales)



$a_1 = 0.72$ mm



$a_1 = 1.00$ mm



$a_1 = 1.40$ mm

Fig.8.2: Surface roughness contours (first-order model) for steel (190 BHN) in-feed planes at selected levels of axial depth of cut (log-scales)

The second-order model for the surface roughness in its transformed state is given by:

$$\begin{aligned} \hat{y}_{(steel)} = & 0.8825 - 0.2056x_1 + 0.5196x_2 + 0.1458x_3 + 0.1998x_1^2 \\ & + 0.12041x_2^2 - 0.0173x_3^2 + 0.2432x_1x_2 - 0.1098x_1x_3 + 0.1218x_2x_3 \end{aligned} \quad (8.9)$$

Equation (8.9) is plotted in Fig. 8.3 as contours for each of the response surfaces at three selected levels of axial depth of cut (note that this figure is on a logarithmic scale). These selected levels were chosen as low ($a_a = 0.72$ mm), centre ($a_a = 1.00$ mm) and high ($a_a = 1.40$ mm). These contours were constructed by computer utilizing "Matlab" computer package for determining the optimum conditions for a required surface roughness. From the contours shown in Fig. 8.3 it is possible to select a combination of cutting speed and feed which produces the same roughness. This can be illustrated by further utilization of the model to include the rate of material removed Q (cm^3/min) as shown in equation (3.16) of chapter 3. Equation of material removal rate, Q can be written as:

$$\ln Q_{(steel)} = \ln f_z + \ln z + \ln N_s + \ln a_a + \ln a_r - \ln 1000 \quad (8.10)$$

For slot milling (20 mm diameter end mill with 2 teeth) at a specified depth of cut, $a_a = 1.00$ mm and using the transformation equations (8.4) and (8.5), equation (8.10) becomes:

$$\ln Q_{(steel)} = 1.01 + 0.21x_1 + 0.69x_2 \quad (8.11)$$

For a constant rate of material removal, equation (8.11) can be represented by a straight line as illustrated in Fig. 8.4. This figure was obtained by superimposing the constant Q lines on the surface roughness contours in the speed-feed plane, for $a_a = 1.40$ mm axial depth of cut. Fig. 8.4 shows that the rate of material removal can be doubled without increasing the surface roughness $R_a = 3 \mu\text{m}$ (CLA). It can be shown that the selection of cutting conditions represented by the point "B" is better than that represented by point "A". This 100% increase in material removal rate is obtained without any sacrifice in quality of the produced surface.

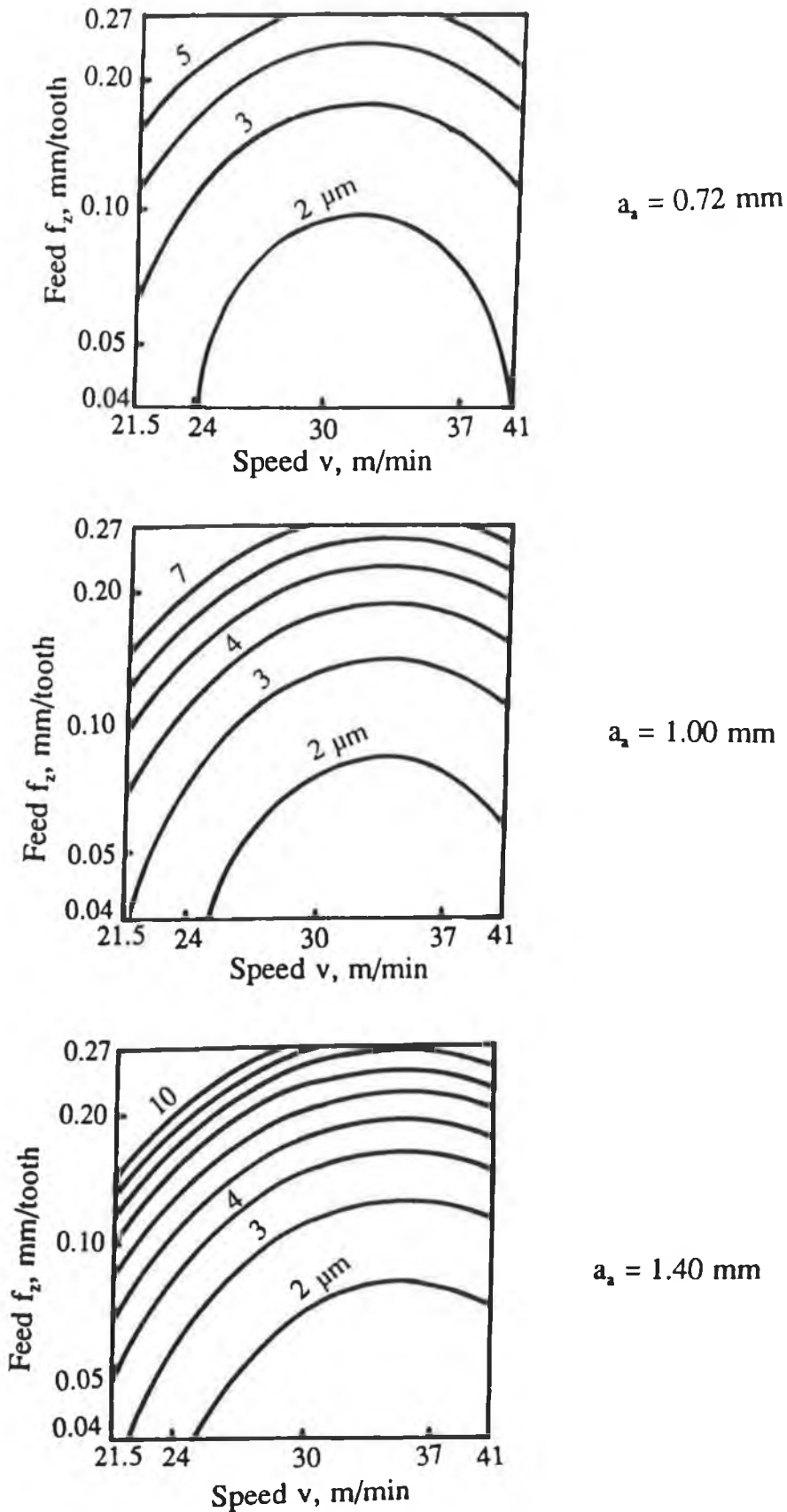


Fig.8.3: Surface roughness contours (second-order model) for steel (190 BHN) in speed-feed planes at selected levels of axial depth of cut (log-scales)

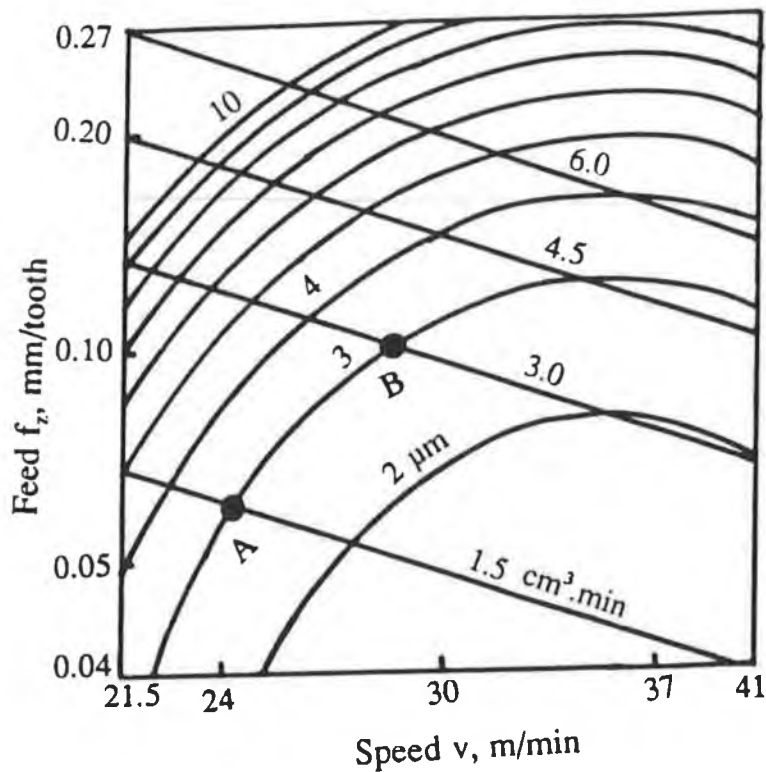


Fig.8.4: Contours of surface roughness (second-order model) and material removal rates steel (190 BHN) in speed-feed planes at 1.40 mm axial depth of cut (log-scales)

(c) Adequacy of the postulated Models

The adequacy of the predicting models are tested by analysis of variance (ANOVA). As per this technique the calculated F_{rat} of the first and second-order models are 5.19 and 3.75 respectively, and the corresponding F_{rat} (95% confidence) for the first and second-order models are 19.30 and 4.07 respectively as obtained from statistical tables. Hence, both the first and second-order models are valid. The detailed formulae of analysis of variance are shown in chapter 4. The results of the analysis of variance for the predicting models are shown in Appendix 4.

(d) Significance of individual variables

The significance testing of the individual variables of the predictive models was done using formula (4.15) of chapter 4. The results of significance testing are shown in

Appendix 4. The calculated F_{rat} of the speed, feed and axial depth of cut for the first-order model are 0.41, 15.25 and 1.49 respectively while the corresponding F_{rat} for 95% confidence is 5.32, and the calculated F_{rat} of the speed, feed and axial depth for the second-order model are 16.85, 100.20 and 7.89 respectively while the corresponding F_{rat} for 95% confidence is 4.60. So, it is observed that the effect of cutting speed (x_1) and axial depth of cut are not so significant in the first order model. It may be due to the fact that within the speed range of the first-order model there is not any significant effect of built up edge on the produced surface and within the axial depth of cut range of the first-order model the cutting force is not sufficient to cause deflection and vibration of the work-tool system. Since speed and axial depth of cut are important variables in material cutting operations and have some effect on the surface roughness, so they are included in the first-order model. But for the case of the second-order model it is seen that the cutting speed and axial depth of cut have a significant effect on surface roughness. This may be attributed to the built up edge formation effect within the speed range which deteriorates the produced surface finish and the cutting force within the axial depth of cut range causes deflection and vibration of the work-tool system which in turn deteriorates the surface finish. The feed effect is significant for both the first and second-order model. This is due to the fact that surface roughness is the result of the feed marks left on the milled surface by the cutter teeth as they slide across the surface. So, within a narrow range of cutting speed and axial depth of cut, surface roughness in end milling mainly depends on feed rate, while within a wide range of cutting speed and axial depth of cut, surface roughness in end milling depends on all variables (i.e. cutting speed, feed and axial depth of cut).

(e) Precision of prediction (Confidence Interval)

Due to experimental error , the estimated parameters hence the estimated surface roughness \hat{y} (R_a) is subjected to a uncertainty. Hence the precision of these quantities has been estimated by calculating the appropriate confidence intervals using formula (4.16) of chapter 4. The resulting 95% confidence intervals of the predictive models are shown in Appendix 4.

(vii) Conclusions

- (a) Reliable surface roughness models have been developed to enhance the efficiency of slot milling steel (190 BHN) when using slot drills.
- (b) The first-order surface prediction equation is valid within the speed range of 24 - 37 m/min, the feed range of 0.05 - 0.20 mm/tooth and the axial depth of cut range of 0.72 - 1.40 mm.
- (c) By utilizing the second-order model, it is possible to extend the variable range. The prediction equation is valid within the speed range of 22 - 40 m/min, the feed range 0.04 - .26 mm/tooth and the axial depth of cut range of 0.62 - 1.60 mm.
- (d) The effect of the cutting speed and axial depth of cut on surface roughness are significant for the second-order model only i.e., over a wide range of the variable of which the feed effect is the most dominant.
- (e) An increase in either the feed or the axial depth of cut increases the surface roughness while an increase in the cutting speed decreases the surface roughness.
- (f) Contours of the surface roughness outputs were constructed in planes containing two of the independent variables. These contours were further developed to select the proper combination of the cutting speed and feed to increase the material removal rate without sacrificing the quality of the produced surface roughness.

8.3 Influence of machining conditions on surface roughness in end milling

Inconel 718.

The influence of machining conditions on surface roughness in end milling Inconel 718 is divided as:

- (1) Influence of cutting speed on surface roughness
- (2) Influence of feed on surface roughness

Influence of axial depth of cut on surface roughness in end milling Inconel 718 is not investigated as it is shown in section 8.2 that when machining steel (190 BHN), low range of axial depth of cut has no significant influence on surface roughness.

8.3.1 Influence of cutting speed on surface roughness in end milling Inconel 718.

A slot milling operation was carried at varying cutting speeds. Surface roughness was measured at 3 location points on the bottom surface of the slot for each cutting condition. The measured surface roughnesses were plotted against the varying cutting speed in Fig.8.5. From the figure it is seen that the surface roughness decreases as the cutting speed is increased, but after a certain speed the rate of decrease is not significant. At lower speeds the surface roughness is influenced by the presence of a built up edge. Higher speed results the higher temperature and consequently reduces the tendency of pressure welding. Thus the surface roughness at higher speeds is reduced due to the disappearance of the built up edge.

8.3.2 Influence of feed on surface roughness in end milling Inconel 718.

A slot milling operation was carried out at varying feeds using carbide insert. Surface roughness was measured at 3 location points on the bottom surface of the slot for each cutting condition. The measured surface roughnesses were plotted against the varying feed rates in Fig. 8.6. From the figure it is seen that surface roughness increases as feed per tooth increases. This is due to the fact that surface roughness is the result of feed marks left on the milled surface by the cutter tooth as they slide across the surface. So, as the feed per tooth increases surface irregularities also increase.

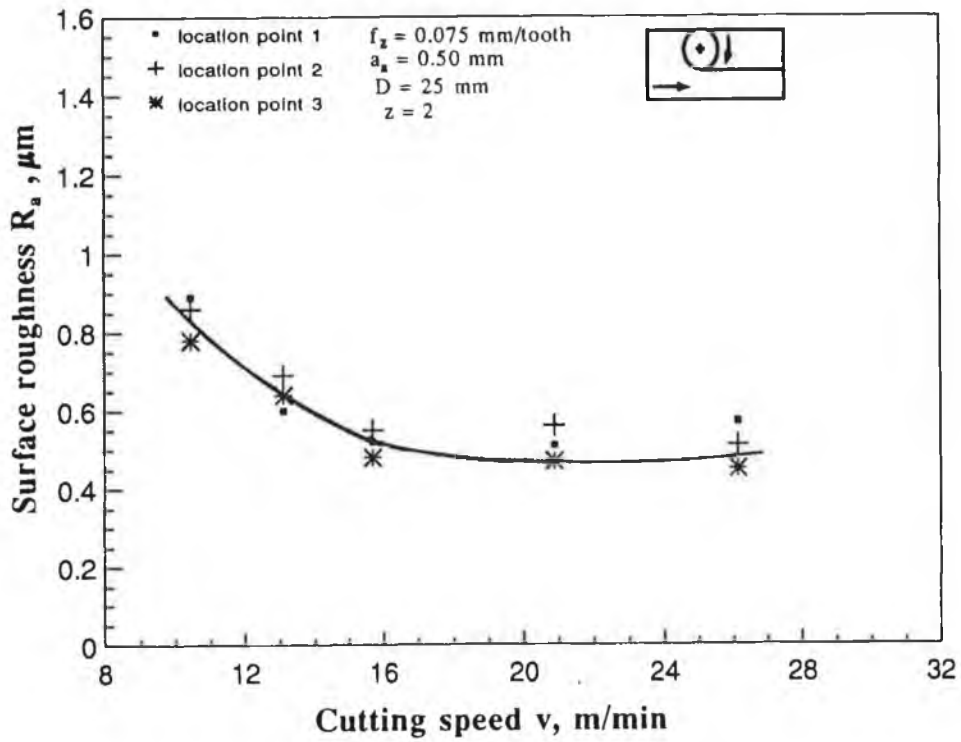


Fig.8.5: Surface roughness versus speed for slot milling Inconel 718 using sharp uncoated carbide under dry condition

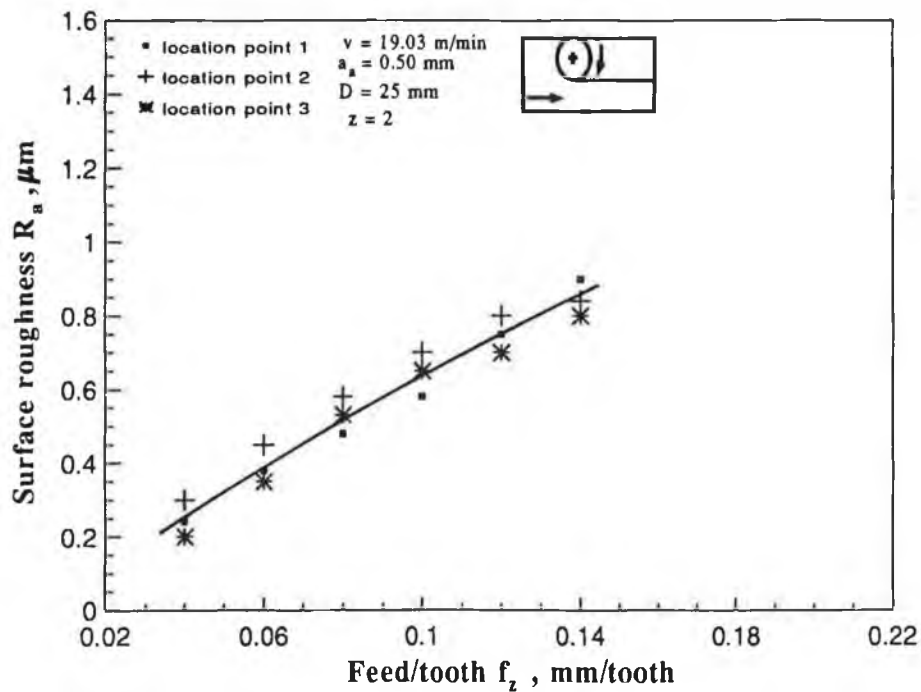


Fig.8.6: Surface roughness versus feed for slot milling Inconel 718 using sharp uncoated carbide insert under dry condition

8.4 Development of surface roughness model in end milling Inconel 718

8.4.1 Introduction

The surface roughness models in slot milling Inconel 718 are developed by RSM. The machining variables like cutting speed and feed are considered in building the models. The optimum cutting conditions is obtained by constructing contours of constant surface roughness by computer.

8.4.2 Development of surface roughness model by RSM.

(i) Postulation of mathematical model

For a particular work-tool geometry, the roughness in end milling is assumed to be a function of the machining conditions. When end milling steel (190 BHN), it has been shown that within low range, axial depth of cut has no significant influence on surface roughness. Hence, surface roughness in end milling Inconel 718 is assumed to be a function of cutting speed and feed i.e.

$$\text{Surface roughness} = f(v, f_z)$$

Where v - cutting speed (m/min) and f_z - feed rate per tooth (mm/tooth).

From the equation (4.6) of chapter 4, the multiplicative model for the predictive surface roughness (response surface) in end milling in terms of the investigated independent variables can be expressed as:

$$\hat{R}_{a(\text{Inconel})} = C_{80} v^{I_8} f_z^{m_8} \quad (8.12)$$

Where $R_{a(\text{Inconel})}$ - predicted surface roughness, CLA (μm) and C_{80} , I_8 , m_8 are model parameters to be estimated using experimental data.

Equation (4.12) can be written as the first-order polynomial as:

$$\hat{y}_{(Inconel)} = b_0x_0 + b_1x_1 + b_2x_2 \quad (8.13)$$

The second- order surface roughness model can be written from equation (4.7) of chapter 4 as:

$$\hat{y}_{(Inconel)} = b_0x_0 + b_1x_1 + b_2x_2 + b_{11}x_1^2 + b_{22}x_2^2 + b_{12}x_1x_2 \quad (8.14)$$

$\hat{y}_{(Inconel)}$ - predictive response (surface roughness) on logarithmic scale, while $x_0 = 1$ and x_1, x_2 - the coded values (logarithmic transformations) of v, f_z respectively and b 's are model parameters to be estimated by the method of least squares using experimentally measured surface roughness data.

(ii) Experimental Design

The orthogonal first-order design and central rotatable composite designs were selected in order to determine the equation of the first-order and the second order surface roughness model respectively. The orthogonal first-order and central rotatable design for two factors are shown in Figs.4.3 and 4.5 respectively in chapter 4.

(iii) Coding of independent variables

The coded values of the variables shown in Table 8.3 for use in equation (8.13) and (8.14) were obtained from the following transforming equations:

$$x_1 = \frac{\ln v - \ln 18.37}{\ln 24.10 - \ln 18.37} \quad (8.15)$$

$$x_2 = \frac{\ln f_z - \ln 0.075}{\ln 0.098 - \ln 0.075} \quad (8.16)$$

Where x_1 - the coded value of the cutting speed corresponding to its natural value v and x_2 - the coded value of the feed per tooth corresponding to its natural value f_z .

The above relationships were obtained from equation (4.10) of chapter 4

Table 8.3: Levels of the Independent Variable and Coding Identification for surface roughness (Inconel 718)

Independent Variables		Levels in Coded form				
		-√2 (lowest)	-1 (low)	0 (centre)	+1 (high)	+√2 (highest)
v , m/min x ₁	Calculated	12.47	14.00	18.37	24.10	26.22
	Used	13.12	14.08	18.37	24.10	26.97
f _z , mm/tooth x ₂	Calculated	0.053	0.057	0.075	0.098	0.109
	Used	0.053	0.057	0.075	0.098	0.107

(iv) Experiment

The process utilized for surface roughness was a slot milling operation, performed on a vertical milling machine (Bridgeport). The cutting tests were carried out using an end mill with carbide inserts under dry conditions. The tool geometry has been shown in chapter 5 and Appendix 1. The reference work material was Inconel 718. The properties of the reference work material has been shown in chapter 5 and Appendix 1. The bottom surface roughness produced in the slot were measured by a stylus type instrument (Taylor Hobson's Talysurf 5-120). Table 8.4 shows the cutting conditions and measured surface roughness results. The measured surface roughness values were obtained at a minimum of three location points of the bottom surface produced in the slot.

(v) Estimation of model parameters

The regression parameters of the selected models were estimated by the method of least square. The basic formula for least square is shown in equation (4.10) of chapter 4.

(vi) Analysis of results

(a) Development of the First-order model

The first-order model of the surface roughness was developed using 9 tests, the parameters in equation (8.13) were estimated , yielding the surface roughness predicting equation as:

$$\hat{y}_{(Inconel)} = -0.6078 - 0.1206x_1 + 0.4609x_2 \quad (8.17)$$

The predicting equation (8.17) can be plotted in Fig.8.7 as contours for each of response surfaces at a selected level of axial depth of cut of 0.5 mm (note that this figure is on a logarithmic scale). This Equation can be transformed using equations (8.15) and (8.16) to provide the surface roughness (CLA, μm) as a function of the cutting speed v (m/min) and feed f_z (mm/tooth) as follows:

$$\hat{R}_a (Inconel) = 172.12 v^{-0.444} f_z^{1.723} \quad (8.18)$$

Equation (8.18) indicates that an increase in the cutting speed decreases surface roughness while an increase in the feed increases the surface roughness. This equation is valid for slot milling Inconel 718 using end mill with carbide inserts and $14.08 \leq v \leq 24.10$ m/min and $0.057 \leq f_z \leq 0.098$ mm/tooth.

Table 8.4: Experimental Results and conditions for surface roughness (Inconel 718).

Trial No.	Speed v m/min	Feed f_z mm/tooth	Coding		Measured Surface roughness R_a , μm
			x_1	x_2	
1	14.08	0.057	-1	<u>-1</u>	0.40
2	24.10	0.057	1	-1	0.35
3	14.08	0.098	-1	1	1.12
4	24.10	0.098	1	1	0.79
5	18.37	0.075	0	0	0.53
6	18.37	0.075	0	0	0.49
7	18.37	0.075	0	0	0.47
8	18.37	0.075	0	0	0.48
9	18.37	0.075	0	0	0.58
10	13.12	0.075	$-\sqrt{2}$	0	0.62
11	26.97	0.075	$\sqrt{2}$	0	0.51
12	18.37	0.053	0	$-\sqrt{2}$	0.37
13	18.37	0.107	0	$\sqrt{2}$	0.64

(b) Development of the second-order model

The second order model was developed to extend the variable range to describe adequately the relationship between slot milling output (surface roughness) and the investigated independent variables. The second order surface roughness model in its transformed state is given as:

$$\hat{y}_{(Inconel)} = -0.6740 - 0.0941x_1 + 0.3267x_2 + 0.0826x_1^2 + 0.0076x_2^2 - 0.0525x_1x_2 \quad (8.19)$$

Equation (8.19) is plotted in Fig.8.8 as contours for each of the response surfaces at a selected level of axial depth of cut (note that this figure is on a logarithmic scale). These contours were constructed by computer utilizing "Matlab" computer package for a required surface roughness. From the contours shown in Fig.8.8 it is possible to select a combination of feed and cutting speed that reduces machining time without increasing the surface roughness, since there is a large number of combinations of cutting speed and feed which produces the same surface roughness. This can be illustrated by further utilization of the model to include the rate of material removed Q (cm^3/min) as shown in equation (3.16) of chapter 3. The rate of material removal Q can be written as:

$$\ln Q_{(Inconel)} = -0.8226 + 0.2715x_1 + 0.2676x_2 \quad (8.20)$$

For a constant rate of material removal, the equation (8.20) can be represented by a straight line as illustrated in Fig. 8.9. This figure was obtained by superimposing the constant Q lines on the surface roughness contours in the speed feed plane, for axial depth of cut (a_a) of 0.5 mm. This figure shows that the rate of material removal can be doubled without increasing the surface roughness $0.6 \mu\text{m CLA}$. It can be shown that the selection of cutting conditions represented by point "B" is better than those represented by point "A". This 100% increase in material removal rate is obtained without any sacrifice in quality of the produced surface finish.

(c) Adequacy of the postulated models

Both the first and second order models were tested by analysis of variance. As per this technique the calculated F_{rat} of the first and second-order models are 4.31 and 8.01 respectively while the corresponding F_{rat} (95% confidence) for the first and second-order

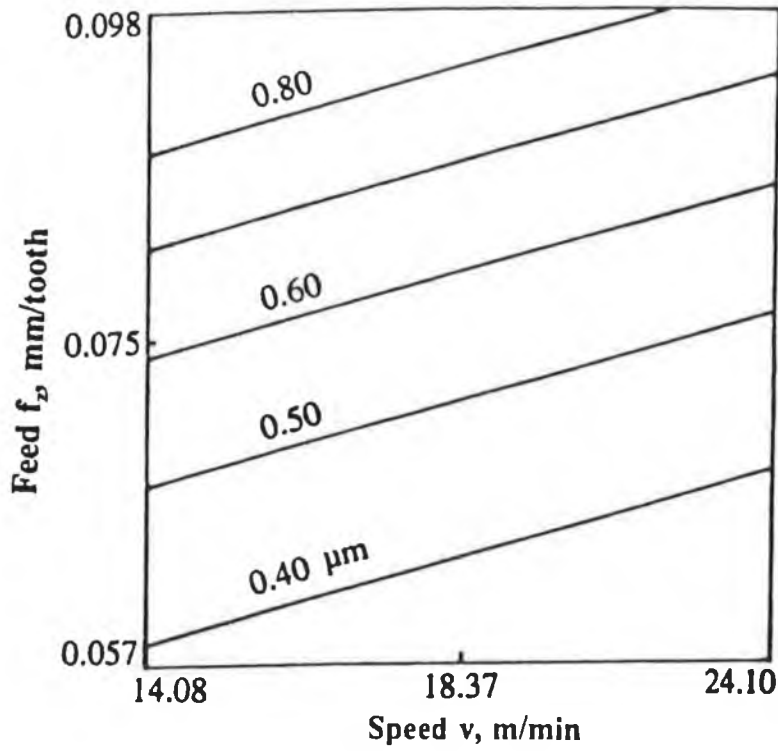


Fig.8.7: Surface roughness contours (first-order model) for Inconel 718 in speed-feed planes at 0.50 mm axial depth of cut (log-scales)

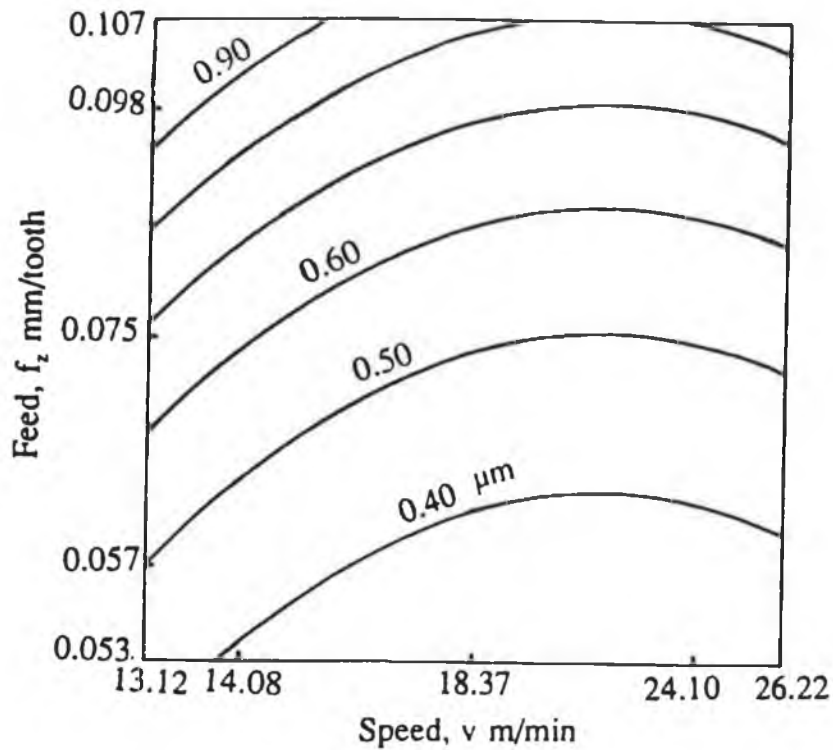


Fig.8.8: Surface roughness contours (second-order) for Inconel 718 in speed-feed planes at 0.50 mm axial depth of cut (log-scales)

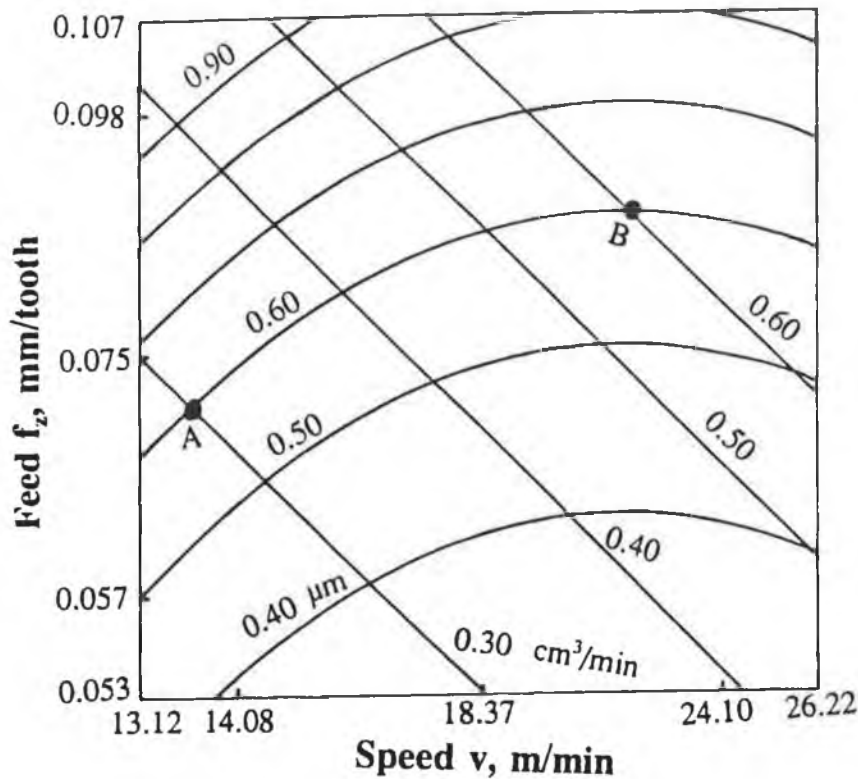


Fig.8.9: Surface roughness contours (second-order model) and material removal rates for Inconel 718 in speed-feed planes at 0.50 mm axial depth of cut (log-scales)

models are 6.94 and 16.69 respectively as obtained from statistical tables. Hence, both the models are valid. The results of analysis of variance for the predicting models are shown in Appendix 4.

(d) Significance of individual variables

The significance testing for the individual variables of the predicting models are shown in Appendix 4. From the significance testing it is seen that the calculated F_{rat} of the speed and feed of the first-order model are 3.70 and 150.25 while the corresponding

F_{rat} is 5.99 as obtained from statistical table, and the calculated F_{rat} of the speed and feed of the second-order model are 2.36 and 28.50 respectively while corresponding F_{rat} is 5.59 as obtained from statistical table. So, the feed effect is significant for both the first and the second-order models.

(e) Precision of prediction (confidence intervals)

The precision of the predictive models can be determined by calculating the appropriate confidence intervals and comparing them with the experimental values. The resulting 95% confidence intervals for the predicted responses are shown in Appendix 4.

(vii) Conclusions

- (a) Reliable surface roughness models have been developed and utilized to enhance the efficiency of slot milling Inconel 718 when using end mills with carbide inserts.
- (b) The first-order surface prediction model is valid within the speed range of 14.08 - 24.10 m/min and the feed range of 0.057 - 0.098 mm/tooth.
- (c) By utilizing the second-order model, it is possible to extend the variable range and the second order prediction model is valid within the speed range of 13.12 - 26.22 mm/min and feed range of 0.053 - 0.107 mm/tooth.
- (d) The feed effect is very dominant in both the first and second order models but the speed effect is not so significant for both the models.
- (e) An increase in the feed increases the surface roughness while an increase in the cutting speed decreases the surface roughness.
- (f) Contours of the surface roughness outputs were constructed in planes containing two of the independent variables. These contours were further developed to select the proper combination of the cutting speed and feed to increase the material removal rate without sacrificing the quality of the produced surface.

8.5 Development of surface roughness models for end milling 2618 MMC

8.5.1 Introduction

Most Metal Matrix Composite(MMC) materials are not produced to a finished net shape, post-production machining of the composite materials is necessary in different engineering components. However, MMCs are difficult to machine due to the use of hard abrasive materials as the reinforcing medium within a more ductile matrix material. A high surface finish is required because the fracture behaviour of MMCs is very sensitive to surface finish. Since MMCs are relatively new materials, so only limited data is available regarding the machinability of MMC using conventional machining methods. Under ideal conditions, the roughness of a machined surface may be a function of feed and tool geometry. But, in actual machining situation deflection, vibration of work-tool system and built up edge formation affect the surface produced in the machining processes which are usually a function of cutting conditions like depth of cut and cutting speed. So, it is necessary to relate surface roughness index, R_a with primary machining variables like speed, feed and depth of cut. RSM is employed to relate surface roughness in end milling 2618 MMC in terms of primary machining variables.

8.5.2 Development of the mathematical models by RSM

(i) Postulation of the mathematical models

For a particular work-tool geometry, the surface roughness in end milling is assumed to be a function of cutting speed (v), feed(f_z) and axial depth of cut(a_a). The multiplicative model for the predicted surface roughness(response surface) in end milling in terms of the investigated independent variables can be expressed from equation (4.6) of chapter 4 as:

$$\hat{R}_{a(MMC)} = C_{90} v^{k_9} f_z^{l_9} a_a^{m_9} \quad (8.21)$$

Where $\hat{R}_{a(MMC)}$ - predicted surface roughness CLA (μm) and C_{90} , k_9 , l_9 , m_9 are model parameters to be estimated by experimental data.

Equation (4.21) can be written as the first-order polynomial from equation (4.5) of chapter 4 as:

$$\hat{y}_{(MMC)} = b_0x_0 + b_1x_1 + b_2x_2 + b_3x_3 \quad (8.22)$$

The first-order model is only accepted over a narrow range of the variables. In order to predict the response reliably over a wide range of the machining variables, the second-order polynomial models are needed in some cases. The second-order model can be written from equation (4.7) of chapter 4 as:

$$\hat{y}_{MMC} = b_0x_0 + b_1x_1 + b_2x_2 + b_3x_3 + b_{11}x_1^2 + b_{22}x_2^2 + b_{33}x_3^2 + b_{12}x_1x_2 + b_{13}x_1x_3 + b_{23}x_2x_3 \quad (8.23)$$

Where $\hat{y}_{(MMC)}$ - proposed predicted response (roughness) on natural logarithmic scale, $x_0 = 1$, and x_1 , x_2 , x_3 are the coded value (logarithmic transformation) of v , f_z , a_a respectively and b 's are model parameters to be estimated using experimentally measured surface roughness data.

(ii) Experimental Design

In order to determine the equations of the first and the second-order model of the response surface the orthogonal first-order design and the central composite second-order design were selected respectively.. The orthogonal first-order design and the central composite design (with three factors) are shown in chapter 4.

(iii) Coding of independent variables

The coded values of the variables shown in Table 8.5 for use in equations (8.22) and (8.23) were obtained from the following transforming equations:

$$x_1 = \frac{\ln v - \ln 52.31}{\ln 78.46 - \ln 52.31} \quad (8.24)$$

$$x_2 = \frac{\ln f_z - \ln 0.10}{\ln 0.20 - \ln 0.10} \quad (8.25)$$

$$x_3 = \frac{\ln a_a - \ln 1.00}{\ln 1.64 - \ln 1.00} \quad (8.26)$$

x_1 - the coded value of the cutting speed of the cutter corresponding to its natural value v , x_2 - the coded value of the feed per tooth corresponding to its natural value f_z and x_3 - the coded value of the axial depth of cut corresponding to its natural value a_a .

The above relationships were obtained from equation (4.10) of chapter 4.

Table 8.5: Levels of the Independent Variables and Coding Identification for surface roughness(MMC)

Independent Variables	Levels in Coded form				
	$-\sqrt{2}$ (lowest)	-1 (low)	0 (centre)	+1 (high)	$+\sqrt{2}$ (highest)
v , m/min (x_1)	29.45	34.87	52.31	78.46	92.83
f_z , mm/tooth (x_2)	0.04	0.05	0.10	0.20	0.27
a_a , mm (x_3)	0.50	0.62	1.00	1.64	2.00

(d) Experiment

The process utilized for surface roughness was a slot milling operation, performed on a vertical milling machine (Bridgeport). The cutting tests were carried out using an end mill with carbide inserts (\approx K20). The detailed specification of the insert has been shown in chapter 5 and Appendix 1. The properties of reference work material(2618 MMC) are also shown in chapter 5 and Appendix 1. The bottom surface roughness (R_a) produced in the slot were measured by a stylus type instrument. Table 8.6 shows the cutting conditions and measured surface roughness results. The measured surface roughness were obtained by averaging the surface roughness values at a minimum of three different location points of the bottom surface of the slot.

(v) Estimation of the model parameters

The regression parameters of the selected models were estimated by the method of least squares, using the basic formula as shown in equation (4.13) of chapter 4.

**Table 8.6 : Experimental Results and Cutting Conditions for surface roughness
(2618 MMC)**

Trial No.	Block No.	Speed v m/min	Feed f_z mm/tooth	Axial depth of cut a_p , mm	Coding			Experimental av. Surface roughness R_a , μm
					x_1	x_2	x_3	
1	1	34.87	0.05	0.62	-1	<u>-1</u>	-1	0.19
2	2	78.46	0.05	0.62	1	-1	-1	0.16
3	2	34.87	0.20	0.62	-1	1	-1	2.25
4	1	78.46	0.20	0.62	1	1	-1	1.10
5	2	34.87	0.05	1.64	-1	-1	1	0.24
6	1	78.87	0.05	1.64	1	-1	1	.21
7	1	34.87	0.20	1.64	-1	1	1	1.53
8	2	78.87	0.20	1.64	1	1	1	1.09
9	1	52.31	0.10	1.00	0	0	0	0.43
10	1	52.31	0.10	1.00	0	0	0	0.53
11	2	52.31	0.10	1.00	0	0	0	0.39
12	2	52.31	0.10	1.00	0	0	0	0.37
13	3	29.45	0.10	1.00	$-\sqrt{2}$	0	0	0.44
14	3	92.83	0.10	1.00	$\sqrt{2}$	0	0	0.58
15	3	52.31	0.04	1.00	0	$-\sqrt{2}$	0	0.18
16	3	52.31	0.27	1.00	0	$\sqrt{2}$	0	2.30
17	3	52.31	0.10	0.50	0	0	$-\sqrt{2}$	0.38
18	3	52.31	0.10	2.0	0	0	$\sqrt{2}$	0.48
19	4	29.45	0.10	1.00	$-\sqrt{2}$	0	0	0.47
20	4	92.83	0.10	1.00	$\sqrt{2}$	0	0	0.44
21	4	52.31	0.04	1.00	0	$-\sqrt{2}$	0	0.25
22	4	52.31	0.27	1.00	0	$\sqrt{2}$	0	2.57
23	4	52.31	0.10	0.50	0	0	$-\sqrt{2}$	0.49
24	4	52.31	0.10	2.00	0	0	$\sqrt{2}$	0.37

(vi) Analysis of results

(a) Development of the first-order model

The first-order model of the surface roughness was developed using 12 tests of the first and second blocks, the parameters in equation (8.22) were estimated, yielding

the surface roughness predicting equation as:

$$\hat{y}_{(MMC)} = -0.7065 - 0.17x_1 + 0.9873x_2 + 0.0139x_3 \quad (8.27)$$

The predicting equation (8.27) can be graphically represented in 3 dimensional space of speed, feed and axial depth of cut as depicted in Fig. 8.10. The predicting equation (8.27) can also be plotted in Fig.8.11 as contours for each of the response surfaces at a selected level of axial depth of cut of 1.00 mm (note that Fig.8.10 and 8.11 are on a logarithmic scale). Equation (8.27) can be transformed using equations (8.24), (8.25) and (8.27) to provide the surface roughness, R_a (CLA, μm) as a function of the cutting speed v (m/min), feed f_z (mm/tooth) and axial depth of cut a_a (mm) as follows:

$$\hat{R}_{a(MMC)} = 68 v^{-0.42} f_z^{1.43} a_a^{0.03} \quad (8.28)$$

Equation (8.28) indicates that an increase in the cutting speed decreases the surface roughness while an increase in either the feed or axial depth of cut increases the surface roughness. But the effect of axial depth of cut is very small which can be neglected in practical machining situation. This equation is valid for slot milling 2618 MMC using end mill with carbide inserts and $34.87 \leq v \leq 78.46$, $0.05 \leq f_z \leq 0.20$ mm/tooth and $0.62 \leq a_a \leq 1.64$ mm.

(b) Development of the second-order model

The second-order model was developed to extend the variable range to describe adequately the relationship between the slot milling output (surface roughness) and the investigated independent variables. The second-order model for surface roughness in its transformed state is given by:

$$\begin{aligned} \hat{y}_{(MMC)} = & -0.82 - 0.07x_1 + 0.925x_2 + 0.003x_3 + 0.003x_1^2 + 0.228x_2^2 \\ & + 0.033x_3^2 - 0.094x_1x_2 + 0.052x_1x_3 - 0.1125x_2x_3 \end{aligned} \quad (8.29)$$

Equation (8.29) is plotted in Fig. 8.12 as contours for each of the response surfaces at a selected level of axial depth of cut of 1.00 mm (note that this figure is on a logarithmic scale). These contours were constructed utilizing "Matlab" computer package for determining the optimum cutting conditions for a required surface roughness.

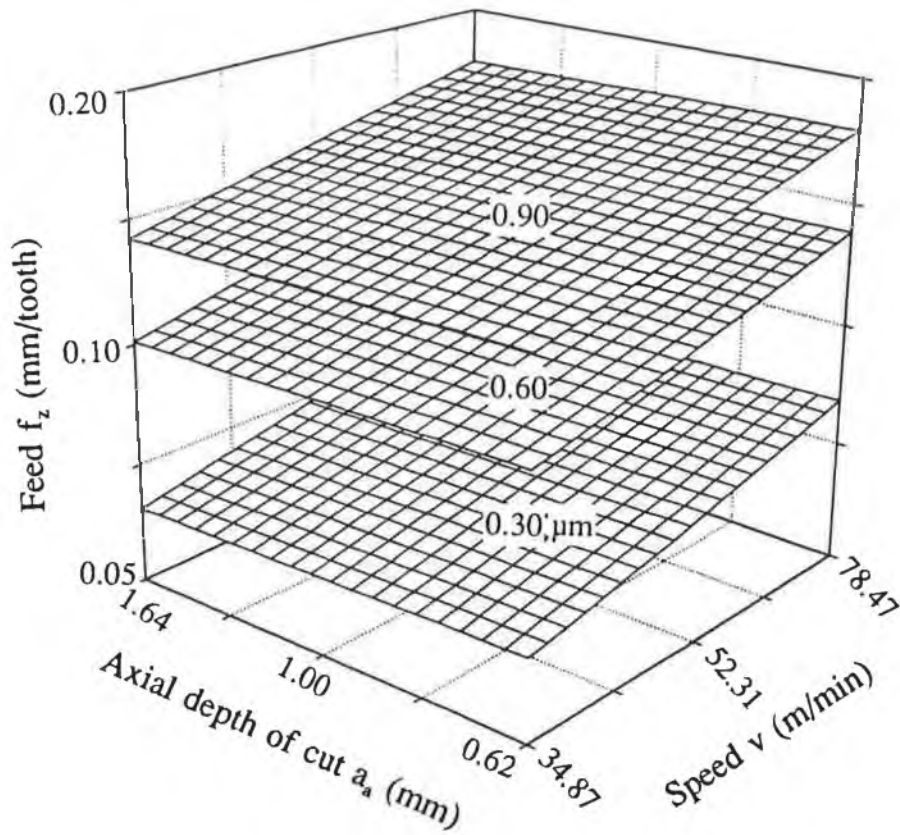


Fig.8.10: Contour surfaces for surface roughness in end milling MMC in 3 dimensional factor space (log-scales)

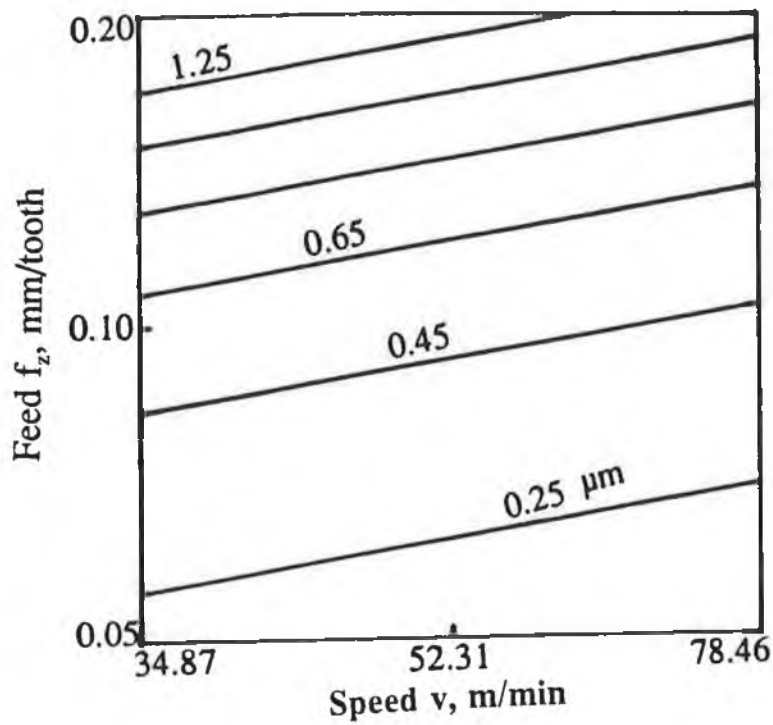


Fig.8.11: Surface roughness contours (first-order model) for MMC in speed-feed planes at 1.00 mm axial depth of cut (log-scale)

From the contours shown in the Fig.8.12 it is possible to select a combination of feed and cutting speed that reduces machining time without increasing the surface roughness, since there is a large number of combinations of cutting speed and feed which produces the same surface roughness. This can be illustrated by further utilization of the model to include the rate of material removed. The rate of material removed Q (cm^3/min) is given by equation (3.16) of chapter 3. For slot milling using a cutter of diameter 25 mm (i.e. $a_r = 25$ mm) and at a specified axial depth of cut, $a_a = 1.00$ and using equations (8.24) and (8.25), the equation of material removal rate (Q) becomes:

$$\ln Q_{(MMC)} = 1.2029 + 0.4054x_1 + 0.6931x_2 \quad (8.30)$$

For a constant rate of material removal, equation (8.30) can be represented by a straight lines as illustrated in Fig.8.13. This figure was obtained by superimposing the constant Q lines on the surface roughness contours in the speed-feed plane, for axial depth of cut $a_a = 1.00$ mm. This figure shows that the rate of material removal can be doubled without increasing the surface roughness $0.45 \mu\text{m}$ (CLA). It can be shown that the selection of cutting condition represented by a point " B " is better than those represented by point " A ". This 100 % increase in material removal rate is obtained without any sacrifice in quality of the produced surface finish.

(c) Adequacy of the postulated models

The analysis of variance (ANOVA) technique was used to check the adequacy of the postulated models. As per this technique the calculated F_{rat} of the first and second-order models are 6.68 and 4.18 respectively while the corresponding F_{rat} (95% confidence) for the first-order model and F_{rat} (99% confidence) of the second-order model are 19.30 and 7.59 as obtained from statistical tables. Hence, the first- and second-order models are valid with 95% and 99% confidence probability. The results of ANOVA are shown in Appendix 4.

(d) Significance of individual variables:

The significance testing for the individual variables of the predictive models are shown in appendix 4. From significance testing it is seen that the calculated F_{rat} of the speed, feed and axial depth of cut for the first-order model are 4.52, 150.25 and 0.03 respectively while the standard F_{rat} is 3.46 , and the calculated F_{rat} of the speed,

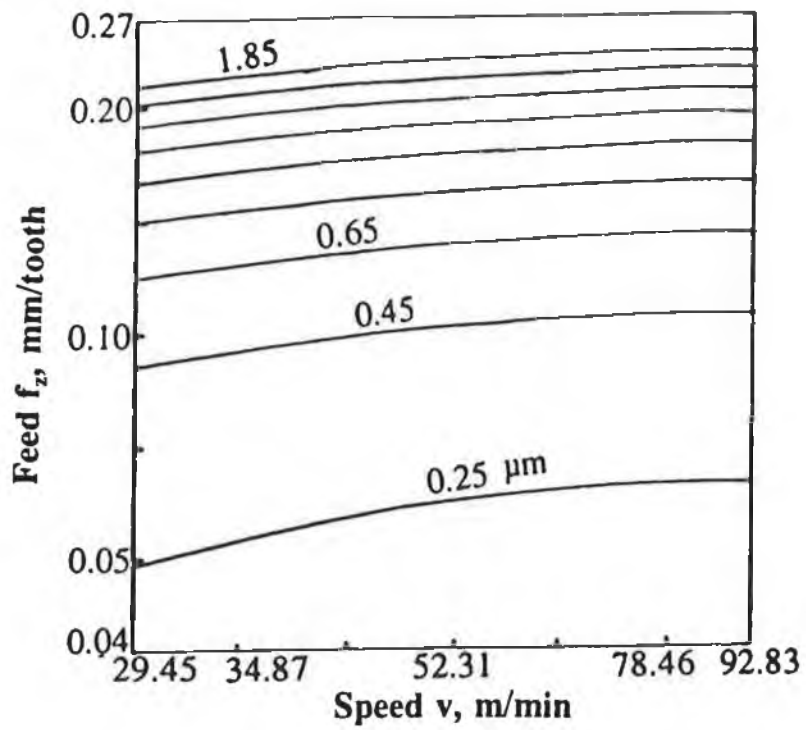


Fig.8.12: Surface roughness contours (second-order model) for MMC in speed-feed planes at 1.00 mm axial depth of cut (log-scales)

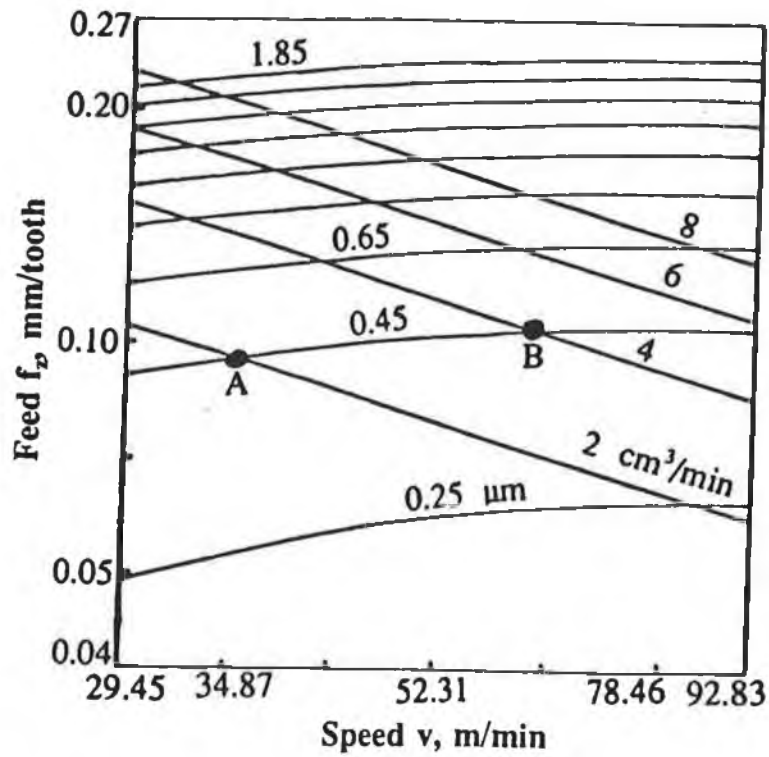


Fig.8.13: Surface roughness contours (second-order model) and material removal rates in speed-feed planes at 1.00 mm axial depth of cut (log-scales)

feed and axial depth of cut of the second-order model are 1.90, 369.02 and 0.008 respectively while the standard F_{rat} is 3.10 as obtained from standard statistical table. So, it is observed that the feed (x_2) effect was significant for both the first- and second-order models. This is because surface roughness is the result of the feed marks left on the milled surface. The effect of cutting speed is significant in the first-order model while in the second order-model the effect of cutting speed is not so significant. This may be attributed to built up edge formation effect within the speed range of the first-order model while the surface finish improves within the speed range of second-order model because of less built up formation. The effect of axial depth of cut was very insignificant for both the first- and second-order model which may be neglected in a practical machining situation. This may be attributed to the fact that within the range of axial depth of cut for both the first- and second-order models the cutting force may not be sufficient to cause deflection and vibration of the work-tool system.

(e) Precision of prediction (Confidence Interval)

The precision of the predicted model can be determined by calculating the appropriate confidence intervals and comparing them with the experimental values. The confidence intervals have been calculated using the formula (4.16) of chapter 4. The resulting 95% and 99% confidence intervals for the first-order and the second-order models respectively are shown in Appendix 4.

(vii) Conclusions

- (a) Reliable surface roughness models have been developed and utilized to enhance the efficiency of slot milling MMC (Al/15% Vf. SiC) when using end mills with carbide inserts.
- (b) The first-order surface roughness prediction model is valid within the speed range of $34.87 \leq v \leq 78.46$, the feed range of $0.05 \leq f_z \leq 0.20$ mm/tooth and the axial depth of cut range of $0.62 \leq a_a \leq 1.64$ mm.
- (c) By utilizing the second-order model, it is possible to extend the variable range. The prediction model is valid within the speed range of $29.45 \leq v \leq 92.83$ m/min, the feed range of $0.04 \leq f_z \leq 0.27$ and the axial depth of cut range of $0.50 \leq a_a \leq 2.00$ mm.

- (d) The feed effect is very dominant in both the first-and second-order models. The effect of cutting speed is significant in the first-order model (i.e. the narrow range of the cutting speed) while in the second-order model(i.e. the wide range of the cutting speed) its effect is not so significant. The effect of axial depth of cut is very insignificant in both the first- and second-order models which may be neglected in practical machining situation.
- (e) An increase in either the feed or the axial depth of cut increases the surface roughness while an increase in the cutting speed decreases the surface roughness.
- (f) Contours of the surface roughness outputs were constructed in planes containing two of the independent variables. These contours were further developed to select the proper combination of the cutting speed and feed to increase the material removal rate without sacrificing the quality of the produced surface finish.

Table 8.7: Summary of Surface roughness equations of the investigated workpiece material (steel, Inconel 718 & MMC) in terms of v (m/min), f_z (mm/tooth) and a_a (mm)

Material	Hardness	Cutting conditions	Equations
Steel	190 BHN	$v = 24 - 37$ m/min $f_z = 0.05 - 0.20$ mm/tooth $a_a = 0.72 - 1.60$ mm	$\hat{R}_a(\text{steel}) = 65.87 v^{-0.40} f_z^{0.74} a_a^{0.48}$
Inconel 718	260 BHN	$v = 14.08 - 24.10$ m/min $f_z = 0.057 - 0.098$ mm/tooth	$\hat{R}_a(\text{Inconel}) = 172.12 v^{-0.444} f_z^{1.7223}$
2618 MMC	145 BHN	$v = 34.87 - 78.46$ m/min $f_z = 0.05 - 0.20$ mm/tooth $a_a = 0.62 - 1.64$ mm	$\hat{R}_a(\text{MMC}) = 68.0 v^{-0.42} f_z^{1.43} a_a^{0.03}$

CHAPTER 9

GENERAL CONCLUSIONS AND SUGGESTIONS FOR FURTHER DEVELOPMENT

9.1 General conclusions

Advanced materials are being used over a wide area of the manufacturing industry. Present research work on the machinability assessment of the two advanced materials, Inconel 718 and 2618 MMC using commercially available end mills with uncoated tungsten carbide inserts under dry conditions leads to the following conclusions:

(1) Conclusions on machining Inconel 718

Cutting condition

- Though the relative machinability of Inconel 718 is poor, it could be machined satisfactorily within a speed range of 14 - 29 m/min, feed range of 0.04 - 0.10 mm/tooth and axial depth of cut up to 2.00 mm.
- In general, it is not convenient to perform machinability assessment of Inconel 718 on a milling machine with a limited number of fixed speeds and feeds.

Cutting forces

- Cutting forces in end milling decrease as the cutting speed increases while cutting forces increase (up to $F_R = 1050$ N) with either an increase in feed or axial depth of cut.
- Normal force (F_y) is the highest in the table system of cutting forces in slot milling while feed force (F_x) and normal force (F_y) are the highest in up cut and down cut end milling respectively.

- There is no significant difference in magnitude of the resultant and tangential cutting force in up cut end milling compared with that of down cut end milling.
- A high powered milling machine of at least 8 kW is required to conduct a machining test on Inconel 718

Tool life

- There is an increase in tool life when slot milling - followed by down cut end milling, then up cut end milling. There is a significant difference in tool life between up cut and down cut end milling.

Surface finish

- Surface roughness in slot milling decreases as the cutting speed increases but after a certain speed the rate of decrease is not significant.
- Surface roughness increases as the feed rate increases in a slot milling operation.
- A good surface finish (0.35 - 1.2 μm) can be achieved at a cutting speed range of 13.12 - 26.97 m/min and feed range of 0.053 - 0.107 mm/tooth in a slot milling operation.

Modelling

- Response surface methodology can be used to develop mathematical models for machining responses (cutting forces and surface roughness) in a slot milling operation by a small number of experiments and these mathematical models can be used to determine the optimum cutting condition for a required machining response.

(2) Conclusions in machining 2618 MMC

Cutting condition and surface finish

- The relative machinability is satisfactory.
- A good surface finish (0.16 - 2.57 μm) can be achieved within a speed range 29.45 - 92.83 m/min, feed range of 0.04 - 0.27 mm/tooth and axial depth range of 0.50 - 2.00 mm in a slot milling operation.
- An increase in the cutting speed increases the surface finish while an increase in the feed rate decreases the surface finish. An increase in the axial depth of cut decreases the surface finish which may be neglected in a practical machining operation.

Modelling

- Response surface methodology can be used to develop mathematical models for surface roughness in slot milling and these models can be used to determine the optimum cutting condition for a required surface finish.

9.2 Recommendations for further works

This work has been conducted as a first step towards the development of machinability data system for advanced materials. In view of this, a study has been carried out on machinability assessment of Inconel 718, a representative nickel base superalloy and 2618 MMC, a representative MMC by the end milling process. It is suggested that further works on the following lines would be useful:

Cutting conditions

- Machinability assessment of Inconel 718 and 2618 MMC using different cutting fluids (i.e. nitrogen gas, air blast, water based coolants etc) and to compare the results of each other as well as that of the results under the dry condition.

Cutting force

- Investigation of machining variables (one variable at a time) on cutting forces in end milling 2618 MMC.

Tool life

- Investigation of machining variables (one variable at a time) on tool life in end milling Inconel 718 and 2618 MMC

Surface finish and Surface integrity

- Investigation of machining variables (one variable at a time) on surface finish in end milling 2618 MMC
- To measure cutting temperatures when machining Inconel 718 and 2618 MMC and investigate the subsurface change of the machined surface.

Modelling

- Modelling of machining responses (cutting forces, power, tool life, surface roughness etc.) in end milling Inconel 718 and 2618 MMC taking into account radial depth (width) of cut.
- Estimation of model parameters of the mathematical models by other techniques i.e. regression techniques (forward selection, backward elimination, stepwise regression etc.) and sequential estimation procedure and compare the results of each other.
- To develop an expert system for automatic selection of optimized machining conditions in end milling of Inconel 718 and 2618 MMC.

Workpiece materials, machining processes and cutting tools

- Machinability assessment of all grades of commercially available nickel base superalloys and MMCs by end milling processes as well as by other conventional mechanical machining processes (turning, drilling, tapping etc.).

- To compare the machining response of Inconel 718 and 2618 MMC in the annealed and age hardened condition as well as that of the forged and cast condition.

- Machinability assessment of Inconel 718 and 2618 MMC using other recently developed cutting tools like coated carbide, CBN, oxide, sialon, PCD etc.

- To investigate machinability assessment of Inconel 718 and 2618 MMC by non-conventional mechanical processes (i.e. abrasive jet, electro chemical, electro discharge machining etc.).

REFERENCES

- [1] Technical report on "Machining Wiggins Nickel alloys", The International Nickel Company, publication 2463, 1980.
- [2] AVALONE, E.A. and BAUMEISTER III, T., "Marks's Standard handbook for mechanical engineers", 9th edition, Mc Graw - Hill Book Co., New York, 1978.
- [3] Technical report on "High temperature MMCs", Version No.1, AICAN, Burslem, UK, 1990.
- [4] WILSON, M., "Machining High Strength Materials: Co-Base Alloys", M.Sc. Thesis, Trinity College, Dublin, 1982.
- [5] SABBERWAL, A.J.P., "Development and Application of a Two-Dimensional Milling Force Dynamometer", M.Sc. Thesis, Victoria University of Manchester, 1958.
- [6] SABBERWAL, A.J.P., "Cutting Forces in Down Milling", Int.J.Mach.Tool Des. Res., Vol.2,pp.27-41, 1962.
- [7] SABBERWAL, A.J.P., "An Investigation into the Chip section and cutting Forces during milling operation", Ph.D Thesis, Victoria University of Manchester, 1961.
- [8] SCHMIDT, A.O., "Heat in Metal Cutting", Machining Theory & Practice, American Society for Metals, 1950.
- [9] MARTELOTTI, M.E., "An Analysis of the milling Process", A.S.M.E.Transaction, Vol.63,pp.677-700, 1941.
- [10] MARTELOTTI, M.E., "A analysis of the Milling Process,Part II-Down Milling", A.S.M.E. Transaction, Vol.67,pp.233-251, 1945.
- [11] KOENIGBERGER, F. AND SABBERWAL, A.J.P., "An investigation into the cutting force pulsations during milling operations", Int.J.Mach.Tool Des. Res., Vol.1,pp.27-41, 1962.
- [12] KLINE, W.A., DeVOR, R.A. and LINDBERG, J.R., "Prediction of cutting forces in End Milling with application to coning cuts", Int.J.Mach.Tool Des.Res.,Vol.22,pp.7-22, 1982.
- [13] KLINE, W.A. and DeVOR, R.E., "The effect of runout on cutting geometry and forces in End Milling", Int.J.Mach.Tool Des.Res., Vol.23,pp.123-140, 1983.
- [14] YELLOWLEY, I., "Observation of mean value of forces, torque and specific power in the peripheral milling Process", Int.J.Mach.Tool Des.Res., Vol.25,pp.337-346, 1985.

- [15] ELBESTAWI, M.A., PAPAZAFIRIOU, T.A. and DU, R., "Inprocess monitoring of tool wear in milling using force signature", *Int.J.Mach.Tool Manufact.*, Vol.31,pp.55-73, 1991.
- [16] MACHINING DATA CENTRE, "Machining Data Handbook" 3rd edition, Vol.1, Metcut Research Associates, Inc., Ohio, 1980.
- [17] SMITH, S. and TLUSTY, J., "An overview of Modeling and Simulation of the Milling Process", *ASME J. Engng. Ind.*, Vol.113,pp.169-175, 1991.
- [18] Milling Handbook of High efficiency Metal cutting Carboly Systems Department, General Electric Company, 1980.
- [19] ARMAREGO, E.J.A., SMITH, A.J.R. AND KARRI, V., "Mechanics of cutting Model for Simulated Oblique Rotary Tool Cutting processes", *J.Materials processing Tech.*, Vol.28,pp.3-14, 1991.
- [20] MAN LIU and STEVEN, Y.L., "Analytical Modeling of Acoustic Emission for monitoring of Peripheral milling Processes", *Int.J.Mach.Tool Des.Res.*, Vol.31,pp.589-606, 1991.
- [21] BOOTHROYD, G. and KNIGHT, W.A, "Fundamentals of machining and Machine Tools", Merce Dekker, Inc., New York, 1989.
- [22] TOBIAS, S.A. and FISHWICK, W., "Theory of Regenerative Machine Tool Chatter" *The Engineer*, Vol.205,pp.199-203, 1958.
- [23] TOBIAS, S.A., "The vibration of vertical milling machine under test and working condition", *Proc. Instn. Mech.Engr.* 173, p.474, 1959.
- [24] SMITH and TOBIAS, "The Dynamic cutting of Metal", *Int.J.Mach.Tool Des.Res.*, Vol.1,pp.283-292, 1961.
- [25] SABRI, O.A., "Dynamics of the Metal Cutting Process", Ph.D thesis, University of Birmingham, 1964.
- [26] SHUMSHERUDDIN, A.A., "Dynamic Metal Cutting", Ph.D thesis, University of Birmingham, 1965.
- [27] DAS, M.K., "Physical aspects of the dynamic cutting of Metals", Ph.D thesis, University of Birmingham, 1965.
- [28] DAS, M.K. and TOBIAS, S.A., "The relation between the Static and Dynamic cutting of Metals", *Int.j.Mach.Tool Des.Res.*, Vol.7,pp.63-89, 1967.
- [29] MaCNAMUS, B.R., "Dynamic Hot Machining and its Relationship to regenerative Chatter", *Proc. of 9th Int. M.T.D.R Conf.*, the university of Birmingham, pp.699-724, 1968.
- [30] KAINTH, G.S., "Investigation into Dynamics of the Metal Cutting Process", Ph.D thesis, University of Birmingham, 1969.

- [31] NIGM, M.M., SADEK, M.M. and TOBIAS S.A, "Determination of dynamic cutting co-efficient from steady-state cutting data", *Int.J.Mach.Tool Des. Res.* Vol.17,pp.19-37, 1977.
- [32] GRASSO, V., DIEGA LA, NOTOLA and PASSANNANTI, A., "Dynamic cutting co-efficients in three dymensional cutting", *Int.J.Mach.Tool Des.Res.* ,Vol.20, pp.235-249, 1980.
- [33] LIN, G.S. and WENG, C.I., "A non linear dynamic model of cutting", *Int. J. Mach.Tool Des.Res.*,Vol.30, pp.53-64, 1990.
- [34] SHINOBO KATO and HIROSHI FUJII, "Characteristics of Cutting Force in Plain Milling operation using helical cutter", *Proc. 17th Int. M.T.D.R Conference*, pp.117-128, 1976.
- [35] TLUSTY, J. and MacNEIL, "Dynamics of Cutting force in the End Milling", *Annals of the CIRP*,Vol.24,pp.21-25, 1975.
- [36] TLUSTY, J. and ISMAIL, F., "Basic non-linearity in machining Chatter", *Annals of the CIRP*,Vol.30,pp.21-25, 1981.
- [37] TLUSTY, J. and TAYLER, T., "Adaptive Control for Die Milling criteria and Stratigies", *PED Vol.32,ASME,WAM*,pp.45-60, 1988.
- [38] SUTHERLAND, J.W. and DeVOR, R.E., "An improved method for cutting force and Surface error prediction in Flexible End Milling", *ASME Journal of Engg. for Industry*,Vol.108,pp.269-279, 1986.
- [39] SUTHERLAND, J.W, "A Dynamic model for the cutting force system in End Milling", *Sensors and Controls for Manufacturing*,*PED Vol.33, ASME, WAM*, 1988.
- [40] MONTGOMERY, D. and ALTINTAS, Y., "Mechanism of Cutting forces and Surface generation in Dynamic Milling", *J.Engng.Ind.*,Vol.113,pp.160-168, 1991.
- [41] KOLARITITS, F.M. and DeVRIES, W.R., "A mechanistic Dynamic model of End Milling for Process Controller Simulation", *J.Engng.Ind.*,Vol.113,pp.176-183, 1991.
- [42] SABBERWAL, A.J.P and FLEISCHER, P., "The effect of material and geometry on the wear characteristics of cutting tools during face milling", *Int.J.Mach.Tool Des.Res.*,Vol.4,pp.47-71, 1964.
- [43] ISO 8688-1, "Tool life testing in milling- Part 1: Face milling", 1989(E).
- [44] ISO 8688-2, "Tool life testing in milling-Part 2: End milling, 1989(E).
- [45] NIKLASSON, G., "Standardized Milling test", *Proc. 3rd Int. MTDR. Conf.*, University of Birmingham, pp.55-67, 1962.

- [46] COLDING, B.N., "A wear relation for turning, milling and grinding", Hakan Ohissons Bokkycherie, Lund, 1959.
- [47] YELLOWLEY, I., "An investigation into the variables affecting the life of cutting tools", M.Sc. Thesis, The Victoria university of Manchester, 1970.
- [48] KULJANIC, E., "An investigation of wear in single-tooth and multi-tooth milling" Int.J.Mach.Tool Des.Res.,Vol14,pp.95-109, 1974.
- [49] YELLOWLEY, I., "The development of machinability testing methods with specific reference to high strength thermal resistant work material", Ph.D Thesis, The Victoria university of Manchester, 1974.
- [50] McGOLDRICK, P. and HIJAZI, M.A.M., "The use of weighing method to determine a tool wear algorithm for end milling", Proc. 20th Int.MTDR Conf.,Birmingham,pp.345-349, 1979.
- [51] LEE, L.C., LEE, K.S. and GAN, C.S., "On the correlation between dynamic cutting force and tool wear", Int.J.Mach.Tools Manufact.,Vol.29,No.3,pp.295-303, 1989.
- [52] RICHARDS, N. and ASPINWALL, "Use of ceramic Tools for machining nickel based alloys", Int.J.Mach.Tool Manufact.,Vol.29,No.4,pp.575-588, 1989.
- [53] FOCKE et al."The deformation of WC tools when cutting Inconel 718", Proc.16th Int.MTDR Conf.,Manchester,pp.565-572, 1975.
- [54] EZUGWU, E.O. and PASHBY, I.R., "High speed Milling of nickel based superalloys", Proc.7th Conf.IMC,pp.540-550,Trinity College,Dublin, 1990.
- [55] EZUGWU, E.O. and TANG S.H., "Surface abuse when machinig cast iron(G-17) and nickel base super alloy(Inconel 718) with ceramic tools", Proc.9th Conf.IMC., UCD, Dublin, pp.436-450, 1992.
- [56] SHAW, M.C., "Metal cutting principles", Oxford University Press,Oxford, 1986.
- [57] TAYLOR, F.W., "On the art of cutting metal", Trans.ASME,Vol.28,pp.1-280 1907.
- [58] JAIN, R.K. and GUPTA S.C., "Production Technology", Khanna Publishers, Delhi, India, 1986.
- [59] COLDING, B.N., "Machinability of metals and machining cost", Int.J.Mach.Tool Des. Res., Vol.1,pp220-248, 1961.
- [60] HIJAZI, M.A.M., "The adaptive control of end milling", Ph.D Thesis.Nottingham University, 1978.
- [61] KRONENBERG, M., "Replacing the Taylor's formula by a new tool life equation", Int.J.Mach.Tool Des. Res.,Vol.10,pp.193-202, 1970.

- [62] BARROW, G., "Tool life equations and machining economics", Proc.12th Int.MTDR. Conf, Manchester,pp.481-493, 1971.
- [63] PILAFIDS, E.J., "Observations on Taylor ' n ' values", Annals of the CIRP, Vol.XVIVI, pp.571-577, 1971.
- [64] COLDING B.N., "A three dimensional tool life equation in machining economics" , J.Engng.Ind.(Trans. ASME),Vol.81,pp.239-250, 1959.
- [65] COLDING, B.N. and KONING, W., "Validity of the Taylor's equation in metal cutting", Annals of the CIRP,Vol.XVIV,pp.793-812, 1971.
- [66] KRONENBERG, M., "Machining Science and Application", Pergemon Press, 1966.
- [67] DeFILIPPI, A. IPPOLITO, R. and MICHELLETTI, G.F., "The influence of constraints on cutting conditions optimization", Annals of the CIRP, Vol.24/1,pp.417-421, 1975.
- [68] MICHELETTI, G BEER, C. Aand VILENCHICH, R., "A statistical model of Taylor's equation for tool life and computer optimization of unit cost and production rates in front milling", Annals of the CIRP,Vol.22/1,pp.45-46, 1973.
- [69] EL-HAKIM, M., "Optimization of the machining variables", The 2nd Annual Operations Research Conf.,Vol.2,pp91-106, 1975.
- [70] BEER,C., MALHERBE, M and VENTOR,R., "Adaptive Control Optimization for Numerically Controlled Milling Process", Proc. 18th Int.MTDR Conf., Manchester , pp.665-671, 1977.
- [71] SAVHN and COLDING, "Machining properties and wear of milling cutters", Tekniska Hogskolan,Avhandling 55, Stochholm, Sweeden, 1948.
- [72] BREWER, R. and REUDA, R., "A simplified approach to optimum machining" Engineers Digest, Vol.24,pp.133-150, 1963.
- [73] WU, S.M., "Tool life testing by Response Surface Methodology", Part-I & Part-2, Trans. ASME ,Series B,Vol.86,pp.105-110, 111-116, 1964.
- [74] YELLOWLEY, I. and BARROW, G., "The assessment of tool life in peripheral milling", Proc. of the 19th Int. MTDR. Conf.,pp443-452, 1978.
- [75] PERA, "Machining Data Bank - continued development of an established Data Bank to include a wide range of processes, materials, cutting tools and proven machining conditions", PERA report No.336, November, 1978.
- [76] GILLIBRAND, D., "Surface formation in metal machining", Ph.D thesis, University of Nottingham, 1975.

- [77] BYRNE, G., "Surface integrity and temperatures in finish machining", M.Engg. thesis, The University of Dublin, Trinity College, 1984.
- [78] KACZMAREK, J., "Principles of machining by cutting, abration and erosion", Peter Peregrinus ltd., England, 1976.
- [79] NATIONAL TWIST DRILL & TOOL CO. and WINTER BROTHER CO., " Accuracy of Milled surfaces, Part 1: Effect of cutter diameter, number of teeth, runout and feed", Metal Cuttings, Vol.9, No.1, pp.1-10, Jan., 1961.
- [80] NATIONAL TWIST DRILL & TOOL CO. and WINTER BROTHER CO., " Accuracy of Milled surfaces, Part 2: Effect of End mill deflection", Metal Cuttings, Vol.9, No.2, pp.2-10, April, 1961.
- [81] NATIONAL TWIST DRILL & TOOL CO. and WINTER BROTHER CO. " Accuracy of Milled surfaces, Part 3: Arbor type cutter versus End mills", Metal Cuttings, Vol.10, No.1, Jan, pp.2-10, 1962.
- [82] ARMAREGO, E.J.A. and BROWN, R.H., "The Machining of metals", Prentice Hall, Inc., New Jersey, 1976.
- [83] KLINE, W.A., DeVOR, R.A. and SHAREEF, I.A., "The prediction of surface geometry in end milling", ASME J.Engng.Ind., Vol.104, pp.272-278, 1982.
- [84] EMA, S. and DAVIES, R., "Cutting performance of end mills with different helix angles", Int.J.Mach.Tool Manufact., Vol.29, No.2, pp.217-227, 1989.
- [85] ELBESTAWI, M.A. and SAGHERIAN, R., "Dynamic modelling for the prediction of surface error in the milling of thin walled section", J. Materials Processing Tech, Vol.25, pp.215-228, 1991.
- [86] ALTINTAS, Y., MONTGOMERY, D. and DUDAK, E., "Dynamic Peripheral Milling of flexible structure", ASME J.Egng.Ind, Vol. 114, pp.137-145, 1992.
- [87] SMITHBERG, D. "Inconel 718 machining manual", No. 6M59-559, Manufacturing Research & Development, Boeing Commercial Airplane Company, 1987.
- [88] SHAW, M.C. and NAKAYAMA, K., " Machining High Strength Materials" Annal of the CIRP, Vol. XV, pp. 45-45, 1967
- [89] GALIMBERTI, J.M., "Improved Metal Removal Rates for Difficult-to Machine Alloys", Creative Manufacturing Seminar, A.S.T.M.E, SP63-194, 1962-63.
- [90] Machining the Huntington Alloys, Technical Bulletin T-12, Huntington Alloy Products Division, The Int. Nickel Company, Inc, Huntington, West Virginia, 1985
- [91] FLEMING, M.G., "Investigation of the wear and Failure Modes of Surface Engineered Multipoint cutting Tools" M.Engg. thesis, Dublin City University, 1992.

- [92] HEWITT, W.R., "TiN Coating benefits apply to solid carbide tools", *Cutting tool Eng.*, Jan./Feb., pp.17-18, 1984.
- [93] THANGARAJ, A.R. and WEINMANN, K.J., "On the wear mechanism and cutting performance of solid Carbide whisker Reinforced Alumina", *ASME J.Engng.Ind.*, Vol.114, pp301-308, 1992.
- [94] DREGER, D.R., "Design guide lines for joining advanced composites", *J.Mach.Design*, Vol.52, pp.89-93, May, 1980.
- [95] KING, R.L., "Production engineers's view of advanced composites", *J.Materials and Design*, Vol.3, pp515-521, August, 1982.
- [96] ALAUDDIN, M., "Machining of non-metallic materials", M.Sc. dissertation, UMIST, Manchester, 1987.
- [97] BARADIE, M.A.E., "Manufacturing aspects of Metal Matrix Composites", *J. Materials Processing Tech.*, Vol.24, pp.261-272, 1990.
- [98] LOONEY, L.A., MONAGHAN, J.M. and TAPLIN, D.M.R., "The turning of an Al/SiC Metal Matrix Composite", *Proc.7th Conf.of IMC*, pp.494-510, Trinity College, Dublin, 1990.
- [99] RELLY, P.O', MONAGHAN, J.M. and TAPLIN, D.M.R., "The machining of Metal Matrix composites - a overview", 6th Irish Materials Forum(IMF), Dublin, pp.183-200, Sept.28-29, 1989.
- [100] CHADWICK, G.A. and HEATH, P.J., " Machining Metal Matrix Composites", *J. Metals and Materials*, pp.73-76, Feb., 1990.
- [101] MCGINTY, M.J. and PREUSS, C.W., "High Productivity Machining Materials and Processes", *ASM Conf.*, ASM Pub., pp.231-244, 1985.
- [102] WALDROP, P.S., "Metal Matrix Composites, Manufacturing challenges", *SME Conf.*, Calif., USA, pp.342-351, 1986.
- [103] ROBERTSON, A.R. and MAIKISH, D.C.R., "Advanced secondary fabrication techniques for Boron/Aluminium", 21st National SAMPE Symposium, Los Angeles, April, 1976.
- [104] DEGARMO, E.P., BLACK, J.T. and KOSHER, R.A., " Materials and Processes in Manufacturing", sixth edition, Macmilan Publishing Co., New York, 1984.
- [105] YELLOWELY, I. and BARROW, G, "The influence of thermal cycling on tool life in peripheral milling", *Int.J.Mach.Tool Des.Res.*, Vol.16, pp.1-12, 1976.
- [106] PAPAZAFIRIOU, T.A. and ELBESTAWI, M.A., "Flank wear modelling in milling", *J.Mechanical Working Technology*, Vol.20, pp.93-104, 1989.

- [107] KING, R., "Handbook of high speed machining Technology", Chapman & Hall, 1985.
- [108] REULEAUX, "Die Praktischen Beziehungen der Kinematik zur Geometrie und Mechanik" Lehrbuch der Kinematik, Vol. 2, pp.685-689, 1900.
- [109] HEGINBOTHAM, "Some aspects of the formation and behaviour of the built-up nose in metal machining", Ph.D thesis submitted at the Manchester University, 1956.
- [110] SEROPE KALPAKJIN, "Manufacturing Process for Engineering materials", Addison Wesley Publishing Co., London, 1984.
- [111] LEE, C.W., CHUNG, S.C. and KIM, J.S., "Geometric adaptive straightness control system for the peripheral end milling process", Int.J.Mach.Tool Des.Res., Vol.27, pp.417-430, 1987.
- [112] FENTON, R.G. and OXLEY, L.B., "Predicting cutting forces at super high cutting speed from work material properties and cutting conditions", Proc. 8th Int. MTDR Conf., Manchester, pp.247-258, 1967.
- [113] FLEISCHER, P. and KOENIGBERGER, "Face milling with artificially restricted tools", Proc.4th Int.MTDR. Conf., Manchester, pp.87-96, 1963.
- [114] AHMED, M.M., HOGAN, B. and GOODE, E., "Machinability tests on cubic boron nitride", Proc. of 5th Conf. of the IMC (IMC-5), The Queen's University of Belfast, Sept., 1988.
- [115] LISTER, P.M. and BARROW, G., "Tool condition monitoring systems", Proc.26th MTDR Conf., Manchester, pp.271-288, 1986.
- [116] KJELD BRUNO PEDERSEN, "Wear measurement of cutting tools by computer vision", Int.J.Mach.Tools Manufact., Vol.30, no.1, pp.131-139, 1990.
- [117] LEE, L.C., LEE, K.C. and GAN, C.S., "On the correlation between dynamic cutting force and tool wear" Int.J.Mach.Tools Manufact., Vol.29, No.3, pp.295-303, 1989.
- [118] SABBERWAL, A.J.P. and KAVINA, Y.B., "An investigation into the cutting forces and wear characteristics of helical milling cutter", Proc.3rd Int. MTDR Conf., Birmingham, pp.245-257, 1962.
- [119] WANG, K.K., WU, S.M. and IWATA, K, " Temperature responses and experimental errors for multitooth milling cutter", ASME J. Ind., pp.353-359, 1968.
- [120] BAILEY, J.A., JEELANI, S. and BECKER, S.E., "Surface Integrity in machining AISI 4340 steel", ASME, WAM, 1975, Paper No.75 WA/Prod.33.

- [121] KLINE, W.A., "The prediction of cutting forces and surface accuracy for the end milling process", Ph D thesis, University of Illinois at Urbana-Champaign, 1982.
- [122] MOORE, A.I.W., "Satisfying industry's needs for improved machining data", Proc.14th Int. MTDR Conf., Manchester,pp.691-695, 1973.
- [123] Machining Data Centre, "Machining Data Handbook", Vol.2, 3rd edition, 1980,Metcut Research Associates Inc., Cincinnati, Ohio.
- [124] EL BARADIE, M. and WILSON, M., "Metal cutting and machinability", Engineering Technology Series, National Board for Science and Technology, Ireland, 1983.
- [125] PERA, "PERA Machining Data Club", PERA Report 263, 1972.
- [126] PERA, "Machining Data Bank - Development of an established Data Bank to include a wider range of processors, materials, cutting tools and proven machining conditions", PERA Report 302, 1976.
- [127] PERA, "Machining Data Bank - Further development of an established Data Bank to include a wider range of processes, materials, cutting tools and proven machining conditions", PERA Report 324, 1977.
- [128] MONTGOMERY, D.C., "Design and Analysis of Experiments", 2nd edition John Wiley & Sons, New York, 1984.
- [129] BOX, G.E.P and YOUNG, P.V., "The exploration and exploitation of Response Surfaces" Biometrics, Vol.11,pp.287-323, 1955.
- [130] BOX, G.E.P. and HUNTER, W.G., "Multifactor experimental Designs for exploring Response Surfaces", Ann. Math. Stat., Vol.28,pp.195-241, 1957.
- [131] BOX, G.E.P. and WILSON K.B., "On the experimental attainment of optimum condition", J. Royal Statistical Society, Vol.13,pp.1-45, 1951.
- [132] HILL, W.J. and HUNTER, W.G., "A review of response surface methodology: A literature survey", Technometrics, Vol.8,pp.571-590, 1966.
- [133] MEAD, R. and PIKE, D.J., "A review of response surface methodology from a biometric viewpoint", Biometrics,Vol.31,pp.803-851, 1975.
- [134] EL BARADIE, M. A., "Computer aided analysis for a surface roughness model for turning", J. Material Processing Technology, Vol.216,pp.207-216,1991.
- [135] TARAMAN, K., "Multi-machning output-multidependent variable turning research by response surface methodology", Int.J.Prod. Res., Vol.12,No.2,pp.233-245, 1974.

- [136] TARAMAN, K and TARAMAN, S., "Optimum selection of machining and cutting tool variables", SME Paper MR 83-182, Presented at The SME Int. Conf. Detroit, Michigan, USA, May, 1983.
- [137] PADMANABHAN, K.K. and MURTY, A.S., "Evaluation of frictional damping by Response Surface Methodology", Int.J.Mach.Tools Manufact., Vol.31, No.1, pp.99-105, 1991.
- [138] PADMANABHAN, K.K., "Prediction of damping in machined joints", Int.J. Mach.Tools Manufact.,Vol.32,No.3,pp.305-314, 1992.
- [139] BOX. G.E.P., HUNTER, W.G. and HUNTER J.S., "Statistics for experimenters Wiley, New York, 1978.
- [140] DAVIES, O.L. and GOLDSMITH P.L, "Statistical methods in research and production", Longman Group Ltd., New York, 1980.
- [141] DAVIES, O.L., "Design and analysis of Industrial Experiments", Oliver and Boyd(Longman Group), Edinburgh, 1971.
- [142] TIPNIS, V.A., BUESCHER, S.C. and GARRISON, R.C., "Mathematically Modelled Machining Data for adaptive control of end milling operations", Proc.NAMRC-iv,pp.279-286, 1976.
- [143] BALAKRISHNAN, P. and DEVRIES, M.F., "Sequential Estimation of Machinability Parameters for adaptive optimization of machinability data base systems", ASME J. Engng. Ind.,Vol 107,pp.159-166, 1985.
- [144] JALALI, S.A. and KOLARIK, W.J., "Tool life and machinability models for drilling steels", Int.J.Mach.Tools Manufact., Vol.31,No.3,pp.273-282, 1991.
- [145] LO, K.C. and CHEN, N.N.S., "Prediction of tool life in hot machining of alloy steel", Int.J.Prod.Res.,Vol.15,No.1, pp.47-63, 1977.
- [146] JOGINDER SING and KHARE, M.K., "A mathematical model for tool wear weight using Response Surface methodology", Pro.12th AIMTDR Conf, IIT Delhi,pp.256-260, 1986.
- [147] COCHRAN, W.G. and COX, G.M.,"Experimental designs", Asia Publishing House, New Delhi, 1959.
- [148] DRAPPER, N.R. and SMITH, H., "Applied Regression Analysis", 2nd edition John Wiley & Sons,New York, 1966.
- [149] BALAKRISHNAN, P. and DEVIRIES, M.F., "Analysis of Mathematical Model building Techniques adaptable to machinability data base systems", Proc. NAMRC-x1,pp.466-474,May, 1983.
- [150] NORUSIS, M.J., "Basic statistics and operations: SPSS Introductory Guide", McGraw Hill Book Co., 1982.

- [151] DUNN, O.J. and CLARK, V.A., "Applied Statistics, analysis of variance and regression", John Wiley, London, 1974.
- [152] EL BARADIE, M.A., "Surface roughness model for turning grey cast iron", Proc. Instn. Mech.Engr., Vol.207.,pp.43-54, 1993.
- [153] HUDA, D., EL BARADIE, M.A. and HASHMI, M.S.J., "Manufacturing aspect of metal matrix composites II", J.Material Processing Tech., Vol.37 , pp.529-541, 1993.
- [154] SANDVIK (Cormant) Catalogue on, "Rotating Tools and Inserts", Sandvik, S-81181 SANDVIKEN, Sweden, 1991.
- [155] TLUSTY, J. and ANDREWS, G.C., "A critical review of sensors for unmanned Machining", Ann. CIRP 32,pp.563-577, 1983.
- [156] KISTLER INSTRUMENT CORP., manual on "Three component dynamometer", Type - 9265, 1989, Whiteoaks, The Grove Hartley, Witney, Hants RG27 8RN, UK.
- [157] SAMUEL D. S. and DON R.H., "Digital Signal Analysis", Prentice Hall, New Jersey, 1990.
- [158] KISTLER INSTRUMENT CORP., manual on "Charge Amplifier" Type - 5011, 1989, Whiteoaks, The Grove Hartley, Witney, Hants RG27 8RN, UK.
- [159] METRABYTE CORP., manual on " DASH - 8 ", 440 Myles Standish B1VD, Taunton, MA 0278 , 1990.
- [160] JUN YAN, "An intelligent Robot Control system for Physiotheraphic applications", Ph.D thesis, Dublin City University, 1991.
- [161] MICRO MOVEMENTS LIMITED, manual on "Lightbeam Oscillograph Recorder", June 5, 1989, The Centre Eversley, Hants, RG27 ONB, UK.
- [162] NICOLLS, M.O., technical report on "The measurement of surface finish", De Beers Technical Service Centre Charters U K.

APPENDIX 1

THE EXPERIMENTAL MACHINE TOOL, WORKPIECE AND MEASUREMENT OF CUTTING FORCES, TOOL LIFE AND SURFACE ROUGHNESS

1.1: The specifications of the apparatus, equipment and machine used in the experiment

The specifications of the apparatus, equipment and machine used in the experiment are shown below:

(i) Three Component Dynamometer

The dynamometer was of the following type:

Type: Piezoelectric (Table type) dynamometer(Kistler Instrument,

Type 9265 A2)

Rigidity:

X, Y axes - 1000 N/ μ m
Z axis - 2000 N/ μ m

Natural frequency:

F_x, F_y - > 1.5 KHz
 F_z - > 2 KHz

Sensitivity: 8 pC/N

Cross talk:

Static - $\leq \pm 2$
Dynamic - $\leq 1 - 3$ (depending on frequency)

(ii) Charge Amplifier

The charge amplifier was of the following type:

Type: one-channel (Kistler Type 5011)

Output voltage: ± 10 V

Frequency range: $\approx 0 \dots 200$ KHz

Lowpass filter: Butterworth 10 Hz - 30 KHz

Measuring range: $\pm 10 \dots 999$ pC

Transducer sensitivity: 0.01 ...9.99 pC/M.U

Scale: 0.001 - 9990 M.U/V

(iii) Lightbeam Oscillograph (Recorder)

The recorder was of the following type:

- Type: M12-150A (Micoro Movement Ltd)
- Magnet block: 500 D.C, insulation, 12 channel
- Galvanometer: Moving coil (Micro Movements type " H ")
- Optical Arm: 150 mm
- Recording Paper: Emulsion In or Out (Kodak 1895 or 2022)

(iv) A/D converter

The A/D converter was of the following type:

- Type: MetraByte's DASH - 8 (8 channel 12 bit)
- Input: ± 5 V per channel
- A/D conversion time: 25 - 35 microsecs
- Interrupt: Programmable (8253) counter timer
- Reference Voltage: + 10 V
- Connection: 37 pin D type male connector

(v) Personal Computer (PC)

The PC was of the following type:

- Type: Quattro Prompt (286) (IBM compatible PC)
- Memory: 640 Kbyte (RAM)
- Hard Disk space: 42 Mbyte

(vi) Surface Roughness Tester (Stylus)

Two surface Roughness Testers were used to measure surface roughness:

- (a) Type: Surftest 402 (Mitutoyo)
- (b) Type: Taylor Hobson's Talysurf 5-120

(vii) Toolmakers' Microscope

The Toolmakers' Microscope is a precision optical measurement device which had the following specifications:

Type: TM300 (Mitutoyo)

Magnification: An Objective (3X) and an eyepiece (10X) are provided with a total magnification of 30X

- Digital Counter (Digimatic Heads which provide digital readouts)
- Column optical distance 148 mm
- Microstage for mounting tools (the stage can be moved smoothly for alignment of tool).

(viii) Scanning Electron Microscope

Type: JOEL JXA - 8600 series electron probe microanalyser
Fitted with link an 1000 Energy Dispersive spectrometer

(ix) Milling Machines

Two types of vertical milling machine were used for the cutting tests as:

- (a) Type: Bridgeport Vertical Milling Machine
- (b) Type: Cincinnati Universal Milling Machine

(a) Bridgeport Vertical Milling Machine

The essential specifications of the machine are:

Horse Power of the Motor: 1.5 KW

Variable Spindle speed range: 67 - 3000 rpm

Table Feed range: 20 - 875 mm/min at interval of 5mm/min.

Longitudinal Traverse: 700 mm

Cross Traverse: 250 mm

Greatest distance between Centre of the spindle and Top
of the table: 120 mm

Radial runout: 50 μ m

(b) Cincinnati Universal Milling Machine

The essential specifications of the machine are:

Horse Power of the Motor: 8 Kw

Fixed Spindle speeds (rpm): 18,21,27,32,40,47,58,70,88,105,128,150, 206

246,310,370,460,550,680,812,1020,1220,1485,1880.

Fixed Feed range (mm/min): 16,22,32,45,64,89,120,165,228,311,
425,585,812,1120,1520

Longitudinal Travel: 865 mm

Traverse Travel: 305 mm

Greatest distance between centre of the Spindle and
top of the Table: 370 mm.

1.2 The properties of reference workpiece materials

(i) The properties of the reference steel workpiece material:

(a) The mechanical properties of steel (190 BHN) are shown in Table 1

Table 1: Mechanical properties of steel 190 BHN

Yield strength	354 MPa
Tensile Strength	540 MPa
Elongation(%)	30

(b) The thermal properties of steel (190 BHN) are shown in Table 2.

Table 2: Thermal properties of steel 190 BHN.

Specific heat	0.90 Cal/cm ³
Co-efficient of linear expansion	11.90 °C ⁻¹ x 10 ⁻⁶
Thermal conductivity	0.089 cal/cm ³ /cm/°C/sec

(ii) The properties of the reference Inconel workpiece material are:

(a) Physical properties of Inconel 718

The physical properties of Inconel 718 are shown in Table 3.

Table 3: Physical Constants of Inconel 718

Density	8.22 gm/cm ³
Specific Gravity	8.22
Melting Range	1260 - 1337°C (2300-2437°F)
Permeability	1.0013 - 1.0011

(b) Thermal properties of Inconel 718

The thermal properties of Inconel 718 are shown in Table 4.

Table 4: Thermal Properties of Inconel 718

Specific Heat	0.435 KJ/Kg °C
Thermal Conductivity	11.25 W/m °C
Mean Linear Expansion	12.82 E ⁻⁰⁶ /K (7.1 x 10 ⁻⁶ /°F)

(c) Mechanical properties of Inconel 718

The mechanical properties of Inconel 718 are shown in Table 5.

Table 5: Mechanical properties of Inconel 718

Yield Strength(0.2%)	1035 MPa (150 Ksi)
Ultimate Tensile Strength	1276 MPa (185 Ksi)
Elastic Modulus (Young's)	206.85 GPa (30 x10 ³ Ksi)
Elongation(% 5 cm)	12
Reduction of Area, %	15

(iii) The properties of 2618 MMC workpiece material are:

(a) The Physical properties of 2168 MMC are shown in Table 6.

Table 6: Physical properties of 2618 MMC

Properties	
Densities	2.84 gm/cm ³ (or 0.1026 lb/in ³)
Expansion co-efficient	1.77 E ⁻⁵ /K (or 9.8 x 10 ⁻⁶ /°F)

(b) Mechanical properties

The mechanical properties of 2618 MMC is shown in Table 7.

Table 7: Mechanical properties of 2618 MMC

Properties	MMC material	Matrix material
Yield strength	460 MPa	369 MPa
Ultimate tensile strength	532 MPa	473 MPa
Elongation (ϵ_f)	3.1 %	9.4 MPa
Elastic modulus	97.7 GPa	74.0 GPa

1.3 The specifications of experimental cutting tools

(i) HSS slot drills

(a) The chemical composition of the reference HSS solid slot drill is shown in Table 8.

Table 8: Chemical composition of HSS slot drill

Element	Symbol	%
Carbon	C	1.07
Chromium	Cr	3.8
Tungsten	W	1.5
Molybdenum	Mo	9.7
Vanadium	V	1.1
Cobalt	Co	8.8
Iron	Fe	Balance

(b) The tool geometry of reference HSS slot drill

The angular designation of the HSS slot drill is shown in Table 9 with reference to Fig.1.

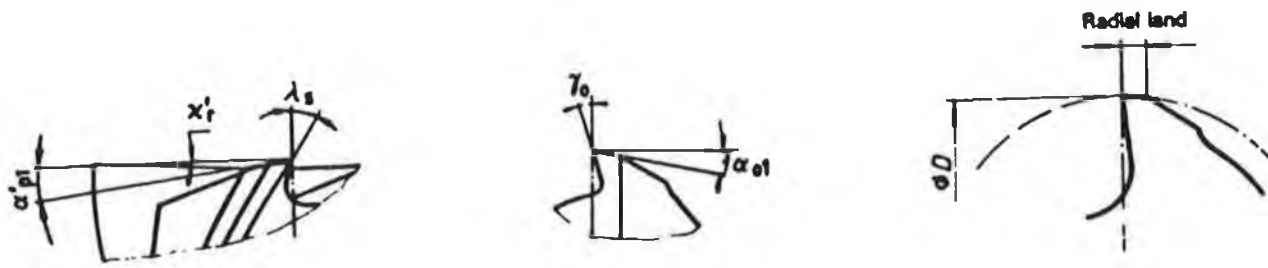


Fig.1: Angular geometries of a slot drill

Table 9: Tool geometry and tolerances for HSS slot drills

Symbol	Terminology according to ISO 3002-1	Terminology in common use.	Geometry and Tolerance
λ_s	Tool cutting edge inclination	Helix angle	$30^\circ \pm 2^\circ$
χ_r'	Tool minor cutting edge angle	Minor cutting edge angle(dishing)	$1\frac{1}{2}^\circ \pm \frac{1}{2}^\circ$
γ_o	Tool orthogonal rake	Radial rake	$9^\circ \pm 3^\circ$
α_{ol}	Tool orthogonal clearance, first flank	Primary clearance angle, Face cutting edge	$10^\circ \pm 2^\circ$
α_{pl}	Tool minor cutting edge back clearance, first minor flank	Primary clearance angle, end cutting edge	$8^\circ \pm 1^\circ$
		Radial land, mm	0.0254 - 0.08
		Radial runout, μm	25
		Axial runout, μm	27
		Corner chamfer	nil

(ii) Carbide inserts

The dimension of carbide end mill inserts and tool holder

The end mill with carbide inserts (Sandvik U-Max R215.44) [5.3] used in this work was 25 mm diameter and had right hand helix. The tool holder (end mill body) is similar to En 46 / En 47 steel with a hardness range of 42 to 46 R_c. The number of indexable uncoated carbide insert (z) of the cutter was 2. The dimensions of these inserts are shown Fig.2.

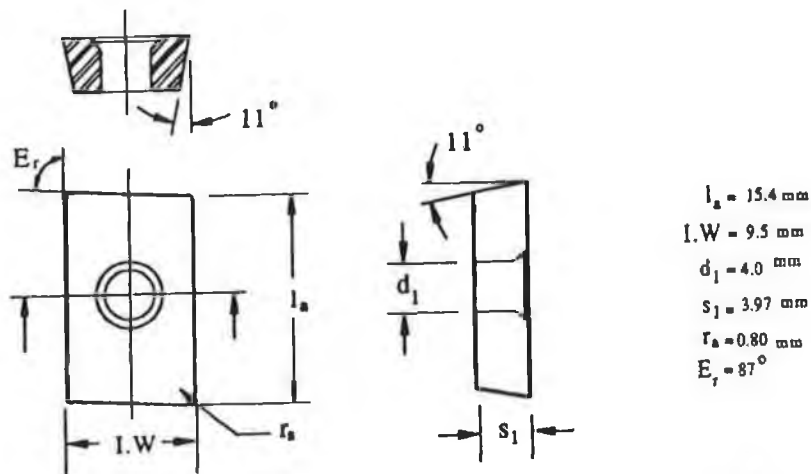


Fig.2: Dimension of the carbide insert of the end mill cutter

1.4 Computer programme for data acquisition of experimental cutting force

```
10 'THIS PROGRAM USES THE METRABYTE FREQUENCY GENERATION PROGRAM
20 'TO GENERATE INTERRUPTS TO INITIATE A/D CONVERSIONS FROM THE
30 KISTLER AMPLIFIERS BY THE DAS-08 INTERFACE CARD.
40 REM
50 REM IT IS IMPORTANT TO HAVE A PRINTER CONNECTED TO RUN THIS
PROGRAM.
100 '*****
110 '*
120 '* SET UP COUNTER 2 TO OUTPUT SQUARE WAVE OF DESIRED FREQUENCY 130
'* MetraByte Corporation          Rev. 1.10 4-9-84  *
140 '*****
150 '
160 '
170 SCREEN 0,0,0:WIDTH 80:CLS:KEY OFF:LOCATE 25,1
175 PRINT"SET COUNTER 2 FOR SQUARE WAVE OUTPUT "METRABYTE CORP"      180
LOCATE 12,19:PRINT"Wait - loading DASH8.BIN and DASH8.ADR"
190 '
200 '----- Load CALL routine & initialize - Contract workspace to 48K -----
210 'Customize this load section to your own requirements:-
220 CLEAR, 49152!
230 DEF SEG = 0
240 SG = 256 * PEEK(&H511) + PEEK(&H510)
250 SG = SG + 49152!/16
260 DEF SEG = SG
270 BLOAD "DASH8.BIN", 0
280 OPEN "DASH8.ADR" FOR INPUT AS #1
290 INPUT #1, BASADR%
300 CLOSE #1
310 DASH8 = 0
320 FLAG% = 0
330 MD% = 0
340 CALL DASH8 (MD%, BASADR%, FLAG%)
350 IF FLAG% <>0 THEN PRINT"INSTALLATION ERROR"
360 CLS:LOCATE 25,1:PRINT "SET COUNTER 2 FOR SQUARE WAVE OUTPUT      365
LOCATE 1,1
370 '
380 '
400 '----- Prompt for desired frequency -----
405 REM
410 INPUT "Desired output frequency in Hz? (Range 37 - 1,000,000): ",FREQ
420 IF FREQ < 37 THEN PRINT:PRINT"Frequency too low ":PRINT:GOTO 400
430 IF FREQ > 1000000! THEN PRINT:PRINT"Frequency too high:PRINT:GOTO 400
```

```

440 '----- Work out closest frequency to desired and inform user -----
450 DIVIDER = 2386400! / FREQ : DIVIDER = INT(DIVIDER + .5)
460 PRINT:PRINT USING "Actual output frequency will be #####.## Hz";2386400!/DIVIDER
465 PRINT:PRINT"-----"
470 '
480 '
500 '----- Set up Counter 2 to provide this frequency -----
510 'Set counter 2 in square wave configuration
520 DIO%(0) = 2 'select counter 2
530 DIO%(1) = 3 'square wave generator
540 MD% = 10 'set config. mode 10
550 CALL DASH8 (MD%, DIO%(0), FLAG%) 'do it
560 'Now load divider
565 IF DIVIDER > 32767 THEN DIVIDER = DIVIDER - 65536! 'correct for 2's comp.
570 DIO%(1) = DIVIDER
580 MD% = 11 'select load mode 11
590 CALL DASH8 (MD%, DIO%(0), FLAG%) 'do it
600 ' O.K. - counter 2 now outputting desired frequency.
610 GOTO 645
620 A$=INKEY$:IF A$ = "" GOTO 620
625 PRINT A$
630 IF A$="Y" OR A$="y" THEN PRINT:PRINT:GOTO 400
635 IF ASC(A$)>=48 AND ASC(A$)<=57 THEN LOCATE CSRLIN-1,1:PRINT SPC(79):LOCATE
CSRLIN-1,1:GOTO 610
637 ' Bypass inadvertent number entry for Y/N response
640 LOCATE 25,1:PRINT SPC(79):END
645 DIM CONVX%(500)
650 LPRINT "THE SELECTED SAMPLING FREQUENCY IS ";FREQ
655 LPRINT
660 REM NOW INITIALIZE SOME VARIABLES TO ZERO
670 INPUT "ENTER NUMBER OF TESTS TO RUN ";TESTS
680 PRINT "WHEN REQUESTED ENTER A FEED-RATE FOR TESTS"
685 PRINT
690 PRINT "TO END SESSION ENTER A FEED-RATE GREATER THAN 600"
695 PRINT
700 LET FEED = 0
710 INPUT "ENTER FEED RATE OF AXIS ";FEED
720 CLS
730 IF FEED > 600 THEN 8000 ELSE 740
740 LET COUNT = 0
750 REM
760 REM
770 REM
780 REM
790 REM TO SET UP THE INTERRUPT LEVEL FOR DAS-8

```

```

800 REM TO USE LEVEL ? BUT THIS CAN BE CHANGED IF NOT SUITABLE.
805 REM THE ACTUAL INTERRUPT SETUP IS DONE IN MAIN A/D SUBROUTINE.
810 FOR I% = 0 TO 499
820 LET CONVX%(I%) = 0
830 NEXT I%
840 REM
850 REM
900 REM TO START CONVERSIONS FOR EACH AXIS WITH THESE SUBROUTINES.
905 REM THIS IS THE SUBROUTINE FOR X-AXIS
910 GOSUB 2000
915 REM THIS IS THE SUBROUTINE FOR Y-AXIS
920 GOSUB 3000
925 REM THIS IS THE SUBROUTINE FOR Z-AXIS
930 GOSUB 4000
940 REM
950 REM
960 REM
970 REM NOW SWITCH OFF INTERRUPTS USING MODE 7
980 MD% = 7
990 LEV% = 7
1000 FLAG% = 0
1010 REM
1015 LPRINT "*****"
1020 GOTO 690
1      9      5      0      R      E      M
XXXXXXXXXXXXXXXXXXXXXXXXXXXXXXXXXXXXXXXXXXXXXXXXXXXXXXXXXXXXXXXXXXXX
2000 REM THIS IS THE ROUTINE WHICH SETS UP DAS-8 FOR THE X-AXIS
2010 REM BE CONNECTED TO CHANNEL 0.(PIN 37. SEE PAGE 78 OF MANUAL.)
2020 REM TO SET THE SCAN LIMIT & STARTING ADDRESS USING MODES 1 & 2
2025 LET CONVERSIONS = 0
2030 MD% = 1
2040 LT%(0) = 0
2050 LT%(1) = 0
2060 FLAG% = 0
2070 CALL DASH8 (MD%, LT%(0), FLAG%)
2080 REM NOW SET STARTING ADDRESS.
2090 MD% = 2
2100 CH% = 0
2110 FLAG% = 0
2120 CALL DASH8 (MD%, CH%, FLAG%)
2130 REM NOW GO TO THE ROUTINE TO DO CONVERSIONS FOR THIS AXIS.
2140 GOSUB 5000
2150 IF CONVERSIONS < 2 THEN 2140 ELSE 2160
2160 LPRINT "THE AV. FORCE(N) ON X-AXIS AT FEEDRATE = ";FEED; "IS: ";FORCE
2170 REM USE DELAY ROUTINE IF NECESSARY

```



```

4100 CH% = 2
4110 FLAG% = 0
4120 CALL DASH8 (MD%, CH%, FLAG%)
4130 REM NOW GO TO THE ROUTINE TO DO CONVERSIONS FOR THIS AXIS.
4140 GOSUB 5000
4150 IF CONVERSIONS < 2 THEN 4140 ELSE 4160
4160 LPRINT "THE AV. FORCE(N) ON Z-AXIS AT FEEDRATE = ";FEED; "IS: ";FORCE
4165 REM
4170 REM
4180 IF CONVERSIONS < TESTS THEN 4140 ELSE 4190
4190 LPRINT "*****"
4200 LPRINT
4210 REM
4220 RETURN
5000 ' THIS IS THE ROUTINE WHICH DOES A/D CONVERSIONS FROM THE
5010 ' KISTLER AMPLIFIERS AND THE CALCULATIONS FOR FORCE.(VOLTS)
5020 ' SCAN LIMIT AND ADDRESS ARE SET BY THE CALLING ROUTINE
5025 ' FIRST SET UP A COUNTER TO DO CONVERSIONS TWICE EACH TIME
5030 LET I = 0
5040 MD% = 6
5050 DIO%(0) = 7
5060 DIO%(1) = 1
5070 FLAG% = 0
5080 CALL DASH8 (MD%, DIO%(0), FLAG%)
5090 ' WE USE MODES 8 AND 9 TO DO THE ACTUAL CONVERSIONS AND
5100 ' TRANSFER TO THE ARRAY IN MEMORY.
5110 REM SET MODE 8 NOW.
5120 MD% = 8
5130 DIO%(0) = 500
5140 DIO%(1) = 20000
5150 FLAG% = 0
5160 CALL DASH8 (MD%, DIO%(0), FLAG%)
5170 ' WE WILL DISPLAY THE FLAG AFTER MODE 8 AS IT MAY BE USEFUL
5180 ' IF THERE ARE PROBLEMS.
5190 PRINT "FLAG AFTER MODE 8 = ";FLAG%
5200 ' NOW SET UP MODE 9 TO TRANSFER CONVERSIONS TO MEMORY.
5210 DEF SEG = SG
5220 MD% = 9
5230 TRAN%(0) = VARPTR(CONVX%(0))
5240 TRAN%(1) = 500
5250 TRAN%(2) = 0
5260 FLAG% = 0
5270 CALL DASH8 (MD%, TRAN%(0), FLAG%)
5280 REM DISPLAY FLAG FOR THIS MODE ALSO
5290 PRINT "FLAG AFTER MODE 9 = ";FLAG%

```

```

5300 MD% = 7
5310 LEV% = 7
5320 FLAG% = 0
5330 REM
5340 REM
5350 REM
5360 REM NOW WE CAN DO THE CALCULATIONS.
5370 LET SUM = 0
5380 FOR I% = 0 TO 499
5390 LET SUM = SUM + CONVX%(I%)
5400 NEXT I%
5410 ' NOW FIND AVERAGE VALUE
5420 LET AVERAGE = 0
5430 LET AVERAGE = SUM/500
5440 '
5550 ' NOW CONVERT THIS VALUE TO FORCE.(VOLTS)
5560 LET VOLTS = 0
5570 LET VOLTS = AVERAGE*10/4096
5571 LET FORCE = VOLTS*200
5575 REM SET ARRAY TO ZERO BEFORE NEXT CONVERSION
5580 FOR I% = 0 TO 499
5590 LET CONVX%(I%) = 0
5600 NEXT I%
5610 LET CONVERSIONS = CONVERSIONS + 1
5660 RETURN
6000 ' THIS IS A DELAY ROUTINE TO GIVE MODE CHANGES TIME TO STABILIZE
6010 ' AND THIS MAY HELP TO SOLVE PROBLEM OF DIFFERENT READINGS
6020 ' BETWEEN THIS PROGRAM AND SINGLE AXIS
6040 ' PROGRAM.(QNCONV.PROGRAM)
6050 FOR I = 0 TO 499
6060 LET DELAY = DELAY + 1
6070 NEXT I
6080 REM
6090 RETURN
8000 END

```


APPENDIX 2

THE CALCULATION OF MODEL PARAMETERS, RESULTS OF ANALYSIS OF VARIANCE, SIGNIFICANCE TESTING OF THE INDIVIDUAL VARIABLES AND CONFIDENCE INTERVALS FOR CUTTING FORCE MODELS FOR STEEL AND INCONEL

2.1 Estimation of model parameters for the resultant cutting force in end milling steel (190 BHN)

(a) Model parameters for 1st block of 6 test

The model parameters of the predictive resultant cutting force model for the first 6 experiments has been estimated by the method of least squares, that is

$$b_m = (X_m^T X_m)^{-1} X_m^T Y_m .$$

The matrix of independent variables X_m for 6 tests is:

$$X_m = \begin{matrix} & \begin{matrix} x_0 & x_1 & x_2 & x_3 \end{matrix} \\ \begin{matrix} 1 \\ 1 \\ 1 \\ 1 \\ 1 \\ 1 \end{matrix} & \begin{vmatrix} -1 & -1 & -1 \\ 1 & 1 & -1 \\ 1 & -1 & 1 \\ 0 & 0 & 0 \\ 0 & 0 & 0 \end{vmatrix} \end{matrix}$$

Hence

$$X_m^T X_m = \begin{vmatrix} 6 & 0 & 0 & 0 \\ 0 & 4 & 0 & 0 \\ 0 & 0 & 4 & 0 \\ 0 & 0 & 0 & 4 \end{vmatrix}$$

$$(X_m^T X_m)^{-1} = \begin{vmatrix} \frac{1}{8} & 0 & 0 & 0 \\ 0 & \frac{1}{4} & 0 & 0 \\ 0 & 0 & \frac{1}{4} & 0 \\ 0 & 0 & 0 & \frac{1}{4} \end{vmatrix}$$

$$Y_m = \begin{vmatrix} 3.8058 \\ 4.6413 \\ 4.4349 \\ 5.3948 \\ 4.6546 \\ 4.5381 \end{vmatrix}$$

$$b_m = \begin{vmatrix} 4.59 \\ 0.03 \\ 0.45 \\ 0.35 \end{vmatrix}$$

(b) Model parameters for the combined block of 12 tests

The matrix of independent variables X_m for 12 tests for the combined blocks is:

$$X_m = \begin{array}{c} x_0 \quad x_1 \quad x_2 \quad x_3 \\ \left| \begin{array}{cccc} 1 & -1 & -1 & -1 \\ 1 & 1 & -1 & -1 \\ 1 & -1 & 1 & -1 \\ 1 & 1 & 1 & -1 \\ 1 & -1 & -1 & 1 \\ 1 & 1 & -1 & 1 \\ 1 & -1 & 1 & 1 \\ 1 & 1 & 1 & 1 \\ 1 & 0 & 0 & 0 \\ 1 & 0 & 0 & 0 \\ 1 & 0 & 0 & 0 \\ 1 & 0 & 0 & 0 \end{array} \right| \end{array}$$

Hence

$$(X_m^T X_m) = \begin{array}{c} \left| \begin{array}{cccc} 12 & 0 & 0 & 0 \\ 0 & 8 & 0 & 0 \\ 0 & 0 & 8 & 0 \\ 0 & 0 & 0 & 8 \end{array} \right| \end{array}$$

and

$$(X_m^T X_m)^{-1} = \begin{array}{c} \left| \begin{array}{cccc} \frac{1}{12} & 0 & 0 & 0 \\ 0 & \frac{1}{8} & 0 & 0 \\ 0 & 0 & \frac{1}{8} & 0 \\ 0 & 0 & 0 & \frac{1}{8} \end{array} \right| \end{array}$$

$$Y_m = \begin{vmatrix} 3.8058 \\ 3.7211 \\ 4.6232 \\ 4.6413 \\ 4.3496 \\ 4.4349 \\ 4.3948 \\ 5.2214 \\ 4.6328 \\ 4.6546 \\ 4.5381 \\ 4.5790 \end{vmatrix}$$

$$b_m = \begin{vmatrix} 4.5475 \\ -0.0200 \\ 0.4463 \\ 0.3262 \end{vmatrix}$$

2.2 Adequacy of the predictive model for the resultant cutting force in end milling steel (190 BHN)

Table 10 shows the results of the analysis of variance of the resultant cutting force model of the combined block of 12 tests.

Table 10: ANOVA for the predictive cutting force model, steel (12 tests)

Source	Sum of Square(SS)	degree of freedom(df)	Mean Square(MS)	$F_{rat(cal)}$	$F_{rat(tab)}$	Remarks
Zero order terms	248.39906	1	248.39906			
First order terms	2.44752	3	0.81584			
Blocks	0.02357	1	0.02357			
Lack of fit	0.01904	5	0.00381	6.93	19.30*	Adequate
Pure error	0.0011	2	0.00055			
Residual	0.04371	8	0.00546			
Total	251.1400	12				

* 95% confidence limit for $F_{rat 5,2}$

2.3 Significance testing of the individual variables of the predictive model for the resultant cutting force in end milling steel (190 BHN)

Table 11 the results of the significance testing of the individual variables of the cutting force model in end milling steel (190 BHN)

Table 11: Significance testing for individual variables (cutting force model, steel)

Source	Sum of Square(SS)	degree of freedom (df)	Mean Square(MS)	$F_{rat(cal)}$	$F_{rat(tab)}$	Remarks
X_1 (v)	0.00280	1	0.00280	0.51	5.32*	Insignificant
X_2 (f ₂)	1.59347	1	1.59347	291.84	"	Significant
X_3 (a _a)	0.85125	1	0.85125	155.91	"	Significant
Residual	0.04371	8	0.00546			

* - 95% confidence limit for $F_{1,8}$

2.4 Calculation of precision of prediction of the predictive cutting force model for steel (12 tests)

The precision of prediction for the predictive model is calculated by $(\hat{y} \pm \Delta\hat{y})$, where $\Delta\hat{y}$ can be shown from equation (4.16) of chapter 4 as:

$$\Delta\hat{y} = t_{df, \frac{\alpha_1}{2}} \sqrt{[V(\hat{y})]}$$

(i) Estimated variance s^2 based on residual sum of square, $\sum (y - \hat{y})^2$ is:

$$s^2 = \frac{\sum (y - \hat{y})^2}{df} = \frac{0.04371}{8} = 0.00546$$

(ii) The variance - covariance matrix for b_m is $(X_m^T X_m)^{-1} s^2$, where $(X_m^T X_m)^{-1}$ is given in section 2.1 of this Appendix.

(iii) Calculation of $V(\hat{y})$

The variance of estimated resultant cutting force $V(\hat{y})$ is calculated according to various cutting conditions as follows:

(a) At the eight corner points (1, 2, 3, 4, 5, 6, 7 or 8),

$$\begin{aligned} V(\hat{y}) &= V(b_0 + b_1 x_1 + b_2 x_2 + b_3 x_3) \\ &= V(b_0) + x_1^2 V(b_1) + x_2^2 V(b_2) + x_3^2 V(b_3) \\ &= (1/12 + 1/8 + 1/8 + 1/8) s^2 \\ &= (11/24) s^2 \end{aligned}$$

Therefore 95% confidence interval for \hat{y} is

$$\begin{aligned} &= \hat{y} \pm t_{8, 0.05/2} \sqrt{\{(11/24) * S^2 \}} \\ &= \hat{y} \pm 3.355 * 0.67700 * 0.07392 \\ &= \hat{y} \pm 0.168 \end{aligned}$$

(b) At the centre point (trials 9, 10, 11 Or 12)

$$V(\hat{y}) = (1/12) s^2$$

Therefore 95% confidence interval for \hat{y} is

$$\hat{y} \pm 0.072$$

(iv) Table 12 shows the Confidence intervals for the predictive cutting force model for steel (12 tests)

Table 12: Confidence intervals (Cutting force Model, Steel 190 BHN)

Tl	F_R	\hat{y}	\hat{y}	\hat{F}_R	$(y-\hat{y})^2$	95% Confidence interval			
						\hat{y}		\hat{F}_R	
						lower	upper	lower	upper
1	44.96	3.8058	3.7955	44.50	0.00011	3.5255	4.0655	33.97	58.29
2	41.31	3.7211	3.7569	42.82	0.00128	3.4869	4.0269	32.68	56.09
3	101.82	4.6232	4.6917	109.04	0.00469	4.4217	4.9617	83.24	142.84
4	103.68	4.6413	4.6531	104.91	0.00014	4.3831	4.9231	80.09	137.43
5	77.45	4.3496	4.4432	85.05	0.00875	4.1732	4.7132	64.92	111.41
6	84.34	4.4349	4.4046	81.83	0.00092	4.1346	4.6746	62.46	107.19
7	220.25	5.3948	5.3394	208.39	0.00307	5.0694	5.6094	159.08	272.98
8	185.20	5.2214	5.3008	200.50	0.00630	5.0308	5.5708	153.06	262.64
9	102.8	4.6328	4.5508	94.71	0.00672	4.4408	4.6608	84.84	105.72
10	105.07	4.6546	4.5508	94.71	0.01078	4.4408	4.6608	84.84	105.72
11	93.51	4.5381	4.5508	94.71	0.00016	4.4408	4.6608	84.84	105.72
12	97.42	4.5790	4.5508	94.71	0.00080	4.4408	4.6608	84.84	105.72

$$\Sigma=0.04371$$

2.5 Adequacy of the predictive model for tangential cutting force in end milling Inconel 718

Table 13 shows the analysis of variance for the predictive model for tangential cutting force in end milling Inconel 718

Table 13: ANOVA for the cutting force model for Inconel 718

Source	Sum of Square(SS)	degree of freedom(df)	Mean Square(MS)	$F_{rat(cal)}$	$F_{rat(tab)}$	Remarks
Zero order terms	272.206	1	272.206			
First order terms	2.52251	2	0.31548			
Lack of fit	0.0169	2	0.00845	3.52	6.94 *	Adequate
Pure error	0.00959	4	0.00240			
Residual	0.02649	6	0.00442			
Total	274.755	9				

* 95% confidence limit for $F_{rat,2,4}$

2.6 Significance testing for individual variables for cutting force model (Inconel 718)

Table 14 shows the significance testing for the individual variables for the tangential cutting force model for Inconel 718.

Table 14: Significance testing for individual variables (tangnetial cutting force model, Inconel 718)

Sources	SS	df	MS	$F_{rat(cal)}$	$F_{rat(tab)}$	Remarks
$X_2 (f_z)$	0.10511	1	0.10511	23.78	5.99*	Significant
$X_3 (a_z)$	2.41740	1	2.41803	547.07	"	Significant
Residual	0.02649	6	0.00442			

* - 95% confidence lim Fit for $F_{1,6}$

2.7 Confidence interval for cutting force model (Inconel 718)

The resulting 95% confidence interval for the tangential cutting model for Inconel 718 is shown in Table 6.15.

Table 15: Confidence intervals for cutting force model for Inconel 718

TI	F_t	\hat{y}	\hat{y}	\hat{F}_t	$(y-\hat{y})^2$	95 % Confidence interval			
						\hat{y}		\hat{F}_t	
						lower	upper	lower	upper
1	89.81	4.4977	4.5612	95.70	0.00403	4.4362	4.6862	84.45	108.44
2	141.40	4.9516	4.8854	132.34	0.00438	4.7604	5.0104	116.79	149.96
3	484.08	6.1823	6.1160	453.05	0.00439	5.9910	6.2410	399.81	513.37
4	587.90	6.3766	6.4402	626.53	0.00405	6.3152	6.5652	552.91	709.95
5	242.04	5.4891	5.5007	244.86	0.00013	5.4474	5.5540	232.15	258.27
6	246.50	5.5074	5.5007	244.86	0.00004	5.4474	5.5540	232.15	258.27
7	255.41	5.5429	5.5007	244.86	0.00178	5.4474	5.5540	232.15	258.27
8	225.48	5.4182	5.5007	244.86	0.00680	5.4474	5.5540	232.15	258.27
9	252.23	5.5303	5.5007	244.86	0.00088	5.4474	5.5540	232.15	258.27

APPENDIX 3

THE CALCULATION OF MODEL PARAMETERS, RESULTS OF ANALYSIS OF VARIANCE, SIGNIFICANCE TESTING OF THE INDIVIDUAL VARIABLES AND CONFIDENCE INTERVALS FOR TOOL LIFE MODELS FOR STEEL (190 BHN) AND THE SEM IMAGE OF THE FLANK WEAR OF THE CARBIDE INSERTS IN END MILLING INCONEL 718

3.1 Calculation of model parameters for the predictive tool life models for steel

The calculation of model parameters for tool life for 12 tests is similar to Appendix 2.

2.1. The calculation of model parameters for tool life for 24 tests is shown below:

The design matrix X_m of independent variables for 24 tests is

$$X_m = \begin{pmatrix} 1 & -1 & -1 & -1 & 1 & 1 & 1 & 1 & 1 & 1 \\ 1 & 1 & -1 & -1 & 1 & 1 & 1 & -1 & -1 & 1 \\ 1 & -1 & 1 & -1 & 1 & 1 & 1 & -1 & 1 & -1 \\ 1 & 1 & 1 & -1 & 1 & 1 & 1 & 1 & -1 & -1 \\ 1 & -1 & -1 & 1 & 1 & 1 & 1 & 1 & -1 & -1 \\ 1 & 1 & -1 & 1 & 1 & 1 & 1 & -1 & -1 & 1 \\ 1 & -1 & 1 & 1 & 1 & 1 & 1 & -1 & -1 & 1 \\ 1 & 1 & 1 & 1 & 1 & 1 & 1 & 1 & 1 & 1 \\ 1 & 0 & 0 & 0 & 0 & 0 & 0 & 0 & 0 & 0 \\ 1 & 0 & 0 & 0 & 0 & 0 & 0 & 0 & 0 & 0 \\ 1 & 0 & 0 & 0 & 0 & 0 & 0 & 0 & 0 & 0 \\ 1 & 0 & 0 & 0 & 0 & 0 & 0 & 0 & 0 & 0 \\ 1 & -1.5 & 0 & 0 & 2.25 & 0 & 0 & 0 & 0 & 0 \\ 1 & 1.5 & 0 & 0 & 2.25 & 0 & 0 & 0 & 0 & 0 \\ 1 & 0 & -1.5 & 0 & 0 & 2.25 & 0 & 0 & 0 & 0 \\ 1 & 0 & 1.5 & 0 & 0 & 2.25 & 0 & 0 & 0 & 0 \\ 1 & 0 & 0 & -1.5 & 0 & 0 & 2.25 & 0 & 0 & 0 \\ 1 & 0 & 0 & 1.5 & 0 & 0 & 2.25 & 0 & 0 & 0 \\ -1 & -1.5 & 0 & 0 & 2.25 & 0 & 0 & 0 & 0 & 0 \\ 1 & 1.5 & 0 & 0 & 2.25 & 0 & 0 & 0 & 0 & 0 \\ 1 & 0 & -1.5 & 0 & 0 & 2.25 & 0 & 0 & 0 & 0 \\ 1 & 0 & 1.5 & 0 & 0 & 2.25 & 0 & 0 & 0 & 0 \\ 1 & 0 & 0 & -1.5 & 0 & 0 & 2.25 & 0 & 0 & 0 \\ 1 & 0 & 0 & 1.5 & 0 & 0 & 2.25 & 0 & 0 & 0 \end{pmatrix}$$

$$(X_m^T X_m) = \begin{vmatrix} 24.0 & 0 & 0 & 0 & 17.0 & 17.0 & 17.0 & 0 & 0 & 0 \\ 0 & 17.0 & 0 & 0 & 0 & 0 & 0 & 0 & 0 & 0 \\ 0 & 0 & 17.0 & 0 & 0 & 0 & 0 & 0 & 0 & 0 \\ 0 & 0 & 0 & 17.0 & 0 & 0 & 0 & 0 & 0 & 0 \\ 17.0 & 0 & 0 & 0 & 28.25 & 8.0 & 8.0 & 0 & 0 & 0 \\ 17.0 & 0 & 0 & 0 & 8.0 & 28.25 & 8.0 & 0 & 0 & 0 \\ 17.0 & 0 & 0 & 0 & 8.0 & 8.0 & 28.25 & 0 & 0 & 0 \\ 0 & 0 & 0 & 0 & 0 & 0 & 0 & 8.0 & 0 & 0 \\ 0 & 0 & 0 & 0 & 0 & 0 & 0 & 0 & 8.0 & 0 \\ 0 & 0 & 0 & 0 & 0 & 0 & 0 & 0 & 0 & 8.0 \end{vmatrix}$$

$$(X_m^T X_m)^{-1} = \begin{vmatrix} 0.2269 & 0 & 0 & 0 & -0.0872 & -0.0872 & -0.0872 & 0 & 0 & 0 \\ 0 & 0.0588 & 0 & 0 & 0 & 0 & 0 & 0 & 0 & 0 \\ 0 & 0 & 0.0588 & 0 & 0 & 0 & 0 & 0 & 0 & 0 \\ 0 & 0 & 0 & 0.0588 & 0 & 0 & 0 & 0 & 0 & 0 \\ -0.0872 & 0 & 0 & 0 & 0.0739 & 0.0246 & 0.0246 & 0 & 0 & 0 \\ -0.0872 & 0 & 0 & 0 & 0.0246 & 0.0739 & 0.0246 & 0 & 0 & 0 \\ -0.0872 & 0 & 0 & 0 & 0.0246 & 0.0246 & 0.0739 & 0 & 0 & 0 \\ 0 & 0 & 0 & 0 & 0 & 0 & 0 & 0.1250 & 0 & 0 \\ 0 & 0 & 0 & 0 & 0 & 0 & 0 & 0 & 0.1250 & 0 \\ 0 & 0 & 0 & 0 & 0 & 0 & 0 & 0 & 0 & 0.1250 \end{vmatrix}$$

$$b_m = \begin{vmatrix} 4.3946 \\ -0.1472 \\ -0.1297 \\ -0.0541 \\ -0.0108 \\ -0.0533 \\ -0.0196 \\ 0.0037 \\ 0.0638 \\ -0.0413 \end{vmatrix}$$

3.2 Adequacy of predictive tool life models in end milling steel (190 BHN)

Table 16 and Table 17 give the results of the analysis of variance for the first and the second-order tool life model respectively. From the above tables it is found that both the first and the second-order model are adequate with 95% confidence probability.

Table 16: ANOVA for The First-order tool life model (steel)

Source	SS	df	MS	$F_{rat(cal)}$	$F_{rat(tab)}$	Remarks
Zero order terms	221.17708	1	221.17708			
First order terms	0.53141	3	0.17714			
Blocks	0.00389	1	0.00389			
Lack of fit	0.06054	5	0.01211	2.12	19.30*	Adequate
Pure error	0.01140	2	0.00570			
Residual	0.07583	8	0.00948			
Total	221.78432	12				

* $F_{rat5,2}$ for 95% confidence probability

Table 17: ANOVA for the Second-order tool life model(steel)

Source	SS	df	Ms	$F_{rat(cal)}$	$F_{rat(tab)}$	Remarks
Zero-order terms	448.1698	1	448.1698			
First-order terms	0.79964	3	0.26655			
Second-order terms	Quadratic	0.05592	3	0.01864		
	Interaction	0.05153	3	0.01718		
Blocks	0.02293	3	0.00764			
Lack of fit	0.03535	3	0.01178	2.39	4.07*	Adequate
Pure error	0.02636	8	0.00329			
Residual	0.08464	14	0.00605			
Total	549.1239	24				

* $F_{rat 3,8}$ for 95% confidence probability

3.3 Significance testing for Individual variables of tool life model in end milling steel

The significance of the individual variables for the first and the second-order tool life predictive models in end milling steel (190 BHN) are shown in Table 18 and Table 19 respectively.

Table 18: Significance testing for individual Variables (First-order Tool life Model, steel)

Source	SS	df	MS	$F_{rat(cal)}$	$F_{rat(tab)}$	Remarks
x_1 (v)	0.26267	1	0.26267	23.94	5.32*	Significant
x_2 (f_2)	0.17123	1	0.17123	15.61	"	Significant
x_3 (a_s)	0.01715	1	0.01715	1.56	"	Insignificant
Residual	0.08774	8	0.01097			

* $F_{1,8}$ for 95% confidence probability

Table 19: Significance testing for Individual variables(Second-order Tool life Model, steel)

Sources	SS	df	MS	$F_{rat(cal)}$	$F_{rat(tab)}$	Remarks
x_1	0.35300	1	0.35300	67.75	4.60*	Significant
x_2	0.26946	1	0.26946	51.72	"	Significant
x_3	0.04115	1	0.04115	7.90	"	Significant
x_1^2	0.00123	1	0.00123	0.24	"	Insignificant
x_2^2	0.07406	1	0.07406	14.21	"	Significant
x_3^2	0.01221	1	0.01221	2.34	"	not so significant
x_1x_2	0.00024	1	0.00024	0.05	"	Insignificant
x_1x_3	0.03287	1	0.03287	6.31	"	Significant
x_2x_3	0.01351	1	0.01351	2.59	"	not so significant
Residual	0.07290	14	0.005521			

* $F_{1,14}$ for 95% confidence probability

3.4 Precision of prediction for the predictive tool life model in end milling steel

The calculation of confidence interval for first-order tool life model (12 tests) is similar to that of the calculation of cutting force predictive model (shown in Appendix 2). So, the calculation of confidence interval for the second-order model (24 tests) is shown below:

(i) Estimated variance s^2 based on residual sum of squares is

$$s^2 = \frac{\sum (y - \hat{y})^2}{df} = \frac{0.08465}{14} = 0.00605$$

(ii) The variance-covariance matrix for b is $(X_m^T X_m)^{-1} s^2$, where $(X_m^T X_m)$ is shown in section 3.1.

(iii) Calculation of $V(\hat{y})$

$$V(\hat{y}) = V(b_0 + b_1 x_1 + b_2 x_2 + b_3 x_3 + b_{11} x_1^2 + b_{22} x_2^2 + b_{33} x_3^2 + b_{12} x_1 x_2 + b_{13} x_1 x_3 + b_{23} x_2 x_3)$$

$$\begin{aligned} & V(b_0) + x_1^2 V(b_1) + x_2^2 V(b_2) + x_3^2 V(b_3) + x_1^4 V(b_{11}) + x_2^4 V(b_{22}) + x_3^4 V(b_{33}) + (x_1 x_2)^2 V(b_{12}) + (x_1 x_3)^2 V(b_{13}) \\ & + (x_2 x_3)^2 V(b_{23}) + 2(x_0 x_1) \text{CoV}(b_0 b_1) + 2(x_0 x_2) \text{CoV}(b_0 b_2) + 2(x_0 x_3) \text{CoV}(b_0 b_3) + 2(x_0 x_1^2) \text{CoV}(b_0 b_1^2) \\ & + 2(x_0 x_2^2) \text{CoV}(b_0 b_2^2) + 2(x_0 x_3^2) \text{CoV}(b_0 b_3^2) \end{aligned}$$

(a) At the eight corner points (trials 1, 2, 3....8),

$$\begin{aligned} V(\hat{y}) &= [0.2269 + 0.0588 + 0.0588 + 3 * 0.0739 + 3 * 0.125 - 2 * (0.0872) * 3 + 2 \\ & * 0.0246 * 3] s^2 \\ &= 0.6244 s^2 \end{aligned}$$

Therefore 95% confidence interval is

$$\hat{y} \pm t_{14, 0.05/2} \sqrt{V(\hat{y})} = \hat{y} \pm 0.1829$$

(b) At the centre point (trials 9, 10, 11, 12)

$$V(\hat{y}) = 0.2269 s^2$$

Therefore 95% confidence interval is

$$\hat{y} \pm 0.2269 s^2$$

Therefore 95% confidence interval is

$$\hat{y} \pm 0.1103$$

(c) At the six augment points (trials 13, 14, 15....18 or 19, 20, 21...24)

$$V(\hat{y}) = [0.2269 + (- 1.5)^2 * 0.0588 + (2.25)^2 * 0.0739 - 2 * (1 * - 1.5)^2 * 0.087]$$

$$= 0.34092 s^2$$

Therefore 95% confidence interval is

$$\hat{y} \pm 0.1352$$

The resulting 95% confidence intervals for the first and the second-order model are shown in Tables 20 and 21 respectively.

Table 20: Confidence intervals for Tool life (First-order Model, steel)

TI	T	\hat{y}	\bar{y}	\hat{T}	$(y-\hat{y})^2$	95 % Confidence interval			
						\hat{y}		\hat{T}	
						lower	upper	lower	upper
1	117	4.7622	4.6958	109.49	0.00441	4.4770	4.9147	87.97	136.27
2	64	4.1589	4.3050	74.07	0.02135	4.0862	4.5239	59.51	92.19
3	84	4.4308	4.3714	79.15	0.00353	4.1526	4.5903	63.60	98.52
4	52	3.9512	3.9806	53.55	0.00086	3.7618	4.1995	43.02	66.65
5	91	4.5109	4.6078	100.26	0.00940	4.3890	4.8267	80.56	124.79
6	77	4.3438	4.2170	67.83	0.01608	3.9982	4.4359	54.50	84.42
7	67	4.2047	4.2834	72.49	0.00619	4.0646	4.5023	58.24	90.22
8	49	3.8918	3.8926	49.04	0.00001	3.6738	4.1115	39.40	61.04
9	70	4.2485	4.2942	73.27	0.00209	4.2005	4.3879	66.72	80.47
10	78	4.3567	4.2942	73.27	0.00391	4.2005	4.3879	66.72	80.47
11	80	4.3820	4.2942	73.27	0.00771	4.2005	4.3879	66.72	80.47
12	72	4.2767	4.2942	73.27	0.00031	4.2005	4.3879	66.72	80.47

Table 21: Confidence intervals for Tool life (Second-order Model, steel)

TI	T	y	\hat{y}	\hat{T}	$(y-\hat{y})^2$	95% Confidence interval			
						\hat{y}		\hat{T}	
						lower	upper	lower	upper
1	117	4.7622	4.7005	110.00	0.00380	4.53979	4.86121	93.67	129.18
2	64	4.1589	4.2273	68.53	0.00468	4.06659	4.38801	58.35	80.48
3	84	4.4308	4.4935	89.43	0.00393	4.33279	4.65421	76.16	105.03
4	52	3.9512	4.0091	55.10	0.00335	3.84839	4.16981	46.92	64.70
5	91	4.5109	4.5093	90.86	0.00001	4.34859	4.67001	77.37	106.70
6	77	4.3438	4.3377	76.53	0.00004	4.17699	4.49841	65.1694	89.87
7	67	4.2047	4.1927	66.20	0.00014	4.03199	4.35341	56.37	77.74
8	49	3.8918	4.0099	55.14	0.01394	3.84919	4.17061	46.96	64.75
9	70	4.2485	4.3378	76.54	0.00798	4.24092	4.43468	69.47	84.33
10	78	4.3567	4.3378	76.54	0.00036	4.24092	4.43468	69.47	84.33
11	80	4.3820	4.3378	76.54	0.00196	4.24092	4.43468	69.47	84.33
12	72	4.2767	4.3378	76.54	0.00374	4.24092	4.43468	69.47	84.33
13	96	4.5643	4.6025	99.73	0.00145	4.48373	4.72123	88.56	112.31
14	63	4.1431	4.1105	60.98	0.00107	3.99173	4.22923	54.15	68.66
15	89	4.4886	4.4684	87.21	0.00041	4.34963	4.58713	77.45	98.22
16	65	4.1744	4.0673	58.40	0.01147	3.94853	4.18603	51.86	65.76
17	82	4.4067	4.3980	81.28	0.00008	4.27920	4.51670	72.18	91.53
18	76	4.3307	4.2552	70.47	0.00571	4.13640	4.37390	62.58	79.36
19	101	4.6151	4.6025	99.73	0.00016	4.48373	4.72123	88.56	112.31
20	68	4.2195	4.1105	60.98	0.01189	3.99173	4.22923	54.15	68.66
21	84	4.4308	4.4684	87.21	0.00141	4.34963	4.58713	77.45	98.22
22	60	4.0943	4.0673	58.40	.00073	3.94853	4.18601	51.86	65.76
23	88	4.4773	4.3980	81.28	0.00630	4.27920	4.51670	72.18	91.53
24	70	4.2485	4.2552	70.47	0.00004	4.13640	4.37390	62.58	79.35

$$\Sigma=0.08465$$

3.5 The SEM image of the flank wear of the carbide insert in end milling Inconel 718

The SEM images of the flank wear of the carbide insert in full and half immersion end milling Inconel 718 are shown in the following figures.



Fig.3: SEM image of the flank wear (VB2/VB3) of the carbide insert (after 10 minutes) in full immersion end milling Inconel 718 at $v = 19.32$ m/min, $f_z = 0.091$ mm/tooth and $a_a = 1.00$ mm

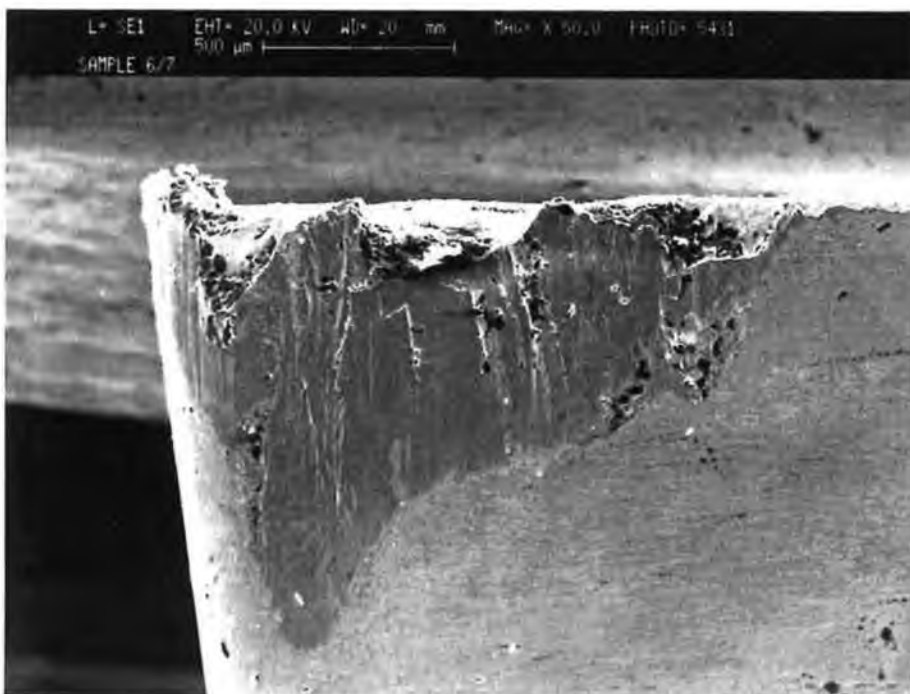


Fig.4: SEM image of the flank wear (VB2/VB3) of the carbide insert (after 5 minutes) in full immersion end milling Inconel 718 at $v = 29.05$ m/min, $f_z = 0.086$ mm/tooth and $a_a = 1.00$ mm



Fig.5: SEM image of the flank wear (VB2/VB3) of the carbide insert (after 2 minutes) in half immersion end milling Inconel 718 at up cut mode at $v = 19.32$ m/min, $f_z = 0.091$ mm/tooth and $a_a = 1.00$ mm

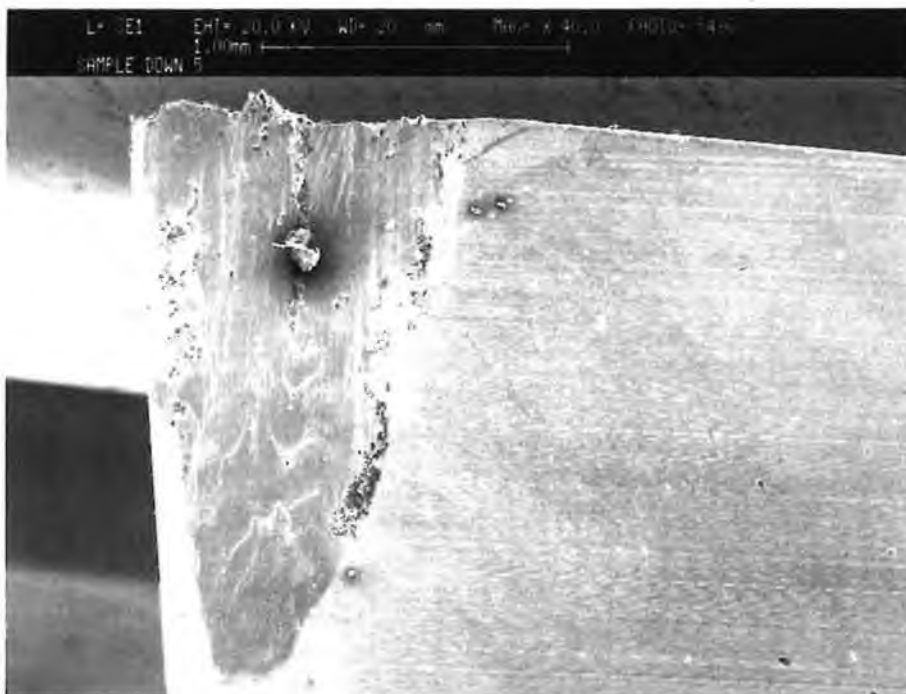


Fig.6: SEM image of the " V " shaped localized flank wear (notching, VB3) of the carbide insert (after 7 minutes) in half immersion end milling Inconel 718 at down cut mode at $v = 19.32$ m/min, $f_z = 0.091$ mm/tooth and $a_a = 1.00$ mm

APPENDIX 4

THE RESULTS OF ANALYSIS OF VARIANCE, SIGNIFICANCE TESTING FOR INDIVIDUAL VARIABLES & CONFIDENCE INTERVALS FOR THE PREDICTIVE SURFACE ROUGHNESS MODELS IN END MILLING STEEL, INCONEL & MMC

4.1 Adequacy of the predictive models for surface roughness for steel (190 BHN)

The results of the analysis of variance for the first and second-order surface roughness models for steel (190 BHN) are shown in Table 22 and 23 respectively.

Table 22: ANOVA for the First-order surface roughness model(Steel)

Source	SS	df	MS	$F_{rat(cal)}$	$F_{rat(tab)}$	Remarks
Zero order terms	15.24966	1	15.24966			
First order terms	2.38347	3	0.79449			
Blocks	0.08100	1	0.08100			
Lack of fit	0.95782	5	0.19156	5.19	19.30*	Adequate
Pure error	0.07382	2	0.03691			
Residual	1.11264	8	0.13908			
Total	18.82677	12				

* - 95% confidence probability for Frat 5,2

Table 23: ANOVA for the Second-order surface roughness model(Steel)

Source	SS	df	MS	$F_{rat(cal)}$	$F_{rat(tab)}$	Remarks
Zero-order terms	28.41638	1	28.41638			
First-order terms	5.38646	3	1.79549			
Second order terms	Quadratic	0.66171	3	0.22057		
	Interaction	0.68968	3	0.22989		
Blocks	0.13548	3	0.04516			
Lack of fit	0.27339	3	0.09113	3.75	4.07	Adequate
Pure error	0.19465	8	0.02433			
Residual	0.60352	14				
Total		24				

* - 95% confidence probability for $F_{rat, 3,8}$

4.2 Significance testing of the individual variables for the predictive models for surface roughness in end milling steel (190 BHN)

Table 24 and Table 25 shows the significance testing for individual variables of the first and the second-order surface roughness model respectively.

Table 24: Test for significance of independent variables(First-order surface roughness model,Steel)

Source	SS	df	MS	$F_{rat(cal)}$	$F_{rat(tab)}$	Remarks
x_1 (v)	0.05564	1	0.05564	0.41	5.32*	Insignificant
x_2 (f_2)	2.12098	1	2.12098	15.25	"	Significant
x_3 (a_2)	0.20685	1	0.20685	1.49	"	Insignificant
Residual	1.11264	8	0.13908			

* $F_{rat 1,8}$ for 95% confidence probability

Table 25: Test for significance of independent variables(Second-order surface roughness model Steel)

Sources	SS	df	MS	$F_{rat(cal)}$	$F_{rat(tab)}$	Remarks
x_1	0.72659	1	0.72659	16.85	4.60*	Significant
x_2	4.31975	1	4.31975	100.20	"	Significant
x_3	0.34012	1	0.34012	7.89	"	Significant
x_1^2	0.51369	1	0.51369	11.92	"	Significant
x_2^2	0.16371	1	0.16371	3.80	"	Almost significant
x_3^2	0.00519	1	0.00519	0.12	"	Insignificant
x_1x_2	0.47317	1	0.47317	10.89	"	Significant
x_1x_3	0.09645	1	0.09645	2.24	"	not so significant
x_2x_3	0.11868	1	0.11868	2.75	"	not so significant
Residual	0.60352	14	0.04311			

* $F_{rat 1,14}$ for 95% confidence probability

4.3 Confidence Interval

The resulting 95% confidence intervals for the first-order and the second-order surface roughness models in end milling steel (190 BHN) are shown in Table 26 and Table 27 respectively.

Table 26: Confidence intervals for surface Roughness (First-order Model, Steel)

TI	R_a	\hat{y}	\hat{y}	\hat{R}_a	$(y-\hat{y})^2$	95 % Confidence interval			
						\hat{y}		\hat{R}_a	
								lower	upper
1	2.73	1.0043	0.5345	1.71	0.22071	- 0.3155	1.3845	0.73	3.99
2	1.41	0.3436	0.3681	1.44	0.0006	- 0.4819	1.2181	0.62	3.38
3	2.94	1.0784	1.5647	4.78	0.2364	0.7147	2.4147	2.04	11.19
4	6.31	1.8421	1.3983	4.05	0.1960	0.5483	2.2483	1.73	9.47
5	2.94	1.0784	0.8561	2.35	0.0494	0.0061	1.7061	1.01	5.51
6	1.53	0.4253	0.6897	1.99	0.0699	- 0.1603	1.5397	0.85	4.66
7	8.07	2.0882	1.8863	6.59	0.0407	1.0363	2.7363	2.82	15.43
8	7.13	1.9643	1.7199	5.58	0.0597	0.8699	2.5699	2.39	13.06
9	2.31	0.8372	1.1272	3.09	0.0840	0.7572	1.4972	2.10	4.47
10	2.88	1.0578	1.1272	3.09	0.0048	0.7572	1.4972	2.10	4.47
11	2.89	1.0613	1.1272	3.09	0.0043	0.7572	1.4972	2.10	4.47
12	2.11	0.7464	1.1272	3.09	0.1447	0.7572	1.4972	2.10	4.47

Table 27: Confidence intervals of surface roughness (Second-order Model, Steel)

TI	R_a	y	\hat{y}	\hat{R}_a	$(y-\hat{y})^2$	95% Confidence interval			
						\hat{y}		\hat{R}_a	
1	2.73	1.0043	0.9919	2.70	0.00015	0.5539	1.4299	1.74	4.18
2	1.41	0.3436	0.2989	1.35	0.00199	- 0.1391	0.7369	0.87	2.09
3	2.94	1.0784	1.3011	3.67	0.04959	0.8631	1.7391	2.37	5.69
4	6.31	1.8421	1.5809	4.86	0.06824	1.1429	2.0189	3.14	7.53
5	2.94	1.0784	1.2595	3.52	0.32794	0.8215	1.6975	2.27	5.46
6	1.53	0.4253	0.1273	1.14	0.08878	- 0.3107	0.5653	0.73	1.76
7	8.07	2.0882	2.0559	7.81	0.00104	1.6179	2.4939	5.04	12.11
8	7.13	1.9643	1.8965	6.66	0.00459	1.4585	2.3345	4.30	10.32
9	2.31	0.8372	0.8861	2.43	0.00238	0.6374	1.1348	1.89	3.11
10	2.88	1.0578	0.8861	2.43	0.02947	0.6374	1.1348	1.89	3.11
11	2.89	1.0613	0.8861	2.43	0.03068	0.6374	1.1348	1.89	3.11
12	2.11	0.7467	0.8861	2.43	0.01943	0.6374	1.1348	1.89	3.11
13	6.71	1.9036	1.6011	4.96	0.09150	1.2866	1.9156	3.62	6.79
14	2.22	0.7975	0.9985	2.72	0.40398	0.6840	1.3130	1.98	3.72
15	1.39	0.3293	0.3849	1.47	0.00309	0.0704	0.6994	1.07	2.01
16	5.6	1.7228	1.8543	6.39	0.01730	1.5398	2.1688	4.66	8.75
17	1.86	0.6206	0.6384	1.89	0.00031	0.3239	0.9529	1.38	2.59
18	3.15	1.1474	1.0507	2.86	0.00935	0.7362	1.3652	2.09	3.92
19	4.88	1.5851	1.6011	4.96	0.00025	1.2866	1.9156	3.62	6.79
20	2.13	0.7561	0.9985	2.72	0.05874	0.6840	1.3130	1.98	3.72
21	1.42	0.3507	0.3849	1.47	0.00117	0.0704	0.6994	1.07	2.01
22	6.83	1.9213	1.8543	6.39	0.00449	1.5398	2.1688	4.66	8.75
23	1.86	0.6206	0.6384	1.89	0.00031	0.3239	0.9529	1.38	2.59
24	2.3	0.8329	1.0507	2.86	0.04743	0.7362	1.3652	2.09	3.92

4.4 Adequacy of the predictive models for surface roughness in end milling Inconel 718

The results of the analysis of variance for the first-order model and the second order surface roughness models for Inconel 718 are shown in Tables 8.28 and 8.29 respectively.

Table 8.28: ANOVA for the First-order surface roughness model(Inconel 718)

Source	SS	df	MS	$F_{rat(cal)}$	$F_{rat(tab)}$	Remarks
Zero order terms	3.32501	1	3.32501			
First order terms	0.90789	2	0.45395			
Lack of fit	0.06450	2	0.03225	4.31	6.94*	Adequate
Pure error	0.02992	4	0.00748			
Residual	0.09442	6	0.01574			
Total	4.32732	9				

* $F_{rat 2,4}$ for 95% confidence probability

Table 8.29: ANOVA for the Second-order surface roughness model(Inconel 718)

Sources	SS	df	Ms	$F_{rat(cal)}$	$F_{rat(tab)}$	Remarks
Zero-order terms	5.00014	1				
First-order terms	0.90789	2				
Second-order terms	0.02210	3				
Lack of fit	0.17981	3	0.05993	8.01	16.69*	Adequate
Pure error	0.02992	4	0.00748			
Residual	0.20973	7				
Total	6.13986	13				

* - $F_{rat 3,4}$ for 95% confidence probability

4.5 Significance of individual variables

Table 8.30 and Table 8.31 were constructed to test the effect of individual variables, adjusted for all other variables for the first and second order surface roughness model (Inconel 718) respectively.

Table 8.30 : Test of significance for individual variables (First-order surface roughness model, Inconel 718)

Sources	SS	df	MS	$F_{rat(cal)}$	$F_{rat(tab)}$	Remarks
x_1 (v)	0.05818	1	0.05818	3.70	5.99*	almost significant
x_2 (f_z)	0.84972	1	0.84972	150.25	"	Significant
Residual	0.09442	6	0.01574			

* $F_{rat 1,6}$ for 95% confidence

Table 31 : Test of significance for individual variables (Second-order surface roughness model, Inconel 718)

Sources	SS	df	MS	$F_{rat(cal)}$	$F_{rat(tab)}$	Remarks
x_1	0.07084	1	0.07084	2.36	5.59*	insignificant
x_2	0.85334	1	28.50	28.50	"	Significant
x_1^2	0.04746	1	0.04746	1.58	"	Insignificant
x_2^2	0.00040	1	0.00040	0.01	"	Insignificant
x_1x_2	0.01103	1	0.01103	0.37	"	Insignificant
Residual	0.20973	7	0.02996	0.02996		

* $F_{rat 1,7}$ for 95% confidence

4.6 Confidence interval for the predictive models for surface roughness for Inconel 718

The resulting confidence intervals for the first and the second order surface roughness model for Inconel 718 is shown in Table 8.32 and 8.33 respectively.

**Table 32: Confidence intervals for the First-order surface roughness model
(Inconel 718)**

Tl	R _a	y	ŷ	R̂ _a	(y-ŷ) ²	95% Confidence interval			
						ŷ		R̂ _a	
1	0.4	- 0.9163	- 0.9481	0.39	0.0010	- 1.1881	- 0.7081	0.30	0.49
2	0.35	- 1.0498	- 1.1893	0.30	0.0195	- 1.4293	- 0.9493	0.24	0.39
3	1.12	0.1133	- 0.0263	0.97	0.0195	- 0.2663	- 0.2137	0.77	1.24
4	0.79	- 0.2357	- 0.2675	0.77	0.0010	- 0.5075	- 0.0275	0.60	0.97
5	0.53	- 0.6349	- 0.6078	0.54	0.0007	- 0.7101	- 0.5055	0.49	0.60
6	0.49	- 0.7133	- 0.6078	0.54	0.0111	- 0.7101	- 0.5055	0.49	0.60
7	0.47	- 0.7550	- 0.6078	0.54	0.0217	- 0.7101	- 0.5055	0.49	0.60
8	0.48	- 0.7340	- 0.6078	0.54	0.0159	- 0.7101	- 0.5055	0.49	0.60
9	0.58	- 0.5447	- 0.6078	0.54	0.0040	- 0.7101	- 0.5055	0.49	0.60

**Table 33: Confidence intervals for the Second-order surface roughness model
(Inconel 718)**

Tl	R _a	ŷ	ŷ	R̂ _a	(y-ŷ) ²	95% Confidence interval			
						ŷ		R̂ _a	
						lower	upper	lower	upper
1	0.40	- 0.9163	- 0.8689	0.42	0.00225	- 1.2022	- 0.5356	0.30	0.59
2	0.35	- 1.0498	- 0.9521	0.39	0.00955	- 1.2854	- 0.6188	0.28	0.54
3	1.12	0.1133	- 0.1105	0.90	0.05010	- 0.4438	0.2228	0.64	1.25
4	0.79	- 0.2357	- 0.4037	0.67	0.02822	- 0.7370	- 0.0704	0.48	0.93
5	0.62	- 0.4780	- 0.3758	0.69	0.01045	- 0.6995	- 0.0521	0.50	0.95
6	0.51	- 0.6733	- 0.6419	0.53	0.00099	- 0.9656	- 0.3182	0.38	0.73
7	0.37	- 0.9943	- 1.1208	0.33	0.01609	- 1.4445	- 0.7971	0.24	0.45
8	0.64	- 0.4463	- 0.1969	0.82	0.06219	- 0.5206	0.1268	0.59	1.14
9	0.53	- 0.6349	- 0.674	0.51	0.00153	- 0.8571	- 0.4909	0.42	0.61
10	0.49	- 0.7133	- 0.674	0.51	0.00155	- 0.8571	- 0.4909	0.42	0.61
11	0.47	- 0.7550	- 0.674	0.51	0.00656	- 0.8571	- 0.4909	0.42	0.61
12	0.48	- 0.7340	- 0.674	0.51	0.00360	- 0.8571	- 0.4909	0.42	0.61
13	0.58	- 0.5447	- 0.674	0.51	0.01671	- 0.8571	- 0.4909	0.42	0.61

4.7 Adequacy of the predictive surface roughness models for 2618 MMC

The results of variance analysis for the first and second-order models are shown in Tables 8.34 & 8.35 respectively.

Table 34: ANOVA for the First-order surface roughness model(2618 MMC)

Source	SS	df	MS	$F_{rat(cal)}$	$F_{rat(tab)}$	Remarks
Zero order terms	5.98985	1	5.98985			
First order terms	8.03112	3	2.67704			
Blocks	0.00118	1	0.00118			
Lack of fit	0.38766	5	.07766	6.68	19.30*	Adequate
Pure error	0.02324	2	0.01162			
Residual	0.41274	8				
Total	14.43305	12				

* - $F_{rat 5,2}$ for 95% confidence probability

Table 35 : ANOVA for the Second-order surface roughness model (2618 MMC)

Source	SS	df	MS	$F_{rat(cal)}$	$F_{rat(tab)}$	Remarks
Zero-order terms	10.87197	1				
First-order terms	13.75667	3				
Second order terms	Quadratic	0.72797	3			
	Interaction	0.19303	3			
Blocks	0.03217	3				
Lack of fit	0.29734	3	0.09911	4.18	7.59*	Adequate
Pure error	0.18986	8	0.02237			
Residual	0.51937	14				
Total		24				

* - $F_{rat 3,8}$ for 99% confidence probability

4.8 Significance of individual variables for the predictive surface roughness model for 2618 MMC

Table 8.36 and Table 8.37 were constructed to test the effect of individual variables, adjusted for all other variables for the first and second-order surface roughness model respectively.

Table 36: Test of significance for individual variables (First-order surface roughness Model, 2618 (MMC)

Source	SS	df	MS	$F_{rat(cal)}$	$F_{rat(tab)}$	Remarks
x_1 (v)	0.2312	1	0.2312	4.52	3.46*	Significant
x_2 (f_z)	7.79809	1	7.79809	150.25	"	Significant
x_3 (a_a)	0.00155	1	0.00155	0.03	"	Insignificant
Residual	0.41274	8	0.05159			

* $F_{rat 1,8}$ for 90% confidence

Table 37: Test of significance for individual variables(Second-order surface roughness Model, 2618 MMC)

Sources	SS	df	MS	$F_{rat(cal)}$	$F_{rat(tab)}$	Remarks
x_1	0.07054	1	0.07054	1.90	3.10*	not so significant
x_2	13.69	1	13.69	369.02	"	Significant
x_3	0.00017	1	0.00017	0.008	"	Insignificant
x_1^2	0.00793	1	0.00793	0.21	"	Insignificant
x_2^2	0.62326	1	0.62326	16.80	"	Significa
x_3^2	0.01291	1	0.01291	0.35	"	Insignificant
x_1x_2	0.07023	1	0.07023	1.89	"	not so significant
x_1x_3	0.02155	1	0.02155	0.58	"	Insignificant
x_2x_3	0.10125	1	0.10125	2.73	"	not so significant
Residual	0.51937	14	0.03709			

* $F_{rat 1,14}$ for 90% confidence

4.9 Precision of prediction for the predictive surface roughness models for 2618 MMC

The precision of the predicted model can be determined by calculating the appropriate confidence intervals and comparing them with the experimental values. The resulting 95% and 99% confidence intervals for the first-order and the second-order surface roughness models are shown in Tables 8.38 and 8.39 respectively.

Table 38: Confidence intervals (First-order surface roughness Model, 2618 MMC)

TI	R_a	\hat{y}	\hat{y}	\hat{R}_a	$(y-\hat{y})^2$	95% Confidence interval			
						\hat{y}		\hat{R}_a	
						lower	upper	lower	upper
1	0.19	- 1.6607	- 1.6149	0.21	0.01514	- 1.9828	- 1.0926	0.14	0.34
2	0.16	- 1.877	- 1.8777	0.15	0.00204	- 2.3228	- 1.4326	0.10	0.24
3	2.25	0.8109	0.4369	1.55	0.13990	- 0.0082	0.8820	0.99	2.42
4	1.10	0.0953	0.0969	1.10	0.00000	- 0.3482	0.5420	0.71	1.72
5	0.24	- 1.4271	- 1.5099	0.22	0.00685	- 1.9550	- 1.0648	0.14	0.34
6	0.21	- 1.5606	- 1.8499	0.16	0.08367	- 2.2950	- 1.4048	0.10	0.25
7	1.53	0.4253	0.4647	1.59	0.00155	- 0.0196	0.9098	1.02	2.48
8	1.09	0.0862	0.1247	1.13	0.00148	- 0.3204	0.5698	0.73	1.77
9	0.43	- 0.8440	- 0.7065	0.49	0.01890	- 0.8964	0.5166	0.41	0.60
10	0.53	- 0.6349	- 0.7065	0.49	0.00513	- 0.8964	0.5166	0.41	0.60
11	0.39	- 0.9416	- 0.7065	0.49	0.05528	- 0.9864	0.5166	0.41	0.60
12	0.37	- 0.9943	- 0.7065	0.49	0.08280	- 0.9864	0.5166	0.43	0.60

Table 39: Confidence intervals (Second-order surface roughness Model, 2618 MMC)

TI	R_a	y	\hat{y}	\hat{R}_a	$(y-\hat{y})^2$	99% Confidence interval			
						\hat{y}		\hat{R}_a	
						lower	upper	low er	uppe r
1	0.19	- 1.6607	- 1.6149	0.20	0.0020	- 1.9869	- 1.2429	0.14	0.29
2	0.16	- 1.8326	- 1.6641	0.19	0.02839	- 2.0361	- 1.2921	0.13	0.27
3	2.25	0.8109	0.6473	1.91	0.02677	- 0.2753	- 1.0193	1.32	2.77
4	1.10	0.0953	0.2233	1.25	0.01638	- 0.1487	- 0.5953	0.86	1.81
5	0.24	- 1.4271	- 1.4883	0.23	0.00374	- 1.8603	- 1.1163	0.16	0.33
6	0.21	- 1.5606	- 1.3299	0.26	0.05324	- 1.7019	- 0.9579	0.18	0.38
7	1.53	0.4253	0.3239	1.38	0.01028	- 0.0481	- 0.6959	0.95	2.01
8	1.09	0.0862	0.1075	1.11	0.00045	- 0.2645	- 0.4795	0.77	1.62
9	0.43	- 0.8440	- 0.8202	0.44	0.00057	- 1.0621	- 0.5783	0.35	0.56
10	0.53	- 0.6349	- 0.8202	0.44	0.03434	- 1.0621	- 0.5783	0.35	0.56
11	0.39	- 0.9416	- 0.8202	0.44	0.01474	- 1.0621	- 0.5783	0.35	0.56
12	0.37	- 0.9943	- 0.8202	0.44	0.03029	- 1.0621	- 0.5783	0.35	0.56
13	0.44	- 0.8210	- 0.6749	0.51	0.02134	- 0.9929	- 0.3569	0.37	0.70
14	0.58	- 0.5447	- 0.8627	0.42	0.10111	- 1.1807	- 0.5447	0.31	0.58
15	0.18	- 1.7148	- 1.6724	0.19	0.00180	- 1.9904	- 1.3544	0.14	0.26
16	2.30	0.8329	- 0.9433	2.57	0.01219	- 0.62532	- 1.2613	1.87	3.53
17	0.38	- 0.9676	- 0.8896	0.41	0.00608	- 1.2076	- 0.5716	0.30	0.56
18	0.48	- 0.7340	- 0.8820	0.41	0.02191	- 1.2000	- 0.5640	0.30	0.57
19	0.47	- 0.7550	- 0.6749	0.51	0.00642	- 0.9929	- 0.3569	0.37	0.70
20	0.44	- 0.8210	- 0.8627	0.42	0.00174	- 1.1807	- 0.5447	0.31	0.58
21	0.25	- 1.3863	- 1.6724	0.19	0.08186	- 1.9904	- 1.3544	0.14	0.26
22	2.57	0.9439	0.9433	2.57	0.00000	- 0.62532	- 1.2613	1.87	3.53
23	0.49	- 0.7133	- 0.8896	0.41	0.03106	- 1.2076	- 0.5716	0.30	0.56
24	0.37	- 0.9943	- 0.8820	0.41	0.01260	- 1.2000	- 0.5640	0.30	0.57

APPENDIX 5: PUBLICATIONS

- [1] M. ALAUDDIN, M.A. EL BARADIE and M.S.J. HASHMI, "Surface roughness model for end milling metal matrix composite (Al/SiC)", Proc. 30th Int. MATADOR Conf., UMIST, pp.135-142, 1993.

- [2] M. ALAUDDIN, M.A. EL BARADIE and M.S.J. HASHMI, "Surface roughness model for end milling Inconel 718", Proc.3rd Int. FAIM (Flexible Automation and Integrated Manufacturing) Conf., University of Limerick, Ireland, pp.810-821, 1993.

- [3] M. ALAUDDIN, M.A. EL BARADIE and M.S.J. HASHMI, " Computer aided analysis of a surface roughness model for end milling", Proc. of the 9th Conf.of the IMC (Irish Manufacturing Committee), University College, Dublin, pp.775-785, 1992.

- [4] M. ALAUDDIN, M.A. EL BARADIE and M.S.J. HASHMI, "Optimization of surface finish in machining Inconel 718" Proc. of 1st Int.Conf. on AMPT (Advances in Materials & Processing Technologies), Dublin City University, August, Vol.1,pp.71-84, 1993.

- [5] M. ALAUDDIN, M.A. EL BARADIE and M.S.J. HASHMI, "Tool life testing in end milling Inconel 718", Proc. of the 1st Int. Conf. on AMPT, Dublin City University, August, Vol.3,pp.1973-1985,1993

- [6] M. ALAUDDIN, M.A. EL BARADIE and M.S.J. HASHMI, " Cutting force model in end milling", Proc. of the 10th Conf. of the IMC, University College, Galway, September, Vol. 2,pp.1013-1024, 1993.